Development of multiscale microbial kinetic-transport models for prediction and optimization of biogenic coalbed methane production

by

Gouthami Senthamaraikkannan

A thesis submitted in partial fulfillment of the requirements for the degree of

Doctor of Philosophy

in

Process Control

Department of Chemical and Materials Engineering
University of Alberta

Abstract

The fundamental objective of this research project is to develop an enzymatic reaction kinetic model for coal bioconversion which, on integration with multiscale transport models, would allow simulation and optimization of field scale biogenic coalbed methane production.

Biogenic coalbed methane (CBM) is an unconventional source of natural gas produced by microbial anaerobic breakdown of coal. Given the many advantages of converting coal to natural gas, much research has been conducted on the enhancement of this natural process at the laboratory scale, and some field scale tests have also been conducted. Commercialization of any such technology requires conceptualization and optimization of field scale strategies. This is a challenge given the complexity and variability of coal, the associated transport processes and the microbial processes involved. In this study, we have used a scaling-up approach starting with the development of reaction kinetics at the smallest scale and the addition of appropriate transport effects at each successive scale to build a model for simulation of CBM in coalbed reservoirs.

The first challenge is to develop a suitable microbial kinetic model with reasonable predictive capability. To this end, microbial reaction networks involved in coal bioconversion were extensively reviewed and complemented with analysis and interpretation of data from laboratory experiments to propose a simplified reaction pathway. An enzymatic reaction kinetic model based on simple and modified Monod models was then derived using lumped species, an approach common in kinetic descriptions of complex

reaction mixtures such as those found in fluid catalytic cracking. The model was then validated by nonlinear regression of data from various coal enrichment cultures.

The kinetic model was next applied to a coreflooding experiment, which is a laboratory scale representation of field conditions, with the inclusion of gas diffusion and sorption behaviour. The model was simplified using computational singular perturbation analysis and an optimal model-based experimental design was devised.

Next, a set of partial differential equations were derived to model the multiple gas transport/storage processes occurring in a coalbed reservoir characterized by dual porosity. After discretization using forward difference formulas and non-dimensionalization, the stiff transport model was solved using the Levenberg-Marquardt algorithm. Dimensionless numbers derived in the course also allow analysis of dominant processes at changing scales. History matching of the transport model was performed against gas production data from Manville wells in Alberta. Finally, gas transport and reaction kinetics were coupled for simulation of biogenic coalbed methane flow and then advanced to multiphase, multicomponent reservoir simulations in CMG STARS for estimation and optimization of commercial biogenic coalbed methane production.

Polynomial chaos expansion (PCE) was used to quantify the effect of parametric uncertainty in the model on estimates of methane production. Legendre orthogonal polynomials were applied in conjunction with PCEs to generate stochastic proxy models for coalbed methane production. In an alternate approach, coefficients of time series models (AR/ARMAX/BJ) were expanded in PCEs to account for dynamic operating variables. Since reservoir models are large and complex with multiple parameters and operating variables, sparse meta models can be employed in proxy model development. The proxy model was then applied for robust optimization based on computationally efficient evaluation of statistical metrics of the costs function at varying operating conditions.

Preface

The research presented in this thesis was carried out under the supervision of Dr. Vinay Prasad and Dr. Ian Gates.

Chapter 2 of this work is submitted as Senthamaraikkanan G., Budwill K., Gates I., Mitra S., Prasad V., 2015 "Kinetic modeling of the biogenic production of coalbed methan", *Energy & Fuels*. Anaerobic serum bottle experiments and results of GC/MS analysis of samples, reported in the work were conducted by Dr. Karen Budwill at Alberta Innovates Technology Futures. I performed analysis of the experimental data, model development and parameter estimation. I wrote the first draft of the paper, which was subsequently reviewed by Dr. Vinay Prasad, Dr. Ian Gates and Dr. Karen Budwill.

Chapter 3 of this work is submitted as Senthamaraikkanan G., Gates I., Prasad V., 2015 "Modeling, estimation and optimization in coreflood experiments for coalbed methane production", *Chemical Engineering Science*. I performed analysis of the experimental data, model development and parameter estimation, along with model based analysis, experimental design and model reduction.

Chapter 4 of this work is submitted as Senthamaraikkanan G., Prasad V., Gates I., 2015 "Development of multiscale microbial kinetics coupled gas transport model for simulation of biogenic coalbed methane production", *Fuel*. I developed the coupled reactive-transport model along with history matching of real time gas production data from Manville gas.

Chapter 5 of this work was presented as Senthamaraikkannan G., Prasad V., Gates I., 2015 "Stochastic proxy modeling for coalbed methane production using orthogonal polynomials" In 9^{th} IFAC symposium on Advanced Control of Chemical Processes. I developed the method described in the paper and applied it for the estimation of coalbed methane production.

Chapter 6 of this work is in preparation for submission as Senthamaraikkannan G., Prasad V., Gates I., 2015 "Multiphase reactive-transport simulations for estimation

and robust optimization of the field scale production of microbially enhanced coalbed methane" to the *Journal of Process Control*. I performed the model development and conducted simulations on CMG STARS. Using the CMG CMOST Studio, I conducted multiple runs to evolve effects of uncertainty and performed robust optimization.

The first draft of chapters 3, 4, 5 and 6 were written by me and then reviewed and refined by Dr. Vinay Prasad and Dr. Ian Gates.

Dedicated to my parents

Acknowledgements

I would like to express my gratitude to my supervisors Dr. Vinay Prasad and Dr. Ian Gates for providing me an ideal environment to enrich my learning and research experience. I take great pride in the fact that throughout the course of my doctoral studies, I have been comfortable despite numerous research challenges, thanks to the many enlightening discussions that I have had with them and the interesting ideas and perspectives that it always resulted in.

I thank Dr. Karen Budwill for her guidance on experimental data related to microbial processes, Jingyi Wang for generously helping me with reservoir simulations and Abhishek Batwara for providing me with real time gas production data extracted from public databases. I would also like to thank Dr. Japan Trivedi for introducing me to new avenues where I can potentially extend the knowledge gained during this program.

I would like to express my sincere appreciation to Artin Afacan for always inspiring me with his refreshing discussions. I also appreciate Ruoxia and Sepideh for the research ideas and useful scientific literature that they have shared with me.

I would like to thank my parents, Mr. Senthamarai Kannan and Mrs. Krishnaveni Senthamarai Kannan, my biggest inspirations, for reminding me everyday the value of hardwork. I thank them for all the selfless sacrifices they have made to let me follow my passions. I also thank Vignesh Senthamarai Kannan, who has been an elder brother to me ever since he ousted my authority as the elder sibling with muscle

power gained overnight. Jokes aside, these four years my brother never failed to check on me even though I was immersed in my own world for the most time.

I wish to thank my husband Dr. Debanjan Chakrabarti for a very many reasons, right from motivating me to pursue doctoral studies, to the constant companionship and moral support he has provided me through thick and thin. It is often that I wonder if I could have faced the varied experiences this entire journey has offered me without him by my side. I also wish to thank my parents-in-law Mr. Durga Shankar Chakrabarti and Mrs. Nivedita Chakrabarti for the support and encouragement they have provided me during their stay in Edmonton.

I wish to thank my wonderful buddies, Babitha Kutty and Sunil Ravinder. Having spent the longest time with them leaves me at a loss of where to begin. What I must mention however is the iron hand that they have had in controlling my stability, everytime I was losing it!

I would like to thank Sriram Ragav for the big smiles he sends all the way from Netherlands; Regena Peter and Dony Alex for the pereptual delight that they generate; Naveen Nayak and Tanni Paul for all the memorable holidays, not to forget Naveen's tremendous culinary skills; Dr. Vinay Bavdekar for the various insightful technical discussions, and his wife Neha Bavdekar who has constantly pampered me with her delicacies; my good friends Priya Baskaran, Dr. Hariprasad Kodamana and Shiv Prakash Upadhyay; and Nivedita Bhaskar, my friend from a very long time, who is going to be a very famous mathematician!

I would like to gratefully acknowledge Carbon Management Canada (CMC) and the Natural Sciences and Energy Research Council (NSERC) for the financial support.

Last but not the least, I feel my acknowledgements would be incomplete without a mention of the myriad of stalwarts in Indian music, who have played a very large role all throughout my research.

Table of Contents

List of Tables

List of Figures

Chapter 1

Introduction

1.1 Introduction to coalbed methane (CBM)

Coalbed methane (CBM) is in fact a mixture of gases, with methane being predominant. Owing to the structural stress caused by the high pressure of the gases, CBM was considered to be a major mine hazard in the early nineteenth century[1]. However, significant research towards identification of alternate unconventional gas resources during the late twentieth century paved the path for CBM's status today as an important unconventional natural gas resource[2]. CBM has higher energy efficiency than coal and burns clean as well, leaving no ash and emits lower GHG and other toxic emissions[3,4]. The International Energy Agency (IEA) reports that in 2008, CBM contributed to 10% natural gas production in the United States, 4% in Canada, and 8% in Australia. Also, there has been increased interest in CBM production in other countries with large coal reserves, such as India, China, Russia, and Indonesia[4]. According to a report on global market volume by Grand View Research in 2014, the power sector is the largest consumer of CBM. In 2013, 35.3% of the total CBM produced globally was used for power generation, with an estimate that the usage would grow at a compound annual growth rate of 8.5% from 2014 to 2020[5].

CBM is generally produced from relatively shallow coal beds (about 1000 -1500 ft) as compared to conventional sources that are contained within sharply defined geological formations (at about 3000 ft). For a coal seam to be economically viable for CBM production, it must typically be at least 20 ft thick, produce 50 - 70 ft^3 of gas/ton of coal, contain 77% - 87% of carbon (normally found in sub-bituminous coal) and contain sufficient water pressure to hold the gas in place[6]. CBM exists in coal seams in three basic states: free gas, gas dissolved in formation waters, and gas adsorbed on solid coal surfaces[7]. When a production well is drilled for CBM

extraction, the hydrostatic pressure decreases to produce formation water, which is followed by the production of free gas and adsorbed gases (which are about 91% - 95% of the total gas content) [8]. The life span of a CBM well typically lies between 5 and 15 years. The three stages of production (U.S. EPA 2010b) are (1) an early stage where the hydrostatic pressure is reduced by the production of formation water, (2) a stable stage where natural gas production increases and water production decreases, and (3) a late stage where gas production declines and water production remains low. Gas transport in coal is a multi-step process consisting of gas diffusion in micropores, gas diffusion through partly blocked microfractures, gas flow through open, un-mineralized microfractures and gas movement through main fractures[9]. For simplification in numerical simulations, this is usually modeled as a two-step transport process consisting of gas diffusion through micropores (or matrix) and gas flow through macropores (or fractures).

There are many issues affecting a CBM project. For high CBM production from wells, desorbed gases have to be able to flow out easily. This depends a great deal on the presence of preexisting natural fracture systems. In the absence of natural fractures (which is typically the case), artificial stimulation by hydraulic fracturing is required. Also, owing to low productivity of gas wells (about 100 - 500 MCF/day), sustained CBM production often requires continued drilling of production wells, causing drilling costs to account for 74% of the total cost that is incurred. Similarly, uncertainties in projected gas and water production due to the vast heterogeneity of coal beds, high investment costs, economics of gas demand and supply, water and environmental management, availability of gas and water pipelines, availability of land and ownership issues are some of the hurdles faced by this industry.

The economic profitability of CBM production can be improved by enhancement of gas recovery. Conventional CBM recovery by reservoir pressure depletion typically recovers only 50% of the gas in place. The recovery of gases adsorbed in the coal matrix can be improved by the use of well-known techniques such as inert gas stripping using nitrogen injection and displacement desorption by CO_2 injection. This process is referred to as enhanced CBM recovery (ECBM)[10]. Nitrogen injection ECBM (N_2-ECBM) works by decreasing the partial pressure of methane in the porous spaces of coal to promote desorption, while carbon dioxide injection (CO_2-ECBM) works on the principle that carbon dioxide preferentially adsorbs in coalbed matrix and promotes methane desorption. In addition, CO_2-ECBM sequesters CO_2, which is a high potent greenhouse gas, simultaneously. Alternatively, CBM production can also be increased by the generation of additional methane. Microbially enhanced CBM (MECoM) is one such technique that has gained interest since it was discovered that approximately 20% natural gas is microbial in origin[11]. This practice of microbial enhancement is in fact already well-known to the oil industry. U.S. Pat. No. 3,185,216,[12] for example, discusses oil metabolization by bacteria injected into oil reservoirs to produce

byproducts and enhance mobility. The method is referred to as microbially enhanced oil recovery (MEOR).

1.2 Microbially enhanced coalbed methane

CBM gases formed from coal are classified as primary, secondary biogenic gas and thermogenic gas based on their source and origin. Primary biogenic CBM is the gas eliminated by aerobic microbial attack of cellulose during coal formation[13]. Thermogenic CBM is the gas generated by catalytic cracking of deeply buried coal beds under high temperature and pressure conditions. Finally, gas produced by anaerobic microbial attack of coal substrate following renewed microbial activity in deeply buried coal beds is known as secondary biogenic CBM[14,15]. High CBM-producing zones in many basins around the world contain a large proportion of secondary biogenic methane generated by microbes transported during water recharge through permeable coal seams[16,17]. Studies by various research groups have shown that secondary biogenic methane generation is still active in many basins around the world[18–21].

The various factors controlling the extent of microbial activity are the bioavailability of coal carbon, the presence of a microbial community to convert coal carbon to methane, and a suitable environment for microbial growth[22]. Theoretically, microbially generated coalbed methane can be increased if the appropriate conditions are made available either by the introduction of anaerobic bacterial consortia, consisting of hydrolyzers, acetogens and methanogens, and/or nutrients into coalbed methane wells[23]. To achieve this, researchers have primarily studied four strategies: microbial stimulation by the addition of nutrients, microbial augmentation by the addition of microbes, physically increasing fracture spacing to provide more access to microbes and nutrient amendments, and chemically increasing the bioavailability of coal organics[11].

Laboratory incubation studies on lignite and subbituminous coals by Harris et al.[24] showed that substantial methane production occurs in the presence of H_2/CO_2 and inorganic nutrient ammendments. Studies by Singh et al.[25] on an Indian coal bed sample showed that methane production in the presence of formation waters and native microbial population improved considerably with the addition of nitrite. Experiments by Opara et al.[26] on lignite, bitminous coal and coal wastes with selected microbial inocula and different types and levels of nutrient amendments showed that methane production increased with increasing nutrient concentrations. The addition of organic nutrients such as tryptone and Brain Heart Infusion (BHI) was shown to improve methane production in sub-bituminous coal samples from western Canada by Penner et al[27]. Jones et al.[28] observed that bioaugmentation with a consortium of

bacteria and methanogens enriched from wetland sediment accompanied by biostimulation with nutrient amendments generated methane more rapidly and to a higher concentration as compared to biostimulation without the amendments. Experiments by Papendick et al.[29] on native Walloon coal with produced waters from the Surat basin showed that initial methane production rate and final methane yield increased by 240% and 180%, respectively on the addition of a Zonyl FSN surfactant to improve coal bioavailability. Similarly, Huang et al.[30] showed that methane production increased when coal samples were treated with potassium permanganate, a depolymerization agent that aids in coal solubilization.

Many field scale studies have also been carried out on biogenic methane production. Succesful pilot scale field tests for microbial stimulation of CBM production were conducted by Luca Technologies, Inc to restore gas production in existing wells in the Powder River Basin, Wyoming. Similarly, Crisis Energy, and Next Fuel, Inc. have also conducted smaller field scale tests. Also, Archtech, Synthetic Genomics and ExxonMobil hold patents related to MECoM[11]. US patent 7696132[31] describes methods for stimulating biogenic production with enhanced hydrogen content using a combination of hydrogen and phosphorous compounds, US patent 5424195[32] describes a method using household sewage injection into an abandoned coal mine to provide feedstock for the bacteria, US patent 20040033557[33] describes a method for injection of bacteria and nutrients under pressure into naturally occurring fractures or cleats as well as fractures induced during the stimulation of coalbed methane gas wells, US patent 20140034297[34] describes methods for dispersion of nutrient amendments and US 7640978[35] describes methods for contacting subsurface coalbeds with microbes under anaerobic conditions to form a reaction mixture.

Although numerous studies have been carried out, a key link in the commercialization of any such technology development is the capacity to conduct model-based analysis for technology transfer over increasing scales along with process estimation, optimization and control at field scales. For instance, Luca's operational approach was batch treatment of wells with nutrient amendments, followed by the assessment of new gas formation after many months or years, whereas Ciris adopted a continuous-flow injection process using 4 injection wells surrounded by 13 production wells, recirculating 1000 - 2000 barrels of water every day. Since there is no rigorous approach for the appraisal of these operating procedures, optimum injection procedures cannot be resolved and process efficiency is compromised. Thus, in the absence of suitable simulation tools, all decisions related to production forecasting, well completions, etc. are likely to be sub-optimal.

1.3 Thesis contributions

Thus, in the light of the above discussion, it is evident that the progress of MECoM projects that can make CBM a long term viable energy source is intertwined with the development of a numerical model that seamlessly and dynamically links reactive and transport phenomena occuring in a coal bed across multiple length and time scales[36]. Such a model that can predict the quantity of biogenic methane production reasonably can play a huge role in the commercialization of microbially enhanced CBM recovery by enabling process analysis, optimization and control. While the modeling of fluid transport in coal beds with multiscale porosities is mature, coupled kinetic and transport models for the simulation of ongoing biogenic methane production are not available. The complexity and variability of coal and the associated microbiota, complicated biodegradation systematics that are not fully understood, ignorance of reactant transport within coal and the inaccessible nature of coal seams are some of challenges in developing such models. Addressing these issues, the work described in this thesis develops a multiscale model by incorporating information from the laboratory to the field scale.

The first step is the modeling of enzymatic reaction kinetics related to coal bioconversion. Since coal biodegradation occurs through a complicated network of many series and parallel reactions, detailed microkinetic models are difficult to develop. Therefore, we identify an approximate simplified reaction pathway based on lumping techniques and use it for developing kinetic models. The estimated kinetic model is then employed to quantify the production of methane and other gases as well as intermediates under different nutrient loadings and injection rates. Model reduction was performed by a time scale analysis of the metabolic network to differentiate fast and slow time scales at different times. It is to be noted that the multistep kinetic scheme proposed in this work for anaerobic coal breakdown is the first of its kind and its predictive ability has been validated for various coal samples.

The next step is to develop a multiscale fluid transport model, which is performed in two stages. In the first stage, we develop a single phase 1D radial gas transport model accounting for adsorption and desorption of methane, surface and bulk diffusion, and convection. Following a global sensitivity analysis of model parameters based on the Morris OAT (one-at-a-time) method, non-dimensionalized implicit formulations of the stiff partial differential transport equations are solved at different parameter value sets for history matching of the real-time gas production data from Manville wells in Alberta, Canada. After validation, the gas transport model is then coupled with the derived microbial kinetic model based on the assumption that microbes reside in the macropore spaces containing residual moisture. Apart from evaluation of the effect of transport parameters based on dimensionless numbers, the effect of

the various kinetic parameters on the enhancement of methane production is also studied. Although gas transport modeling has been dealt with adequately prior to this work, reactive-transport models for simulation of microbially enhanced coalbed methane were not available.

In the second stage, we use the model parameter values in multicomponent two-phase reservoir simulations in CMG STARS (Steam, Thermal and Advanced Processes Reservoir Simulator).[37] A physical model for the coal reservoir is simulated using the Warren-Root dual porosity model with matrix-fracture flow transmissibility defined by Kazemi-Gilman formulations. The coal component is assumed to react only in the fractures (macropores) where microbes exist, while the matrix (micropores) only functions as a storage medium for the gases. Using this field scale reservoir model, biogenic methane production is optimized based on model analysis under different nutrient loadings and injection systems including well configuration, injection rates and pressures. The integrated efforts for model development in this study traversing across multiple scales, finally produce simulation tools required in the assessment of commercial recovery of microbially enhanced coalbed methane. The motivation behind this multiscale modeling approach is prediction and control of the various phenomena occurring at different length and time scales. Ultimately, we aim to achieve robust optimization of commercially produced microbially enhanced coalbed methane, based on manipulating operation scale variables.[38] The schematic representation of the scaling approach adopted in this study is shown in Figure 1.1.

Physical systems that are of multiscale nature require mathematical models that look beyond differential equations at the continuum level. This coupled with the rapid growth in computational speed has resulted in widespread use of multiscale modeling approaches in various scientific and engineering applications. [38,39] Several multiscale model simulation approaches exist in literature. Based on the distance of separation between scales, they are broadly classified as hybrid & multi-grid hybrid type simulations. Hybrid simulations are conducted by advancing a large scale model at large length and time scales with simultaneous information transfer from small scale model simulations. Multi-grid type hybrid simulations on the other hand employ coarse grid models with small scale information estimated from small model simulations on fine grids.[38] The various algorithms for conducting multiscale simulations and multiscale model reduction based on user-accepted error thresholds are summarized in Givon et al.[40]

Another research challenge that is dealt with is the computational expense attached to model-based optimization studies combined with effects of parameter uncertainty. Since parametric uncertainty can significantly affect the optimality of the calculated solution, robust optimization incorporating a degree of caution in the results is also considered. Several uncertainty propagation methods are available from literature.

Among them, the traditional approach is Monte Carlo based on standard or Latin Hypercube sampling. A low-cost alternative to this is the perturbation method or sensitivity analysis, which produces reliable predictions for small perturbations without predicting the shape of the whole distribution. Overcoming these drawbacks, computationally efficient uncertainty propagation methods based on probability theory are also available. One of these is the use of first and second order power series approximations which combines sensitivity analysis & probability theory techniques. Since these expansions do not capture the shape and tails of non Gaussian distributions, in this study, we employ the more generic method known as polynomial chaos expansion - a method in which model output is expanded as sum of orthogonal polynomials in the underlying random variables.[41] By retaining the functional relation between input and output variables in the polynomial chaos expansion, we have proposed proxy/surrogate models that can be employed to perform low cost robust optimization of commercially enhanced coalbed methane production at varying injection pressures and nutrient injection compositions.

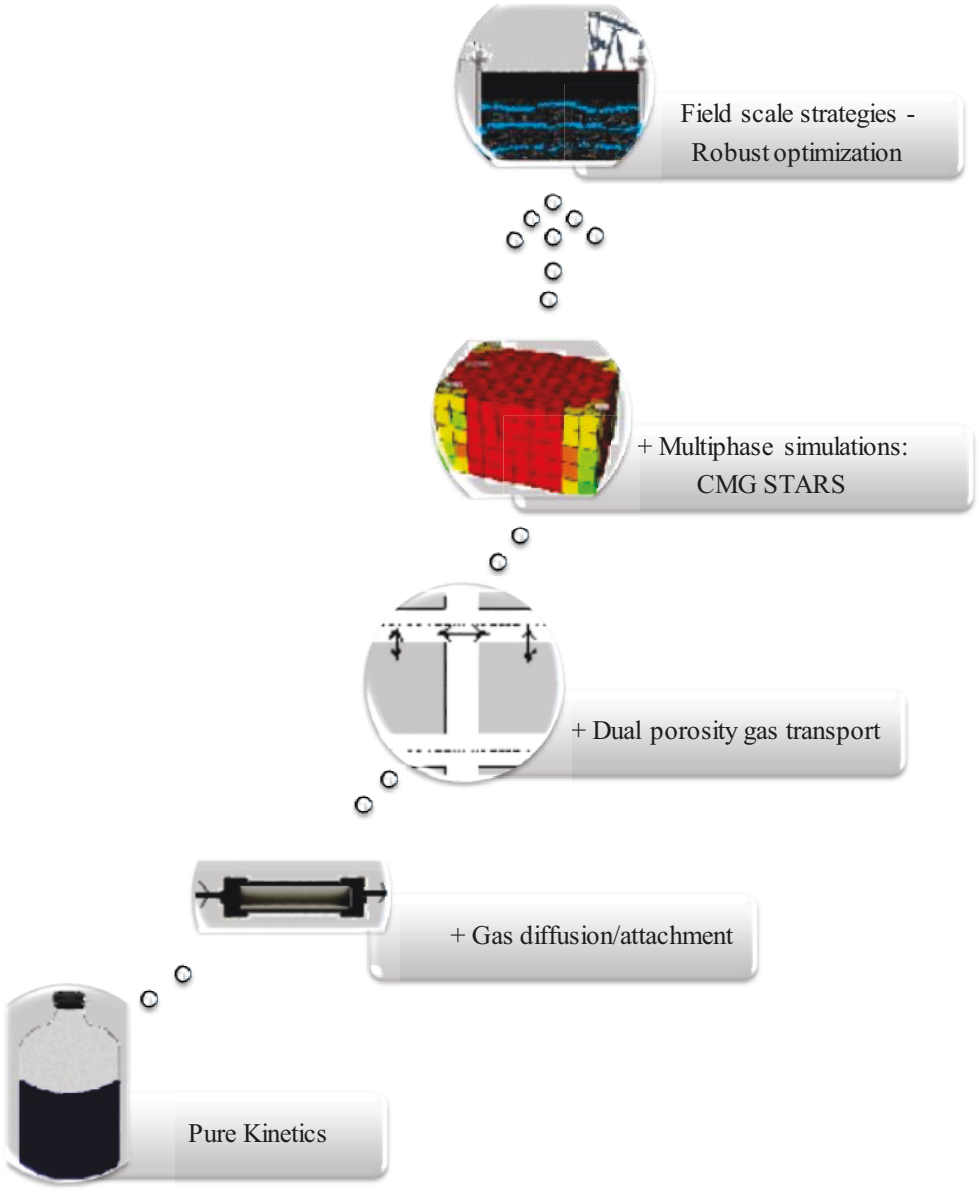

Figure 1.1: *Schematic of the scaling approach adopted in this work.*

1.4 Thesis outline

The following is a brief description of each chapter in this thesis:

Chapter 2: Kinetic modeling of the biogenic production of coalbed methane

In this chapter, a simplified reaction pathway using lumped species is derived for coal bioconversion based on data from laboratory scale experiments. Kinetic models are then developed for single substrate (carbon) limitation using simple and modified Monod models. The model is validated against experimental data from anaerobic serum bottle experiments with crushed coal in the presence of inoculum and nutrients.

Chapter 3: Modeling, estimation and optimization in coreflood experiments for coalbed methane production

In this chapter, coreflooding experiments conducted to mimic field operations on laboratory scale are modeled using a tanks-in-series model with an enzymatic reaction kinetic model modified from the previous chapter to account for multiple substrate (carbon and nitrogen) limitations. Since the coreflood is simulated with an overburden pressure, sorption processes are also accounted for in the model.

Chapter 4: Modeling of methane production in coal seams with dual porosity characteristics in the presence of microbial activity

In this chapter, a dual porosity coalbed is projected on a 1D radial co-ordinate system and multiscale coalbed methane gas transport and storage processes are modeled. The stiff transport equations are non-dimensionalized and solved with implicit formulations. The transport model is then coupled with enzymatic reaction kinetics, based on the assumption that microbial growth is supported by residual pore water in the macropores/fractures.

Chapter 5: Stochastic proxy modeling of coalbed methane production using orthogonal polynomials

In this chapter, a proxy model is built for the stochastic solutions of transport equations describing coalbed methane (CBM) production at different well bottomhole pressures, based on a polynomial chaos framework. The proxy model enables computationally efficient robust optimization using statistical metrics of CBM production calculated over the entire parameter space, as opposed to running multiple full model simulation runs, which would be computationally expensive.

Chapter 6: Multiphase reactive-transport simulations for estimation and robust op-

timization of the field scale production of microbially enhanced coalbed methane

In this chapter, multiphase multi-component enzymatic kinetic models and transport models are simulated for field scale gas production from dual porosity coal bed reservoirs in STARS. Simulations are used to evaluate the effect of changing operating conditions such as injection pressure, nutrient composition in injection fluid and well patterns. Robust optimization in the presence of uncertainty in model parameters is also performed based on the technique developed in the previous chapter, to identify the optimal values of injection bottomhole pressure and nutrient composition.

Chapter 7: Conclusions

This chapter summarizes the thesis, provides conclusions and discusses future research directions.

Finally, it is to be noted that since the thesis is paper-based, repetitions may occur, especially in the "Introduction" section of each chapter.

References

[1] Flores, R. M. Coalbed methane: from hazard to resource. *International Journal of Coal Geology*, 35(1):3–26, 1998.

[2] Soot, P. Tax incentives spur development of coalbed methane. *Oil & Gas Journal*, 89(23):40, 1991.

[3] Senthamaraikkannan, G. and Prasad, V. Coalbed methane. In M.R.Riazi and Gupta, R., editors, *Coal Production and Processing Technology*. Taylor & Francis Group, (in press).

[4] Stevens, P. The shale gas revolution: Hype and reality. *Chatham House London*, 2010.

[5] Stiller, B., Bocek, T., Hecht, F., Machado, G., Racz, P., and Waldburger, M. Coal Bed Methane (CBM) Market Analysis By Application (Industrial, Power Generation, Residential, Commercial and Transportation) And Segment Forecasts To 2020. Technical report, Grand View Research, 2014.

[6] Young, E. . Shale gas and coal bed methane: Potential sources of sustained energy in the future. Technical report, 2010. URL `http://www.ey.com/Publication/vwLUAssets/Shale_gas_and_coal_bed_methane/$File/Shale_gas_and_coal_bed_methane_-__Potential_sources_of_sustained_energy_in_the_future.pdf`.

[7] U.S. Environmental Protection Agency (U.S. EPA). Technical Development Document for the Coalbed Methane (CBM) Extraction Industry. Technical report, 2013. URL `http://water.epa.gov/scitech/wastetech/guide/oilandgas/upload/cbmttd2013.pdf`.

[8] U.S. Environmental Protection Agency (U.S. EPA). Characteristics of coalbed methane production and associated hydraulic fracturing practices, 2004. URL `http://water.epa.gov/type/groundwater/uic/class2/hydraulicfracturing/wells_coalbedmethanestudy.cfm`.

[9] Wei, X., Wang, G., Massarotto, P., Golding, S., and Rudolph, V. Numerical simulation of multicomponent gas diffusion and flow in coals for CO_2 enhanced coalbed methane recovery. *Chemical engineering science*, 62(16):4193–4203, 2007.

[10] White, C. M., Smith, D. H., Jones, K. L., Goodman, A. L., Jikich, S. A., LaCount, R. B., DuBose, S. B., Ozdemir, E., Morsi, B. I., and Schroeder, K. T. Sequestration of carbon dioxide in coal with enhanced coalbed methane recovery: A review. *Energy & Fuels*, 19(3):659–724, 2005.

[11] Ritter, D., Vinson, D., Barnhart, E., Akob, D. M., Fields, M. W., Cunningham, A. B., Orem, W., and McIntosh, J. C. Enhanced microbial coalbed methane generation: A review of research, commercial activity, and remaining challenges. *International Journal of Coal Geology*, 146:28–41, 2015.

[12] Hitzman, D. Use of bacteria in the recovery of petroleum from underground deposits. May 25 1965. US Patent 3,185,216.

[13] Rice, D. D. Composition and origins of coalbed gas. *Hydrocarbons from coal: AAPG Studies in Geology*, 38(1):159–184, 1993.

[14] Parkes, R. J., Cragg, B. A., and Wellsbury, P. Recent studies on bacterial populations and processes in subseafloor sediments: A review. *Hydrogeology Journal*, 8(1):11–28, 2000.

[15] Martini, A., Walter, L., Budai, J., Ku, T., Kaiser, C., and Schoell, M. Genetic and temporal relations between formation waters and biogenic methane: Upper Devonian Antrim Shale, Michigan Basin, USA. *Geochimica et Cosmochimica Acta*, 62(10):1699–1720, 1998.

[16] Faiz, M. Microbial influences on coal seam gas reservoirs: A review. 6(2004):133–42, 2004.

[17] Faiz, M. and Hendry, P. Significance of microbial activity in Australian coal bed methane reservoirs: A review. *Bulletin of Canadian Petroleum Geology*, 54(3):261–272, 2006.

[18] Cokar, M., Ford, B., Kallos, M., and Gates, I. New gas material balance to quantify biogenic gas generation rates from shallow organic-matter-rich shales. *Fuel*, 104:443–451, 2013.

[19] Ulrich, G. and Bower, S. Active methanogenesis and acetate utilization in Powder River Basin coals, United States. *International Journal of Coal Geology*, 76(1):25–33, 2008.

[20] Kirk, M. F., Martini, A. M., Breecker, D. O., Colman, D. R., Takacs-Vesbach, C., and Petsch, S. T. Impact of commercial natural gas production on geochemistry and microbiology in a shale-gas reservoir. *Chemical Geology*, 332:15–25, 2012.

[21] Strapoc, D., Mastalerz, M., Eble, C., and Schimmelmann, A. Characterization of the origin of coalbed gases in southeastern illinois basin by compound-specific carbon and hydrogen stable isotope ratios. *Organic Geochemistry*, 38(2):267–287, 2007.

[22] Jones, E. J., Voytek, M. A., Warwick, P. D., Corum, M. D., Cohn, A., Bunnell, J. E., Clark, A. C., and Orem, W. H. Bioassay for estimating the biogenic methane-generating potential of coal samples. *International Journal of Coal Geology*, 76(1):138–150, 2008.

[23] Scott, A. R. Improving coal gas recovery with microbially enhanced coalbed methane. In Mastalerz, M., Glikson, M., and Golding, S., editors, *Coalbed Methane: Scientific, Environmental and Economic Evaluation*, pages 89–110. Springer Netherlands, 1999. ISBN 978-90-481-5217-9.

[24] Harris, S. H., Smith, R. L., and Barker, C. E. Microbial and chemical factors influencing methane production in laboratory incubations of low-rank subsurface coals. *International Journal of Coal Geology*, 76(1):46–51, 2008.

[25] Singh, D. N., Kumar, A., Sarbhai, M. P., and Tripathi, A. K. Cultivation-independent analysis of archaeal and bacterial communities of the formation water in an Indian coal bed to enhance biotransformation of coal into methane. *Applied microbiology and biotechnology*, 93(3):1337–1350, 2012.

[26] Opara, A., Adams, D., Free, M., McLennan, J., and Hamilton, J. Microbial production of methane and carbon dioxide from lignite, bituminous coal, and coal waste materials. *International Journal of Coal Geology*, 96:1–8, 2012.

[27] Penner, T. J., Foght, J. M., and Budwill, K. Microbial diversity of western Canadian subsurface coal beds and methanogenic coal enrichment cultures. *International Journal of Coal Geology*, 82(1):81–93, 2010.

[28] Jones, E. J., Voytek, M. A., Corum, M. D., and Orem, W. H. Stimulation of methane generation from nonproductive coal by addition of nutrients or a microbial consortium. *Applied and Environmental Microbiology*, 76(21):7013–7022, 2010.

[29] Papendick, S. L., Downs, K. R., Vo, K. D., Hamilton, S. K., Dawson, G. K., Golding, S. D., and Gilcrease, P. C. Biogenic methane potential for Surat Basin, Queensland coal seams. *International Journal of Coal Geology*, 88(2):123–134, 2011.

[30] Huang, Z., Urynowicz, M. A., and Colberg, P. J. Stimulation of biogenic methane generation in coal samples following chemical treatment with potassium permanganate. *Fuel*, 111:813–819, 2013.

[31] Pfeiffer, R., Ulrich, G., and Finkelstein, M. Chemical amendments for the stimulation of biogenic gas generation in deposits of carbonaceous material. April 13 2010. US Patent 7,696,132.

[32] Volkwein, J. Method for in situ biological conversion of coal to methane. June 13 1995. US Patent 5,424,195.

[33] Scott, A. R. and Guyer, J. E. Method of generating and recovering gas from subsurface formations of coal, carbonaceous shale and organic-rich shales. February 19 2004. US Patent 20040033557.

[34] Mahaffey, W., Bradfish, J., Haveman, S., Sutton, B., and Greaser, L. Dispersion of compounds for the stimulation of biogenic gas generation in deposits of carbonaceous material. February 6 2014. US Patent 20140034297.

[35] Pfeiffer, R., Ulrich, G., Vanzin, G., Dannar, V., DeBruyn, R., and Dodson, J. Biogenic fuel gas generation in geologic hydrocarbon deposits. January 5 2010. US Patent 7,640,978.

[36] Vlachos, D., Mhadeshwar, A., and Kaisare, N. S. Hierarchical multiscale model-based design of experiments, catalysts, and reactors for fuel processing. *Computers & Chemical Engineering*, 30(10):1712–1724, 2006.

[37] Computer Modelling Group: Calgary, Alberta, Canada. *Computer Modelling Group STARS Version 2011.10 Users Guide*, 2011.

[38] Vlachos, D. G. A review of multiscale analysis: Examples from systems biology, materials engineering, and other fluid–surface interacting systems. *Advances in Chemical Engineering*, 30:1–61, 2005.

[39] Ricardez-Sandoval, L. A. Current challenges in the design and control of multiscale systems. *The Canadian Journal of Chemical Engineering*, 89(6):1324–1341, 2011.

[40] Givon, D., Kupferman, R., and Stuart, A. Extracting macroscopic dynamics: model problems and algorithms. *Nonlinearity*, 17(6):R55, 2004.

[41] Nagy, Z. and Braatz, R. Distributional uncertainty analysis using power series and polynomial chaos expansions. *Journal of Process Control*, 17(3):229–240, 2007.

Chapter 2

Kinetic modeling of the biogenic production of coalbed methane

Abstract

Biogenic production of coalbed methane under anaerobic conditions occurs through a large number of reactions involving a community of micro-organisms. A kinetic scheme for such a complicated reaction network has been proposed using lumped species reacting in a series of enzymatic reaction blocks consisting of coal solubilization, hydrolysis, acidogenesis, acetogenesis and methanogenesis. Amongst these pathways, acetoclastic methanogenesis is assumed to be dominant. Based on implications from experimental data, tryptone (a nitrogen rich nutrient used in the stimulation of methane production) is assumed to produce aromatic ring intermediates. Monod kinetics is applied to the enzymatic reactions, but methanogenesis is modeled with modified Monod kinetics to account for substrate inhibition. The kinetic model thus established can estimate the concentration of products as well as intermediate species in the conversion of coal. An analytical solution to the model is derived and its parameter sensitivity is investigated at different operating regions. Model parameters are estimated for data from various anaerobic bottle experiments by nonlinear regression using the particle swarm optimization algorithm, and the model's predictive ability has been validated for various coal samples.

2.1 Introduction

Gases stored at high densities (approximately between 0.0003 and 18.66 m^3/metric ton)[1] in the multi-porous structure of coalbeds[2] are known as coalbed methane (CBM). The gas consists of methane (80 - 99% by volume) and minor amounts of carbon dioxide, nitrogen, hydrogen sulphide, sulphur dioxide and heavier hydrocarbons such as ethane, propane and butane. In the early 19^{th} century, CBM was recognised as a major mine hazard before being commercially produced as an unconventional resource of natural gas in the 1970's. Compared to coal, CBM is a better fuel with higher calorific value and burns cleaner with lower greenhouse gas emissions, particulate emissions and other toxic emissions, while also producing no solid wastes[3]. CBM is produced by two major processes - thermogenic and biogenic. Biogenic CBM is produced by the anaerobic microbial attack of organic matter in coal and thermogenic CBM is generated by thermal cracking. Biogenic gas generation is very often triggered in coal seams that are no longer conducive to microbial activity by events such as basin uplift and cooling, flow of associated ground water, and the dilution of salinity levels[4].

Various factors are evaluated for assessing the desirability of CBM extraction in a certain coal seam. These include gas content, gas sorption capacity, permeability, reservoir pressure, and geometry and coal chemistry[5]. Conventional core/rock samples, full size wellbores and five-spot pilot production tests provide data that can be used to estimate characteristics of coal seams and their production potential. However, in the case of coalbeds with microbial activity, it is also necessary to quantify the reaction kinetics. A possibility that is currently being researched is the enhancement of the microbial processes producing biogenic CBM[6–10].

To address the rate of gas production from microbial activity, we identify a simplified reaction pathway for coal bioconversion and develop the corresponding reaction kinetic model and overall reaction rate using experimental data and existing literature on anaerobic digestion processes. The identification of reaction kinetics provides a rational basis for process analysis, control and design[11]. At smaller scales (laboratory experiments), the kinetic model can aid in the design of experiments to study optimum reaction conditions. At larger scales, simulation of a flow model coupled with the kinetic model will aid in estimating commercial gas production from coal seams on field scales while taking ongoing bioconversion into account.

2.2 Coal degradation reaction network

2.2.1 Coal and coal precursor: Lignin

CBM associated with coal deposits consists of gas molecules that are either eliminated from organic matter during compaction/transformation processes associated with coal formation or produced by microbial attack or thermal cracking of coal. Based on the source/origin, CBM is classified as primary biogenic, thermogenic and secondary biogenic gas. Primary biogenic gas begins in peat swamps[12] by aerobic microbial attack on cellulosic material leading to the formation of anaerobic conditions. As coalification progresses, the anaerobic microbial attack on cellulosic breakdown products occurs in the presence of inorganic electronic acceptors such as CO_2 and H_2 ultimately providing the substrates for methanogenesis. The degraded peat material becomes deep coal beds over geological time and generates thermogenic gas by thermal cracking. Microbial activity in these coal beds is suppressed or killed due to extreme conditions of pressure and temperature. Microbial activity may be renewed or the population re-inoculated in these layers by changes in geochemical conditions or triggering events[4,13]. The new microbial communities in these layers feed on the highly recalcitrant organic matter and continue to evolve by adapting a strategy of high biomass and low growth rate thus producing secondary biogenic gas[4]. An example of secondary biogenic gas generation is the Sydney Basin formed post the cretaceous uplift (during which a large quantity of thermogenic gases were lost)[14]. Various production data indicate that coal deposits of high rank with intense secondary biogenic gas generation have high gas content and hydrostatic pressure conditions approaching their maximum sorption capacity. Apart from gas produced in-situ by the degradation of coal/gas components, CBM beds are also saturated with allochthonous gas components that migrated from other strata.

Since coalification occurs by compaction of peat swamps through cycles of subsidence and emergence, plant organic matter spends quite some time under microbial attack. From petrographic studies[15], it has been shown that coalification does not occur as degradation followed by the re-organisation/condensation of smaller molecules to form larger ones. The preservation of parts of plant material as fossils is proof of this. Coal is formed from transformations of the resistant biopolymers (e.g., cutan, lignin, alganean) that are left behind in plant matter after the rapid elimination of cellulose by aerobic bacteria. Hence, lignin, the largest fraction amongst the biopolymer constituents, is generally considered the precursor of coal[16]. Lignin is a random, complex, irregular, heterogeneous, three dimensional (3D), varyingly branched network of cross linked phenolic (aromatic) biopolymers.

2.2.2 Anaerobic breakdown of coal: Ongoing biogenic gas generation

The biogenic CBM gas found in coal beds is the product of the anaerobic breakdown of the complex structure of coal by a microbial food chain. This is established from various anaerobic microcosm studies such as those by Ulrich et al.[13]. The anaerobic breakdown or digestion of coal is similar to the anaerobic breakdown of any complex organic matter. It is broadly classified into (1) hydrolysis/fermentation of coal macromolecules into smaller molecules (2) acidogenesis (3) acetogenesis, and (4) methanogenesis.[13,17] Since all of these reaction steps are microbial processes, the coal substrate must be solubilised in water. Thus, the coal solubilisation rate is a variable in coal degradation.

2.2.3 Solubilization

Coal is a large cross linked 3D network of macromolecules and lower molecular substances[18–20] held together by attractive forces such as pi-pi interactions, hydrogen bonds, electrostatic and electrodynamic interactions. Therefore, it is generally very insoluble in water or organic solvents at ambient temperatures and pressures. Lignin, the structure that coal preserves, also has poor solubility owing to its large molecular size, complex cross linking and aromaticity.[16] Studies on extraction indicate that solubility can be improved by increasing cooperative interactions between coal and solvents through hydrogen bonds and aromatic pi-pi interactions. Adding a base (nucleophile/electron donor) significantly affects these interactions. In the presence of a base, the solubilization mechanism is a substitution reaction of an electron-donor participating in the intermolecular forces of coal[19–21]. The complete solubilization mechanism, identifying which covalent bonds are broken by the solvent, is not known yet. Studies have also shown that solubilization can occur even at room temperature in the presence of microbes.[22–24]

Biological solubilization of coal is an area that gained interest in 1982 following a report that lignite could be degraded to recoverable liquid products by a certain fungus[22]. Since then, several works have been published[22–24] which suggest that the biocatalytic solubilization of coal can be mediated by microbes and enzymes in aqueous or other organic media; specifically, the alkaline cell metabolites produced by these microbes.[24]. Apart from requiring mild physiological conditions, coal biosolubilisation is also dependent on many other factors such as the size of coal particles, pH, the concentration of free cells and the concentration of other inorganic ions.[25]

2.2.4 Hydrolysis

Hydrolysis of complex coal macromolecules in the soluble phase produces simpler polymers or monomers. Products of hydrolysed coal have been identified in many experiments such as those by Young et al.[26]. These products are acids and alcohols that bear structural similarities to the constituents of lignin or lignin monomers such as vanillic acid, ferullic acid, cinnamic acid, benzoic acid, catechol, protocatechuic acid, phenol, p-hydroxybenzoic acid, syringic acid and syringaldehyde. This is consistent with the theory that lignin structure is preserved in coal formations.

2.2.5 Acidogenesis and acetogenesis

Hydrolysed products are then fermented into fatty acids, volatile fatty acids, ketones, alcohols and even simple one-carbon compounds such as acetate and carbon dioxide. This process is known as acidogenesis and is aided by acidogenic bacteria. Several other factors such as temperature, pH and the availability of nutrients determine favourable conditions for acidogenesis. Acetogenesis is the anaerobic breakdown of the products of acidogenesis, producing smaller acids such as acetate, formate and hydrogen and carbon dioxide. This process is aided by acetogenic bacteria. Ferry and Wolfe[17] indicate that benzoate degradation (an acidogenesis reaction) proceeds only with the continuous removal of the products acetate, formate, and hydrogen.

2.2.6 Methanogenesis

Methanogenesis is the terminal step where microbes known as methanogens produce methane by the conversion of methanogenic substrates such as acetate, formate, hydrogen and carbon dioxide. The various possible pathways of methanogenesis are acetoclastic methanogenesis, hydrogenotrophic methanogenesis, syntrophic acetate oxidation followed by hydrogenotrophic methanogenesis and acetogenesis followed by acetoclastic methanogenesis[13]. Each of these pathways employs different substrates. Numerous studies have indicated that methanogenesis may occur via different predominant mechanisms in different coal beds with varying conditions[27]. For example, laboratory and field studies by Ulrich et al.[13] on coal seams in Powder River Basin (where acetate was found to be an important intermediate) or rapid stimulation of methane production in the presence of acetate as compared to hydrogen in coal samples from an abandoned coal mine in the Ruhr basin[28] provide evidence that acetoclastic methanogenesis is the dominant pathway. However, a few other studies such as the work by Harris et al.[29], which proved that methane production from

coals in the Powder River Basin improved in the presence of H_2/CO_2 amendments, and that by Thielemann et al.[30] on methane production in samples from the Ruhr basin which were incubated in the presence of H_2 and fatty acids, show that hydrogenotrophic methanogenesis is the dominant pathway. It would appear that the dominant methanogenetic pathways may differ from basin to basin and within a basin itself, and the relation between carbon isotopes of methane and carbon dioxide that has been used to infer methanogenetic pathways may more accurately describe the extent of methanogenesis[31].

A very significant factor affecting the dominant methanogenesis pathway is temperature. Investigation of the effect of temperature on methanogenesis[32] has shown that in a psychrophilic community (enriched at about 5°C), 95% of the methane originated from acetate, whereas for a thermophilic community (50°C), 98% of the methane was formed from bicarbonate. A mesophilic community (at 30°C) exhibited both pathways, but about 80% methane was produced using acetate as precursor. Also, it is observed that in young organic systems, acetoclastic methanogenesis is the dominant pathway while carbon dioxide reduction is predominant in older systems. Methanogenesis is usually inhibited at low pH values (< 6)[33,34].

2.3 Kinetic model development

2.3.1 Experimental methods

Coal bioconversion experiments were conducted using accepted standard anaerobic culturing techniques[35]. Two different methanogenic enrichment cultures, T-1610 and QSAF, which had been enriched from coal cuttings obtained from drilling operations in two different coal formations in the Western Canadian Sedimentary Basin, Alberta[6], were used. Different batch experiments were conducted in the presence of these two enrichment cultures in bottles containing mineral salts medium (MSM)[36] amended with tryptone (nutrient). Tryptone is a nitrogen-rich, protein-based nutrient proven to be effective in stimulating biogenic methane production[6]. The coal used was the same source coal used in the original enrichments. The cultures were incubated stationary at 30°C in the dark. The initial headspace was 100% N_2 and the subsequent gas production was measured by gas chromatography[35]. Replicate samples of each culture were periodically sacrificed in order to collect the culture fluid for volatile fatty acid analyses (Extractable Priority Pollutants in Water Method, Alberta Innovates - Technology Futures Method 2054M-EC 3/11 version 9.1).

A kinetic model for biogenic methane production from coal is presented in the fol-

lowing sub-sections.

2.3.2 Simplified reaction pathway

Coal degradation occurs through a complicated reaction network involving many different species (summarized by Jones et al.[37]) It is impractical to build a kinetic model by evaluating all the elementary reaction steps. Parameter estimation for such a model would also be unworkable, given the minimal availability of data on the intermediates. A reasonable kinetic model can be built by lumping intermediates belonging to the major steps involved in coal degradation. We consider these to be solubilization, hydrolysis, acidogenesis, acetogenesis and methanogenesis. Solubilization/hydrolysis and methanogenesis are known to be the slowest steps. The reactants for acidogenesis (lignin and lignin-like monomers) and acetogenesis (benzoate-like components) are found at significant concentration in many experimental studies conducted on coal degradation and in formation waters[13,38–42]. Components belonging to each of the reaction classes - hydrolysis, acidogenesis and acetogenesis, are lumped and represented with a compound or marker that is the most common structure involved in the process. This marker is used to represent the aggregate kinetic characteristics of the components involved. This is similar to the method of lumping (grouping) for kinetic modeling that is employed in complex chemical reaction systems[43,44]. The various assumptions in our kinetic model are:

1. Each reaction step (i) is carried out by one class of microbes X_i and its corresponding enzyme E_i.

2. The carbon source is considered to be the only limiting nutrient for all the microbes. The nitrogen source (tryptone) is assumed to be in excess and does not appear explicitly in the model.

3. The product of solubilization is solubilized coal and is considered to have the same molar mass as coal.

4. The product of hydrolysis/fermentation is fragmented coal. This represents smaller fragments of the coal macromolecule which are compositionally similar to lignin and lignin-like monomers. Therefore, we choose the representative compound to be syringic acid, a common lignin monomer.

5. The products of acidogenesis are putative aromatic ring intermediates which are lumped and represented by benzoate/benzoic acid, since benzoate is a dominant intermediate in coal formation waters[13,27,42].

6. Short chain acids, which are the products of acetogenesis, are lumped and represented by acetate/acetic acid, since they are among the most common intermediates found in coal formation waters[13,37,45,46].

7. The main products of methanogenesis are methane, carbon dioxide and hydrogen. Acetoclastic methanogenesis is assumed to be the major pathway, since H_2 and CO_2 feeding hydrogenotrophic methanogens usually favor high temperatures and are found in deeper layers of sediments[47], while acetoclastic methangens favour low/moderate temperatures and are found in relatively young systems, which is the case with the anaerobic microcosm systems under study. Thus, acetate is the substrate for methanogenesis.

8. A negative effect on rate of methanogenesis has been observed with increasing acetate concentration in many studies[47–52]. Further, acetate is usually found in low concentrations in formation waters of coal seams with ongoing gas generation [13,42,46]. This implies inhibition to acetoclastic methanogenesis from its substrate (acetate). Lokshina et al.[50] have implemented this effect in the kinetic rate expression for methanogenesis, using Haldane models (which are modified Monod models accounting for substrate inhibition) and have proved that these explain experimental data better than Monod kinetics.

9. Among the products of methanogenesis, only methane is modeled quantitatively.

10. To account for the initial inoculation period, a delay that is estimated from the experimental data is introduced into the kinetic model.

2.3.3 Stoichiometry

Coal is very heterogeneous and does not have a constant composition; however, proximate and ultimate analysis can provide an estimate of its stoichiometry[53]. Using Buswell's equation for methane fermentation by bacteria[54], $C_nH_aO_b + (n - \frac{a}{4} - \frac{b}{2})\ H_20 \rightarrow (\frac{n}{2} - \frac{a}{8} + \frac{b}{4})\ CO_2 + (\frac{n}{2} + \frac{a}{8} - \frac{b}{4})\ CH_4$, and extrapolation of the methanogenesis rate from Strapoc et al.[46], we obtain an approximate molecular formula for sub-bituminous coal as $C_{100}H_{100}O_9$ (sub-bituminous coal is commonly associated with CBM). The rest of the dominant reaction intermediates are fragmented coal (syringic acid, $C_{10}H_{10}O_5$), benzoate/benzoic acid ($C_7H_6O_2$), acetate/acetic acid (CH_3COOH) and the products CH_4, CO_2 and H_2. Therefore, the stoichiometry for the lumped

reaction system is

$$
\begin{aligned}
C_{100}H_{100}O_9 + 41H_2O &\rightarrow 10C_{10}H_{10}O_5 + 41H_2 \\
C_{10}H_{10}O_5 + 3H_2O &\rightarrow C_7H_6O_2 + 5H_2 + 3CO_2 \\
C_7H_6O_2 + 6H_2O &\rightarrow 3CH_3COOH + 3H_2 + CO_2 \\
CH_3COOH &\rightarrow CH_4 + CO_2
\end{aligned}
$$

In cases where other dominant methanogenic pathways are present, the stoichiometry and kinetic model can be modified appropriately.

2.3.4 Model

In this section, reaction kinetics are modeled for the lumped reaction system: coal → solubilized coal → fragmented coal → benzoate → acetate → products. The concentrations of coal, solubilised coal, fragmented coal, benzoate, acetate and products are represented by C, S, W, B, A and P, respectively.

Crushed coal particles in water first undergo solubilization. Let the initial mass of coal be m_0 and its density be ρ_0. The particles are assumed to be uniformly spherical with initial radius r_0. The rate of solubilization of coal is modeled according to the dissolution rate law of Noyes and Whitney based on diffusion layer model/film theory[55]. The model assumes that

- There exists an interface between the solid and liquid phases.
- Equilibrium exists at the interface, i.e., the rate of transfer to the interface is set equal to the rate of transfer from the interface. The resistance to mass transfer is a combination of resistances in both phases.
- The concentration in the bulk liquid phase is constant throughout the volume.

The solubilization rate is given by

$$
R = -\frac{1}{X_1}\frac{dC}{dt} = K_1 A(S^* - S) = K_1 \frac{3m_0}{r_0\rho} f_b \left(\frac{C}{C_0}\right)^{2/3} (S^* - S) \tag{2.1}
$$

where K_1 is the overall mass transfer coefficient, S^* is the equilibrium solubility of coal, C_0 is the initial concentration of coal, A is the cross-sectional area of coal particles in contact with water, f_b is the fraction of the surface area covered by microbes and X_1 is the concentration of microbes involved in solubilization.

The rest of the enzymatic reactions, each assumed to be a single-substrate limited microbial process, are modeled by the empirical Monod equation for a substrate, Q. The Monod equation generates a sigmoidal curve for the growth rate. At high substrate concentrations, the growth rate is constant, while at low concentrations, the growth rate is first order.

$$\mu = \frac{\mu_{max} Q}{K + Q}; \quad q = \frac{q_{max} Q}{K + Q} \tag{2.2}$$

$$\tag{2.3}$$

where $\mu = \frac{1}{X}\frac{dX}{dt}$ is the specific growth rate of microbes and $q = \frac{1}{X}\frac{dQ}{dt}$ is the substrate utilization/removal rate. μ_{max} and q_{max} are the maximum growth rates and K is the substrate concentration at half the maximum growth rate. To account for inhibition to methanogenesis at high acetate concentrations, the Monod model is modified as[50]

$$q = \frac{q_{max} Q}{K + Q + \frac{Q^2}{I}} \text{ where } I \text{ is the inhibition constant.} \tag{2.4}$$

By considering bacterial density to be high relative to substrate concentrations, the kinetic equations are considered for the case of no-growth kinetics, i.e, the organism concentration is assumed to remain essentially constant even as the substrate is degraded[56,57]. In other words, the Michaelis-Menten kinetic model is applied. Based on the derived stoichiometry, the overall model describing the chain of enzymatic reactions using a series of Monod models is

$$\frac{dC}{dt} = -K_1 X_1 \frac{3m_0}{r_0 \rho} f_b \left(\frac{C}{C_0}\right)^{2/3} (S^* - S) \tag{2.5a}$$

$$\frac{dS}{dt} = K_1 X_1 \frac{3m_0}{r_0 \rho} f_b \left(\frac{C}{C_0}\right)^{2/3} (S^* - S) - \frac{k_2 X_2 S}{K_2 + S} \tag{2.5b}$$

$$\frac{dW}{dt} = 10\frac{k_2 X_2 S}{K_2 + S} - \frac{k_3 X_3 W}{K_3 + W} \tag{2.5c}$$

$$\frac{dB}{dt} = \frac{k_3 X_3 W}{K_3 + W} - \frac{k_4 X_4 B}{K_4 + B} \tag{2.5d}$$

$$\frac{dA}{dt} = 3\frac{k_4 X_4 B}{K_4 + B} - \frac{k_5 X_5 A}{K_5 + A + A^2/K_5'} \tag{2.5e}$$

$$\frac{dP}{dt} = \frac{k_5 X_5 A}{K_5 + A + A^2/K_5'} \tag{2.5f}$$

Figure 2.1 shows results of GC-MS analysis on samples from the anaerobic serum bottle study conducted with QSAF enrichment culture in the presence of coal and a mineral salts medium (MSM) amended with tryptone. As is seen, benzeneacetic acid is a common intermediate at all times (even at $t = 0$). Short chain acids such as

pentanoic acid and butanoic acid, which would be lumped into acetate due to similar kinetic characteristics, are also present at $t = 0$. Lumped acetate and benzoate concentrations from GC/MS analysis on samples from the anaerobic serum bottle study conducted with T-1610 enrichment culture and a mineral salts medium amended with tryptone with/without coal are seen in Figure 2.2a. These results also indicate that a benzoate and an acetate pool were present at $t = 0$ even when coal was absent. Also, results of GC/MS analysis on an uninoculated tryptone medium are shown in Figure 2.2b[58].

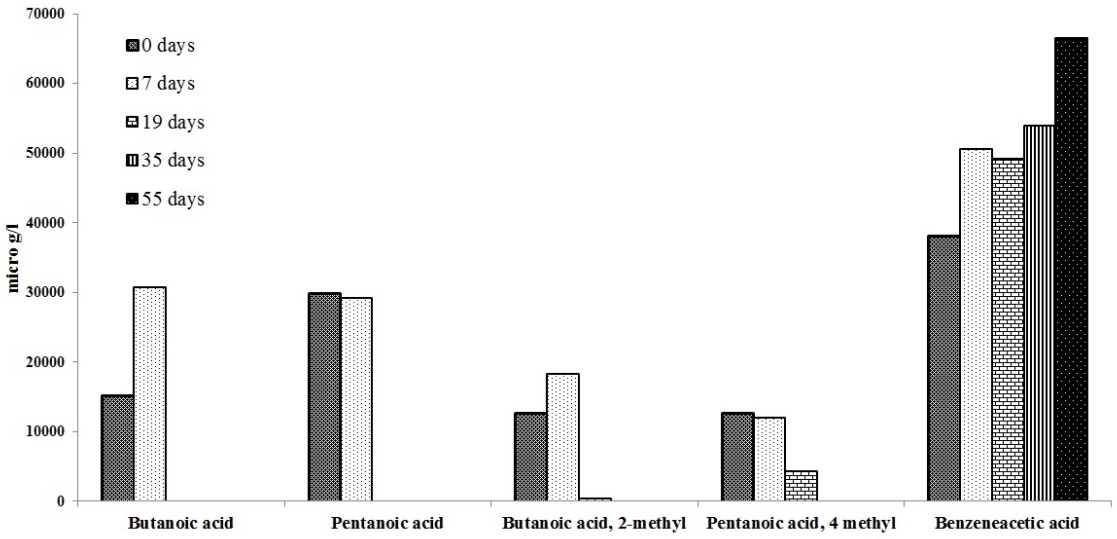

Figure 2.1: *GC-MS analysis on samples of an anaerobic serum bottle study conducted with QSAF enrichment culture in the presence of coal and MSM amended with tryptone.*

These observations lead us to believe that a benzoate pool becomes available from tryptone and this, on undergoing acetogenesis, produces acetate. To account for this, we modify the rate of change of benzoate concentration in the model as

$$\frac{dB}{dt} = \frac{k_3 X_3 W}{K_3 + W} + \nu - \frac{k_4 X_4 B}{K_4 + B} \tag{2.6}$$

where ν is the zero-order rate of benzoate generation from tryptone, which is assumed to be present in excess.

To simplify the model, the Monod expressions are reduced to first order rate expressions by assuming low substrate concentrations (since the coal solubilization rate is very low). However, substrate inhibition is preserved in methanogenesis to account for acetate inhibition. At high methanogenesis rates where the acetate concentration is quite low, there is no difference in the Monod and first order rates. However, at low

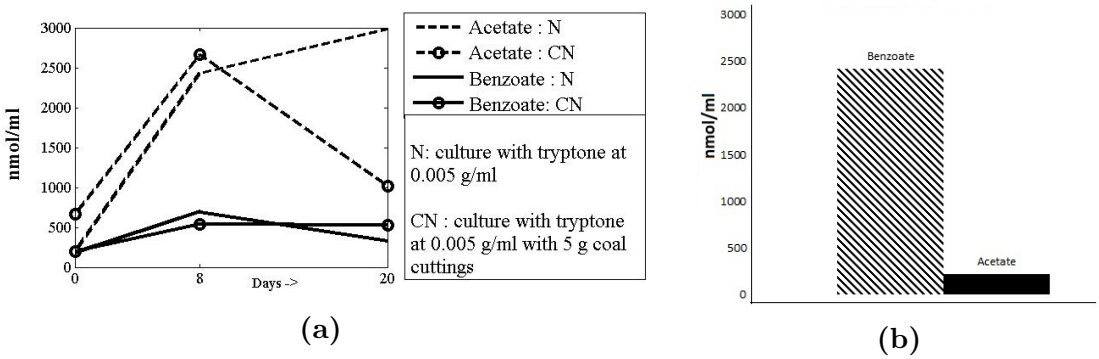

Figure 2.2: *Results of GC/MS analysis (a) From analysis on samples from experiments conducted with/without coal in the presence of tryptone (b) From analysis on uninoculated tryptone medium.*[58]

methanogenesis rates, acetate accumulation and consequently the cut-off of product generation is manifested only with the modified Monod model with the substrate-inhibition component. The reduced model is

$$\frac{dC}{dt} = -a([S^*] - [S])(\frac{C}{C_0})^{2/3} \tag{2.7a}$$

$$\frac{dS}{dt} = a([S^*] - [S])(\frac{C}{C_0})^{2/3} - b[S] \tag{2.7b}$$

$$\frac{dW}{dt} = 10b[S] - r[W] \tag{2.7c}$$

$$\frac{dB}{dt} = r[W] + \nu - d[B] \tag{2.7d}$$

$$\frac{dA}{dt} = 3d[B] - \frac{e[A]}{f + [A] + \frac{[A]^2}{g}} \tag{2.7e}$$

$$\frac{dP}{dt} = \frac{e[A]}{f + [A] + \frac{[A]^2}{g}} \tag{2.7f}$$

$$\text{where } a = K_1\frac{3m_0}{r_0\rho}f_b; b = \frac{k_2X_2}{K_2}; r = \frac{k_3X_3}{K_3}; d = \frac{k_4X_4}{K_4}; e = k_5X_5; f = K_5; g = K_5' \tag{2.7g}$$

2.4 Analytical solution

It is difficult to obtain analytical solutions for the model described above. However, by making the assumption that solubilisation is the slowest step ($\frac{dC}{dt} \approx 0$), the equa-

tions can be solved using Laplace transforms. The analytical solutions are found in Equation 2.8. For $b \neq r \neq d \neq \frac{e}{f}$,

$$S(t) = S_0 e^{-bt} \tag{2.8a}$$

$$W(t) = W_0 e^{-rt} + \frac{10bS_0}{(b-r)}(e^{-rt} - e^{-bt}) \tag{2.8b}$$

$$B(t) = B_0 e^{-dt} + \int_t \nu e^{-dt} dt + \frac{rW_0}{(r-d)}(e^{-dt} - e^{-rt}) + \frac{10brS_0}{b-r}\left(\frac{e^{-dt} - e^{-rt}}{(r-d)} - \frac{e^{-dt} - e^{-bt}}{(b-d)}\right) \tag{2.8c}$$

when A(t) is low;

$$A(t) = A_0 e^{-\frac{e}{f}t} + \frac{3dB_0}{d-\frac{e}{f}}(e^{-\frac{e}{f}t} - e^{-dt}) + \frac{3drW_0}{(r-d)}\left(\frac{e^{\frac{-e}{f}t} - e^{-dt}}{d-\frac{e}{f}}\frac{e^{\frac{-e}{f}t} - e^{-rt}}{r-\frac{e}{f}}\right) + \tag{2.8d}$$

$$\frac{30dbrS_0}{(b-r)}\left(\frac{e^{\frac{-e}{f}t} - e^{-dt}}{(d-\frac{e}{f})(r-d)} - \frac{e^{\frac{-e}{f}t} - e^{-dt}}{(d-\frac{e}{f})(b-d)} - \frac{e^{\frac{-e}{f}t} - e^{-rt}}{(r-\frac{e}{f})(r-d)} + \frac{e^{\frac{-e}{f}t} - e^{-bt}}{(b-\frac{e}{f})(b-d)}\right) \tag{2.8e}$$

and $P(t) = P_0 + \frac{e}{f}\int_t A(t)dt$

when A(t) is high; $A(t) = A_0 + 3d\int_t B(t)dt$; and $\frac{dP}{dt} = 0$ (2.8f)

where S_0, W_0, B_0, A_0 and P_0 are the initial concentrations of solubilised coal, fragmented coal, benzoate, acetate and product. Concentration profiles of coal, intermediates and products in the presence of low and high acetate concentrations were computed using the analytical solution. The results are seen in Figure 2.3. As is seen in Figure 2.3a, product generation continues as acetate decreases as compared to Figure 2.3b, where product generation is inhibited due to high acetate concentration.

2.5 Parametric sensitivity analysis

We use sensitivity analysis to reduce the number of parameters to be estimated. Since we are interested in the concentrations of produced methane, normalized sensitivity coefficients are evaluated for methane with respect to various model parameters.

$$NSC = \frac{(P - P_0)/P_0}{(p - p_0)/p_0}$$

where p and P are the parameter and the corresponding output, and p_0 and P_0 represent nominal values, respectively. The sensitivity analysis is based on the numerical

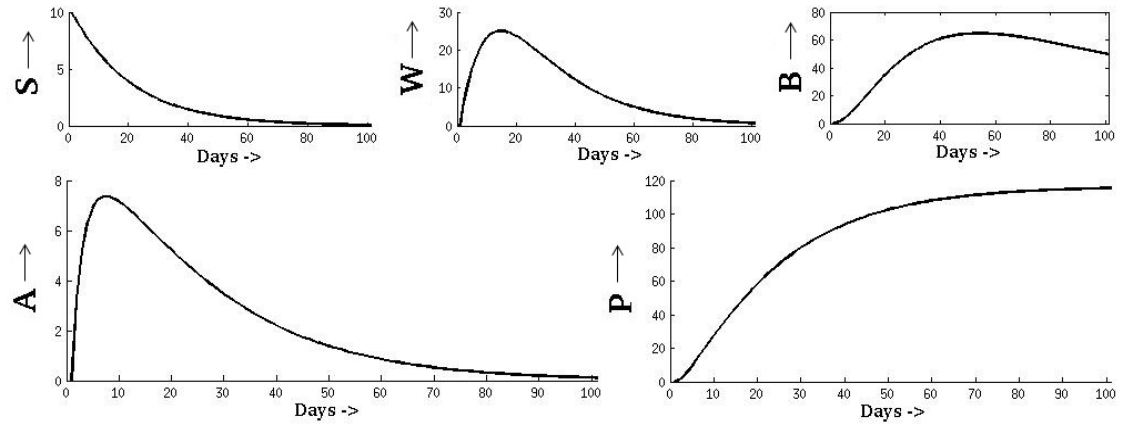

Figure 2.3: *Profiles of intermediate products using the analytical solution from Equation 2.8. S, W, B, A and P denote concentrations of solubilized coal, fragmented coal, benzoate, acetate and products in μmol/ml, respectively. (a) Low acetate concentration with methane production (b) High acetate concentration inhibiting methane production.*

solution of the model in Equation 2.7 for two different sets of nominal parameter values. Nominal set 1 is [$a = 0.025$, $S^* = 75$, $b = 5$, $r = 5$, $d = 2$, $e = 1$, $f = 1$, $g = 0.1$] and nominal set 2 is [$a = 0.001$, $S^* = 10$, $b = 10$, $r = 5$, $d = 1$, $e = 0.04$, $f = 1$, $g = 1$]; ν was chosen to be 0.01 in both the cases. Set 1 operates in a region of high acetate and low product concentration, while set 2 operates in a region of low acetate and high product concentration.

Normalized sensitivity analysis reveals that a, S^* and e are the most sensitive parameters. Apart from this, f is sensitive in regions of low acetate concentrations and g

is sensitive in regions of high acetate concentrations (when its nominal value is not large). a, S^* and e, f, g together control solubilization and methanogenesis, respectively. b, r and d are not very sensitive parameters and ν is not a sensitive parameter at large times. In spite of this, we include b, r, d and ν in the estimation to ensure accurate prediction of product concentrations.

2.6 Parameter estimation

Having identified the most sensitive parameters, we use particle swarm optimization (PSO) to solve the nonlinear regression problem to estimate these parameters. PSO is a population-sample based optimization algorithm inspired by social behaviour in animals such as bird flocking, fish schooling and bees swarming[59]. In this method, randomly generated particles (parameter sets) are allowed to move around the solution space with velocities determined by the algorithm so that they move towards a global optimal solution[60]. The various experimental data sets employed were:

1. *Enrichment studies using only coal as carbon substrate conducted by Harris et al.[29]. Two low rank (lignite A) coal samples were obtained from separate coal seams at different depths (referred to as Alaska deep and Alaska shallow) in a single borehole in Fort Yukon, Alaska, USA. The experiments were conducted with 8 g of crushed coal transferred to 10 ml of inorganic medium (which is a solution of trace metals, minerals and 40mM bicarbonate).*

   The rate of methane production was higher in Alaska shallow coals (obtained at a depth of 381 m) compared to Alaska deep coals (obtained at a depth of 582 m). Harris et al. also observed that high acetate concentration amendments to enrichment cultures do not support substantive methane production, indicating that acetoclastic methanogenesis may not occur. However, in the absence of H_2 and CO_2 measurements, this cannot be verified and the low activity could also be attributed to inhibition at high acetate concentrations. Based on this assumption, the kinetic model derived with acetoclastic methanogenesis as the dominant pathway was still applied to the data set and a good fit was observed. ν is set as zero as there is no addition of nitrogen-rich nutrient (tryptone).

2. *Methane production data from degradation experiments conducted by us with two different enrichment cultures, T-1610 and QSAF, on 5 g coal cuttings, with other conditions such as bottle volume and tryptone concentration being kept constant in both cases.*

Table 2.1 shows the estimated model parameters, while Figure 2.4 shows the comparison of model predictions against experimental data for the cases mentioned above. Parameters b, r and d were kept constant as they have very low sensitivity values. Parameter g is more sensitive in the case of studies conducted by Harris et al.[29] due to inhibition from acetate.

3. *A series of anaerobic serum bottle studies conducted with different quantities of coal (at constant volume) and with a constant coal ratio (while varying the quantity of coal and bottle volume), both in the presence and absence of tryptone.*

Tables 2.2 and 2.3 show the estimated model parameters, while Figures 2.5 to 2.8 show the comparison of model predictions against experimental data for data set 3. As is seen, $K_1 f_b$, S^* and e are generally higher for the case with tryptone as compared to that without tryptone. For the experiments conducted in the absence of tryptone, it is seen that $K_1 f_b$ decreases when the quantity of coal increases. This could indicate the effect of crowding of coal particles in solution. It does not affect the experiments conducted in the presence of tryptone significantly, since a benzoate pool is already available. Since the role of ν diminishes with increasing time, it is kept constant in our model in all of the cases.

The developed model can be applied for quantification of methane and other gases, as well as other intermediates in the coal bio-degradation network. It can then be used to optimize the recovery of other value-added products also using the intermediates that are produced (such as aromatic compounds, which are lumped as benzoate in our model, and short chain acids, which are lumped as acetate in our model, and so on). Figure 2.9 shows intermediate profiles in anaerobic experiments conducted at constant volume and coal ratio, predicted up to a year of production. It is seen that intermediate concentrations are higher when the nutrient (tryptone) is available. Acetate concentrations are highest and continue to increase as compared to other intermdiates. The constant increase is due to inhibition of methane production by acetate.

We present a simple example to illustrate the use of the model in optimization studies at different scales. Let us consider a continuous stirred tank reactor (CSTR) with anaerobic coal bioconversion. To improve product generation by removing acetate, water (amended with tryptone) can be continuously injected into the CSTR. Figure 2.10 shows product profiles at different flow rates ($F = 0, 0.04, 5$ ml/day) and it can be seen that with an increase in the flow rate, there is almost a 10-fold improvement in product generation along with acetate recovery in the outlet stream.

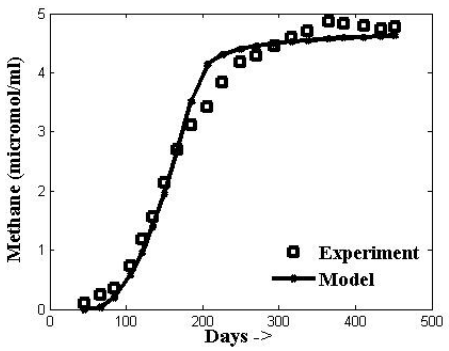

(a) *Alaska deep.*[29]

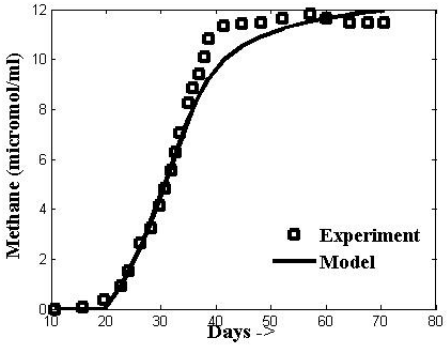

(b) *Alaska shallow.*[29]

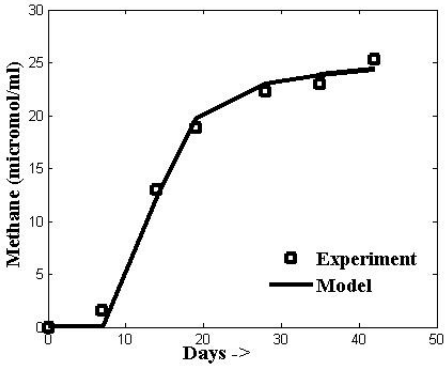

(c) *T-1610*

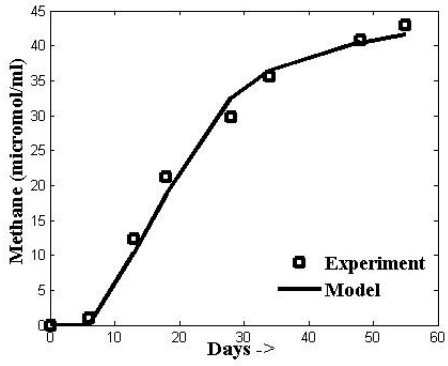

(d) *QSAF*

Figure 2.4: *Comparison of model predictions against methane production data. (a) Alaska coal (deep), (b) Alaska coal (shallow), (c) T-1610 enrichment culture, and (d) QSAF enrichment culture. Data sets for (a) and (b) were obtained from Harris et al.*[29]*. Data sets for (c) and (d) were obtained from experiments conducted by us.*

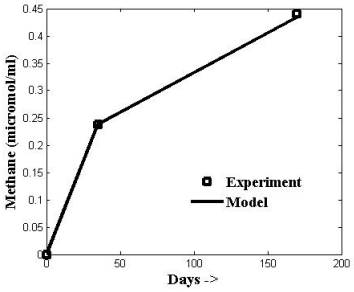

(a) *Methane production for* $m_0 = 0.1g$.

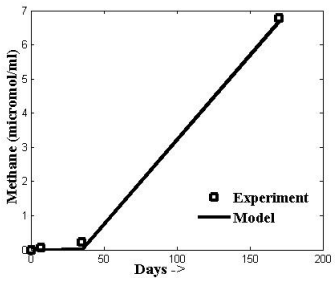

(b) *Methane production for* $m_0 = 0.5g$.

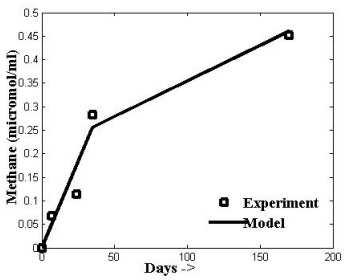

(c) *Methane production for* $m_0 = 1g$.

Figure 2.5: *Regression of kinetic model against data from experiments conducted without tryptone at constant volume for different quantities of coal.*

Table 2.1: *Estimated model parameters based on anaerobic studies conducted with enrichment cultures T-1610 and QSAF, and anaerobic studies conducted by Harris et al.*[29].

Parameter	unit	Alaska shallow	Alaska deep	T1610	QSAF
a	day^{-1}	0.0005	0.0001	0.00155	0.0175
S^*	$\frac{\mu mol}{ml}$	56	43	38.67	3.4
b	day^{-1}	10	10	5	5
r	day^{-1}	10	10	5	5
d	day^{-1}	10	10	5	5
e	$\frac{\mu mol}{ml \text{ day}}$	10	1	24.2	61.22
f	$\frac{\mu mol}{ml}$	4.66	1	4	30
g	$\frac{\mu mol}{ml}$	0.15	0.01	0.1	0.1
ν	$\frac{\mu mol}{ml \text{ day}}$	0	0	0.01	0.01

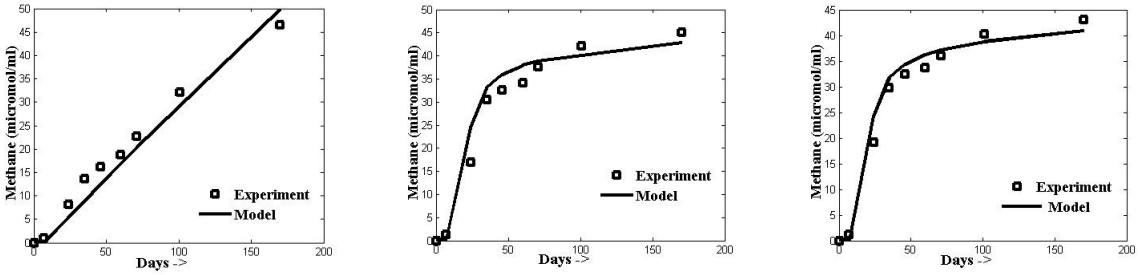

(a) *Methane production for* $m_0 = 0.1g$.

(b) *Methane production for* $m_0 = 0.5g$.

(c) *Methane production for* $m_0 = 1g$.

Figure 2.6: *Regression of kinetic model against data from experiments conducted with tryptone at constant volume for different quantities of coal.*

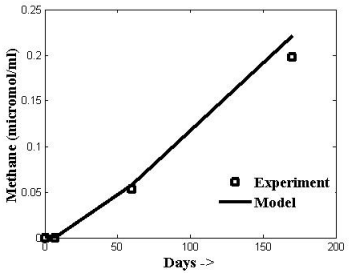

(a) *Methane production at* $V = 2ml$.

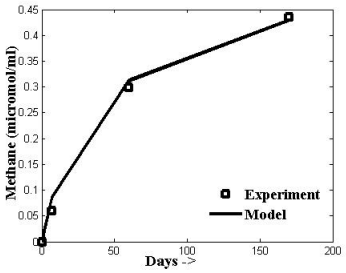

(b) *Methane production for* $V = 10ml$.

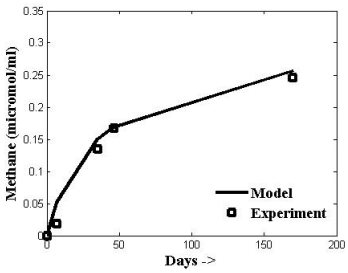

(c) *Methane production for* $V = 20ml$.

Figure 2.7: *Regression of kinetic model against data from experiments conducted without tryptone at a constant coal ratio (even though the quantity of coal and the volume were varied).*

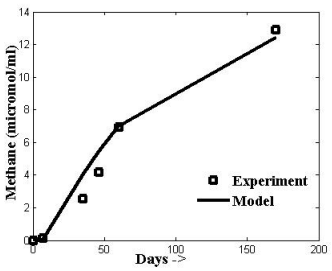

(a) *Methane production at* $V = 2ml$.

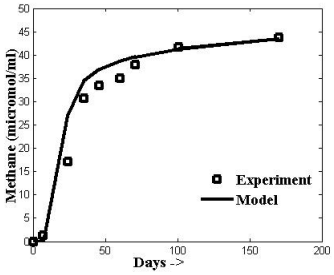

(b) *Methane production for* $V = 10ml$.

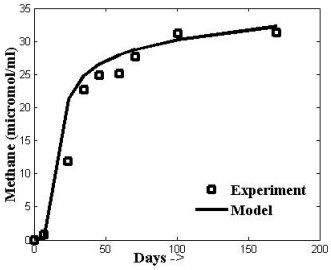

(c) *Methane production for* $V = 20ml$.

Figure 2.8: *Regression of kinetic model against data from experiments conducted with tryptone at a constant coal ratio (even though the quantity of coal and the volume were varied).*

This strategy (and other similar approaches) can be mimicked in laboratory scale and coreflooding experiments and also be extended to methane production at field scales through optimally placed and operated injection wells.

To adapt the kinetic model for different coals, the following considerations exist: stoichiometric ratios will vary with the rank of coal, nutrient limitations may need to be taken into account, and the dominant methanogenic pathway may change based on the operating conditions. However, all of these can be captured in the same modeling framework.

The reaction kinetic model, in conjunction with a fluid transport/storage model, can be adapted for reservoir simulation of CBM production with ongoing bioconversion at the field scale. The effect of varying injection systems, producing well configurations

Table 2.2: *Estimated model parameters based on anaerobic serum studies conducted at constant volume and differing quantities of coal. N_0 ml/ml is the tryptone concentration, m_0 g is the mass of coal, V ml is the volume of the bottle, and C_0 μmol/ml is the initial concentration of coal. Units of model parameters are identical to those defined in Table 2.1.*

$\mathbf{N_0}$	$\mathbf{m_0}$	**V**	$[\mathbf{C_0}]$	**a**	$\frac{\mathbf{3m_0}}{\rho \mathbf{r_0}}$	$\mathbf{K_1 f_b}$	$\mathbf{S^*}$	**b**	**r**	**d**	**e**	**f**	**g**	ν
Without tryptone														
0	0.1	10	6.9	0.001	10.55	9e-5	10	10	5	1	0.04	1	1	0
0	0.5	10	34.77	0.005	52.75	9e-5	10	10	5	1	4.15	1	1	0
0	1	10	69.44	0.001	105.45	9e-6	10	10	5	1	0.043	1	1	0
With tryptone														
0.1	0.1	10	6.9	0.001	10.55	9e-5	10	10	5	1	1	1	1	0.01
0.1	0.5	10	34.77	0.005	52.75	9e-5	10	10	5	1	4.44	1	1	0.01
0.1	1	10	69.44	0.005	105.45	4.5e-5	10	10	5	1	4.455	1	1	0.01

and nutrient loadings can be predicted and optimized for such cases. Along with core-holder studies, this forms the basis of our future work.

Table 2.3: *Estimated model parameters based on anaerobic serum studies conducted at a constant coal ratio (even though the quantity of coal and the volume were varied). N_0 ml/ml is the tryptone concentration, m_0 g is the mass of coal, V ml is the volume of the bottle, and C_0 μmol/ml is the initial concentration of coal. Units of model parameters are identical to those defined in Table 2.1.*

$\mathbf{N_0}$	$\mathbf{m_0}$	**V**	$[\mathbf{C_0}]$	**a**	$\frac{\mathbf{3m_0}}{\rho \mathbf{r_0}}$	$\mathbf{K_1 f_b}$	$\mathbf{S^*}$	**b**	**r**	**d**	**e**	**f**	**g**	ν
Without tryptone														
0	0.1	2	34.7	0.0001	10.55	9.5e-6	10	10	5	1	0.005	1	1	0
0	0.5	10	34.7	0.001	52.75	1.9e-5	15	10	5	1	0.05	1	1	0
0	1	20	34.7	0.001	105.45	9.5e-6	15	10	5	1	0.03	1	1	0
With tryptone														
0.1	0.1	2	34.7	0.0005	10.55	4.7e-5	10	10	5	1	0.44	1	1	0.01
0.1	0.5	10	34.7	0.005	52.75	9.5e-5	10	10	5	1	4.44	1	1	0.01
0.1	1	20	34.7	0.005	105.45	4.75e-5	10	10	5	1	4.36	1	1	0.01

2.7 Conclusions

By considering the major reaction classes in coal bioconversion, i.e., solubilization, hydrolysis, acidogenesis, acetogeneis and methanogenesis; and taking into account information on dominant intermediates, we have simplified the reaction pathway to a series of enzymatic reactions using lumped species, with acetoclastic methanogenesis being assumed to be the dominant methanogenic pathway in the microcosm studies considered in this work. The rate of coal solubilisation was described by a diffusion layer model; hydrolysis, acidogenesis and acetogenesis were based on Monod kinetics (reduced to first order rates for low substrate concentrations), and the methanogenesis rate was modeled with modified Monod kinetics to account for substrate inhibition from acetate. Anaerobic serum bottle culture experiments conducted with and without tryptone, a nutrient, revealed that the addition of tryptone produces a pool of benzoate.

A kinetic model was developed using the these observations and assumptions, and was validated against experimental coal bioconversion data for many different coal samples, both with and without nutrient addition. The estimates of the parameters of the model were consistent with the assumption that the addition of the nutrient, tryptone, led to the production of a pool of benzoate. Additionally, the parameters

controlling solubilization and methanogenesis were found to be the most sensitive parameters that affected the methane production predicted by the model. The kinetic model was also used to infer the concentrations of intermediate products in the bioconversion of coal and to devise optimal operating strategies for maximizing the production of methane and/or intermediate products. Our future work focuses on the use of the kinetic model in conjunction with fluid transport and storage models to predict the performance of enhanced biogenic methane production in the presence of nutrient amendments and/or varying production cycles[8] at reservoir and field scales.

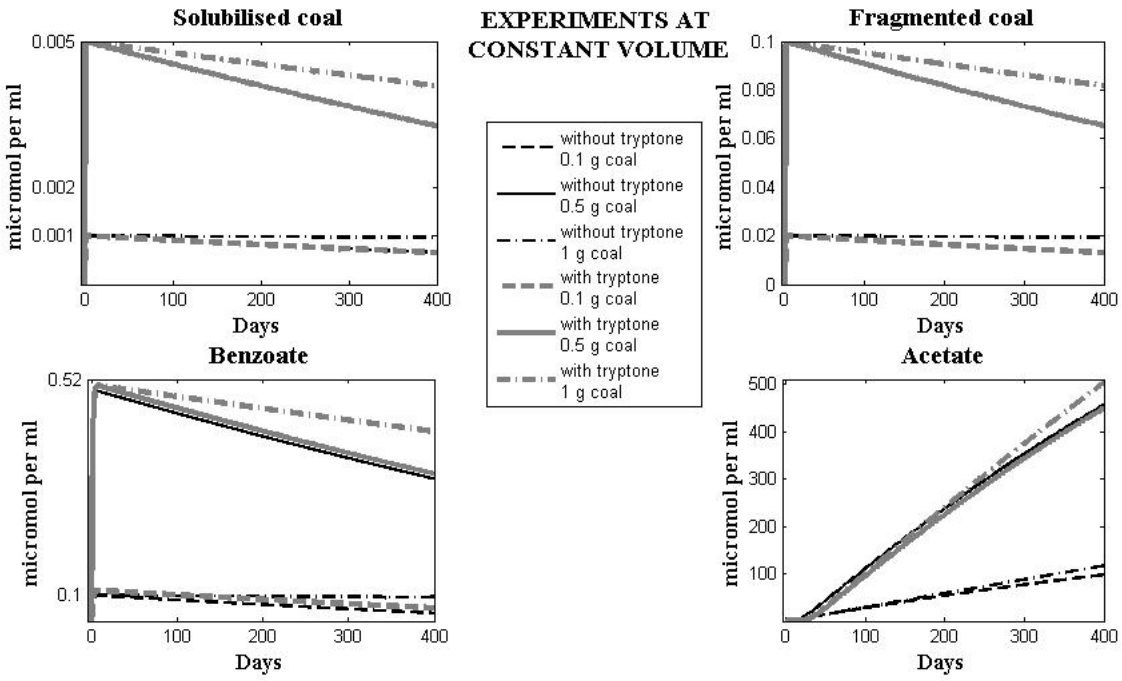

(a) *Intermediate profiles for anaerobic bottle experiments at constant volume.*

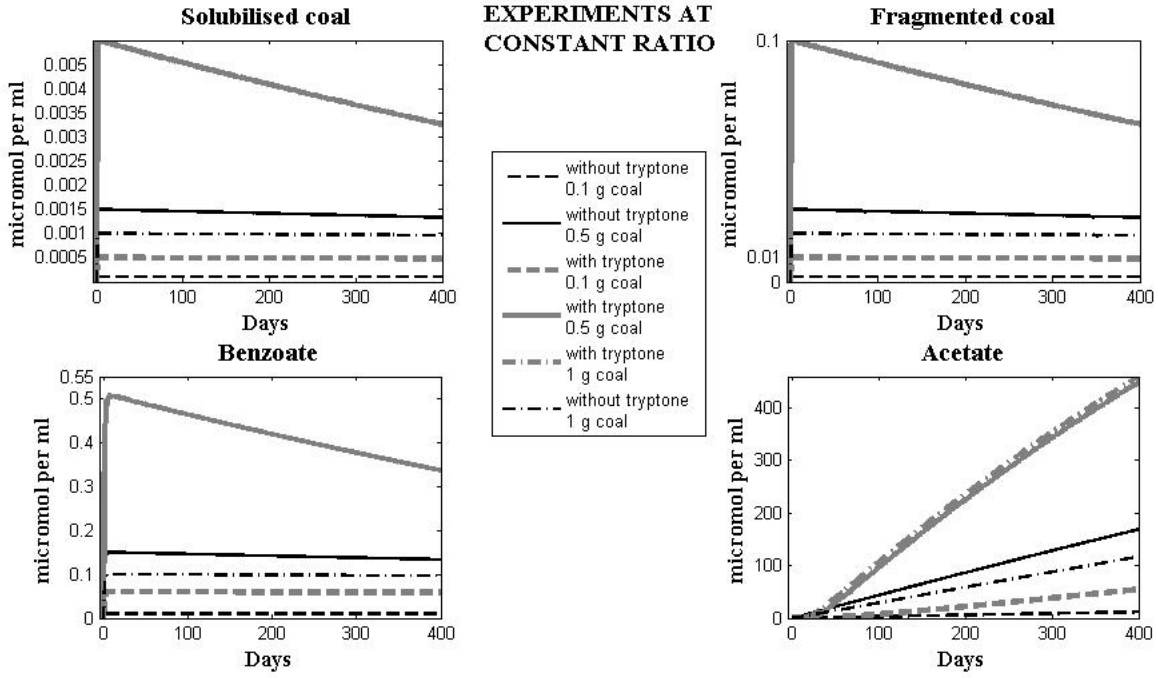

(b) *Intermediate profiles for anaerobic bottle experiments at constant coal ratio.*

Figure 2.9: *Profiles of intermediate products for anaerobic experiments at constant volume and coal ratio.*

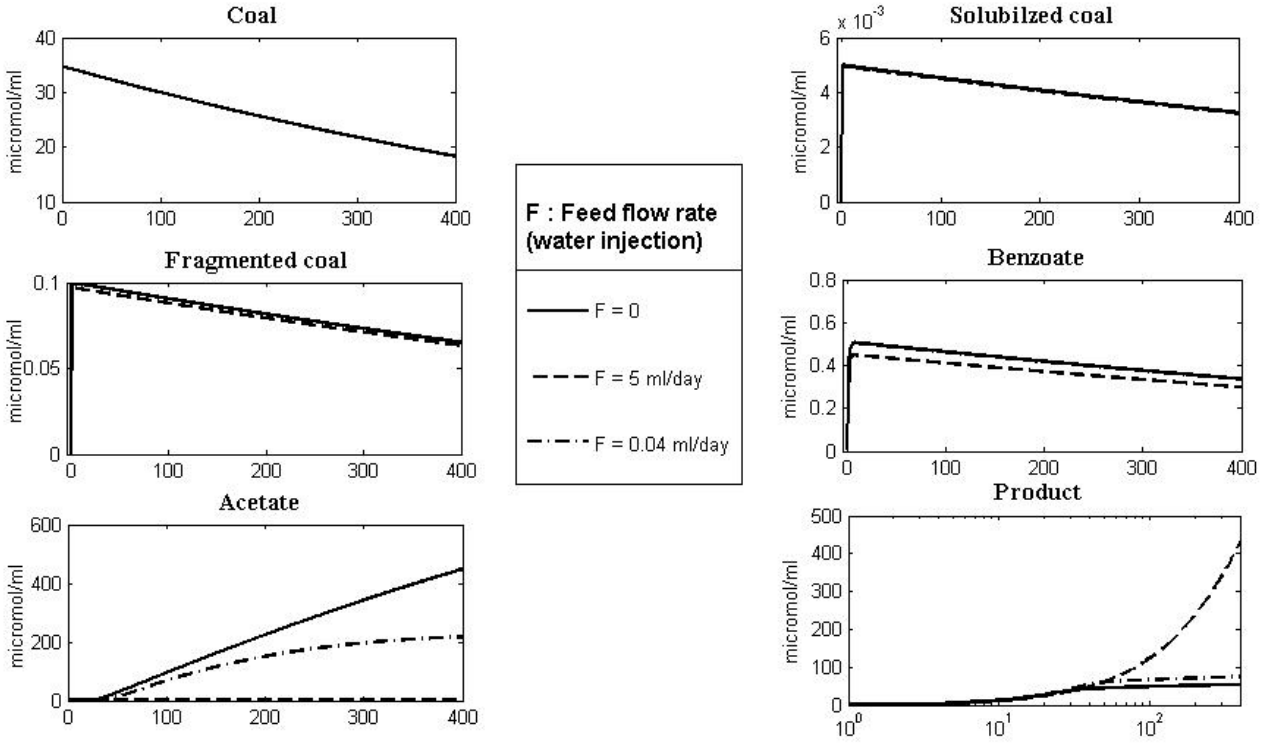

Figure 2.10: *Increased product generation along with the recovery of lumped acetate components at the outlet for anaerobic bioconversion coal in a continuous stirred tank reactor with water (amended with tryptone) injection.*

References

[1] Flores, R. M. Coalbed methane: from hazard to resource. *International Journal of Coal Geology*, 35(1):3–26, 1998.

[2] Patching, T. and Mikhail, M. Studies of gas sorption and emission on Canadian coals. *CIM Bulletin*, 79(887):104–109, 1986.

[3] Das, L., Gulati, R., and Gupta, P. A comparative evaluation of the performance characteristics of a spark ignition engine using hydrogen and compressed natural gas as alternative fuels. *International Journal of Hydrogen Energy*, 25(8):783–793, 2000.

[4] Parkes, R. J., Cragg, B. A., and Wellsbury, P. Recent studies on bacterial populations and processes in subseafloor sediments: A review. *Hydrogeology Journal*, 8(1):11–28, 2000.

[5] Al-Jubori, A., Johnston, S., Boyer, C., Lambert, S. W., Bustos, O. A., Pashin, J. C., and Wray, A. Coalbed methane: Clean energy for the world. *Oilfield Review*, 21(2):4–13, 2009.

[6] Budwill, K., Koziel, S., and Vidmar, J. Advancements in understanding and enhancing biogenic methane production from coals. In *Canadian Unconventional Resources Conference*. Society of Petroleum Engineers, 2011.

[7] Gray, N. D., Sherry, A., Larter, S. R., Erdmann, M., Leyris, J., Liengen, T., Beeder, J., and Head, I. M. Biogenic methane production in formation waters from a large gas field in the North Sea. *Extremophiles*, 13(3):511–519, 2009.

[8] Converse, D., Hinton, S., Hieshima, G., Barnum, R., and Sowlay, M. Process for stimulating microbial activity in a hydrocarbon-bearing, subterranean formation, April 8 2003. US Patent 6,543,535.

[9] Jin, S., Bland, A., and Price, H. Biogenic methane production enhancement systems, November 16 2010. US Patent 7,832,475.

[10] Scott, A. Improving coal gas recovery with microbially enhanced coalbed methane. In Mastalerz, M., Glikson, M., and Golding, S., editors, *Coalbed Methane: Scientific, Environmental and Economic Evaluation*, pages 89–110. Springer Netherlands, 1999. ISBN 978-90-481-5217-9.

[11] Lawrence, A. W. and McCarty, P. L. Kinetics of methane fermentation in anaerobic treatment. *Journal (Water Pollution Control Federation)*, 41(2):R1–R17, 1969.

[12] Rice, D. D. Composition and origins of coalbed gas. *Hydrocarbons from coal: AAPG Studies in Geology*, 38:159–184, 1993.

[13] Ulrich, G. and Bower, S. Active methanogenesis and acetate utilization in Powder River basin coals, United States. *International Journal of Coal Geology*, 76(1):25–33, 2008.

[14] Faiz, M. and Hendry, P. Significance of microbial activity in Australian coal bed methane reservoirs – A review. *Bulletin of Canadian Petroleum Geology*, 54(3):261–272, 2006.

[15] Hatcher, P. G. and Clifford, D. J. The organic geochemistry of coal: from plant materials to coal. *Organic Geochemistry*, 27(5-6):251–257, 1997.

[16] Achyuthan, K. E., Achyuthan, A. M., Adams, P. D., Dirk, S. M., Harper, J. C., Simmons, B. A., and Singh, A. K. Supramolecular self-assembled chaos: polyphenolic lignin's barrier to cost-effective lignocellulosic biofuels. *Molecules*, 15(12):8641–8688, 2010.

[17] Ferry, J. and Wolfe, R. Anaerobic degradation of benzoate to methane by a microbial consortium. *Archives of Microbiology*, 107(1):33–40, 1976.

[18] Fakoussa, R. and Hofrichter, M. Biotechnology and microbiology of coal degradation. *Applied Microbiology and Biotechnology*, 52(1):25–40, 1999.

[19] Bodzek, D. and Marzec, A. Molecular components of coal and coal structure. *Fuel*, 60(1):47–51, 1981.

[20] Marzec, A. Towards an understanding of the coal structure: A review. *Fuel Processing Technology*, 77:25–32, 2002.

[21] Makgato, M., Moitsheki, L., Shoko, L., Kgobane, B., Morgan, D., and Focke, W. W. Alkali-assisted coal extraction with polar aprotic solvents. *Fuel Processing Technology*, 90(4):591–598, 2009.

[22] Cohen, M. S. and Gabriele, P. D. Degradation of coal by the fungi *Polyporus versicolor* and *Poria monticola*. *Applied and Environmental Microbiology*, 44(1):23–27, 1982.

[23] Faison, B., Scott, C., and Davison, B. Biosolubilization of coal in aqueous and non-aqueous media. *Preprints of the American Chemical Society, Div. Fuel Chem., United States*, 33(conf 8809269), 1988.

[24] Cohen, M. S., Feldman, K. A., Brown, C. S., and Gray, E. T. Isolation and identification of the coal-solubilizing agent produced by *Trametes versicolor*. *Applied and Environmental Microbiology*, 56(11):3285–3291, 1990.

[25] Cohen, M., Aronson, H., Feldman, K., Brown, C., and Gray Jr, E. Recent progress in cell-free solubilization of coal. *Preprints of the American Chemical Society, Div. Fuel Chem.; United States*, 33(conf 8809269):., 1988.

[26] Young, L. and Frazer, A. The fate of lignin and lignin-derived compounds in anaerobic environments. *Geomicrobiology Journal*, 5(3-4):261–293, 1987.

[27] Wawrik, B., Mendivelso, M., Parisi, V. A., Suflita, J. M., Davidova, I. A., Marks, C. R., Van Nostrand, J. D., Liang, Y., Zhou, J., and Huizinga, B. J. Field and laboratory studies on the bioconversion of coal to methane in the San Juan Basin. *FEMS Microbiology Ecology*, 81(1):26–42, 2012.

[28] Krüger, M., Beckmann, S., Engelen, B., Thielemann, T., Cramer, B., Schippers, A., and Cypionka, H. Microbial methane formation from hard coal and timber in an abandoned coal mine. *Geomicrobiology Journal*, 25(6):315–321, 2008.

[29] Harris, S. H., Smith, R. L., and Barker, C. E. Microbial and chemical factors influencing methane production in laboratory incubations of low-rank subsurface coals. *International Journal of Coal Geology*, 76(1):46–51, 2008.

[30] Thielemann, T., Cramer, B., and Schippers, A. Coalbed methane in the Ruhr basin, Germany: a renewable energy resource? *Organic Geochemistry*, 35(11):1537–1549, 2004.

[31] Ritter, D., Vinson, D., Barnhart, E., Akob, D. M., Fields, M. W., Cunningham, A. B., Orem, W., and McIntosh, J. C. Enhanced microbial coalbed methane generation: A review of research, commercial activity, and remaining challenges. *International Journal of Coal Geology*, 146(1):28–41, 2015.

[32] Nozhevnikova, A. N., Nekrasova, V., Ammann, A., Zehnder, A. J., Wehrli, B., and Holliger, C. Influence of temperature and high acetate concentrations on methanogenensis in lake sediment slurries. *FEMS Microbiology Ecology*, 62(3):336–344, 2007.

[33] Kessel, J. A. S. and Russell, J. B. The effect of pH on ruminal methanogenesis. *FEMS Microbiology Ecology*, 20(4):205–210, 1996.

[34] Kim, I. S., Hwang, M. H., Jang, N. J., Hyun, S. H., and Lee, S. Effect of low pH on the activity of hydrogen utilizing methanogen in bio-hydrogen process. *International Journal of Hydrogen Energy*, 29(11):1133–1140, 2004.

[35] Penner, T. J., Foght, J. M., and Budwill, K. Microbial diversity of western Canadian subsurface coal beds and methanogenic coal enrichment cultures. *International Journal of Coal Geology*, 82(1):81–93, 2010.

[36] Fedorak, P. M. and Hrudey, S. E. The effects of phenol and some alkyl phenolics on batch anaerobic methanogenesis. *Water Research*, 18(3):361–367, 1984.

[37] Jones, E. J., Voytek, M. A., Corum, M. D., and Orem, W. H. Stimulation of methane generation from nonproductive coal by addition of nutrients or a microbial consortium. *Applied and Environmental Microbiology*, 76(21):7013–7022, 2010.

[38] Keith, C., Bridges, R., Fina, L., Iverson, K., and Cloran, J. The anaerobic decomposition of benzoic acid during methane fermentation. *Archives of Microbiology*, 118(2):173–176, 1978.

[39] Healy, J. and Young, L. Anaerobic biodegradation of eleven aromatic compounds to methane. *Applied and Environmental Microbiology*, 38(1):84–89, 1979.

[40] Colberg, P. J. and Young, L. Biodegradation of lignin-derived molecules under anaerobic conditions. *Canadian Journal of Microbiology*, 28(7):886–889, 1982.

[41] Colberg, P. and Young, L. Aromatic and volatile acid intermediates observed during anaerobic metabolism of lignin-derived oligomers. *Applied and Environmental Microbiology*, 49(2):350–358, 1985.

[42] Orem, W., Tatu, C., Varonka, M., Lerch, H., Bates, A., Engle, M., Crosby, L., and McIntosh, J. Organic substances in produced and formation water from unconventional natural gas extraction in coal and shale. *International Journal of Coal Geology*, 126:20–31, 2014.

[43] Okino, M. S. and Mavrovouniotis, M. L. Simplification of mathematical models of chemical reaction systems. *Chemical Reviews*, 98(2):391–408, 1998.

[44] Jacob, S. M., Gross, B., Voltz, S. E., and Weekman, V. W. A lumping and reaction scheme for catalytic cracking. *AIChE Journal*, 22(4):701–713, 1976.

[45] Susilawati, R., Esterle, J. S., Golding, S. D., and Mares, T. E. Microbial methane potential for the South Sumatra basin coal: Formation water screening and coal substrate bioavailability. *Energy Procedia*, 65:282–291, 2015.

[46] D Strapoc, D., Mastalerz, M., Dawson, K., Macalady, J., Callaghan, A. V., Wawrik, B., Turich, C., and Ashby, M. Biogeochemistry of microbial coal-bed methane. *Annual Review of Earth and Planetary Sciences*, 39:617–656, 2011.

[47] Kotsyurbenko, O. R., Chin, K.-J., Glagolev, M. V., Stubner, S., Simankova, M. V., Nozhevnikova, A. N., and Conrad, R. Acetoclastic and hydrogenotrophic methane production and methanogenic populations in an acidic West-Siberian peat bog. *Environmental Microbiology*, 6(11):1159–1173, 2004.

[48] Joulian, C., Patel, B., Ollivier, B., Garcia, J.-L., and Roger, P. A. Methanobacterium *Oryzae sp. nov.*, a novel methanogenic rod isolated from a Philippines ricefield. *International Journal of Systematic and Evolutionary Microbiology*, 50(2):525–528, 2000.

[49] Demirel, B. and Scherer, P. The roles of acetotrophic and hydrogenotrophic methanogens during anaerobic conversion of biomass to methane: A review. *Reviews in Environmental Science and Biotechnology*, 7(2):173–190, 2008.

[50] Lokshina, L. Y., Vavilin, V. A., Kettunen, R. H., Rintala, J. A., Holliger, C., and Nozhevnikova, A. N. Evaluation of kinetic coefficients using integrated Monod and Haldane models for low-temperature acetoclastic methanogenesis. *Water Research*, 35(12):2913–2922, 2001.

[51] Westermann, P., Ahring, B. K., and Mah, R. A. Temperature compensation in *Methanosarcina barkeri* by modulation of hydrogen and acetate affinity. *Applied and Environmental Microbiology*, 55(5):1262–1266, 1989.

[52] Rebac, S., Ruskova, J., Gerbens, S., Van Lier, J. B., Stams, A. J., and Lettinga, G. High-rate anaerobic treatment of wastewater under psychrophilic conditions. *Journal of Fermentation and Bioengineering*, 80(5):499–506, 1995.

[53] Scott, R. G., Moore, L. P., and Studier, M. H. Structural characterization of coal: lignin-like polymers in coals. In *Coal structure: based on a symposium sponsored by the Division of Fuel Chemistry at the ACS/CSJ Chemical Congress, Honolulu, Hawaii, April 3-4, 1979*, volume 192, page 133. ACS Publications, 1981.

[54] Buswell, A. and Mueller, H. Mechanism of methane fermentation. *Industrial & Engineering Chemistry*, 44(3):550–552, 1952.

[55] Noyes, A. A. and Whitney, W. R. The rate of solution of solid substances in their own solutions. *Journal of the American Chemical Society*, 19(12):930–934, 1897.

[56] Bekins, B. A., Warren, E., and Godsy, E. M. A comparison of zero-order, first-order, and Monod biotransformation models. *Groundwater*, 36(2):261–268, 1998.

[57] Simkins, S. and Alexander, M. Models for mineralization kinetics with the variables of substrate concentration and population density. *Applied and Environmental Microbiology*, 47(6):1299–1306, 1984.

[58] Stephen, A., Adebusuyi, A., Baldygin, A., Shuster, J., Southam, G., Budwill, K., Foght, J., Nobes, D., and Mitra, S. Bioconversion of coal: New insights from a core flooding study. *RSC Advances*, 4(43):22779–22791, 2014.

[59] Kennedy, J. and Eberhart, R. Particle swarm optimization. In *Encyclopedia of Machine Learning*, pages 760–766. Springer, 2010.

[60] Lee, C. J., Prasad, V., and Lee, J. M. Stochastic nonlinear optimization for robust design of catalysts. *Industrial and Engineering Chemistry Research*, 50(7):3938–3946, 2011.

Chapter 3

Modeling, estimation and optimization in coreflood experiments for coalbed methane production

Abstract

We extend a previously derived kinetic model for coal bioconversion and couple it with a transport model to simulate coreflooding experiments with packed crushed coal, which are representations of a coalbed methane (CBM) reservoir at the laboratory scale. We apply a tanks-in-series model to simulate plug flow in the core, and the nonlinear model is regressed against experimental data using particle swarm optimization. The validated model is used to analyze CBM production at different operating conditions and subsequently for optimization of gas production. Model-based experimental design is applied to improve the accuracy of parameter estimation, and computational singular perturbation analysis is applied to develop a better understanding of the important species and reaction at each stage of the coreflooding experiment, and to develop reduced order kinetic models that can be used in process optimization.

3.1 Introduction

Gases produced and stored or trapped in coalbeds with multiple scales of porosity are known as coalbed methane (CBM). They are usually a mixture of methane (80 - 99% by volume) and minor amounts of carbon dioxide, nitrogen, hydrogen sulphide, sulphur dioxide and heavier hydrocarbons such as ethane, propane and butane. CBM is an unconventional resource of natural gas and is a better fuel than its precursor, coal, in terms of calorific value and impact on the environment. Interest in CBM extraction for commercial production began in the 1970s and has rapidly increased since the early 1990s.

CBM is produced by two major processes, biogenic and thermogenic. While thermogenic CBM is produced by thermal cracking at elevated pressure and temperature, biogenic methane is produced by anaerobic microbial attack on the organic matter in coal. Various events such as basin uplift/cooling, the flow of associated groundwater or dilution in salinity levels can trigger biogenic methane generation in coal beds that are no longer conducive to any microbial growth, and this methane is referred to as secondary biogenic CBM. Simulation of CBM production in the presence of ongoing microbial activity requires quantification of reaction kinetics along with characterisation of the coalbeds. To address this, we have developed a simplified reaction pathway and a corresponding kinetic model based on existing literature on anaerobic digestion processes and experimental data from anaerobic microcosm studies conducted with crushed coal in serum bottles[1–4]. However, these closed system laboratory culture bottle experiments are conducted at very high ratios of medium to coal substrate. Since this is not the case in an actual CBM reservoir, models estimated with such experimental data cannot be applied directly for the simulation of biogenic CBM production at commercial field scales.

To overcome these limitations of the bottle experiments, coreflooding experiments, similar in principle to coreflooding experiments conducted by petroleum reservoir engineers for studies related to crude oil and gas recovery[5–7], were conducted by Stephen et al.[8]. These laboratory scale experiments mimic underground reservoir conditions more closely, in the sense that they treat the coal sample as a porous medium that permits migration of fluids (flow of water, microbes and flow/diffusion/sorption of gases) at high operating pressures. Data from these experiments is therefore more suitable for use in scale-up.

In this study, we have developed a fundamental model that includes reaction kinetics describing the coreflooding experiments of Stephen et al.[8], conducted parameter estimation and model validation, analyzed the dynamic features of the model and used it for process optimization. First, we modify our previously developed enzymatic

kinetic model[1] to accommodate for varying nutrient limitations along with the integration of gas diffusion and sorption kinetics. A tanks-in-series model is then built to simulate the flow and changing species concentrations within the core. Particle swarm optimization is used for estimation of the parameters of the model to validate it against the production data from the experiment. The validated model is then used for model-based analysis of the effects of varying operating conditions, which subsequently enables optimization of gas production. In addition, we devise an optimal experimental design for parameter estimation based on a D-optimal measure. Analysis of the important species and reactions at different stages of the coreflooding experiments is also performed using computational singular perturbation (CSP).

3.2 Coreflooding experiments

For clarity of exposition, we provide a brief description of the coreflooding experiments of Stephen et al.[8], for which we develop a model in this work.

A core holder was filled with crushed coal of different mesh sizes simulating a heterogeneous porous medium as in an actual reservoir. Before starting the coreflood experiment, 3 pore volumes of MSM-tryptone solution were injected (until saturation) followed by inoculation with 1.25 pore volumes of microbial culture and two weeks of incubation at room temperature. During the experiment, the core was continuously flooded with MSM-tryptone solution (nutrient) at $0.006\ ml/min$ and the effluent sample was collected at the downstream section of the core holder. Dissolved gases were desorbed from the effluent by pressure reduction,and were then analysed for the presence of CH_4 and CO_2 in a gas chromatograph (GC) using two different methods. In one, the gas collected in a Tedlar bag was directly injected into the GC column, and in the other, the gas samples were transferred to a sealed vial before injection into the GC. Gas chromatography-mass spectrometry (GC-MS) was performed on the effluent to analyse the composition of the intermediate products[8]. Table 3.1 lists the properties of the coal sample and core holder used in these experiments.

3.3 Kinetic model development

In our previous work[1], the complicated reaction network for biogenic CBM production from coal was simplified by using lumped species reacting in a series of enzymatic reaction blocks consisting of coal solubilization, hydrolysis, acidogenesis, acetogenesis and methanogenesis. The lumped components involved in each block are coal (C), solubilized coal (S), i.e., coal solubilized in water, fragmented coal (W) denoting

Coal:	
Mass	300.4 g
Average particle size	200 μm
Density	1422 kg/m^3
Core	
Length	30.5 cm
Diameter	3.81 cm
Bulk volume	347.5 ml
Pore volume	131.95 ml

Table 3.1: *Coal and core holder properties.*

the products of hydrolysis and represented by a common lignin monomer (syringic acid), benzoate (B) denoting the products of acidogenesis and represented by benzoate/benzoic acid, which is the most common aromatic ring intermediate found in these systems, acetate (A) denoting products of acetogenesis and represented by acetate/acetic acid and finally the products (P) of methanogenesis, which are methane, carbon dioxide and hydrogen. Thus, the simplified reaction pathway is

Coal **C** $\rightarrow$ Solubilized coal **S** $\rightarrow$ Fragmented coal **W** $\rightarrow$ Benzoate **B** $\rightarrow$ Acetate **A** $\rightarrow$ Products **P**

A kinetic model was proposed for this reaction scheme using a series of Monod models which was then validated against experimental data from various closed static low pressure anaerobic microcosm studies conducted in bottles with crushed coal[1]. Various assumptions were considered in the development of the kinetic model, including assuming that carbon is the only limiting substrate while nitrogen (from the nutrient, tryptone) is present in excess for the entire microbial chain. This was reasonable in the case of bottle experiments where the medium to substrate ratios were high. However, in the case of coreflooding experiments, the concentration of nitrogen (from tryptone) is not in excess in different parts of the core at all times. For instance, for a core with volume $V = 347.5\ ml$ and tryptone supplied at a feed flow rate of $F = 0.006\ ml/min$, there is a constant fresh supply of tryptone at the inlet, while there is a fresh supply only every 40 days (the residence time) at the outlet. Thus, nitrogen limitations due to low tryptone concentrations have to be introduced into the kinetic model for coal breakdown.

Table 3.4 lists the notation for all the variables introduced in the following sections.

Nitrogen as a limiting substrate

Tryptone, which is the nutrient used in the experiment, is an assortment of peptides providing a source of amino acids (i.e., supply of nitrogen [N]) to growing bacteria. The growth rate in the presence of heterogeneous limiting substrates, i.e., the carbon and nitrogen sources ([C] and [N] respectively), can be expressed by modifying the Monod model as[9]

$$\mu = \mu_m \frac{[N]}{K_N + [N]} \frac{[C]}{K_C + [C]} \tag{3.1}$$

Since the nitrogen is derived from tryptone, $[N]$ is replaced by $[Nu]$, which denotes the concentration of the external nutrient supply (tryptone). It is to be noted that complex structures such as peptides and amino acids present in tryptone are usually broken down by higher microbes[10], making simpler compounds available to the rest of the microbial chain.

Apart from providing a source of nitrogen, anaerobic digestion of tryptone also produces a pool of aromatic ring intermediates lumped into benzoate, as established in our previous study[1]. Figure 3.1 shows the concentrations of benzoate-like and acetate-like components from GC/MS analysis on uninoculated tryptone medium.[8,11] Compounds such as p-tolylacetic acid, phenylacetic acid, o-pthalate were lumped under the marker benzoate, whereas compounds such as methyl succinate and succinic acid were lumped under the marker acetate. A high concentration of benzoate-like components indicates that the benzoate pool was produced from tryptone in the presence of indigenous microbes present in the inoculum.

Since benzoate-like components are produced by acidogenesis of fragmented coal components as well as by microbial attack on tryptone, they are both assumed to be competing substrates at low concentrations. To model this, the Monod model is modified based on the purely competitive substrate kinetics proposed by Yoon et al.[12].

Apart from this, tryptone is also assumed to influence the rate of coal solubilisation owing to its nucleophilic property. The solubilisation constant in the kinetic model is accordingly modified as $ke^{S_n[Nu]}$. A schematic of the reaction network is shown in Figure 3.2.

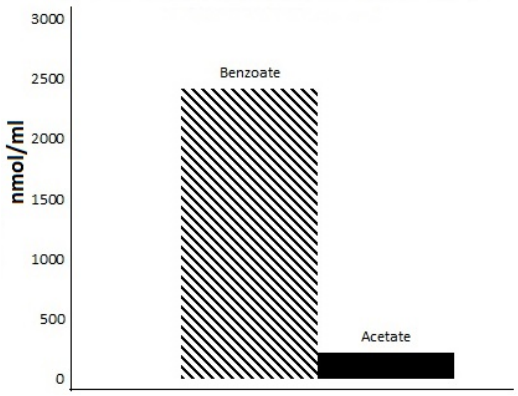

Figure 3.1: *Lumped benzoate and acetate concentrations from GC/MS analysis on MSM-tryptone medium.*

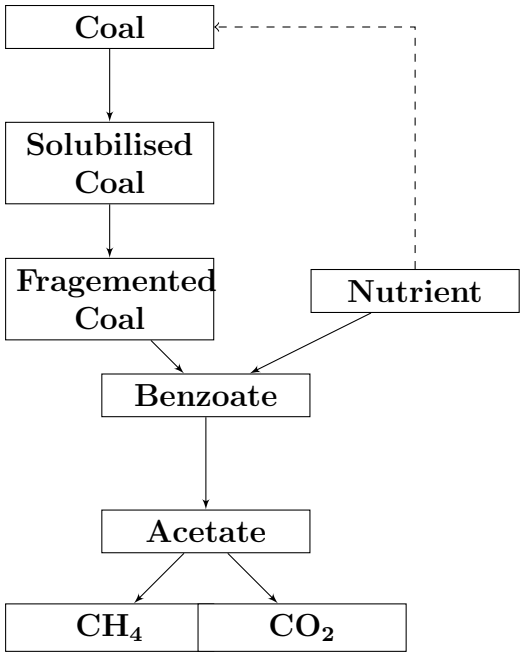

Figure 3.2: *Schematic of the reaction network.*

Acetoclastic methanogenesis with substrate inhibition

In our previous study[1], the dominant pathway for methanogenesis was assumed to be acetoclastic methanogenesis with substrate inhibition. The results from 16s rRNA pyrotag sequencing of the core material from the inlet, center and outlet sections reported in Stephen et al.[8] further support this claim.

According to the results of the 16S rRNA gene pyrotag sequencing, *Methanobacterium*, a methanogen that uses the hydrogenotrophic pathway is found at 17.9% relative abundance at the inlet of the core, but completely disappears at the outlet. The absence of *Methanobacterium* at the core outlet where there is a high concentration of CO_2 implies that hydrogenotrophic methanogenesis is not dominant. *Methanosarcina*, a methanogen that uses the acetoclastic pathway, is found at 5.4% relative abundance at the inlet, but also completely disappears towards the center and outlet of the core. However, this can be explained by inhibition to microbial activity of these methanogens from growing acetate concentrations along the core; this is supported by the decrease in the average pH of the effluent from 6.04 to 5.9. The dominance of *Clostridia*, which are fermentative anaerobic bacteria, at the core outlet further supports the claim that methanogenesis is highly inhibited at high concentrations of acetate (A), leaving fermentation/hydrolysis as the dominant reaction. The only inconsistency with this description is the relatively higher survival rate of

hydrogenotrophic methangens at the inlet of the core. It can be reasoned that hydrogenotrophic methanogens thrive at the inlet because of the constant fresh supply of MSM (containing NH_4Cl), as they are a source of simple nitrogen containing compounds for these methanogens. The absence of acetoclastic methanogens here can be attributed to their low activity in the presence of free ammonia[13]. This speculation can be clarified by performing pyrotag sequencing of the core material at different times in the coreflooding experiment.

Gas sorption

Since the coreflooding experiment was conducted at different pressure conditions (3.45 MPa at the beginning and 0.069 MPa towards the end), the rate of gas diffusion between different phases and sorption on solid coal must also be considered in the kinetic model. First, since the experiment is conducted at relatively high operating pressures, the gases produced during methanogenesis are assumed to be completely dissolved in the water. Hence, all components are assumed to be present in the water phase. At high pressures, the gas dissolved in the liquid phase is assumed to diffuse and adsorb on to the surface of the solid. By assuming that the rate of attachment is fast[14], the rate of gas diffusion from water to the surface of the solid is expressed as

$$r_{ad} = k_{ad} M([G] - [G]_s) \tag{3.2}$$

where k_{ad} is the diffusion rate constant ($1/s.m^2$), M is the surface area available for adsorption, $[G]$ is the gas concentration in the liquid bulk (mol/m^3) and $[G]_s$ is the concentration of gas molecules attached to the surface of the coal ($\frac{mol}{m^2}\frac{m^2}{m^3}$). CO_2 is also quantified in this kinetic model, and it is assumed to face competition from CH_4 during sorption. Competition for solid sites between the gases is reflected in the available surface area M as

$$\begin{aligned} dM &= \frac{\partial M}{\partial [CH_{4s}]} d[CH_{4s}] + \frac{\partial M}{\partial [CO_{2s}]} d[CO_{2s}] \\ &= -kads_m[M]d[CH_{4s}] - kads_c[M]d[CO_{2s}] \\ M &= M_0 \exp(-kads_m[CH_{4s}] - kads_c[CO_{2s}]) \end{aligned} \tag{3.3}$$

When the pressure drops, gas molecules desorb and are assumed to follow a simple first order reaction law

$$r_d = k_d[Gas]_s \text{ where } k_d \text{ is the desorption rate constant} \tag{3.4}$$

The rate constants corresponding to adsorption and desorption, i.e., $k_a d$ and k_d are dependent on pressure. We assume all the reactions to occur under non-growth conditions (i.e., the total microbe quantity is constant). With these assumptions, the kinetic model is derived as

$$r_C = \underbrace{-ke^{S_n[Nu]}}_{\text{Effect of } [Nu] \text{ on solubilization rate}} \left(\frac{C}{C_0}\right)^{2/3} ([S^*] - [S]) \tag{3.5a}$$

$$r_S = ke^{S_n[Nu]} \left(\frac{C}{C_0}\right)^{2/3} ([S^*] - [S]) - b[S] \underbrace{\left(\frac{[Nu]}{k_1 + [Nu]}\right)}_{\text{Limiting } [Nu] \text{ in Hydrolysis}} \tag{3.5b}$$

$$r_W = 10b\frac{[Nu][S]}{k_1 + [Nu]} - \mu_1 \underbrace{\left(\frac{[Nu]}{k_2 + [Nu]}\right)}_{\text{Limiting } [Nu] \text{ in Acidogenesis}} \left(\frac{[W]}{Ks_1 + [W] + \frac{Ks_1}{Ks_2}[Nu]}\right) \tag{3.5c}$$

$$r_B = \mu_1 \underbrace{\left(\frac{[Nu]}{k_2 + [Nu]}\right)\left(\frac{[W]}{Ks_1 + [W] + \frac{Ks_1}{Ks_2}[Nu]}\right)}_{[B] \text{ from } [W] \text{ under competition from } [Nu]} + \underbrace{\frac{\mu_2[Nu]}{Ks_2 + [Nu] + \frac{Ks_2}{Ks_1}[W]}}_{[B] \text{ from } [Nu] \text{ under competition from } [W]} \tag{3.5d}$$

$$- d[B] \underbrace{\left(\frac{[Nu]}{k_3 + [Nu]}\right)}_{\text{Limiting } [Nu] \text{ in Acetogenesis}} \tag{3.5e}$$

$$r_A = \frac{3d[Nu][B]}{k_3 + [Nu]} - \underbrace{\left(\frac{[Nu]}{k_4 + [Nu]}\right)}_{\text{Limiting } [Nu] \text{ in Methanogenesis}} \left(\frac{e[A]}{f + [A] + [A]^2/g}\right) \tag{3.5f}$$

$$r_{Nu} = \underbrace{-\frac{\mu_3[Nu]}{Ks_2 + [Nu] + \frac{Ks_2}{Ks_1}W]}}_{\text{Nutrient consumed to produce } [B]} - \underbrace{K_{Nu_s}[Nu]}_{\text{Total [Nu] consumed to provide [N] to microbes}} \tag{3.5g}$$

$$r_{CH_4} = \frac{e[Nu][A]}{(k_4 + [Nu])(f + [A] + [A]^2/g)} \underbrace{-r_{CH_{4ads}} + r_{CH_{4des}}}_{\text{Net } [CH_4] \text{ molecules available after adsorption/desorption}} \tag{3.5h}$$

$$r_{CO_2} = \left(\frac{\mu_1[Nu][W]}{(k_2 + [Nu])(Ks_1 + [W] + \frac{Ks_1}{Ks_2}[Nu])}\right) + \frac{d[Nu][B]}{k_3 + [Nu]} + r_{CH_4} \tag{3.5i}$$

$$\underbrace{-r_{CO_{2ads}} + r_{CO_{2des}}}_{\text{Net } [CO_2] \text{ molecules available after adsorption/desorption}} \tag{3.5j}$$

$$r_{CH_{4ads}} = kad_m M([CH_4] - [CH_{4s}]) \tag{3.5k}$$
$$r_{CH_{4des}} = kd_m[CH_{4s}] \tag{3.5l}$$
$$r_{CO_{2ads}} = kad_c M([CO_2] - [CO_{2s}]) \tag{3.5m}$$
$$r_{CO_{2des}} = kd_c[CO_{2s}] \tag{3.5n}$$
$$k = k_0 X f_b \frac{m_{coal}/n}{r_{coal}\rho_{coal}} \tag{3.5o}$$

3.4 Tanks-in-series model

A tanks-in-series model is developed to simulate the rate of change of various species concentrations along the core. The first assumption made is that the fluid present in the core moves as a series of plugs with no mixing in the axial direction and perfect mixing in the radial direction, which is reasonable based on the low flow rate of the injected fluid in the experiment (0.006 ml/min). Using a sufficient number of continuous stirred tank reactors (CSTRs) in series reduces the error arising from this approximation of the plug flow.

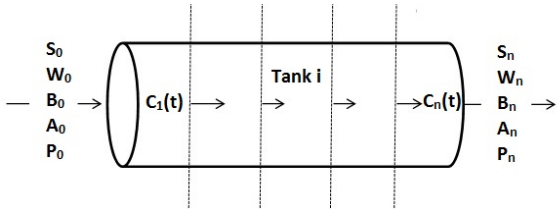

Figure 3.3: *Tanks-in-series model for coreflood experiments.*

Figure 3.3 shows the core volume divided into n CSTRs. The coupled differential equations used to simulate the coreflooding experiment are shown in Equation 3.6 below, and the rates of reactions for the species are obtained from the kinetic model described above in Equation 3.5. Simultaneous integration of the coupled differential equations for all of the tanks provides us with the dynamic variation of the concentrations of the species in different regions of the core holder.

In any tank i,

$$\frac{d[C_i]}{dt} = r_{Ci} \tag{3.6a}$$
$$\frac{d[S_i]}{dt} = \frac{F}{V}([S_{i-1}] - [S_i]) + r_{S_i} \tag{3.6b}$$

$$\frac{d[W_i]}{dt} = \frac{F}{V}([W_{i-1}] - [W_i]) + r_{W_i} \tag{3.6c}$$

$$\frac{d[B_i]}{dt} = \frac{F}{V}([B_{i-1}] - [B_i]) + r_{B_i} \tag{3.6d}$$

$$\frac{d[A_i]}{dt} = \frac{F}{V}([A_{i-1}] - [A_i]) + r_{A_i} \tag{3.6e}$$

$$\frac{d[CH_{4i}]}{dt} = \frac{F}{V}([CH_{4i-1}] - [CH_{4i}]) + r_{CH_{4i}} - r_{CH_4ads_i} + r_{CH_4des_i} \tag{3.6f}$$

$$\frac{d[CH_{4is}]}{dt} = r_{CH_4ads_i} - r_{CH_4des_i} \tag{3.6g}$$

$$\frac{d[CO_{2i}]}{dt} = \frac{F}{V}([CO_{2i-1}] - [CO_{2i}]) + r_{CO_{2i}} - r_{CO_2ads_i} + r_{CO_2des_i} \tag{3.6h}$$

$$\frac{d[CO_{2is}]}{dt} = r_{CO_2ads_i} - r_{CO_2des_i} \tag{3.6i}$$

$$\frac{d[Nu_i]}{dt} = \frac{F}{V}([Nu_{i-1}] - [Nu_i]) + r_{Nu_i} \tag{3.6j}$$

3.5 Estimation and model-based optimal experimental design

Parameter estimation was carried out with the nonlinear model and the coreflooding data for generated methane and carbon dioxide using particle swarm optimization (PSO). PSO is a population sample-based optimization algorithm inspired by social behaviour in animals such as bird flocking, fish schooling and bees swarming[15]. In this method, randomly chosen samples are allowed to move around a solution space with velocities that are iteratively updated so as to converge at a global optimal solution[16].

We also explore the use of optimal experimental design for improving the accuracy of the parameter estimation. Model based design of experiments (DOE) for dynamic systems typically uses scalar metrics of the Fischer Information Matrix (FIM)[17].

$$FIM = N_{SC}^T N_{SC} \tag{3.7}$$

where N_{SC} is the sensitivity matrix containing normalized sensitivity coefficients of the response of the model with respect to its various parameters. In this work, we use the D-optimal criterion, which maximizes the determinant of the FIM. Underdetermined systems have FIM of low rank[18], and this can be avoided by reducing the parameter space based on identifiability analysis using the sensitivity matrix.

3.6 Computational singular perturbation

The reaction kinetic model developed for coal bioconversion in Equation 3.5 faces various difficulties during estimation and simulation. First, the large dimension of the parameter space added to limited availability of observed model responses leads to reduced identifiability. Second, the presence of coupled equations with different time scales coupled together leads to a stiff system of equations. Model reduction can be used to address both issues, and a method that identifies rate-controlling reactions and the subset of reactions that are active at each time can also aid in analysis and optimization. We employ computational singular perturbation (CSP)[19–21] for this purpose. CSP seeks to iteratively separate the fast and slow reaction subspaces by finding a transformation for the vector of the rate of change of species concentrations (g). Given a kinetic model with N species and R reactions, the rate of change of species concentrations is expressed as

$$g = \frac{dy}{dt} = \sum_{r=1}^{R} S^r F^r \tag{3.8}$$

where y is the species vector at any time t, S^r is the stoichiometric matrix and F^r is the reaction rate vector. g can be transformed to N modes using a set of N linearly independent row basis vectors b^i as

$$g = \sum_{i=1}^{N} a_i f^i \tag{3.9}$$

where $f^i = b^i \odot g, i = 1, .., N$. a_i represents the direction of the modes and f^i, the corresponding amplitude. Vectors a_j are the inverse of the column basis vectors, i.e., b^i, $b^i \odot a_j = \delta^i_j, i, j = 1$ to N. The rate of change of amplitude of the modes, f^i is given by

$$\frac{df^i}{dt} = \sum_{j=1}^{N} \left[\frac{db^i}{dt} + b^i \odot \frac{\partial g}{\partial y} \right] \odot a_j f^j = \sum_{j=1}^{N} \Lambda^i_j f^j \tag{3.10}$$

Reciprocals of the eigen values of Λ are the time scales of the N modes, denoted by $\tau(i)$, where i is the index of the mode. Modes can be speed ranked by ordering the time scales in increasing magnitudes as,

$$|\tau(1)| < \cdots |\tau(i)| < \cdots |\tau(N)| \tag{3.11}$$

The fast modes are those with time scale $\tau(m)$ smaller than a desired time resolution δt. In our analysis, since we are interested in exhausted modes at all times, δt is

considered to be the current time scale. A set of ideal basis vectors would be one that block diagonalizes Λ, separating the fast and slow modes with as little mixing as possible, and it can be identified using refinement strategies[19–21]. Information on kinetic model reduction can then be recovered from the CSP radical pointers and reaction pointers. For instance, the species y_i contributing the most to a certain fast mode j can be deduced from the largest value in the corresponding diagonal matrix $a_j b^j$. It is known as the CSP radical pointer. The corresponding fast reaction attributed to the exhaustion of y_i can then be derived from reaction pointers given by $P_j(r) = s_r^{-1} \odot a_j b^j \odot s_r$, where s_r is the stoichiometric column vector corresponding to the reaction rate F^r. g can be represented with the elimination of fast modes as

$$\begin{aligned} g^{\text{slow}}(M) &= (I - Q(M)) \odot g, \text{ where} \\ Q(M) &= \sum_{m=1}^{M} a_m b^m; M \text{ is the number of fast modes} \end{aligned} \tag{3.12}$$

3.7 Results

Estimation using particle swarm optimization

As mentioned earlier, particle swarm optimization was used to fit the tanks-in-series model incorporating the reactions for biogenic methane production and the coreflooding data for generated methane and carbon dioxide. 70 particles were employed and updated over 5 iterations to obtain a suitable parameter set. 10 tanks in series were chosen in the model, and it was verified that increasing the number of tanks beyond this did not change the outputs of the model significantly. The estimated values of the parameters of the model are shown in Table 3.2, and the performance of the model predictions against experimental data in shown in Figure 3.4. The predicted concentrations of methane and carbon dioxide match the experimental data closely. The lumped acetate concentration from GC/MS analysis of the effluent and that predicted by the model have similar trends (increasing with time) but are of different scales of magnitude. However, the trends in the simulated benzoate concentration do not match the lumped benzoate concentration from the GC/MS analysis data at smaller times; however, there is potentially greater error in the benzoate data due to incomplete information from GC/MS analysis.

Stephen et al.[8] have speculated that methane production by hydrogenotrophic methanogenesis might be responsible for the observed decrease in the $CO_2 : CH_4$ ratio over time in the coreflooding experiment. However, they did not consider the fact that CO_2 adsorbs better than CH_4[22,23], and the large volume of CO_2 collected at the end of

the experiment when the operating pressure was lowered to 0.069 MPa supports the conclusion that acetoclastic methanogenesis is dominant. Running the coreflooding experiment with methanogenesis inhibitors could resolve this issue unambiguously. Further, running a coreflood experiment with inert packing material and a continuous feed of nutrient would allow for accurate quantitative estimation of methane production from tryptone alone. The availability of such data can improve the identification of model parameters involving the production of the benzoate pool from tryptone.

The validated kinetic model was used to simulate experiments conducted with and without tryptone, the nutrient source. Figure 3.4e) reveals that the model respects the nitrogen requirement of microbes. The estimated values of the half-saturation constants k_1, k_2, k_3, k_4, which correspond to tryptone limitations, are very low (see the highlighted values in Table 3.2). Since this implies that the model is not very sensitive to tryptone limitation in the hydrolysis, acidogenesis, acetogenesis and methanogenesis steps, the simplification $\frac{[Nu]}{k+[Nu]} = 1$ is applied to the model in the following analysis.

Model-based analysis of the effect of varying operating conditions

Figure 3.5a shows the cumulative methane generated at different initial nutrient concentrations. The cumulative methane produced increases with an increase in the initial nutrient concentration initially, starts decreasing later before leveling out. This is due to the increase in acetate acumulation, which will inhibit methanogenesis. Figure 3.5b shows that with an increase in the feed flow rate, i.e., a decrease in the residence time, the cumulative methane produced decreases. Since the removal of acetate will improve methane production, we simulate a series of experiments using the coreflood model with injection of a fresh batch of nutrient rich fluid at each successive tank i (apart from the inlet tank) in succesive runs at a flow rate F_i. When nutrient is injected closer to the core outlet, more methane is generated. Also, the effect of residence time varies with the location of the injection point. Closer to the core inlet, methane generation is higher at low flow rates. However, closer to the core outlet, methane generation is higher at intermediate flow rates. The observations indicate that methane generation improves with the removal of acetate, which is effected by the dilution caused by nutrient injection.

Model based D-optimal experiment design

As mentioned earlier, a D-optimal experimental design was carried out using the estimated model with the feed flow rate and initial nutrient concentration are the inputs to be varied, the results of which are shown in Figure 3.6. The optimal experimental conditions where the D-optimal metric is highest are at a feed flow rate of $F = 0.009\ ml/min$ and an initial nutrient concentration of $Nu_0 = 0.5\ mol/m^3$.

Computational singular perturbation-based analysis of the kinetic model

Computational singular perturbation (CSP) is used for model analysis and reduction; g, which represents the rate of change of the species concentrations, is transformed to an alternate basis that separates the fast and slow reaction subspaces. The period of initial delay in the methane production is disregarded in this analysis. The reaction rate vectors are analysed only up to 80 days, at which time desorption is limited due to the large operating pressure (between 1.7 MPa and 3.5 MPa). Trial basis vectors were chosen by computing the left and right eigenvectors of $\frac{\partial g}{\partial y}$. The refinement strategy[19–21] is then iteratively applied to the basis vectors to block diagonalise Λ at all instants such that the ten modes corresponding to the ten species $[C], [S], [W], [B], [A], [Nu], [CH_4], [CH_{4s}], [CO_2], [CO_{2s}]$ are separated with little mixing. Figure 3.7d shows the trends of the time scales of the modes with increasing time; the nonlinear nature of the model results in variations in the time scales with time. Figure 3.7c shows the number of exhausted modes, which are those modes with time scales lesser than the current time and negligible contribution to $\frac{dg}{dt}$ (of order $<1E-4$). Radical pointers indicate which components may be chosen as CSP radicals to provide equations of state and reaction pointers indicate which reaction associated with each exhausted mode is fast. Dormant reactions have low reaction rates that do not exhaust over long periods. The reduced reaction rate vector, g, after the identification of fast reactions and CSP radicals is shown in Table 3.3. As seen, after 28 days, there is one exhausted mode $\left(\frac{d[S]}{dt} \approx 0\right)$, a second mode is exhausted after 37 days $\left(\frac{d[CO_2]}{dt} + \frac{d[CO_{2s}]}{dt} \approx 0\right)$ and a third mode is exhausted after 40 days $\left(\frac{d[B]}{dt} \approx 0\right)$. The exhausted reactions corresponding to the fast exhausted modes are hydrolysis rate $b[S]$, the carbon dioxide adsorption rate $r_{CO_{2ads}}$ and the acetogenesis rate $d[B]$, respectively. The mode $\frac{d[CO_2]}{dt} + \frac{d[CO_{2s}]}{dt}$ connected with

the exhausted reaction $r_{CO_{2ads}} = kad_cM([CO_2] - [CO_{2s}]) \approx 0$ indicates that the rate of carbon dioxide production is approximately equal to the rate of its adsorption onto the surface of the coal. Reflecting on its insignificant presence in $\frac{d[S]}{dt}$, r_C is considered to be a dormant reaction.

Thus, accounting for only the slow reactions, the use of CSP results in a reduction in the parameter dimensions by 5 in the reduced model. Figures 3.7a and 3.7b compare the performances of the original and reduced models, and prove that the predictions of the reduced order model do not deviate significantly from that of the original model. Due to the elimination of exhausted modes, the issue of stiffness of the system of differential equations is also resolved, thereby making it suitable for use in simulation at larger length and time scales. The differential equation system corresponding to the reduced kinetic model is shown in the Appendix A.1.

Parameter	Value	Unit
k	7.8×10^{-6}	h^{-1}
S_n	10^{-4}	$\frac{m^3}{mol}$
b	0.1	h^{-1}
k_1	10^{-5}	$\frac{mol}{m^3}$
μ_1	0.001	$\frac{mol}{m^3.h}$
μ_2	0.0312	$\frac{mol}{m^3.h}$
μ_3	0.0029	$\frac{mol}{m^3.h}$
Ks_1	0.3842	$\frac{mol}{m^3}$
Ks_2	0.4922	$\frac{mol}{m^3}$
k_2	10^{-5}	$\frac{mol}{m^3}$
d	0.015	h^{-1}
k_3	10^{-5}	$\frac{mol}{m^3}$
e	19.608	$\frac{mol}{m^3.h}$
k_4	10^{-5}	$\frac{mol}{m^3}$
f	215.805	$\frac{mol}{m^3}$
g	0.0011	$\frac{mol}{m^3}$
K_{Nu_s}	10^{-5}	h^{-1}
kad_m	0.0017	$\frac{1}{m^2.h}$
$kads_m$	0.01	$\frac{m^3}{mol}$
kd_m	10.5	h^{-1}
kad_c	0.01	$\frac{1}{m^2.h}$
$kads_c$	0.01	$\frac{m^3}{mol}$
kd_c	10^{-4}	h^{-1}

Table 3.2: *Values of model parameters estimated using particle swarm optimization.*

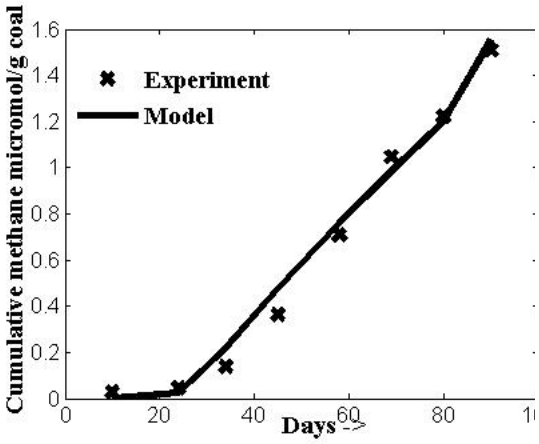

(a) *Comparison of the experimental cumulative CH_4 production data against model predictions.*

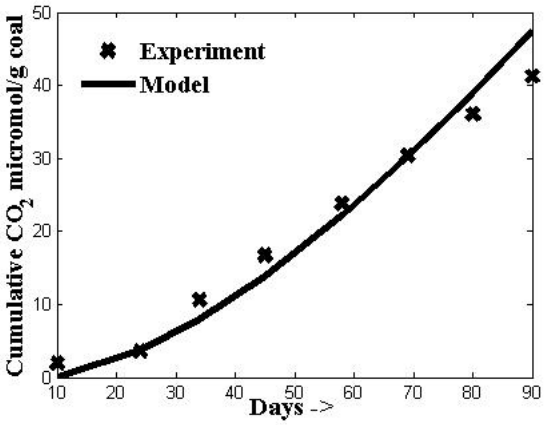

(b) *Comparison of the experimental cumulative CO_2 production data against model predictions.*

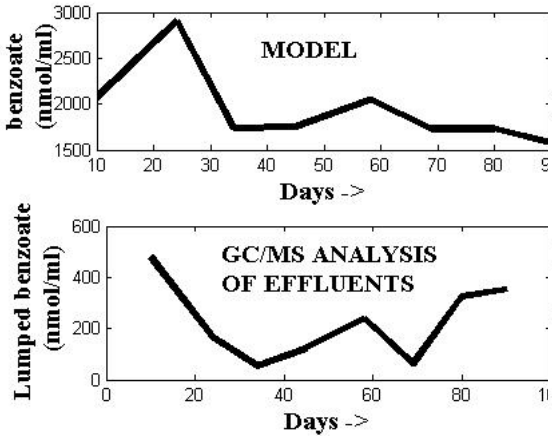

(c) *Comparison of the lumped benzoate concentration from GC/MS analysis against model predictions.*

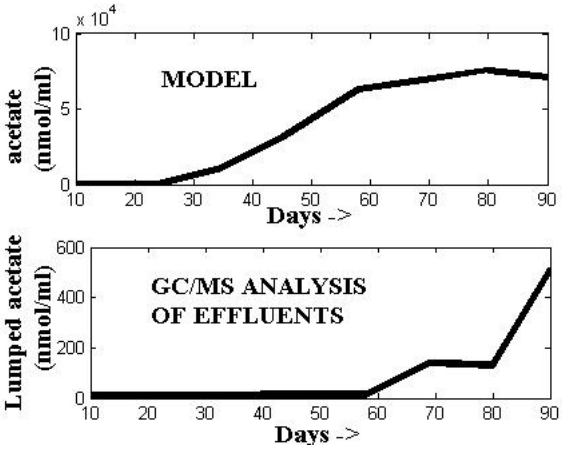

(d) *Comparison of the lumped acetate concentration from GC/MS analysis against model predictions.*

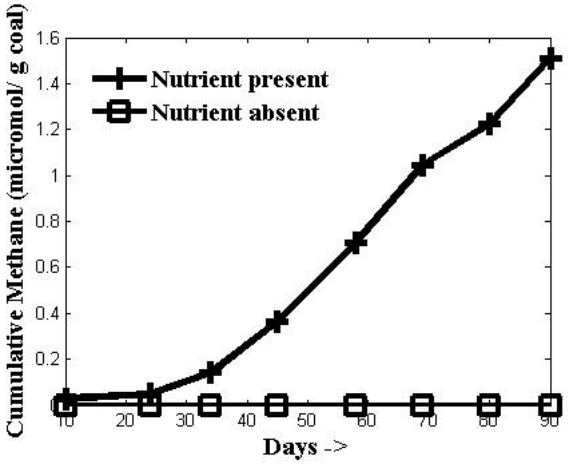

(e) *Cumulative methane generation with and without nutrient addition.*

Figure 3.4: *Comparison of model predictions against the experimental coreholder data.*

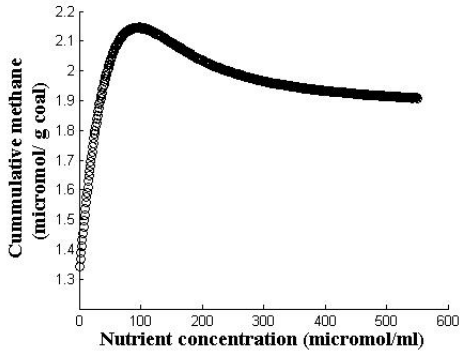

(a) *Cumulative methane generated at the end of* 90 *days for different initial nutrient concentrations.*

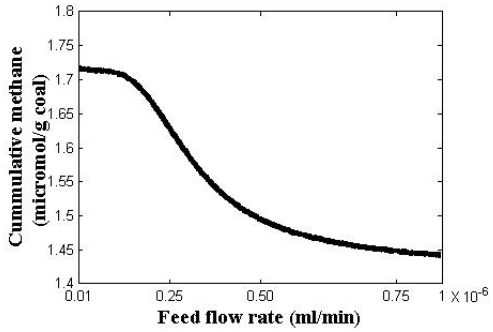

(b) *Cumulative methane generated at the end of* 90 *days for different feed flow rates.*

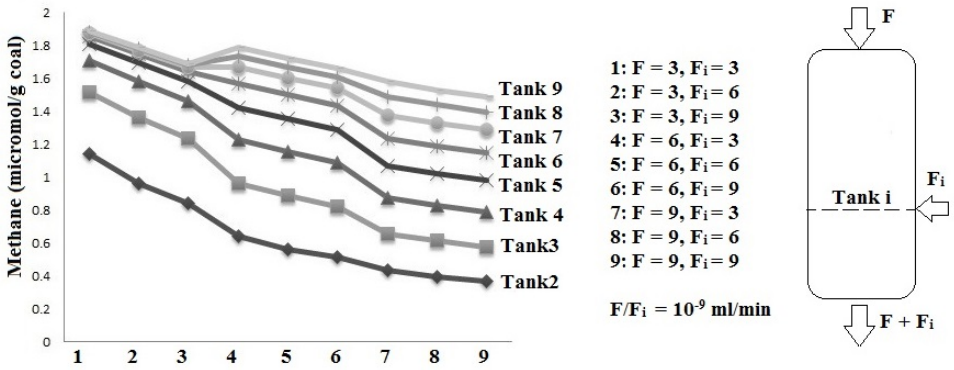

(c) *Cumulative methane generated at the end of* 90 *days with additional fresh nutrient injection in the core.*

Figure 3.5: *Model-based analysis of the effect of varying operating conditions.*

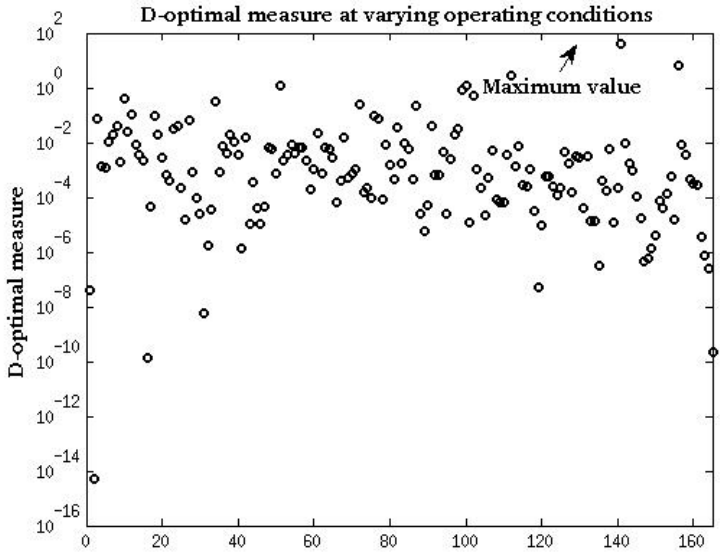

Figure 3.6: *D-optimal metric at different operating conditions.*

g	Stoichiometry											Reaction rate
t > 28 days, One mode exhausted; CSP radical: d[S]/dt = 0												
$\frac{d[C]}{dt}$	-1	0	0	0	0	0	0	0		0		$\underbrace{ke^{S_n[Nu]}\left(\frac{C}{C_0}\right)^{2/3}([S^*]-[S])}_{\text{Dormant}}$
$\frac{d[S]}{dt}$	0	0	0	0	0	0	0	0		0		$b[S]$
$\frac{d[W]}{dt}$	10	0	-1	0	0	0	0	0		0		$\frac{\mu_1[W]}{Ks_1+[W]+Ks_1/Ks_2[Nu]}$
$\frac{d[B]}{dt}$	0	0	1	1	-1	0	0	0		0		$\frac{\mu_2[Nu]}{Ks_2+[Nu]+Ks_2/Ks_1[W]}$
$\frac{d[A]}{dt}$	0	0	0	0	3	-1	0	0		0		$d[B]$
$\frac{d[Nu]}{dt}$	0	0	0	0	0	0	1	0		0		$\frac{e[A]}{f+[A]+[A]^2/g}$
$\frac{d[CH_4]}{dt}$	0	0	0	0	0	1	0	-1		0		r_{Nu}
$\frac{d[CH_{4s}]}{dt}$	0	0	0	0	0	0	0	1		0		r_{CH_4ads}
$\frac{d[CO_2]}{dt}$	0	0	3	0	1	1	0	-1		-1		r_{CH_4des}
$\frac{d[CO_{2s}]}{dt}$	0	0	0	0	0	0	0	0		1		r_{CO_2ads}
		Indicating fast reaction identified by reaction pointer; **b[S]** corresponding to hydrolysis										r_{CO_2des}
		Indicating CSP radical; **[S]**										
Brief time, 37 < t < 40 days, Two modes exhausted; CSP radicals $\frac{d[S]}{dt}=0$, $\frac{d[CO_2]}{dt}+\frac{d[CO_{2s}]}{dt}=0$												
40 <= t < 80 days, Three modes exhausted; CSP radicals $\frac{d[S]}{dt}=0$, $\frac{d[CO_2]}{dt}+\frac{d[CO_{2s}]}{dt}=0$, $\frac{d[B]}{dt}=0$												
$\frac{d[C]}{dt}$	-1	0	0	0	0	0	0	0		0		$\underbrace{ke^{S_n[Nu]}\left(\frac{C}{C_0}\right)^{2/3}([S^*]-[S])}_{\text{Dormant}}$

$\frac{d[S]}{dt}$	0	0	0	0	0	0	0	0		0	$b[S]$
$\frac{d[W]}{dt}$	10	0	-1	0	0	0	0	0		0	$\frac{\mu_1[W]}{Ks_1+[W]+Ks_1/Ks_2[Nu]}$
$\frac{d[B]}{dt}$	0	0	0	0	0	0	0	0		0	$\frac{\mu_2[Nu]}{Ks_2+[Nu]+Ks_2/Ks_1[W]}$
$\frac{d[A]}{dt}$	0	0	2	3	0	-1	-0.7	0		0	$d[B]$
$\frac{d[Nu]}{dt}$	0	0	0	0	0	0	1	0		0	$\frac{e[A]}{f+[A]+[A]^2/g}$
$\frac{d[CH_4]}{dt}$	0	0	0	0	0	1	0	-1		0	r_{Nu}
$\frac{d[CH_{4s}]}{dt}$	0	0	0	0	0	0	0	1		0	r_{CH_4ads}
$\frac{d[CO_2]}{dt}$	0	0	2	0.5	0	0.5	0	-0.5		0	r_{CH_4des}
$\frac{d[CO_{2s}]}{dt}$	0	0	2	0.5	0	0.5	0	-0.5		0	r_{CO_2ads}
		Indicating fast reaction identified by reaction pointer; **b**[**S**] corresponding to hydrolysis; **d**[**B**] corresponding to acidogenesis and $\mathbf{r_{CO_2ads}}$ corresponding to CO_2 adsorption are the fast reactions in this case									r_{CO_2des}
		Indicating CSP radicals; [**S**], [**B**] and $\frac{\mathbf{d[CO_2]}}{\mathbf{dt}} + \frac{\mathbf{d[CO_{2s}]}}{\mathbf{dt}} = \mathbf{0}$									
		0 since desorption rates are not applicable under high pressure at $t < 80$ days									

Table 3.3: *Reduced model based on computational singular perturbation (CSP) with the matrix representation g = Stoichiometry × Reaction rate.*

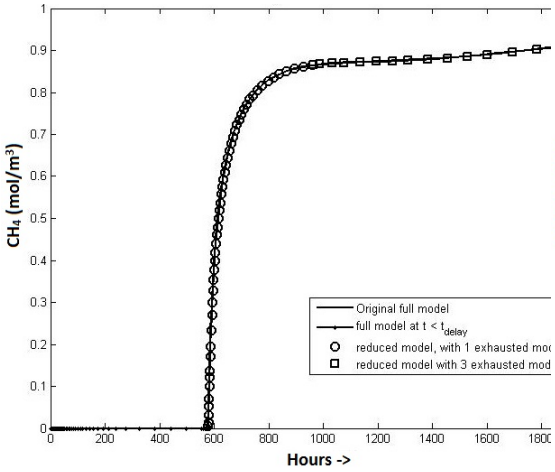

(a) *Prediction of methane production with the reduced model.*

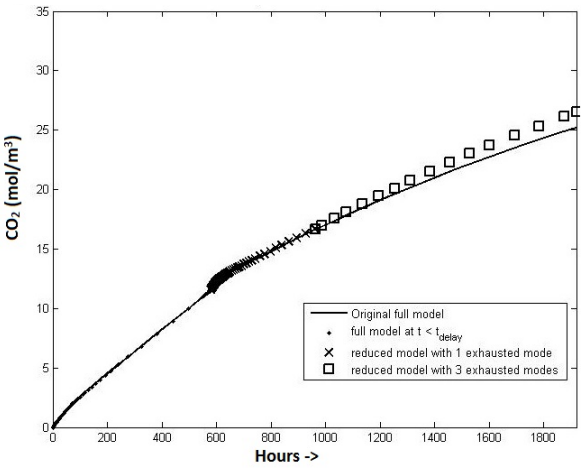

(b) *Prediction of carbon dioxide production with the reduced model.*

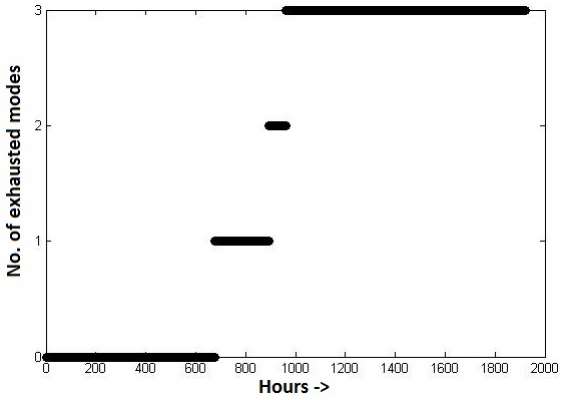

(c) *Number of exhausted modes.*

3.8 Conclusions

In this work, we extend a kinetic model derived to describe the bioconversion of crushed coal in bottles for use in coreflooding experiments, which are used to mimic coalbed methane (CBM) reservoir conditions in terms of porosity, fluid migration and high pressure conditions. Since the concentration of nutrient amendment in the form of tryptone varies along the core (unlike in a small scale bottle), nitrogen-limited microbial growth is included into the model, along with kinetics of the adsorption and desorption of dissolved gases on the surface of the coal. A tanks-in-series model is used to simulate the plug flow in the core, and particle swarm optimization is used to estimate the parameters of the model by minimizing the error between the model predictions and experimental data for methane and carbon dioxide production. The estimated model is then used to study the effect of varying operating conditions and

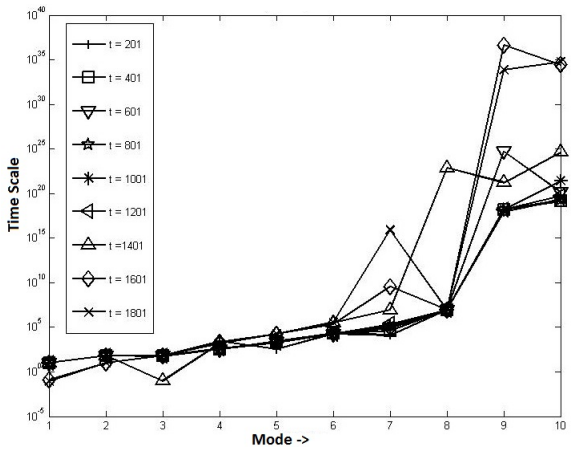

(d) *Time scales of different modes at different times.*

Figure 3.7: *Analysis based on computational singular perturbation.*

to evaluate alternate injection patterns to maximize methane production, and we show that additional nutrient injection at different points in the core can reduce the effects of acetate inhibition and boost methane production. In addition, we suggest operating conditions to perform additional experiments to improve the parameter estimation and the predictive capabilities of the model using the D-optimal criterion. Finally, computational singular perturbation is used to build a reduced order model (with the number of parameters reduced by 5) that can be used more effectively for estimation, prediction and optimization. Our future work focuses on extending the coupled transport and kinetic models to the field scale for estimation and optimization of CBM production.

m_{coal}	Mass of coal in core holder (kg)
r_{coal}	Average radius of coal particle (m)
ρ_{coal}	Density of coal (kg/m^3)
n	Number of tanks in series
V	Volume of each tank (m^3)
F	Feed flow rate into the core (ml/min)
C_0	Initial coal concentration (mol/m^3), $\frac{m_{coal}}{V_{core}}$
M	Total surface area of coal available for adsorption in any tank (m^2)
$[Nu]$	Total concentration of the nitrogen-providing nutrient, tryptone (mol/m^3)
$[C]$	Concentration of coal in any tank (mol/m^3)
$[S]$	Concentration of solubilised coal (mol/m^3)
$[W]$	Concentration of fragmented coal components (mol/m^3)
$[B]$	Concentration of the lumped "benzoate-like" intermediates (mol/m^3)
$[A]$	Concentration of the lumped "acetate-like" intermediates (mol/m^3)
$[CH_4]$	Concentration of methane (mol/m^3)
$[CO_2]$	Concentration of carbon dioxide (mol/m^3)
$[CH_{4s}]$	Concentration of adsorbed methane
$[CO_{2s}]$	Concentration of adsorbed carbon dioxide
k	Reaction rate for microbe-aided solubilization under non-growth conditions (h^{-1})
k_0	Mass transfer coefficient for coal solubilisation in the absence of nutrient ($\frac{mol/m^3/h.m^2}{mol/m^3}$)
X	Quantity of microbes aiding coal solubilization (m^3/m^3)
f_b	Fraction of the surface area of coal particles available for solubilisation; $f_b = k_b\left(\frac{\epsilon}{\epsilon_0}\right)$
S_n	Factor in the exponential scaling of the solubilization rate with respect to the nutrient concentration
b	Rate constant for enzymatic hydrolysis with excess nutrient (h^{-1})
k_1	Nutrient concentration at half the maximum rate of enzymatic hydrolysis under limiting solubilized coal ($\frac{mol}{m^3}$)
μ_1	Maximum reaction rate of of enzymatic acidogenesis at excess fragmented coal and excess nitrogen ($\frac{mol}{m^3.h}$)

μ_2	Maximum rate of lumped benzoate produced from tryptone when it is present in excess ($\frac{mol}{m^3.h}$)
μ_3	Maximum rate at which the nutrient (tryptone) is consumed to produce lumped benzoate when tryptone is in excess ($\frac{mol}{m^3.h}$)
Ks_1	Fragmented coal concentration at half the maximum rate of benzoate, produced in the absence of significant competition from the nutrient (mol/m^3)
Ks_2	Nutrient concentration at half the maximum rate of benzoate produced, in the absence of significant competition from fragmented coal (mol/m^3)
k_2	Nutrient concentration at half the maximum rate of enzymatic acidogenesis under limiting fragmented coal ($\frac{mol}{m^3}$)
d	Rate constant for enzymatic acetogenesis reaction with excess nutrient
k_3	Nutrient concentration at half the maximum rate of enzymatic acetogenesis under limiting benzoate ($\frac{mol}{m^3}$)
k_4	Nutrient concentration at half the maximum rate of enzymatic acidogenesis under limiting acetate ($\frac{mol}{m^3}$)
e/f	First order rate constant for of methanogenesis at low acetate concentrations (h^{-1})
eg	Negative first order rate constant for methanogenesis at high acetate concentrations ($(mol/m^3)^2 h^{-1}$)
K_{Nus}	First order reaction rate for nutrient consumed while providing nitrogen to microbes (h^{-1})
kad_m	Rate constant for diffusion of methane from liquid bulk to the solid surface ($1/h.m^2$)
$kads_m$	Fraction of surface area occupied per mole of methane per m^2 area available (m^3/mol)
kd_m	Desorption rate constant for adsorbed methane (h^{-1})
kad_c	Rate constant for diffusion of carbon dioxide from liquid bulk to the solid surface ($1/h.m^2$)
$kads_c$	Fraction of surface area occupied per mole of carbon dioxide per m^2 area available (m^3/mol)
kd_c	Desorption rate constant for adsorbed methane (h^{-1})
r_i	Reaction rate for species i

Table 3.4: *Table of Notation*

References

[1] Senthamaraikkannan, G., Budwill, K., Gates, I., Mitra, S., and Prasad, V. Kinetic modeling of the biogenic production of coalbed methane. *(submitted)*, 2015.

[2] Harris, S. H., Smith, R. L., and Barker, C. E. Microbial and chemical factors influencing methane production in laboratory incubations of low-rank subsurface coals. *International Journal of Coal Geology*, 76(1):46–51, 2008.

[3] D Strapoc, D., Mastalerz, M., Dawson, K., Macalady, J., Callaghan, A. V., Wawrik, B., Turich, C., and Ashby, M. Biogeochemistry of microbial coal-bed methane. *Annual Review of Earth and Planetary Sciences*, 39:617–656, 2011.

[4] Budwill, K., Koziel, S., and Vidmar, J. Advancements in understanding and enhancing biogenic methane production from coals. In *Canadian Unconventional Resources Conference*. Society of Petroleum Engineers, 2011.

[5] Mazumder, S., Wolf, K., Van Hemert, P., and Busch, A. Laboratory experiments on environmental friendly means to improve coalbed methane production by carbon dioxide/flue gas injection. *Transport in porous media*, 75(1):63–92, 2008.

[6] Nobakht, M., Moghadam, S., and Gu, Y. Mutual interactions between crude oil and CO2 under different pressures. *Fluid Phase Equilibria*, 265(1):94–103, 2008.

[7] Shen, P., Wang, J., Yuan, S., Zhong, T., Jia, X., et al. Study of enhanced-oil-recovery mechanism of alkali/surfactant/polymer flooding in porous media from experiments. *SPE Journal*, 14(02):237–244, 2009.

[8] Stephen, A., Adebusuyi, A., Baldygin, A., Shuster, J., Southam, G., Budwill, K., Foght, J., Nobes, D. S., and Mitra, S. K. Bioconversion of coal: new insights from a core flooding study. *RSC Advances*, 4(43):22779–22791, 2014.

[9] Davidson, K. Modeling microbial food webs. *Marine Ecology Progress Series*, 145(1):279–296, 1996.

[10] Bryant, M., Tzeng, S., and Robinson, I. Nutrient requirements of methanogenic bacteria. *Urbana*, 101:61801, 1971.

[11] Stephen, A. private communication, 2015.

[12] Yoon, H., Klinzing, G., and Blanch, H. Competition for mixed substrates by microbial populations. *Biotechnology and Bioengineering*, 19(8):1193–1210, 1977.

[13] Demirel, B. and Scherer, P. The roles of acetotrophic and hydrogenotrophic methanogens during anaerobic conversion of biomass to methane: a review. *Reviews in Environmental Science and Bio/Technology*, 7(2):173–190, 2008.

[14] Jalali, J. *A Coalbed Methane simulator designed for the independent producers*. Master's thesis, West Virginia University, 2004.

[15] Kennedy, J. and Eberhart, R. Particle swarm optimization. In *Encyclopedia of Machine Learning*, pages 760–766. Springer, 2010.

[16] Lee, C. J., Prasad, V., and Lee, J. M. Stochastic nonlinear optimization for robust design of catalysts. *Industrial & Engineering Chemistry Research*, 50(7):3938–3946, 2011.

[17] Asprey, S. and Macchietto, S. Designing robust optimal dynamic experiments. *Journal of Process Control*, 12(4):545–556, 2002.

[18] Vlachos, D., Mhadeshwar, A., and Kaisare, N. S. Hierarchical multiscale model-based design of experiments, catalysts, and reactors for fuel processing. *Computers & Chemical Engineering*, 30(10):1712–1724, 2006.

[19] Lam, S. Using CSP to understand complex chemical kinetics. *Combustion Science and Technology*, 89(5-6):375–404, 1993.

[20] Lam, S. and Goussis, D. The CSP method for simplifying kinetics. *International Journal of Chemical Kinetics*, 26(4):461–486, 1994.

[21] Zagaris, A., Kaper, H. G., and Kaper, T. J. Two perspectives on reduction of ordinary differential equations. *Mathematische Nachrichten*, 278(12-13):1629–1642, 2005.

[22] Burruss, R. C. CO_2 adsorption in coals as a function of rank and composition: A task in USGS research on geologic sequestration of CO_2. In *Presentation on the Second International Forum on Geologic Sequestration of CO2 in Deep, Unmineable Coalseams (Coal-Seq II), Washington DC*. 2003.

[23] Bromhal, G. S., Sams, W. N., Jikich, S., Ertekin, T., and Smith, D. H. Simulation of CO_2 sequestration in coal beds: The effects of sorption isotherms. *Chemical Geology*, 217(3):201–211, 2005.

Chapter 4

Development of multiscale microbial kinetics coupled gas transport model for simulation of biogenic coalbed methane production

Abstract

In this chapter, we develop a multiscale model to simulate coalbed methane (CBM) production from reservoirs along with the inclusion of secondary biogenic gas generated by the continued anaerobic breakdown of coal. A two-step gas transport model is derived for this purpose, based on the assumption that coal porosity can be classified into two scales, macropores and micropores. The model assumes laminar gas flow in macropores and diffusive flow in micropores, driven by desorption. Surface diffusion of gas due to the Klinkenberg effect occurring at low permeability and pressure conditions is also considered. The transport model built for gas flow simulation in a 1D radial reservoir is non-dimensionalized and solved using the Levenberg-Marquardt method. The Morris OAT (one-at-a-time) method for global sensitivity analysis is used to identify important gas transport/storage parameters to perform model refinement for history matching of production data from the gas producing phase of Manville wells found in Alberta. The validated transport model is then combined with a suitably modified enzymatic reaction kinetic model for coal bioconversion that was originally developed by us for lab-scale experiments. Finally, parametric investigations revealed that an increase in the methanogenesis rate can significantly improve biogenic gas recovery, and the next most significant parameter is the solubilization rate.

4.1 Introduction

Coalbed methane (CBM) is a mixture of methane (approximately 80 - 99% by volume) and other gases such as carbon dioxide, nitrogen, hydrogen sulphide, sulphur dioxide and heavier hydrocarbons such as ethane, propane and butane. It is an unconventional source of natural gas produced from gas wells drilled into relatively shallow coal beds (typically around 1000-1500 ft). Today, it is a rapidly growing significant energy source for various reasons, the most attractive of them being the higher calorific value and cleaner burning properties as compared to coal. According to reports from the International Energy Agency in 2008, CBM contributed to 10% of natural gas production in US, followed by 4% in Canada and 8% in Australia. It is also being extracted in countries with large coal reserves such as India, China, Russia and Indonesia[1].

CBM is produced in coalbeds either by thermocatalytic cracking at elevated pressures and temperatures (known as thermogenic methane) or by the anaerobic attack of organic matter in coal (known as biogenic methane). Biogenic methane production in coalbeds following the restoration of viable conditions for microbial growth is known as secondary biogenic methane production. A rational approach to improve or enhance biogenic methane generation requires real-time dynamic modeling and simulation of CBM generation and recovery from coal fields. However, this is a challenging proposition mainly because of the presence of heterogeneous multiscale porous structures in coalbeds and the associated multiscale gas transport and storage processes coupled with complicated heterogeneous networks for enzymatic coal breakdown. While production curves were used in the past, many models are available today for the prediction of gas production in CBM reservoirs, following the use of dual mechanism gas transport models by King[2] in 1985. However, the models do not account for ongoing microbial activity.

In this study, we have simulated coalbed methane production with ongoing microbial activity by solving gas transport equations that contain source terms relating to gas production due to coal bioconversion. For simplification, we have analysed gas flow in a one dimensional (1D) radial field. The sequence of model development is presented in the following sections. A gas transport model is derived based on dual porosity characteristics and scaling analysis is performed to deduce dimensionless numbers useful in scale-up applications. The transport model is validated by history matching production data from different Manville wells in Alberta and later simulated in conjunction with an enzymatic reaction kinetic model for coal bioconversion that was developed in our previous study[3]. This model simulating secondary biogenic CBM production can potentially be upscaled for multi-phase field scale reservoir simulations of commercial CBM production.

4.2 Gas transport in coal seams

4.2.1 Dual porosity characterization of coalbeds

CBM reservoirs are highly heterogeneous with pore scales varying on a wide range. Based on SEM studies on Australian coals, pore structures (occurring in varying proportions depending on the type/rank of coal) were classified into micropores (<2 nm), mesopores (2-50 nm) macropores (>50 nm), open fractures (0.05 - 20μ m wide) and main fractures (0.1 - 2 mm wide).[4–6] However since there are many validated mathematical models simulating coalbeds with only two scales of porosity, dual porosity has been accepted as a reasonable assumption. The two levels of pore spaces in a dual porosity model are macropores and micropores, interchangeably referred to as fracture porosity and matrix porosity, respectively. Macropores are the natural fractures inherent in coal seams and micropores, surrounded by macropores constitute the primary porosity system. While only a small amount of gas is present in its free state within macropore spaces, micropores usually account for as much as 85% of total coal porosity,[7] storing most of the gas in its adsorbed state. Also, micropores are considered inaccesible to water owing to small pore dimensions.[8]

4.2.2 Dual mechanism gas transport

Methane drainage process from dual porosity reservoirs is treated as a two-step process, consisting of laminar flow through macropores and diffusional flow out of micropores. When production begins, water filled in macropores starts draining out. This leads to reduced pressure in coal seams causing the flow of free gas in macropores as well as desorption and diffusion of stored gases out of the micropores towards a producer well. Based on dual porosity characteristics, there are many available models for simulation of fluid flow in coal seams. King et al.[8] and Remner et al.[9] developed single permeability flow models based on non-equilibrium sorption using a pseudo steady-state formulation that was extended to hydraulically fractured coal seams by Sung et al.[10] Clarkson et al.[11] incorporated a pressure dependent sorption component to a gas flow model and Sawyer et al.[12] simulated two phase flow in 3-dimensional grid blocks with multiple wells, accounting for matrix shrinkage and swelling. Manik et al.[13] introduced dual permeability for application in ECBM (enhanced coal bed methane) recovery, while Thararoop et al.[14] developed a dual porosity dual permeability model by considering the presence of water within the micropore matrix, too.

In this work, gas transport equations in a dual porosity single permeability reservoir with non-equilibrium sorption proposed by King et al.[8] are coupled with a reaction

kinetic model for coal bioconversion to simulate radial gas inflow into a horizontal well. Since the model only considers gas flow, the water required for the survival and growth of microbes is assumed to be available from residual water left in macropore spaces after drainage. Also, since microbes can only access fractures[15,16] and micropores are inaccessible to water,[6,8,17–20] microbial activity is assumed to occur only on the surface of the macropores.

4.3 Gas transport model development

First, gas transport equations are derived by superimposing a one-dimensional (1D) radial coordinate system on a coal seam and performing material balances on an elemental volume of the coal seam (or reservoir). Darcy's law is applied to model laminar flow of gases in the macropores. Since coal seams usually have low pressures and low absolute permeabilities, gas slippage is also included in the transport equation by introducing an effective permeability. Based on the Klinkenberg effect, the effective gas permeability k' at a finite pressure is given by[21,22]

$$k' = k\left(1 + \frac{b(P_g)}{P_g}\right) \text{ where } b = \frac{c_g P_g D_{ma} \mu}{k} \tag{4.1}$$

Gas diffusion in coals from micropores into the macropore spaces is controlled by desorption and diffusion rates. The two processes are generally lumped in numerical models. Among the different models available for simulating gas diffusion[23], the non-equilibrium sorption model with a pseudo steady-state formulation as proposed by King[8] is considered. The various assumptions in model development are listed below.

4.3.1 Assumptions in modeling

1. The flow velocity is assumed to have only a radial component, $\overrightarrow{u} = u * \overrightarrow{e}_{radial}$, since 1D radial gas inflow into a horizontal well is modeled (Figure 4.1a).
2. Gas flow through macropores follow Darcy's law and obey the real gas law. Since the gas deviation factor Z changes insignificantly with pressure, it is considered to be constant. Similarly, the gas viscosity μ is also assumed to remain constant.
3. There is no change in the temperature during degasification. The isothermal gas compressibility c_g in Equation 4.1 is approximated as $c_g \approx 1/P_g$.
4. Gas found adsorbed in micropores is always at a pseudo steady-state or pseudo equilibrium with gas pressure in the macropores and is modeled by the Langmuir isotherm.

5. The permeability of gas in the macropores, surface diffusion constant, micropore gas diffusion time constant and the corresponding geometry dependent factor are assumed to be homogeneous and isotropic.

6. All water in the coal seam is assumed to be produced, and only the gas phase is considered. Water necessary for microbial activity is assumed to be available between macropore spaces.

7. Also, it is assumed that the gas phase contains a single component - methane.

8. Changes in the macropore porosity and permeability due to matrix shrinkage or swelling caused by gas sorption is not considered by assuming that these effects are negligible.

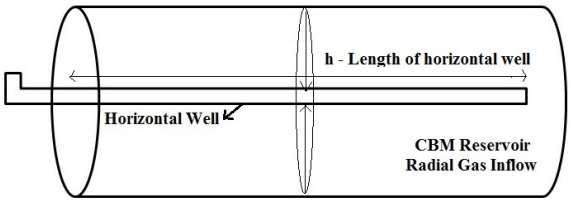

(a) *Gas inflow into a horizontal well in a one-dimensional radial gas reservoir.*

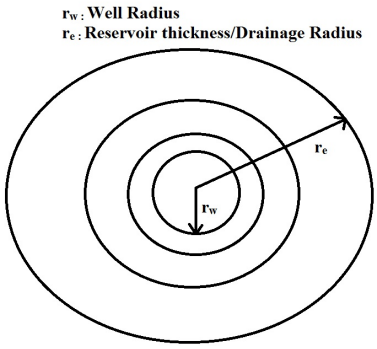

(b) *Logarithmically spaced radial co-ordinates*

Figure 4.1: *Coalbed methane reservoir model for radial gas inflow.*

4.3.2 Coupled nonlinear gas transport equations

Single phase radial gas transport in a dual porosity coalbed reservoir is described by the equation of continuity as

$$\begin{aligned} -\frac{1}{r}\frac{\partial}{\partial r}(r\rho_g\vec{u_g}) + \frac{Q_t}{V_{bma}} &= \frac{\partial}{\partial t}(\rho_g\phi_{ma}), \\ \overrightarrow{u_g} &= -\frac{k}{\mu}\frac{\partial P_g}{\partial r} \end{aligned} \tag{4.2}$$

where V_{bma} is the macropore volume, $\vec{u_g}$ is the laminar gas velocity defined by Darcy's law, $\frac{k}{\mu}$ or λ is the mobility of gas in macropores, $\frac{Q_t}{V_{bma}}$ is the amount of gas diffusing from micropores per unit macropore volume, ρ_g is the gas density and ϕ_{ma} is the macropore porosity. Based on the real gas law, $\rho_g = \frac{P_g M}{ZRT}$. Substituting for ρ_g and $\overrightarrow{u_g}$, we get

$$\frac{1}{r}\frac{\partial}{\partial r}\left(\frac{rP_g}{Z}\frac{k}{\mu}\frac{\partial P_g}{\partial r}\right) + \frac{P_{sc}T}{T_{sc}}\frac{q_t}{V_{bma}} = \frac{\partial}{\partial t}\left(\frac{P_g\phi_{ma}}{Z}\right) \tag{4.3}$$

where $\frac{q_t}{V_{bma}}$ is the amount of gas diffusing from micropores per unit macropore volume, at standard conditions and P_{sc}, T_{sc} are the standard pressure and temperature, respectively.

To account for gas slippage, macropore permeability is replaced with effective permeability (from Equation 4.1) giving

$$\frac{1}{r}\frac{\partial}{\partial r}\left(\frac{rP_g}{Z}\left(\frac{k}{\mu} + \frac{D_{ma}}{P_g}\right)\frac{\partial P_g}{\partial r}\right) + \frac{P_{sc}T}{T_{sc}}\frac{q_t}{V_{bma}} = \frac{\partial}{\partial t}\left(\frac{P_g\phi_{ma}}{Z}\right) \tag{4.4}$$

where D_{ma} is the Klinkenberg factor.

Integrating Equation 4.4 over V_{bma}, we obtain the volumetric weighted average of the quantity of gas diffusing from micropores, denoted by $\left[\frac{q_t}{V_{bma}}\right]$.

$$\int_{V_{bma}} \frac{1}{r}\frac{\partial}{\partial r}\left(\frac{rP_g}{Z}\left(\frac{k}{\mu} + \frac{D_{ma}}{P_g}\right)\frac{\partial P_g}{\partial r}\right)dV + \frac{P_{sc}T}{T_{sc}} \underbrace{\left[\frac{q_t}{V_{bma}}\right]}_{\textit{(averaged quantity)}} = \int_{V_{bma}} \frac{\partial}{\partial t}\left(\frac{P_g\phi_{ma}}{Z}\right)dV \tag{4.5}$$

Based on a lumped diffusion-desorption model, which assumes desorption to be a fast step, $\left[\frac{q_t}{V_{bma}}\right]$ is evaluated as

$$\left[\frac{q_t}{V_{bma}}\right] = -L_{mi}\frac{\partial V_{mi}}{\partial t};\ \text{where } \frac{\partial V_{mi}}{\partial t} = \tau_{mi}(V_E(P_g) - V_{mi}) \tag{4.6}$$

where τ_{mi} is the micropore gas diffusion time constant, L_{mi} is the corresponding geometry dependent factor, V_{mi} is the gas quantity within the micropores and V_E is

the pseudo equilibrium quantity of gas adsorbed on the surface of micropores, defined by the Langmuir isotherm as, $V_E = \frac{V_l P_g}{P_l + P_g}$.

Discretising Equations 4.5 and 4.6 with forward derivative approximations, we get

$$\begin{aligned}
&(PF_{ma})_{i+1/2}\left[\frac{P_g}{Z}\left(\frac{k}{\mu}+\frac{D_{ma}}{P_g}\right)^{N+1}_{i+1/2}({P_{g_{i+1}}}^{N+1}-{P_{g_i}}^{N+1})\right]- \\
&(PF_{ma})_{i-1/2}\left[\frac{P_g}{Z}\left(\frac{k}{\mu}+\frac{D_{ma}}{P_g}\right)^{N+1}_{i-1/2}({P_{g_i}}^{N+1}-{P_{g_{i-1}}}^{N+1})\right] \\
&+\frac{P_{sc}T}{T_{sc}}\left[\frac{q_t}{V_{bma}}\right]_i^{N+1/2}=\frac{1}{\delta t}\left(\frac{\phi_{ma}{P_g}^{N+1}}{Z}_i-\frac{\phi_{ma}{P_g}^{N}}{Z}_i\right) \\
&\text{where } (PF_{ma})_{i+1/2}=\frac{2r_{i+1/2}}{(r^2_{i+1/2}-r^2_{i-1/2})(r_{i+1}-r_i)} \\
&\text{and } (PF_{ma})_{i-1/2}=\frac{2r_{i-1/2}}{(r^2_{i+1/2}-r^2_{i-1/2})(r_i-r_{i-1})}
\end{aligned} \tag{4.7a}$$

$$\begin{aligned}
\left[\frac{q_t}{V_{bma}}\right]_i^{N+1/2} &= L_{mi}\left(\frac{1-exp(-\frac{\delta t}{\tau})}{\delta t}\right)\left({V_{mi}}_i^N - V_E(P_g)_i^N\right) \text{ where,} \\
{V_{mi}}_i^{N+1} &= \exp(-\frac{\delta t}{\tau}){V_{mi}}_i^N + \left(1-\exp(-\frac{\delta t}{\tau})\right)V_E(P_g)_i^N \text{ and} \\
V_E({P_g^N}_i) &= \frac{V_E({P_g^{N+1}}_i)+V_E({P_g^N}_i)}{2}
\end{aligned} \tag{4.8}$$

The implicit formulations in coupled Equations 4.7a and 4.8 are solved by the Levenberg-Marquardt algorithm for an initial reservoir gas pressure P_g^0 and an initial micropore surface gas concentration, $V_{mi}^0 = \frac{V_l P_g^0}{P_l + P_g^0}$. The boundary conditions are defined by a constant well operating pressure P_{wf}, applied at the inner boundary and a pressure far field condition applied at the external boundary (as seen in Equation 4.9).

$$\left.\frac{\partial P_g}{\partial r}\right|_{\text{External boundary}} = \alpha(P_g - P_g^0) \tag{4.9}$$

Thus coalbed methane gas flow in a dual porosity reservoir is evolved based on the above gas transport model. Solutions are obtained at logarithmically spaced radial

co-ordinates, $r_i = r_w \left(\frac{r_e}{r_w}\right)^{\frac{i-1}{NI-1}}$ and discrete time steps, $0\ \delta t\ 2\delta t \ldots T$; where NI is the number of radial grids the reservoir volume is divided into and T is the total simulation time. Logarithmic grid spacing (shown in Figure 4.1b) is relevant because pressure gradients are higher in the vicinity of well bores[23].

4.3.3 Non-dimensionalization of the gas transport model

We introduce the dimensionless variables

$$\tilde{r} = \frac{r}{R_0}, \tilde{P}_g = \frac{P_g}{P_0}, \tilde{t} = \frac{t}{t_0} \tag{4.10}$$

where R_0, P_0 and t_0 are the reference length, pressure and time, characteristic of the system. Substituting the dimensionless variables in Equation 4.10 into Equations 4.7a and 4.8, we get dimensionless equations of the form

$$\begin{aligned}
&\frac{(\tilde{PF}_{ma})_{i+1/2}}{\Pi_1'}\left[\tilde{P}_{gi+1/2}^{N+1} + \frac{\Pi_1'}{\Pi_2'}\right]\left(\tilde{P}_{gi+1}^{N+1} - \tilde{P}_{gi}^{N+1}\right) - \\
&\frac{(\tilde{PF}_{ma})_{i-1/2}}{\Pi_1'}\left[\tilde{P}_{gi-1/2}^{N+1} + \frac{\Pi_1'}{\Pi_2'}\right]\left(\tilde{P}_{gi}^{N+1} - \tilde{P}_{gi-1}^{N+1}\right) \qquad (4.11a)\\
&+ \frac{P_{sc}TZL_{mi}}{P_0T_{sc}}\frac{(1-exp(-\delta\tilde{t}\Pi_3'))}{\delta\tilde{t}}\left(V_{mi}^N - V_E(P_g)_i^N\right) = \frac{\left(\tilde{P}_{gi}^{N+1} - \tilde{P}_{gi}^N\right)}{\delta\tilde{t}/\phi_{ma}}\\
&{V_{mi}}_i^{N+1} = \exp(-\delta\tilde{t}\Pi_3'){V_{mi}}_i^N + (1-\exp(-\delta\tilde{t}\Pi_3'))V_E(P_g)_i^N \qquad (4.11b)\\
&\text{where } \Pi_1' = \frac{R_0^2}{\lambda P_0 t_0},\ \Pi_2' = \frac{R_0^2}{D_{ma}t_0} \text{ and } \Pi_3' = \frac{t_0}{\tau} \qquad (4.11c)
\end{aligned}$$

By combining Π_1' and Π_2', we get

$$\Pi_4' = \frac{\Pi_1'}{\Pi_2'} = \frac{D_{ma}/P_0}{\lambda} \equiv \frac{\text{Klinkenberg effect}}{\text{Laminar flow}} \tag{4.12}$$

where Π_4' is a measure of the ratio between Klinkenberg effect and laminar Darcy flow in macroporous spaces. When Π_4' is low, gas flow is dominated by Darcy's flow, whereas, gas slippage (or Knudsen diffusion) dominates at high values. Under such

conditions, molecules no longer behave as a viscous fluid; instead they act like independent molecules, colliding back and forth between flow boundaries as they travel through pore spaces[24]. Similarly, $\Pi'_3 = \frac{t_0}{\tau}$ is a measure of the ratio between the characteristic time scale and the micropore diffusion time constant. The contribution of micropore diffusion is significant only at low characteristic reservoir pressure, P_0. Table 4.1 shows the role of dimensionless numbers Π'_3 and Π'_4 in the analysis of the different forms of gas transport occurring in the dual porosity reservoir. Apart from this, when values of reference variables are appropriately chosen, non-dimensionalization also reduces the computational difficulty involved in solving stiff multiscale transport equations.

<table>
<tr><th></th><th>Laminar flow</th><th>Gas Slippage</th><th>Micropore gas diffusion</th><th></th></tr>
<tr><td>$\mathbf{\Pi'_4 >> \tilde{P}^{N+1}_{gi+1/2}}$</td><td>✗</td><td>✓</td><td rowspan="2"></td><td></td></tr>
<tr><td>$\mathbf{\Pi'_4 << \tilde{P}^{N+1}_{gi+1/2}}$</td><td>✓</td><td>✗</td><td></td></tr>
<tr><td>$\mathbf{\Pi'_3 << 1}$</td><td rowspan="2" colspan="2"></td><td>$\propto \Pi'_3(V^N_{mi} - V_E(P^N_{gi}))$</td><td>$\downarrow P_0$</td></tr>
<tr><td>$\mathbf{\Pi'_3 >> 1}$</td><td>$\propto \frac{(V^N_{mi} - V_E(P^N_{gi}))}{\tilde{\delta t}}$</td><td></td></tr>
<tr><td colspan="2"></td><td>≈ 0</td><td>$\uparrow P_0$</td></tr>
</table>

Table 4.1: *Analysis of laminar flow and gas slippage in macropores and gas diffusion from micropores, based on dimensionless numbers* Π'_3 *and* Π'_4.

4.4 Model validation based on history matching of production data

History matching is the process of reservoir model refinement to match historical production data. To validate the transport model developed in the previous sections,

we perform history matching of coalbed methane production data from Manville wells in Alberta as available from public databases[25]. Prior to this, we perform sensitivity analysis to identify the most important parameters in the model.

4.4.1 Sensitivity analysis

Global sensitivity analysis was conducted for the model described above based on the Morris one-at-a-time (OAT) sensitivity method. In this method, each parameter in the parameter space is scaled to the unit interval $[0, 1]$ and partitioned into $(p-1)$ intervals[26,27]. Nominal parameter sets are then chosen by randomly selecting values from the set $\{0, 1/(p-1), 2/(p-1), ...1-\Delta\}$, where $\Delta = \frac{p}{2(p-1)}$ is the fixed increment added to each parameter in random order to compute elementary effects of each parameter. The elementary effect of each parameter is then computed as

$$EE_i = \frac{1}{\Delta}\frac{P(p_1, \cdots p_i + \Delta, \cdots p_n) - P(p_1 \cdots p_n)}{\tau_y}$$

where i is the index of the parameter, P is the gas production evaluated at $[p_1 \cdots p_n]$ and τ_y is the output scaling factor. Statistical metrics of elementary effects (EE) computed for each parameter over an ensemble of nominal parameter sets are then evaluated, with the mean value representing the average effect of each parameter and the standard deviation representing nonlinearities and/or interaction effects.[26]

The range of model parameters considered for global sensitivity sensitivity analysis in this study is shown in Table 4.2.

Parameter	Unit	Range
λ	mD	[0.01 - 0.1]
D_{ma}	cm^2/s	[0.0001 - 0.01]
τ	days	[12 - 60]
V_l	$\frac{m^3}{m^3}$	[150 - 300]
P_l	MPa	[0.5 - 10]

Table 4.2: *Range of the model parameters analysed using global sensitivity.*

Gas production at each parameter set is evaluated based on solutions to the non-dimensional gas transport model in Equation 4.11. The reference scales are chosen as $R_0 = \sqrt{D_{ma}\tau}$, $P_0 = \frac{D_{ma}}{\lambda}$ and $t_0 = \tau$ such that $\Pi_1' = \Pi_2' = \Pi_3' = 1$, indicating that

flow in macropores is a combination of laminar flow and gas slippage with significant contribution from micropore gas diffusion as well. Figure 4.2 shows the mean and standard deviation of the ensemble of elementary effects of each parameter, evaluated at an initial reservoir pressure of $P_g^0 = 1$ MPa and a constant well operating pressure of $P_{wf} = 0.14$ MPa. It is to be noted that elementary effects may vary with change in initial and boundary conditions.

Figure 4.2a shows the average of the ensemble of elementary effects for each parameter with time. D_{ma} is the most sensitive parameter, followed by λ. However, the effects of both D_{ma} and λ diminish with time. V_l is the next most sensitive parameter, with its effect on gas production increasing over time. P_l has low sensitivity, whereas τ has a negative effect on production, indicating that production decreases with increase in τ. The effects of both τ and P_l remain almost constant with time.

Figure 4.2b shows the standard deviation of the ensemble of elementary effects for each parameter with time. Since the standard deviation reflects nonlinearities/interaction effects, we interpret that τ has the least effect on the response, followed by P_l. λ and D_{ma} are affected the most, although this diminishes with time. V_l, on the other hand, appears undisturbed in the beginning, but gradually responds significantly to other parameter value changes.

4.4.2 Results of history matching of gas production from Manville wells

In this section, reservoir parameters in the gas transport model (in Equation 4.7a) are estimated based on history matching of gas production data from 8 different Manville wells, managed and made commercially available to the public by IHS Inc.[25] The appropriate single phase gas production is obtained by truncation of the water producing phase occurring prior to the gas producing phase (as seen in Figure 4.3). During history matching, transport model parameters λ and D_{ma} are varied, based on the results of sensitivity analysis. Apart from reservoir parameters, the initial reservoir pressure P_g^0 and α, determining the external boundary condition (Equation 4.9), are also varied. The reservoir model variables that are unchanged during history matching of all the 8 wells are shown in Table 4.3. Results of history matching and the corresponding model parameters are shown in Figure 4.4 and Table 4.4, respectively.

Parameter	Value
Coal seam thickness (drainage radius) r_e	15 m
Reservoir temperature T	300 K
Well radius r_w	0.086 m
Length of horizontal well h	630 m
Well operating pressure P_{wf}	0.14 MPa
Number of radial grid points NI	40
Simulation time step dt	8640 s

Table 4.3: *Values of reservoir model variables that are unchanged during history matching of gas production from 8 different Manville wells.*

	λ mD	D_{ma} cm^2/s	τ days	V_l m^3/m^3	P_l MPa	P_g^0 MPa	ϕ_{ma} %	α -
W172	0.5	0.013	12	150	1	10	2	-0.01
W188	0.5	0.02	12	150	1	10	2	-0.005
W191	0.1	0.012	12	150	1	10	2	-0.01
W205	0.1	0.03	12	150	1	10	2	-0.02
W209	0.1	7×10^{-3}	12	150	1	10	2	0
W263	0.06	10^{-4}	12	150	1	20	2	0
W270	0.1	0.02	12	150	1	10	2	-0.04
W284	0.07	7×10^{-3}	12	150	1	12	2	-0.01

Table 4.4: *Input parameters used in the history matching of production data from the Manville wells.*

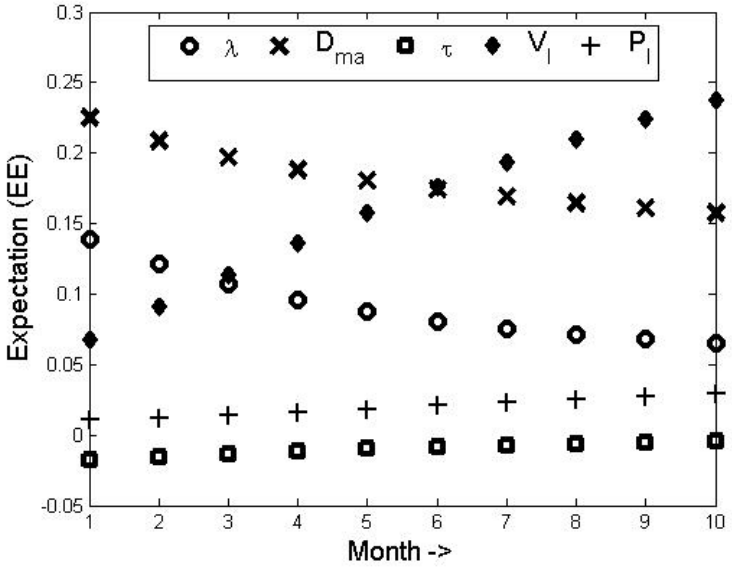

(a) *Expectation of the ensemble of elementary effects (EE), evaluated for each parameter.*

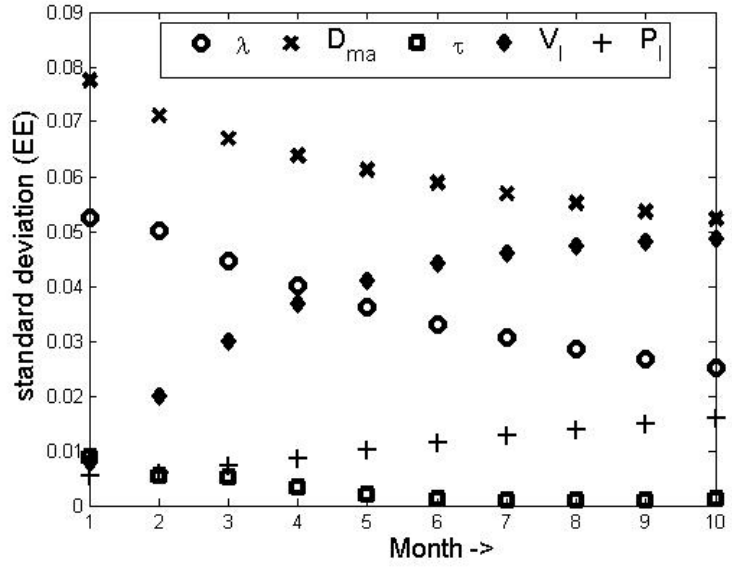

(b) *Standard deviation of the ensemble of elementary effects (EE), evaluated for each parameter.*

Figure 4.2: *Results of global sensitivity analysis by the Morris OAT (one-at-a-time) method.*

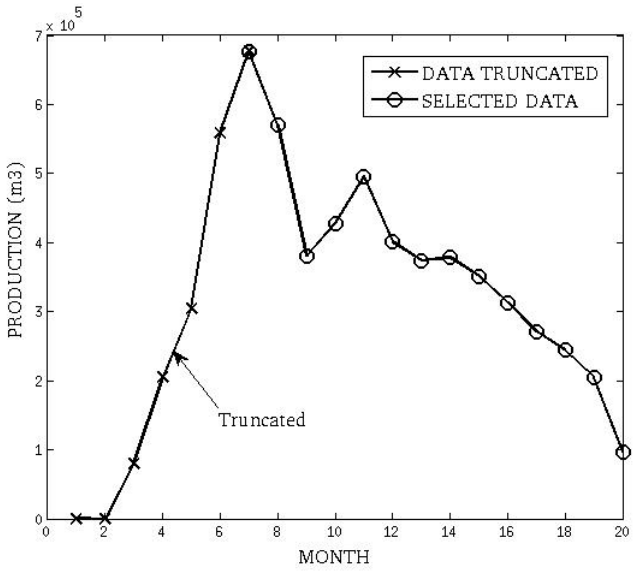

Figure 4.3: *Gas production after the end of the dewatering phase.*

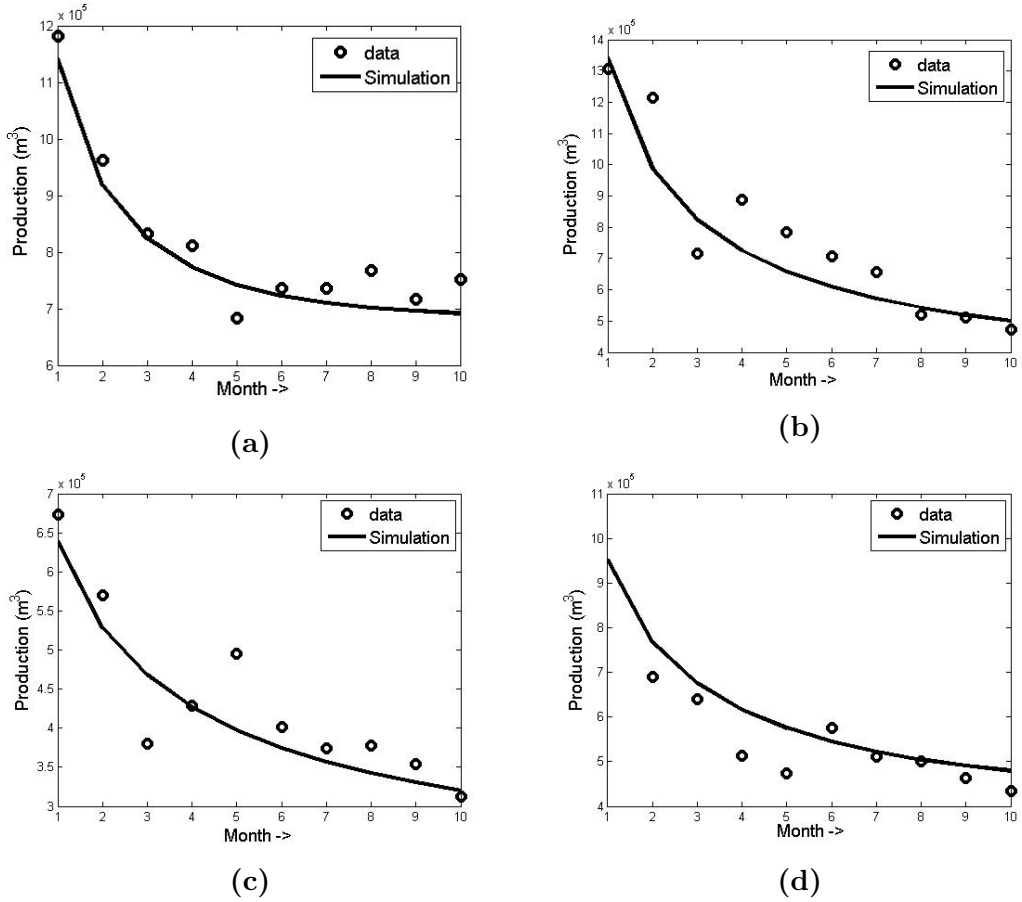

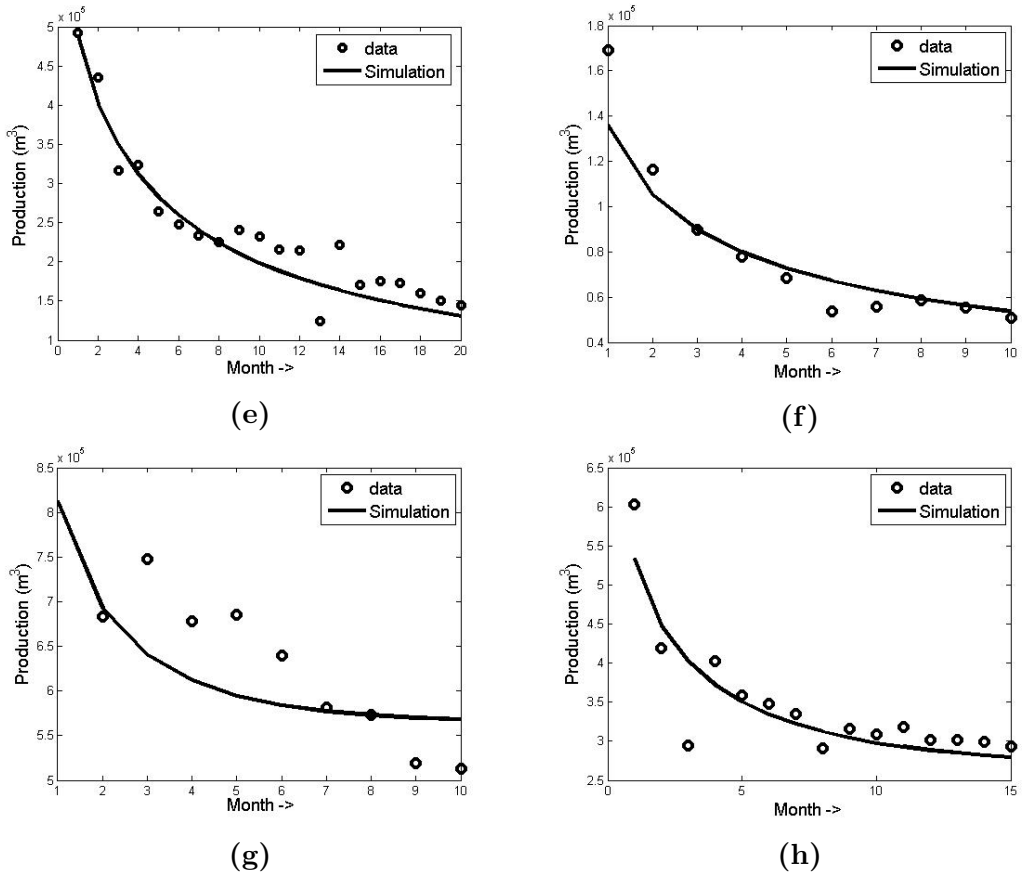

Figure 4.4: *History matching of production from various Manville wells.*

4.5 Development of coupled reaction and transport models

Microbially generated coalbed methane can be increased if appropriate conditions are provided to enhance microbial activity. In connection to this, researchers have conducted many laboratory incubation studies with crushed coal based on the introduction of new microbial consortia, supply of additional nutrients, increase in the availability of carbon substrate, etc.[28–34] To analyse and compare the rate of coal bioconversion in various experiments, we proposed enzymatic reaction kinetic models with reasonable predictive capabilities in our previous studies.[3,35] Following that, we develop multiscale microbial reaction coupled transport models to enable knowledge transfer from laboratory to field scales in this study. Apart from investigation of the effects of kinetic, transport/storage parameter effects on field scale gas production, such models are potentially instrumental in developing field scale strategies for microbially enhanced coalbed methane production also.

4.5.1 Enzymatic reaction kinetic model

In our previous study,[3] we proposed a simplified reaction pathway involving lumped components for coal breakdown, based on literature and experimental data. Major steps in coal bioconversion are coal solubilization, hydrolysis, acidogenesis, acetogenesis and methanogenesis were considered in the reaction network. The products of hydrolysis were represented by a representative lignin monomer, syringic acid. The products of acidogenesis were lumped and represented by benzoate/benzoic acid, which is a common intermediate and the products of acetogenesis were lumped and represented by acetate, a small chain acid with similar characteristics as other products of acetogenesis. The products of methanogenesis are considered to be methane, carbon dioxide and hydrogen.

> Coal **C** $\rightarrow$ Solubilized coal **S** $\rightarrow$ Fragmented coal **W** $\rightarrow$ Benzoate **B** $\rightarrow$ Acetate **A** $\rightarrow$ Products **P**

The corresponding enzymatic reaction kinetic model was built with a series of simple and modified Monod models. The resulting kinetic model was validated for different laboratory scale bottle experiments conducted with crushed coal in the presence of tryptone which is a source of nitrogen for the microbes. Also, in another one of our studies, we have addressed nitrogen limitations based on varying tryptone concentration along the core in a coreflooding experiment[35].

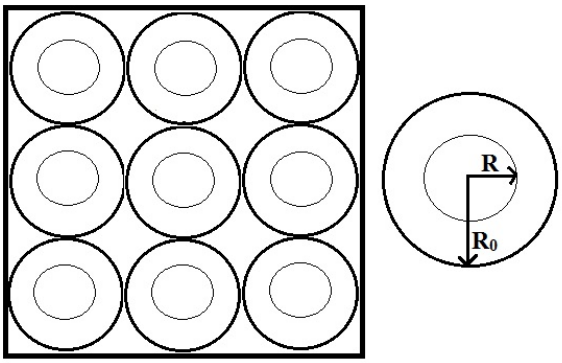

Figure 4.5: *Schematic of spherical shaped particles constituting macropore spaces*

4.5.2 Assumptions in the enzymatic reaction kinetic model

- For simplicity, we assume only carbon substrate limitation in the microbial reactions.[3]
- Since the transport model is developed only for gas flow, the water required for microbial growth is assumed to be available from the residual water concentration in the macropore spaces (micropores are inaccessible to water).[6,8]
- Coal particles composing the reservoir macropore spaces are assumed to be spherical with pore radius R_0. Figure 4.5 represents a schematic of the spherical shaped particles constituting the macropore spaces. With the progress of coal bioconversion, the particle radius R decreases and the macropore porosity ϕ_{ma} increases.

4.5.3 Integration of kinetic and transport models

In this section, we discuss the integration of the validated kinetic and transport models. First, the coal solubilization rate is given by

$$\frac{1}{X}\frac{dC}{dt} = -KA(S^* - [S]) \tag{4.13}$$

where X is the quantity of microbes, K is the solubilization constant and $A = 4\pi R^2 N f_b$ is the surface area available. R is the size of particles composing the macropore space, N is the total number of particles and f_b is the fraction of the surface area available. All particles are assumed to degrade at the same rate; consequently, N is assumed to be constant. Equation 4.13 is rewritten as

$$\frac{dC}{dt} = -K' \left(\frac{C}{C_0}\right)^{2/3} (S^* - [S]) \tag{4.14}$$

where $K' = XK\ \dfrac{3m_{coal}f_b}{R_0\rho_{coal}}$, m_{coal} is total mass of coal present in the reservoir and ρ_{coal} is the coal density. As the reaction progresses, coal is consumed and the particle size reduces to R. The increase in porosity corresponding to reducing the particle size is manifested by the correlation in Equation 4.15, where the correlation exponent nc is negative.

$$\frac{R}{R_0} = \left(\frac{C}{C_0}\right)^{1/3} = \left(\frac{\phi_{ma}}{\phi^0_{ma}}\right)^{nc} \tag{4.15}$$

nc can be experimentally determined by measuring porosity over time in coreflooding experiments. The empirical correlation between porosity and permeability as proposed by Advanced Resources International (ARI)[36] is shown in Equation 4.16.

$$\frac{k}{k_0} = \left(\frac{\phi_{ma}}{\phi^0_{ma}}\right)^3 \tag{4.16}$$

Finally, on coupling the kinetic and transport equations based on the above assumptions and modifications, we get

$$\frac{(\tilde{PF}_{ma})_{i+1/2}}{\Pi'_1}\left[\tilde{P}^{N+1}_{gi+1/2} + \frac{\Pi'_1}{\Pi'_2}\right]\left(\tilde{P}^{N+1}_{gi+1} - \tilde{P}^{N+1}_{gi}\right) - \frac{(\tilde{PF}_{ma})_{i-1/2}}{\Pi'_1}\left[\tilde{P}^{N+1}_{gi-1/2} + \frac{\Pi'_1}{\Pi'_2}\right]\left(\tilde{P}^{N+1}_{gi} - \tilde{P}^{N+1}_{gi-1}\right) +$$
$$\frac{P_{sc}TZL_{mi}}{P_0T_{sc}}\frac{(1 - exp(-\delta\tilde{t}\Pi'_3))}{\delta\tilde{t}}\left(V^N_{mi} - V_E(P_g)^N_i\right) + \frac{t_0P_{sc}T}{P_0T_{sc}}\left[\frac{q_R}{V_{bma}}\right]^{N+1}_i = \frac{\left(\tilde{P}^{N+1}_{gi} - \tilde{P}^N_{gi}\right)}{\delta\tilde{t}/[\phi_{ma}]^{N+1}_i} \tag{4.17a}$$

where k and ϕ_{ma} vary according to Equations 4.15 and 4.16 and

$$\frac{q_R}{V_{bma}} \equiv \frac{\text{standard gas volume from methanogenesis}}{\text{macropore volume}}$$

$$V_{mii}{}^{N+1} = \exp(-\delta\tilde{t}\Pi'_3)V_{mii}{}^N + (1 - \exp(-\delta\tilde{t}\Pi'_3))V_E(P_g)^N_i \tag{4.17b}$$

$$\left[\frac{q_R}{V_{bma}}\right]^{N+1}_i m^3/m^3 = 0.022\frac{m^3}{mol}\left[\frac{d[CH_4]}{dt}\right]^{N+1}_i \frac{mol}{m^3} = \frac{0.022e[A]^{N+1}_i}{f + [A]^{N+1}_i + \dfrac{([A]^{N+1}_i)^2}{g}}\frac{m^3}{m^3} \tag{4.17c}$$

where e, f and g are kinetic parameters related to methanogenesis.

$$\left[\frac{d[A]}{dt}\right]_i^{N+1} = 3d[B]_i^{N+1} - \frac{e[A]_i^{N+1}}{f + [A]_i^{N+1} + \frac{([A]_i^{N+1})^2}{g}} \tag{4.17d}$$

d is the kinetic parameter related to acetogenesis.

$$\left[\frac{d[B]}{dt}\right]_i^{N+1} = r[W]_i^{N+1} + \nu - d[B]_i^{N+1} \tag{4.17e}$$

r and ν are the kinetic parameters related to acidogenesis.

$$\left[\frac{d[W]}{dt}\right]_i^{N+1} = 10b[S]_i^{N+1} - r[W]_i^{N+1} \tag{4.17f}$$

b is the kinetic parameter related to hydrolysis.

$$\left[\frac{d[S]}{dt}\right]_i^{N+1} = K'\left(\frac{C}{C_0}\right)^{2/3}([S^*] - [S]]_i^{N+1}) - b[S]_i^{N+1} \tag{4.17g}$$

$K'$is the solubility constant and S^* is the equilibrium coal solubility concentration

$$\left[\frac{dC}{dt}\right]_i^{N+1} = -K'\left(\frac{C}{C_0}\right)^{2/3}([S^*] - [S]]_i^{N+1}) \tag{4.17h}$$

All the variables and parameters in the model are defined in Table 4.6.

Coupled Equations 4.17a to 4.17h are solved by the Levenberg-Marquardt method for an initial reservoir pressure of 10 MPa, well operating pressure of 0.14 MPa, a no-flow external boundary condition and reaction kinetic parameter values obtained by the nonlinear regression of data from coreflood experiments in our previous study,[35] modified for excess nitrogen concentration. Accordingly, ν, representing the kinetics of nitrogen concentration in acidogenesis, is a zero-order rate term. Also, a large absolute value of nc is chosen to minimize large changes in macropore porosity with progress in coal bioconversion.

Figure 4.6 compares gas production over 20 months with and without the inclusion of coal bioconversion reaction kinetics, for the nominal kinetic parameter values shown in Table 4.5. The increase in gas production is small, although it appears to improve with

Parameter	Unit	Value
e	mol/m^3h	20
f	mol/m^3	215
g	mol/m^3	0.0011
r	mol/m^3h	0.1
ν	mol/m^3h	10^{-4}
d	h^{-1}	0.015
b	h^{-1}	0.1
S^*	mol/m^3	1
K'	h^{-1}	10^{-7}
nc	-	-20

Table 4.5: *Kinetic parameters for enzymatic bioconversion.*

time. The model was then employed to observe the effect of an increase in biogenic gas production over a period of 5 months with respect to changes in individual kinetic rate parameters. Figure 4.7 compares the increase in gas production for a ten-fold increase in the solubilization rate ($K' = 10K'_{\text{nominal}}$). It is seen that K' has quite a large effect on biogenic gas production. Figure 4.8 compares the increase in gas production for a ten-fold increase in the methanogenesis rate ($e = 10e_{\text{nominal}}$). An increase in e significantly improves biogenic gas recovery at field scales. Figure 4.9 shows an increase in gas production for a ten-fold increase in the acidogenesis rate ($d = 10d_{\text{nominal}}$). Its effect is small, although it appears to increase with time. For small changes in parameter values b and r, the model is insensitive. It is to be noted that the effect of parameters f and g can be evaluated only if the acetate concentrations are significant. This will be analysed in our future work, which will consider multiphase multicomponent coupled reactive and transport models for simulation of microbially enhanced coalbed methane.

4.6 CONCLUSION

In this study, we have developed a multiscale microbal reaction kinetics coupled gas transport model for simulation of coalbed methane (CBM) production from reservoirs

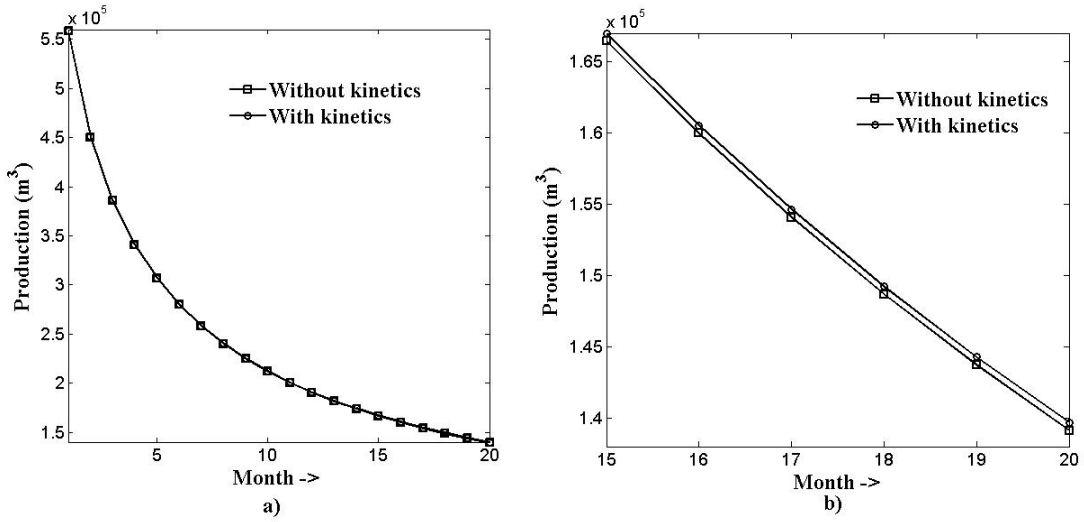

Figure 4.6: *a) Comparison of coalbed methane production with and without coal bioconversion b) Enlarged view of Figure 4.6a between months 15 - 20.*

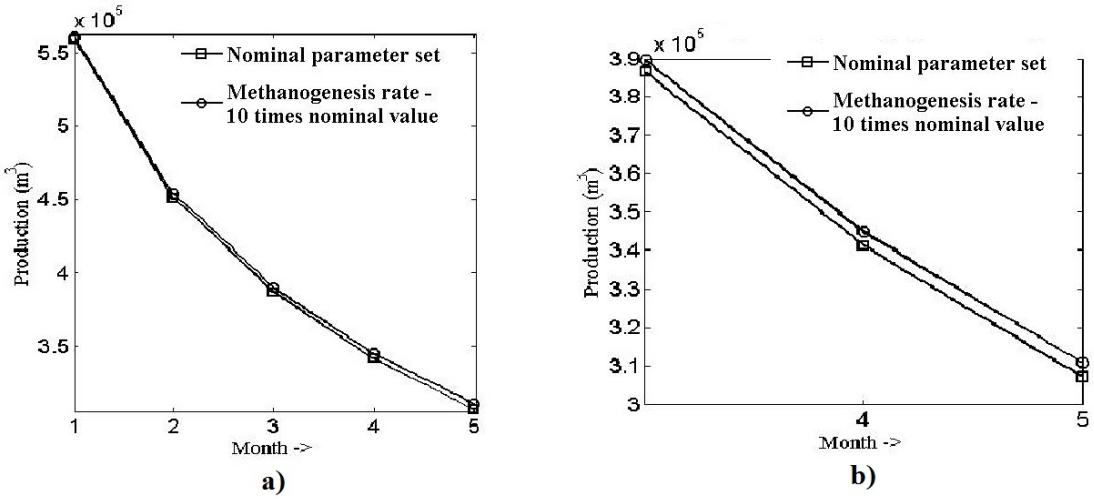

Figure 4.7: *a) Increase in coalbed methane production for a 10-fold increase in solubilization rate ($K' = 10K'_{nominal}$), and b) Enlarged view of Figure 4.7a between months 3 - 5 .*

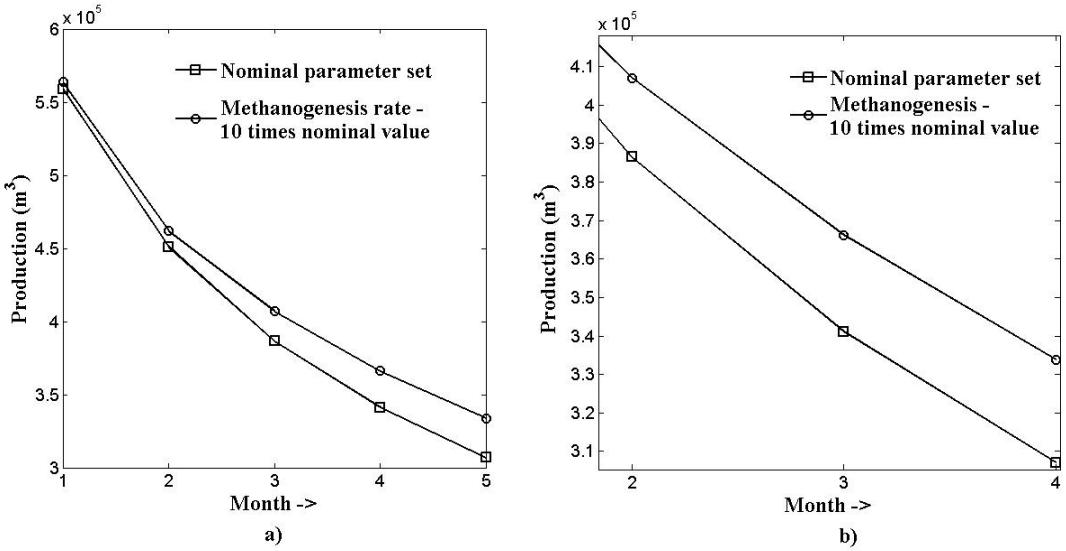

Figure 4.8: *a) Increase in coalbed methane production for a 10-fold increase in methanogenesis rate ($e = 10e_{nominal}$), and b) Enlarged view of Figure 4.8a between months 2 - 4.*

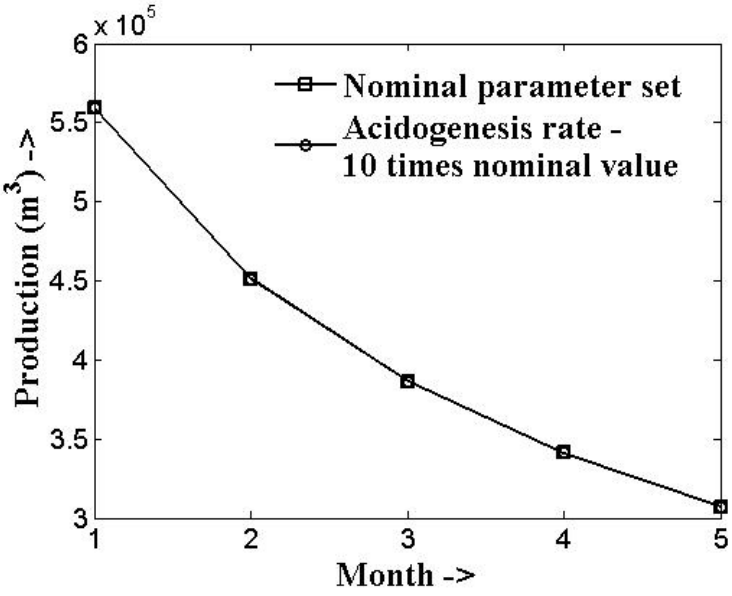

Figure 4.9: *Increase in coalbed methane production for a 10-fold increase in acidogenesis rate ($d = 10d_{nominal}$*

.)

with ongoing anaerobic breakdown of coal. Based on the assumption of dual porosity characteristics in coal seams, gas transport equations were derived for a one dimensional (1D) radial coal bed reservoir by considering laminar flow and gas slippage in macropores and gas diffusion from micropores driven by desorption. The multiscale stiff transport equations were non-dimensionalized to produce dimensionless numbers that can provide insights on the dominant physical process at various scales. A global sensitivity analysis of transport model parameters was conducted by the Morris OAT (one-at-a-time) method, which indicated that gas mobility and the surface diffusion constant affect the gas production the most. Following this, history matching of gas production data from Manville wells in Alberta was performed by solving the transport equations by the Levenberg-Marqardt method. The validated transport model was then combined with an enzymatic reaction kinetic model for coal bioconversion developed in the previous chapters. Based on an analysis of the effects of kinetic rate parameters on gas production, it was observed that an increase in the methanogenesis rate can significantly improve biogenic gas recovery, followed by an increase in the coal solubilization rate. These effects maybe brought out by a combination of strategies such as - biostimulation, bioaugmentation, increase of bioavailability and increased fracture spacing for greater nutrient dispersion and physical space for microbial growth. With the inclusion of the water phase in the macropore system and nitrogen's role as a limiting substrate in the kinetic model[35], the transport model can be updated for application to field scale simulations in the presence of nutrient injection. The effect of varying injection rates, varying nutrient concentrations and varying production rates on CBM production can then be studied and optimized with model-based computational experiments. This forms the basis for our future work.

Symbol	Units	Description
T	K	Reservoir temperature
P_{g0}	MPa	Initial reservoir pressure
P_{wf}	MPa	Well operating pressure
μ	$kg/s.m$	Gas viscosity
ϕ_{ma}		Macropore porosity
$\frac{Q_t}{V_{bma}}$	kg/m^3	Amount of gas diffusing from micropore surface per unit macropore volume
$\frac{q_t}{V_{bma}}$	kg/m^3	Volume of gas at standard conditions diffusing from micropore surface per unit macropore volume
r_e	m	Coal seam thickness (Extent of reservoir)
r_w	m	Well radius
h	m	Length of horizontal well bore
P_{sc}	Pa	Pressure at standard conditions
T_{sc}	K	Temperature at standard conditions
P_0	Pa	Reference pressure
R_0	m	Reference radius
t_0	s	Reference time with respect to dt
k	m^2	Absolute permeability
D_{ma}	m^2/s	Diffusion coefficient in Klinkenberg effect
τ	s	Time constant for micropore gas diffusion
L_{mi}	-	Geometry prefactor for micropore diffusion
V_l	m^3/m^3	Langmuir volume constant
P_l	MPa	Langmuir pressure constant
$[S]$	mol/m^3	Solubilised coal concentration
$[W]$	mol/m^3	Fragmented coal components concentration
$[B]$	mol/m^3	Lumped "benzoate-like" intermediate concentration
$[A]$	mol/m^3	Lumped "acetate-like" intermediate concentration
$[CH_4]$	mol/m^3	Methane concentration (mol/m^3)
b	h^{-1}	First order reaction constant for the enzymatic hydrolysis reaction at low concentrations of $[S]$
r	h^{-1}	First order reaction constant for the enzymatic acidogenesis reaction at low concentrations of $[W]$
d	h^{-1}	First order reaction constant for the enzymatic acetogenesis reaction at low concentrations of $[B]$

ν	mol/m^3h	Zero order reaction rate corresponding to benzoate pool production from tryptone
e	$\frac{mol}{m^3.h}$	Maximum rate for methanogenesis under non-growth conditions
f	mol/m^3	Methanogenic substrate concentration at half the maximum rate of methanogenesis
g	mol/m^3	Substrate inhibition constant for methanogenesis
S^*	mol/m^3	Equilibrium solubility concentration of solubilised coal $[S]$
K'	h^{-1}	Rate constant of solubilisation
nc	-	Exponent in the correlation between R and ϕ_{ma}

Table 4.6: *Table of Notation*

References

[1] Senthamaraikkannan, G. and Prasad, V. Coalbed methane. In M.R.Riazi and Gupta, R., editors, *Coal Production and Processing Technology*. Taylor & Francis Group, (in press).

[2] King, G. Numerical simulation of the simultaneous flow of methane and water through dual porosity coal seams during the degasification process. Technical report, Pennsylvania State Univ., University Park (USA), 1985.

[3] Senthamaraikkannan, G., Budwill, K., Gates, I., Mitra, S., and Prasad, V. Kinetic modeling of the biogenic production of coalbed methane. *(submitted)*, 2015.

[4] Laxminarayana, C. and Crosdale, P. J. Role of coal type and rank on methane sorption characteristics of Bowen Basin, Australia coals. *International Journal of Coal Geology*, 40(4):309–325, 1999.

[5] Gamson, P., Beamish, B., and Johnson, D. Coal microstructure and secondary mineralization: their effect on methane recovery. *Geological Society, London, Special Publications*, 109(1):165–179, 1996.

[6] Wei, X., Wang, G., Massarotto, P., Golding, S., and Rudolph, V. Numerical simulation of multicomponent gas diffusion and flow in coals for CO_2 enhanced coalbed methane recovery. *Chemical Engineering Science*, 62(16):4193–4203, 2007.

[7] Mohaghegh, S. and Ertekin. A type-curve solution for coal seam degasification wells producing under two-phase flow conditions. In *SPE Annual Technical Conference and Exhibition*. Society of Petroleum Engineers, 1991.

[8] King, G. R., Ertekin, T., and Schwerer, F. C. Numerical simulation of the transient behavior of coal-seam degasification wells. *SPE Formation Evaluation*, 1(02):165–183, 1986.

[9] Remner, D. J., Ertekin, T., Sung, W., and King, G. R. A parametric study of the effects of coal seam properties on gas drainage efficiency. *SPE Reservoir Engineering*, 1(6):633–646, 1986.

[10] Sung, W., Ertekin, T., and Schwerer, F. The development, testing, and application of a comprehensive coal seam degasification model. In *SPE Unconventional Gas Technology Symposium*. Society of Petroleum Engineers, 1986.

[11] Clarkson, C. R., Jordan, C. L., Ilk, D., and Blasingame, T. A. Production data analysis of fractured and horizontal CBM wells. In *SPE Eastern Regional Meeting*. Society of Petroleum Engineers, 2009.

[12] Sawyer, W., Paul, G., and Schraufnagel, R. Development and application of A 3-D coalbed simulator. In *Annual Technical Meeting*. Petroleum Society of Canada, 1990.

[13] Manik, J., Ertekin, T., and Kohler, T. Development and validation of a compositional coalbed simulator. In *Canadian International Petroleum Conference*. Petroleum Society of Canada, 2000.

[14] Thararoop, P., Karpyn, Z. T., and Ertekin, T. Development of a multi-mechanistic, dual-porosity, dual-permeability, numerical flow model for coalbed methane reservoirs. *Journal of Natural Gas Science and Engineering*, 8:121–131, 2012.

[15] Ritter, D., Vinson, D., Barnhart, E., Akob, D. M., Fields, M. W., Cunningham, A. B., Orem, W., and McIntosh, J. C. Enhanced microbial coalbed methane generation: A review of research, commercial activity, and remaining challenges, 2015.

[16] Scott, A. and Guyer, J. Method of generating and recovering gas from subsurface formations of coal, carbonaceous shale and organic-rich shales, February 2004.

[17] Bustin, R. and Clarkson, C. Geological controls on coalbed methane reservoir capacity and gas content. *International Journal of Coal Geology*, 38(1):3–26, 1998.

[18] Kolesar, J., Ertekin, T., and Obut, S. The unsteady-state nature of sorption and diffusion phenomena in the micropore structure of coal: Part 1-theory and mathematical formulation. *SPE Formation Evaluation*, 5(01):81–88, 1990.

[19] Prinz, D. and Littke, R. Development of the micro-and ultramicroporous structure of coals with rank as deduced from the accessibility to water. *Fuel*, 84(12):1645–1652, 2005.

[20] Goktas, B. and Ertekin, T. Production performance analysis of cavity-completed wells. In *SPE Eastern Regional Meeting*. Society of Petroleum Engineers, 1998.

[21] Ertekin, T., King, G. A., and Schwerer, F. C. Dynamic gas slippage: a unique dual-mechanism approach to the flow of gas in tight formations. *SPE formation evaluation*, 1(01):43–52, 1986.

[22] Wu, Y.-S. and Pruess, K. Gas flow in porous media with Klinkenberg effects. *Transport in Porous Media*, 32(1):117–137, 1998.

[23] Jalal, J. and Mohaghegh, S. D. A coalbed methane reservoir simulator designed and developed for the independent producers. In *SPE Eastern Regional Meeting*. Society of Petroleum Engineers, 2004.

[24] Heller, R., Vermylen, J., and Zoback, M. Experimental investigation of matrix permeability of gas shales. *AAPG bulletin*, 98(5):975–995, 2014.

[25] IHS Inc. AccuMap oil and gas database for Alberta, Canada, 2013.

[26] Wainwright, H. M., Finsterle, S., Jung, Y., Zhou, Q., and Birkholzer, J. T. Making sense of global sensitivity analyses. *Computers & Geosciences*, 65:84–94, 2014.

[27] Saltelli, A. Sensitivity analysis: Could better methods be used? *Journal of Geophysical Research: Atmospheres (1984–2012)*, 104(D3):3789–3793, 1999.

[28] Harris, S. H., Smith, R. L., and Barker, C. E. Microbial and chemical factors influencing methane production in laboratory incubations of low-rank subsurface coals. *International Journal of Coal Geology*, 76(1):46–51, 2008.

[29] Singh, D. N., Kumar, A., Sarbhai, M. P., and Tripathi, A. K. Cultivation-independent analysis of archaeal and bacterial communities of the formation water in an Indian coal bed to enhance biotransformation of coal into methane. *Applied microbiology and biotechnology*, 93(3):1337–1350, 2012.

[30] Opara, A., Adams, D., Free, M., McLennan, J., and Hamilton, J. Microbial production of methane and carbon dioxide from lignite, bituminous coal, and coal waste materials. *International Journal of Coal Geology*, 96:1–8, 2012.

[31] Penner, T. J., Foght, J. M., and Budwill, K. Microbial diversity of western canadian subsurface coal beds and methanogenic coal enrichment cultures. *International Journal of Coal Geology*, 82(1):81–93, 2010.

[32] Jones, E. J., Voytek, M. A., Corum, M. D., and Orem, W. H. Stimulation of methane generation from nonproductive coal by addition of nutrients or a microbial consortium. *Applied and Environmental Microbiology*, 76(21):7013–7022, 2010.

[33] Papendick, S. L., Downs, K. R., Vo, K. D., Hamilton, S. K., Dawson, G. K., Golding, S. D., and Gilcrease, P. C. Biogenic methane potential for Surat Basin, Queensland coal seams. *International Journal of Coal Geology*, 88(2):123–134, 2011.

[34] Huang, Z., Urynowicz, M. A., and Colberg, P. J. Stimulation of biogenic methane generation in coal samples following chemical treatment with potassium permanganate. *Fuel*, 111:813–819, 2013.

[35] Senthamaraikkannan, G., Gates, I., and Prasad, V. Modeling estimation and optimization in coreflooding experiments for coalbed methane production. *(submitted)*, 2015.

[36] Pekot, L. J. Matrix shrinkage and permeability reduction with carbon dioxide injection. Coal-Seq II Forum, Washington DC, 2003.

Chapter 5

Stochastic proxy modeling for coalbed methane production using orthogonal polynomials

Abstract

Uncertainty in data or in the parameters of models occurs in many real world applications. Quantifying this uncertainty and its effects is required for robust design, control and optimization. In this chapter, we attempt to build a proxy model for the stochastic solutions of coupled governing equations describing coalbed methane (CBM) production at different well bottomhole pressures. To achieve this, monthly production from wells (output) is expanded as a linear combination of Legendre orthogonal polynomials in the input (well bottomhole pressure) and the Wiener-Askey polynomial chaos is used to propagate the uncertainty of the model parameters. A Gaussian quadrature technique is then employed to solve for the coefficients of the basis functions in the proxy model. Alternatively, nonlinear least squares curve fitting using the Levenberg-Marquardt algorithm (LMA) is also used with polynomial chaos expansion to generate the stochastic proxy model. The proxy model now enables robust optimization using statistical metrics of CBM production calculated over the entire parameter space. In the case of multiple decision variables, the appropriate proxy model built using these techniques will allow for robust optimization without the use of any search algorithms.

5.1 Introduction

Many applications in science and engineering require mathematical models which can simulate solutions for a physical variable of interest along spatial and temporal dimensions. The simulations are usually not fully deterministic due to the presence of uncertain parameters/input random variables[1]. Different methods are available for the propagation of uncertainty. The Monte Carlo method is a popular technique where simulations are performed for a large number of values sampled from a known distribution of the random source. Although this method is robust, it requires a large number of simulations, and is therefore computationally expensive. Another method, the power series expansion (PSE), coupled with contour mapping techniques was explored for distributional robustness analysis in the work by Nagy et al.[2]. However, the same work establishes that the polynomial chaos expansion (PCE) method for uncertainty propagation usually gives better results even with relatively lower order approximations.

PCE is a method used for uncertainty propagation in nonlinear dynamic systems and was introduced by Wiener as homogeneous chaos. It is derived from the Cameron-Martin theorem which states that an expansion in Hermite polynomials in Gaussian random variables converges in the L_2 sense for any arbitrary stochastic process with finite second moment[3]. Xiu et al.[4] extended these results to represent stochastic processes with an optimum trial basis from the Askey family of orthogonal polynomials that reduces dimensionality of the polynomial chaos expansions and leads to exponential convergence of error. This came to be known as the Wiener-Askey polynomial chaos. It expands a stochastic output X as

$$X(\theta) = \sum_{j=0}^{p} a_j \Psi_j(\xi)$$

where Ψ_j is the polynomial basis (in the random variable ξ) belonging to a complete orthogonal basis. The best choice of orthogonal polynomials for a PCE is related to the probability distribution of the random source. Projection of the PCE onto each polynomial basis Ψ_j will result in estimation of expansion coefficients a_j and the expansion error is orthogonal to the functional space spanned by the basis functions[5].

PCE for an output variable is thus an effective way to track uncertainty evolution. In this chapter, we introduce the input variable also into the PCE, thus developing a robust proxy model that can significantly reduce computational time in optimization studies. The main concern in building the proxy model, however, is obtaining the underlying functional relation between the input and output in the presence of uncertainty. When the analytical structure of the relation is explicitly known, the

Levenberg-Marquardt algorithm (LMA) is used with PCE to generate the stochastic proxy model.When this is not the case, we suggest the use of orthogonal polynomials to weave the input variable(s) into the PCE. Orthogonal polynomials in the input variable will allow accurate evaluation of coefficients of the proxy model (by Gaussian quadrature rules) using only a few simulations according to the dimensionality. Thus, a robust proxy model can be built for a certain output variable by expansion with two orthogonal basis sets, the Legendre orthogonal polynomials corresponding to the input (assuming uniform distribution for the input to avoid any preferences while choosing collocation points) and the Hermite orthogonal polynomials corresponding to the random source from a known/assumed distribution or a Bayesian estimate as suggested by Mandur et al.[6]. This technique would be computationally superior to other robust optimization methods presented by Mandur et al.[6], Xiong et al.[7] and Molina-Cristobal et al.[8], which evaluate metrics of the objective function (by constructing a PCE) at each decision variable (input) value in the search space.

The approach to proxy model development is demonstrated on coalbed methane production. Coalbed methane is the gas naturally occuring in coalbeds due to thermogenic or biogenic processes, and is an important unconventional source of natural gas. Geologic heterogeneity, the existence of multiple porosity scales, coal matrix shrinkage/swelling, varying pressure-temperature conditions and many other phenomena lead to significant uncertainty in assessing CBM production. For simplicity, a proxy model for monthly coalbed methane gas production is built with respect to the input parameter (well bottomhole pressure), while considering uncertainty only in the micropore diffusion time constant (τ).

5.2 CBM Model

Coalbed seams are highly heterogeneous with a wide range in the scale of pore spaces occurring within coal. For simulation purposes, coal seams are broadly assumed to have two levels of porosity - micropores and macropores. In this study, the production of gas from a hortizontal well drilled into a coalbed seam containing only gas phase is simulated by solving a 1D radial equation representing the multi-step transport process described using a pseudo steady-state sorption model for gas desorption, Fick's law for diffusion through micropores, Darcy's law for gas flow through open fractures (i.e., the macroporous spaces) and gas slippage factor for surface diffusion through the surface of solid coal[9,10]. A cylindrical volume of a coal reservoir, considered for simulations with a horizontal well drilled at its center, is shown in Figure 5.1. The other assumptions made in the model are:

1. Gas permeability through macropores, the gas diffusion constant and the geom-

etry dependent factor for diffusion through the micropore matrix are constant throughout the spatial volume and over time.

2. The flow velocity is assumed to have only a radial component.

3. There is no change of temperature in the coal seam during degasification. The gas compressibility factor Z and viscosity μ are considered to be constant.

Consider a small cylindrical control volume dV in the macroporous space consisting of micropores. The following coupled governing equations are derived for radial gas flow into a producer well operating at a constant pressure of P_{wf}:

$$\begin{aligned} \int_{V_{bma}} \frac{1}{r}\frac{\partial}{\partial r}(\frac{rP_g}{Z}(\frac{k}{\mu}+\frac{D_{ma}}{P_g})\frac{\partial P_g}{\partial r})dV + \\ \int_{V_{bma}} \frac{P_{sc}T}{T_{sc}}\frac{q_t}{V_{bma}}dV = \int_{V_{bma}} \frac{\partial}{\partial t}(\frac{P_g\phi_{ma}}{Z})dV \end{aligned} \tag{5.1a}$$

$$\frac{q_t}{V_{bma}} = \frac{dV_{mi}}{dt} - L_{mi}\tau(V_E(P_g) - V_{mi}); V_{mi}^0 = \frac{V_l P_{g0}}{P_l + P_{g0}} \tag{5.1b}$$

$$\text{Production} = 2\pi r_{well} h_{well} \left(\lambda + D_{ma}/P_g\right)\frac{dP}{dr}\Big)_{well} \tag{5.1c}$$

The partial differential equations were discretised at equally separated time intervals and logarithmically spaced spatial co-ordinates, and was solved using the implicit method. The model variables and parameters are defined in Table 5.1. The nominal values of all the parameters were obtained by history matching the model against existing CBM production data from Manville wells.

$$\begin{aligned} &\pi_1 \left(P\tilde{F}_{ma}\tilde{P}_g^{N+1}\right)_{i+1/2}(\pi_2 + \frac{1}{\tilde{P}_{gi+1/2}^{N+1}})(\tilde{P}_{gi+1}^{N+1} - \tilde{P}_{gi}^{N+1}) - \\ &\pi_1 \left(P\tilde{F}_{ma}\tilde{P}_g^{N+1}\right)_{i-1/2}(\pi_2 + \frac{1}{\tilde{P}_{gi-1/2}^{N+1}})(\tilde{P}_{gi}^{N+1} - \tilde{P}_{gi-1}^{N+1}) + \\ &\pi_3(V_{mi}^N - \frac{P_{gi}^N V_l}{P_l + P_{gi}^N}) = \frac{(\tilde{P}_{gi}^{N+1} - \tilde{P}_{gi}^N)}{\delta T} \end{aligned} \tag{5.2a}$$

$${V_{mi}}_i^{N+1} = exp(-\tau\delta t){V_{mi}}_i^N + (1 - exp(-\tau\delta t))\, V_E(P_g)_i^N \tag{5.2b}$$

$$\begin{aligned} &\text{Production} = \\ &2\pi r_{well} h_{well}(\lambda + D_{ma}/P_{gr_{well}}^N)\left(\frac{P_{g(r_{well}-1)}^N - P_{wf}}{r_{well} - r_{well-1}}\right) \end{aligned} \tag{5.2c}$$

Table 5.1: *Model parameters and variables.*

$\lambda = k/\mu$	Mobility
D_{ma}	Gas slippage
τ	Micropore diffusion time constant
L_{mi}	Geometry dependent factor for micropore diffusion
P_l, V_l	Langmuir adsorption constants
ϕ_{ma}	Macropore porosity
V_{bma}	Macropore volume
r_{well}, h_{well}	Dimensions of producing well
r, t	Continuous spatial and temporal coordinate
N	N^{th} discrete spatial co-ordinate
i	i^{th} discrete time step
$PF_{mai+1/2}$	$\frac{2r_{i+1/2}}{(r_{i+1/2}^2 - r_{i-1/2}^2)(r_{i+1} - r_i)}$
P_g	Gas pressure at r, t
V_{mi}	Volume of gas from micropores diffusing into the macroporous space
V_E	Volume of gas adsorbed in micropore spaces
π_1	$\frac{D_{ma} t_0}{R_0^2 \phi}$
π_2	$\frac{\lambda P_0}{D_{ma}}$
π_3	$\frac{P_{sc} T L_{mi} t_0 Z}{P_0 T_{sc} \tau \phi}$

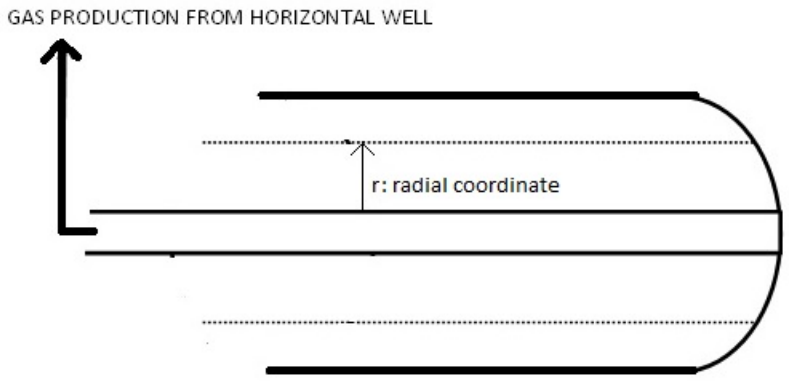

Figure 5.1: *Gas production from a horizontally drilled well in a cylindrical reservoir volume.*

A proxy to the above model is built with P_{wf}, the well bottomhole pressure, as the input (u) and τ, the micropore diffusion time constant, as the only source of uncertainty (ξ). The operating range of P_{wf} is assumed to lie between 1×10^6 N/m^2 to 1×10^7 N/m^2. τ is assumed to belong to a Gaussian distribution with mean value of 5000 s and standard deviation of 500 s. The output is the CBM gas production in the first month (m^3), denoted as Y. The functional dependence of the CBM production on time can be estimated by aggregating proxy models built at different time instants. It is to be noted here that including all the input variables and uncertain sources into the proxy model will increase dimensionality and consequently, the computational expense.

5.3 Proxy model development

The first step is to establish a functional relation between the input (u) and the output (Y). Any given function $f(x)$ can be approximated by minimizing the inner product $\langle f(x) - p(x), f(x) - p(x) \rangle$, where $p(x)$ is a combination of a sequence of orthogonal polynomials, $p_0(x), ..., p_k(x)$. The chosen family of orthogonal polynomials represent an orthogonal basis for the subspace of polynomial functions of degree $\leq k$. The inner product is defined as

$$\langle g, h \rangle = \int_a^b g(x)h(x)w(x)dx = \sum_{i=1}^{n} g(x_i)h(x_i)w(x_i) \tag{5.3}$$

where $g(x)$ and $h(x)$ belong to the class of orthogonal polynomials and $w(x)$ is the

weighting function.

Thus, Y can be expanded as

$$Y = a_0 + a_1 L_1(u) + a_2 L_2(u) + a_3 L_3(u) + ... \tag{5.4}$$

where u is the input variable and $L_0, L_1, ..$ belong to the sequence of Legendre polynomials that are orthogonal on the interval $[-1, 1]$. Legendre polynomials are chosen because their weighting function is a constant (this will prevent any bias in the selection of the input variable during estimation or prediction). The range for P_{wf} is projected onto a range of $[-1, 1]$ for u.

The next step is uncertainty propagation on the orthogonal polynomials in the expansion of Equation 5.4 using Wiener-Askey chaos. To illustrate this, let Y be defined as a second-order polynomial (in u) and the stochastic process in each direction (i.e., the orthogonal basis used to define Y) be approximated by second order Hermite polynomials in the standard Gaussian random variable, ξ. Hermite polynomials are orthogonal on $[-\infty, \infty]$ relative to the weight function $e^{\frac{-x^2}{2}}$, which is similar to the probability density function of a Gaussian distribution.

$$\begin{aligned} Y = & a_0(b_0^1 + b_1^1 H_1(\xi) + b_2^1 H_2(\xi))(L_0(u)) \\ & + a_1(b_0^2 + b_1^2 H_1(\xi) + b_2^2 H_2(\xi))(L_1(u)) \\ & + a_2(b_0^3 + b_1^3 H_1(\xi) + b_2^3 H_2(\xi))(L_2(u)) \end{aligned} \tag{5.5}$$

The random variable τ in the CBM model and ξ are linearly related as $\frac{\tau - 5000}{500} = \xi$.

The first few Legendre and Hermite polynomials are shown in Table 5.2. These are generated using ORTHOPOL.[11]

At certain known values of the input, the expansion in Equation 5.5 reduces to

$$\begin{aligned} Y = & (a_0 b_0^1 L_0(u) + a_1 b_0^2 L_1(u) + a_2 b_0^3 L_2(u)) \\ & + (a_0 b_1^1 L_0(u) + a_1 b_1^2 L_1(u) + a_2 b_1^3 L_2(u)) H_1(\xi) \\ & + (a_0 b_2^1 L_0(u) + a_1 b_2^2 L_1(u) + a_2 b_2^3 L_2(u)) H_2(\xi)) \end{aligned} \tag{5.6}$$

The statistical moments (mean and variance) of the output distribution would then be

$$\mu = a_0 b_0^1 L_0(u) + a_1 b_0^2 L_1(u) + a_2 b_0^3 L_2(u) \tag{5.7a}$$

$$var = (a_0 b_1^1 L_0(u) + a_1 b_1^2 L_1(u) + a_2 b_1^3 L_2(u))^2 + (a_0 b_2^1 L_0(u) + a_1 b_2^2 L_1(u) + a_2 b_2^3 L_2(u))^2 \tag{5.7b}$$

The accuracy of this proxy model depends on the set of basis polynomials chosen for the expansion and accurate evaluation of the coefficients of the basis polynomials in the proxy model.

Table 5.2: *Orthogonal polynomials.*

Hermite	Legendre
$H_0(\xi) = 1$	$L_0(u) = 1$
$H_1(\xi) = \xi$	$L_1(u) = u$
$H_2(\xi) = \xi^2 - 1$	$L_2(u) = u^2 - 0.33$
$H_3(\xi) = \xi^3 - 3\xi$	$L_3(u) = u^3 - 0.6u$
$H_4(\xi) = \xi^4 - 6\xi^2 + 3$	$L_4(u) = u^4 - 0.8571u^2 + 0.0848$
$H_5(\xi) = \xi^5 - 10\xi^3 + 15\xi$	$L_5(u) = u^5 - 1.11u^3 + 0.2372u$
$H_6(\xi) = \xi^6 - 15\xi^4 + 45\xi^2 - 15$	$L_6(u) = u^6 - 1.364u^4 + 0.4549u^2 - 0.0214$

5.4 Estimating coefficients of basis functions in the proxy model

The coefficients of the basis functions in the proxy model are estimated using the orthogonal property of the expanding polynomials. A simple model of Y expanded using first order polynomials in u and ξ is considered to illustrate this.

$$Y = a_0(b_0^1 + b_1^1(\xi)) + a_1(b_0^2 + b_1^2(\xi))(u) \tag{5.8}$$

The inner product of Y with each of the Hermite polynomials and Legendre polynomials (according to the definition in Equation 5.3) give

$$\int_{-1}^{1}\int_{-\infty}^{\infty}\frac{Y}{5}e^{\frac{-\xi^2}{2}}d\xi du = a_0 b_0^1; \int_{-1}^{1}\int_{-\infty}^{\infty}\frac{Y}{5}\xi e^{\frac{-\xi^2}{2}}d\xi du = a_0 b_1^1 \tag{5.9a}$$

$$\int_{-1}^{1}\int_{-\infty}^{\infty}\frac{Y}{1.67}e^{\frac{-\xi^2}{2}}d\xi u du = a_1 b_0^2; \int_{-1}^{1}\int_{-\infty}^{\infty}\frac{Y}{1.67}\xi e^{\frac{-\xi^2}{2}}d\xi u du = a_1 b_1^2 \tag{5.9b}$$

The parameters of the proxy model are estimated by evaluating the above integrals. If an analytical expression was available for Y, the integrals could be evaluated easily. In its absence, non-intrusive methods characterised either as Galerkin projection methods or least squares methods are used. Galerkin projection evaluates the integrals in Equation 5.9 using sampling approaches or Gaussian quadrature rules. The

linear least squares method employed is a regression approach, also known as point collocation or the stochastic response surface method.[12,13]

The sampling approach evaluates products in the integrals of Equation 5.9 at samples within the density of the weighting function. The quadrature approach evaluates the inner products as a summation of the product of basis functions at the roots of the next higher order polynomials as described by the Gaussian quadrature technique[14]. According to Gaussian quadrature rules

$$\text{if } \int_a^b f(x)dx = \int_a^b w(x)g(x)dx; \text{ then } \int_a^b f(x)dx \simeq \sum_c w(x)g(x)dx$$

where there are c roots of the next higher order orthogonal polynomial $h(x)$; $\int_a^b w(x)g(x)h(x)dx = 0$. It is a very useful method when the number of basis functions in the proxy model are small, since the number of collocation points exponentially increases with an increase in the dimensionality of the expansion. The regression approach uses a linear squares solution of the form $\Psi\alpha = R$ to solve for expansion coefficients that provide the best match for a set of response values R. However, it requires oversampling, i.e., the number of samples needs to be at least twice the number of parameters. In spite of this, the approach may still be significantly more affordable than quadrature for large problems.

Since there are only two variables in the proxy model developed in this study, the Gaussian quadrature approach is chosen as it provides accurate results with a lower number of samples. Figure 5.2 represents the work flow for building the proxy model. Along with the application of this technique, a nonlinear least squares method employing the Levenberg-Marquardt algorithm for parameter estimation is also used to estimate the proxy model, provided that the structure of the functional relation between Y and u is identified. For example,

$$Y = Y_0(u) + Y_1(u)H_1(\xi) + Y_2(u)H_2(\xi) \tag{5.11a}$$

if it is known that the relation between Y and u is expontential

$$Y = ae^{f(u)} + be^{g(u)}H_1(\xi) + ce^{h(u)}H_2(\xi) + ... \tag{5.11b}$$

Y_0, Y_1, Y_2 for a set of collocation points in ξ are evaluated at different values of u. These values are regressed against the functions $ae^{f(u)}, be^{g(u)}, ce^{h(u)}$ at the corresponding values of u.

5.5 Results and discussion

Four different model orders - $[1,1]$, $[2,1]$, $[3,1]$, $[3,2]$ (denoting the model order in u and ξ, respectively) were tested. The expansion coefficients of the basis functions

Polynomial	Model order in u and ξ			
	$[1,1]$	$[2,1]$	$[3,1]$	$[3,2]$
1	185215	200030	204450	204490
ξ	303	396	-436	-4976
u	-174081	-228396	-244600	-244830
$u\xi$	422	717	851	9709
$u^2 - 0.33$		188730	245050	245160
$u^2 - 0.33.\xi$		-767	-1164	-13267
$u^3 - 0.6u$			-202320	-202270
$u^3 - 0.6u.\xi$			1135.4	12991
$\xi^2 - 1$				-4350
$\xi^2 - 1.u$				1820
$\xi^2 - 1.u^2 - 0.33u$				38820
$\xi^2 - 1.u^3 - 0.6u$				34770

Table 5.3: *Coefficients corresponding to each polynomial in proxy model.*

for all the four models are shown in Table 5.3. Collocation points of prediction were chosen to be zeros of polynomials two orders higher than the order of the model. Model predictions were compared against data obtained from simulations of the original model (Equation 5.1), and the results are shown in Figure 5.3. The adjusted coefficient of determination (R_a^2) was computed in each case to test the goodness of fit. Figure 5.4 shows that R_a^2 increases with an increase in model order with respect to u but decreases when the order of the polynomial in ξ is increased to 2. The decrease in R_a^2 at this model order could indicate over-fitting. However, computation of the expansion coefficients at this model order ($[u(3), \xi(2)]$) also involved the division of very small numbers, which could have led to numerical issues. It is to be noted that R_a^2 as a criterion discredits increase in number of model parameters. Thus, the model of order $[u(3), \xi(1)]$ has the lowest prediction error. Thus, it is accepted as the proxy model for $Y = F(P_{wf}, \tau(\theta))$, where Y is the CBM production in the first month, P_{wf} is the bottomhole pressure and $\tau(\theta)$ represents the uncertain value of the micropore diffusion time constant. Moments of the distribution at a known value of input u obtained from this proxy model are

$$\mu = 204450 - 244600u + 245050(u^2 - 0.33) - 202320(u^3 - 0.6u) \tag{5.14a}$$

$$\sigma = \sqrt{436^2 + 851^2u^2 + 1164^2(u^2 - 0.33u)^2 + 1135^2(u^3 - 0.6u)^2} \tag{5.14b}$$

Figure 5.6 shows the probability distribution of the normalized values of τ, the uncertain parameter and Y, the output at different input values, u.

Since there is approximation in the way Gaussian quadrature evaluates integrals, some inner products $< \Psi_i \Psi_j >$ with $i \neq j$ are not equal to zero. As a result, the error of the estimated proxy model is not orthogonal to the subspace spanned by the basis functions present in it. Thus, the best values are not obtained for the coefficients in the proxy model resulting in errors when using it for the evaluation of higher order statistical moments of the output distribution. The inaccurate approximation of inner products also increases computational expense.

Nonlinear least squares regression was also applied for the proxy model development. Plotting $\int_{-\infty}^{\infty} Y e^{\frac{-\xi^2}{2}} d\xi$ against u revealed that the underlying functional relation between Y and u is exponential. The proxy model was developed by considering it to be second order in ξ. Model coefficients were evaluated using just 16 collocation points (chosen as roots of 4th order Legendre and Hermite polynomials for a good sample space). The proxy model obtained is

$$\begin{aligned} Y = {} & 7525e^{-4.305u} + 129800e^{-0.7288u} \\ & - 7.648e^{-6.066u}\xi - 141.8e^{-1.398u}\xi \\ & + 3.639e^{-4.5625u}\xi^2 - 1 + 6.604e^{-0.4735u}(\xi^2 - 1) \end{aligned} \tag{5.15}$$

Figure 5.5 compares the prediction (over a large number of simulation points) based on models of order $[u(3)\xi(1)]$, $[u(3), \xi(2)]$ and when the relation between Y and u is considered to be exponential. The model of order $[u(3)\xi(2)]$ does not have adequate predictive capability whereas the model considering an exponential input-output relation displays more accurate prediction with Hermite polynomials in ξ of the order 2. This indicates that the model with order $[u(3), \xi(2)]$ would perform better if interactions between third order terms in u and second order terms in ξ are omitted.

5.6 Robust optimization

Robust optimization is usually performed as a trade-off between maximum performance and robustness[6]. In this study, we employ a weighted mean-variance formulation for the robust optimization strategy, as seen in Equation 5.16, to find an optimum bottomhole pressure value compromising between maximum gas production (performance) and variability (robustness).

$$\max_u \; L = (1 - \alpha) * E(Y, u, \xi) - \alpha * V(Y, u, \xi) \tag{5.16}$$

where α is the degree of caution in the results, and E and V are the expectation and variance of production Y. Equation 5.14 provides both E and V as functions of u (P_{wf}). As is seen in Figure 5.7, the expectation of the production value increases with decreasing u, while the variance has a minimum at $u = 0$. Figure 5.8 shows performance and robustness at varying degrees of caution. As expected, with increasing degree of caution, robustness is increased at the cost of a lower performance.

5.7 Conclusions

We have developed a stochastic proxy model that propagates uncertainty in the micropore diffusion time constant (random source) sampled from a Gaussian distribution, to the monthly coalbed methane gas production (output) at different well bottomhole pressures (input) using Legendre polynomials and Hermite polynomial chaos. The coefficients of the basis functions in the proxy model are estimated by Galerkin projection using the Gaussian quadrature technique. Trial and error evaluation of model structures in increasing order shows that a model that is third order in the input variable and first order in the random source has the lowest relative sum square-root error of prediction. Although Gaussian quadrature is an efficient non-intrusive method of evaluating coefficients of basis functions, the computational expense increases with increasing dimension of the proxy model. The error of approximation of inner products occurring from use of Gaussian quadrature reduces accuracy of the higher order statistical moments of the distribution of the gas production obtained from a proxy model that appears to predict well at the collocation points. Nonlinear least squares regression was also tested for developing a proxy model, and can be employed if the underlying functional relation between the input and output variables is identifiable. The results indicate that the least squares method gives better predictions compared to Galerkin projection of the expansion of output in an orthogonal polynomial basis. However, the input-output relation is not always easily identifiable. The stochastic proxy model developed was then used for robust optimization of gas production. It is seen that the optimal point varies depending on whether performance or robustness is weighed more in the objective function.

References

[1] Fagiano, L. and Khammash, M. Simulation of stochastic systems via polynomial chaos expansions and convex optimization. *Physical Review E*, 86(3):036702, 2012.

[2] Nagy, Z. and Braatz, R. Distributional uncertainty analysis using power series and polynomial chaos expansions. *Journal of Process Control*, 17(3):229–240, 2007.

[3] Dutta, P. and Bhattacharya, R. Nonlinear estimation with polynomial chaos and higher order moment updates. In *American Control Conference (ACC), 2010*, pages 3142–3147. IEEE, 2010.

[4] Xiu, D. and Karniadakis, G. E. The Wiener–Askey polynomial chaos for stochastic differential equations. *SIAM Journal on Scientific Computing*, 24(2):619–644, 2002.

[5] Ghanem, R. and Dham, S. Stochastic finite element analysis for multiphase flow in heterogeneous porous media. *Transport in Porous Media*, 32(3):239–262, 1998.

[6] Mandur, J. and Budman, H. A polynomial-chaos based algorithm for robust optimization in the presence of Bayesian uncertainty. In *Proc. 8th IFAC Symposium on Advanced Control of Chemical Processes*. 2012.

[7] Xiong, F., Xue, B., Yan, Z., and Yang, S. Polynomial chaos expansion based robust design optimization. In *Quality, Reliability, Risk, Maintenance, and Safety Engineering (ICQR2MSE), 2011 International Conference on*, pages 868–873. IEEE, 2011.

[8] Molina-Cristobal, A., Parks, G., and Clarkson, P. Finding robust solutions to multi-objective optimisation problems using polynomial chaos. In *Proc. 6th ASMO UK/ISSMO Conference on Engineering Design Optimization*. 2006.

[9] Wei, X., Wang, G., Massarotto, P., Golding, S., and Rudolph, V. Numerical simulation of multicomponent gas diffusion and flow in coals for CO2 enhanced coalbed methane recovery. *Chemical Engineering Science*, 62(16):4193–4203, 2007.

[10] Jalal, J. and Mohaghegh, S. D. A coalbed methane reservoir simulator designed and developed for the independent producers. In *SPE Eastern Regional Meeting*. Society of Petroleum Engineers, 2004.

[11] Gautschi, W. Algorithm 726: ORTHPOL–a package of routines for generating orthogonal polynomials and Gauss-type quadrature rules. *ACM Transactions on Mathematical Software (TOMS)*, 20(1):21–62, 1994.

[12] Eldred, M., Webster, C., and Constantine, P. Evaluation of non-intrusive approaches for Wiener-Askey generalized polynomial chaos. In *Proceedings of the 10th AIAA Non-Deterministic Approaches Conference, number AIAA-2008-1892, Schaumburg, IL*, volume 117, page 189. 2008.

[13] Kewlani, G. and Iagnemma, K. A stochastic response surface approach to statistical prediction of mobile robot mobility. In *Intelligent Robots and Systems, 2008. IROS 2008. IEEE/RSJ International Conference on*, pages 2234–2239. IEEE, 2008.

[14] Webster, M. D., Tatang, M. A., and McRae, G. J. Application of the probabilistic collocation method for an uncertainty analysis of a simple ocean model. *MIT Joint Program on the Science and Policy of Global Change*, 1996.

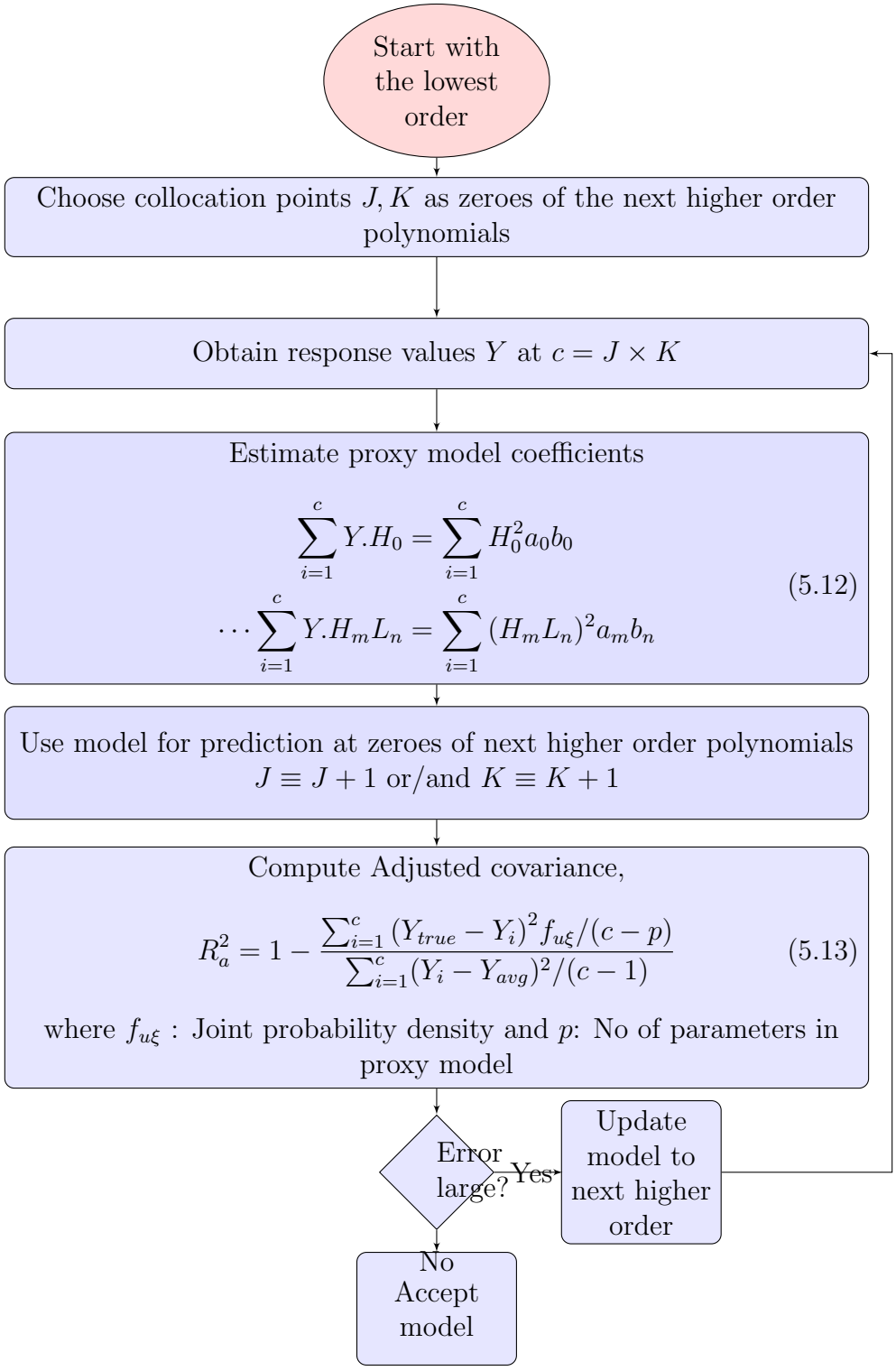

Figure 5.2: *Work flow for proxy model development.*

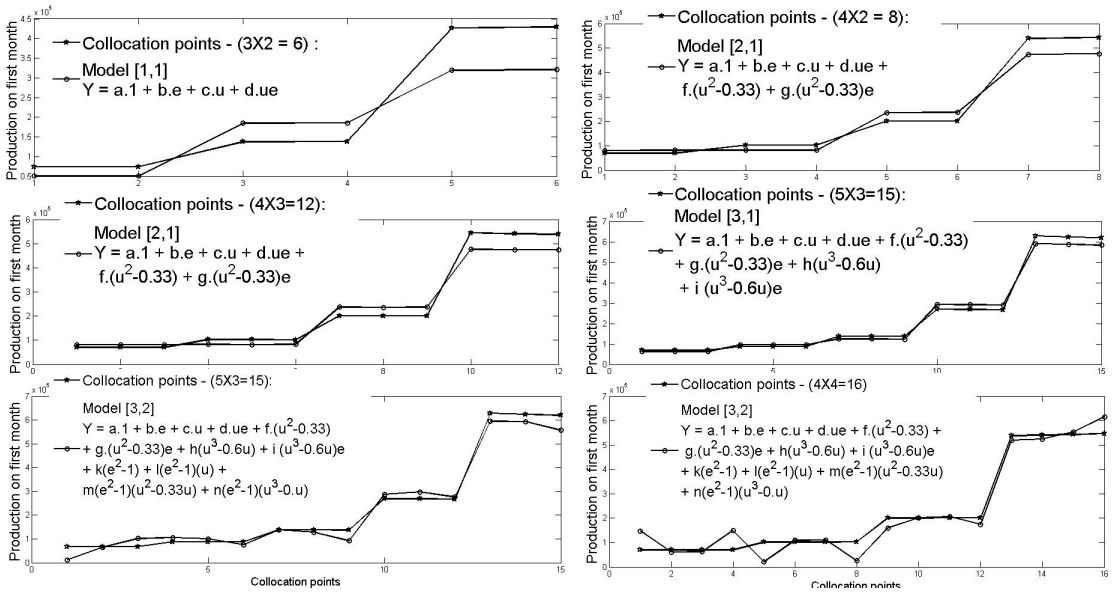

Figure 5.3: *Comparing performances of models built with Gaussian quadrature with simulation data from original model, Equation 5.1.*

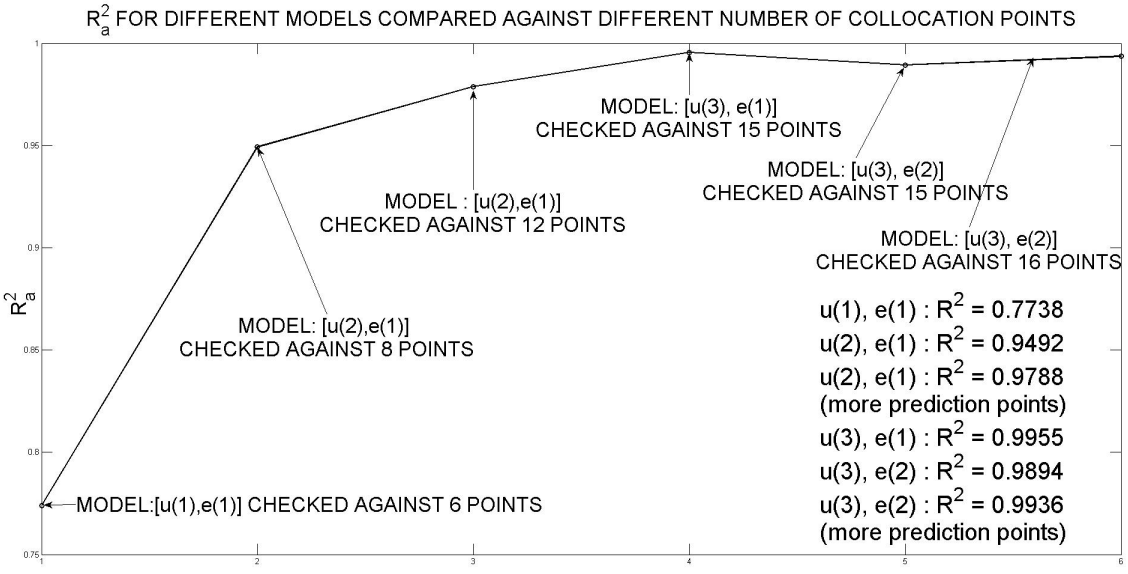

Figure 5.4: *Adjusted coefficient of determination for different models.*

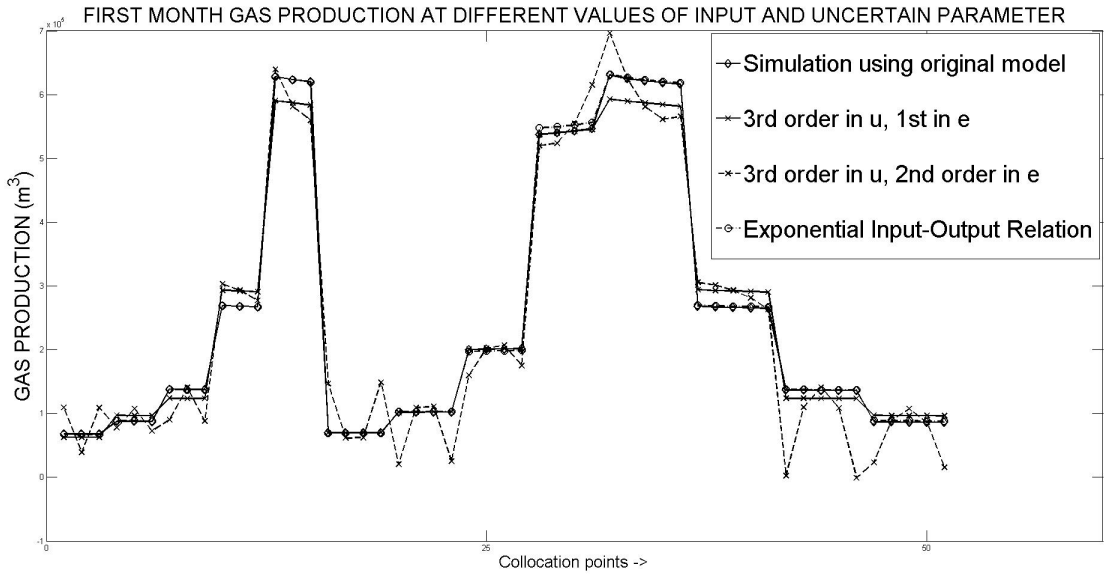

Figure 5.5: *Comparing third order models built with Gaussian quadrature and the Levenberg-Marquardt algorithm for a large number of collocation points against simulation data.*

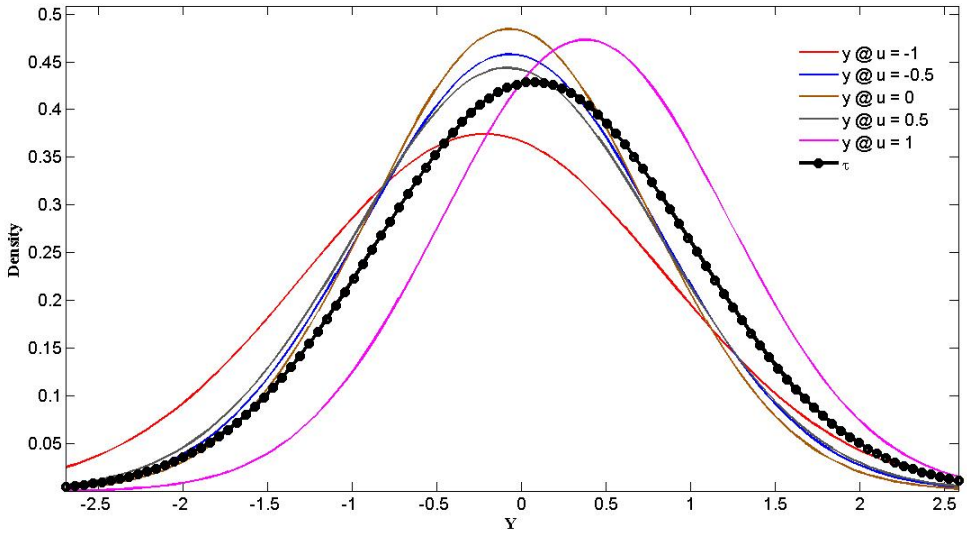

Figure 5.6: *Probability distribution of the normalized values of τ and Y at different input values, u*

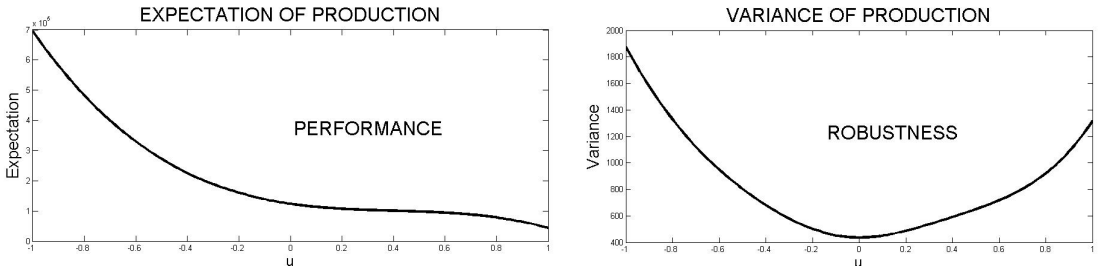

Figure 5.7: *Expectation & Variance of production.*

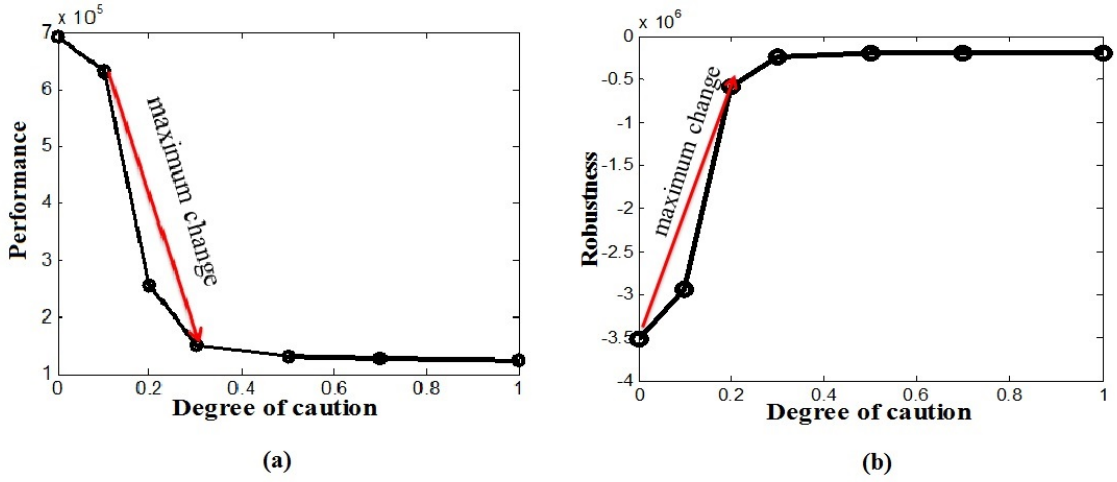

Figure 5.8: *Performance and robustness at varying degrees of caution.*

Chapter 6

Multiphase reactive-transport simulations for estimation and robust optimization of the field scale production of microbially enhanced coalbed methane

Abstract

The discovery that approximately 20% of natural gas is microbial in origin has elevated interest in microbially enhanced coalbed methane (MECoM). However, a rational approach to exploit this calls for the development of reservoir scale models that includes the effect of microbial activity. To address this, we have developed a multiscale, multiphase, multicomponent reactive-transport model for the production of microbially enhanced coalbed methane (MECoM) that includes microbial kinetics. The model is used to evaluate field scale strategies for commercial MECoM production. Optimization studies are also conducted over a range of injection nutrient composition and injector bottomhole pressures. In order to account for the effect of uncertainty in the model parameters, robust optimization is performed. Proxy models are constructed using a multivariate polynomial chaos expansion framework to evaluate the cost functions involved in the robust optimization. The use of sparse polynomial chaos expansions to deal with issues related to high dimensionality is also explored. The results of robust optimization indicate local as well as global optimal points. Also, since the measure of robustness from the proxy model is independent of input variables, the location of the robust optimal point does not vary for different degrees of caution.

6.1 Introduction

Coalbed methane (CBM) is the gas stored/trapped in coalbeds. It is a mixture of methane (80 - 90% by volume) and minor amounts of carbon dioxide, nitrogen, hydrogen sulphide, sulphur dioxide and heavier hydrocarbons such as ethane, propane and butane. CBM was first explored as a source of fuel in the 1990s. Since then, rapid technology developments, coupled with CBM's higher efficiency, lower GHG/toxic gas emissions and zero waste disposal compared to its predecessor coal, has elevated CBM's status as a significant source of natural gas. The International Energy Agency reports that in 2008, CBM accounted for 10%, 4% and 8% of natural gas production in the United States, Canada and Australia respectively. Countries with large coal reserves such as India, China, Russia and Indonesia are also investing in CBM extraction on large scales[1,2]. However, there are many key issues impeding the development of commercial scale CBM production. Amongst these, the low productivity of gas wells and the ensuing high investment requirement in drilling multiple wells is a big challenge, apart from the issues of heterogeneity of coal beds, economics of gas demand and supply, water and environmental management, the availability of gas and water pipelines and land and ownership issues.[3]

There are two dominant processes by which CBM is produced - thermocatalytic cracking at elevated temperatures and pressures, and anaerobic microbial attack of organic matter. When thermal processes begin to dominate during coal formation, microbial activity is usually suppressed. However, recent laboratory and field experiments have indicated that in addition to microbial CBM generated in the past, many basins have active ongoing biogenic methane generation.[4–6] Restoration of microbial activity in these basins is considered to be the result of triggering events such as basin uplift and cooling, the flow of underground water, and the dilution of salinity levels.[6,7] The microbial CBM produced after these events is referred to as secondary biogenic methane. It is estimated that approximately 20% of the methane produced worldwide is microbial in origin[8]. Microbially enhanced coal bed methane production (MECoM) seeks to enhance the production of secondary biogenic methane through improved productivity of existing gas wells along with bioconversion of deep, unmineable coal into fuels.

6.2 Microbially enhanced coalbed methane

The four primary strategies employed for MECoM are microbial stimulation by addition of nutrients, microbial augmentation by addition of microbes, physically increasing fracture spacing to provide more access to microbes and nutrient amendments, and

chemically increasing the bioavailability of coal organics[4]. Many laboratory studies have been conducted to evaluate each of these effects. Laboratory incubation studies on lignite and subbituminous coals by Harris et al.[9] showed that substantial methane production occurs in the presence of H_2/CO_2 and inorganic nutrient amendments. Studies by Singh et al.[10] on an Indian coal bed sample showed that methane production in the presence of formation waters and native microbial population improved considerably with the addition of nitrite. Experiments by Opara et al.[11] on lignite, bitminous coal and coal wastes with selected microbial inocula and different types and levels of nutrient amendments showed that methane production increased with increasing nutrient concentrations. The addition of organic nutrients such as tryptone and Brain Heart Infusion (BHI) was shown to improve methane production in sub-bituminous coal samples from western Canada by Penner et al.[12]. Jones et al.[13] observed that bioaugmentation with a consortium of bacteria and methanogens enriched from wetland sediment accompanied by biostimulation with nutrient amendments generated methane more rapidly and to a higher concentration as compared to biostimulation without the amendments. Experiments by Papendick et al.[14] on native Walloon coal with produced waters from the Surat basin showed that the initial methane production rate and the final methane yield increased by 240% and 180%, respectively, on the addition of a Zonyl FSN surfactant to improve coal bioavailability. Similarly, Huang et al.[15] showed that methane production increased when coal samples were treated with potassium permanganate, a depolymerization agent that aids in coal solubilization.

Many field scale studies have also been carried out on biogenic methane production. Succesful pilot scale field tests for microbial stimulation of CBM production were conducted by Luca Technologies, Inc. to restore gas production in existing wells in the Powder River Basin, Wyoming. Similarly, Crisis Energy and Next Fuel, Inc. have also conducted smaller field scale tests. Also, Archtech, Synthetic Genomics and ExxonMobil hold patents related to MECoM[4]. US patent 7696132[16] describes methods for stimulating biogenic production with enhanced hydrogen content using a combination of hydrogen and phosphorous compounds, US patent 5424195[17] describes a method using household sewage injection into an abandoned coal mine to provide feedstock for the bacteria, US patent 20040033557[18] describes a method for injection of bacteria and nutrients under pressure into naturally occurring fractures or cleats as well as fractures induced during the stimulation of coalbed methane gas wells, US patent 20140034297[19] describes methods for dispersion of nutrient amendments and US 7640978[20] describes methods for contacting subsurface coalbeds with microbes under anaerobic conditions to form a reaction mixture.

Although numerous studies have been carried out, a key link in the commercialization of any such technology development is the capacity to conduct model-based analysis for technology transfer over increasing scales along with process estimation, optimiza-

tion and control at field scales. For instance, Luca's operational approach was batch treatment of wells with nutrient amendments, followed by the assessment of new gas formation after many months or years, whereas Ciris adopted a continuous-flow injection process using 4 injection wells surrounded by 13 production wells, recirculating 1000 - 2000 barrels of water every day. Since there is no rigorous approach for the appraisal of these operating procedures, optimum injection procedures cannot be resolved and process efficiency is likely to be compromised. Thus, in the absence of suitable simulation tools, decisions related to production forecasting, well completions, etc. are likely to be sub-optimal.

In this work, we construct a field scale reservoir simulator in the simulation environment of CMG STARS[21] and use it to conduct studies on enhancement and optimization of microbial methane production.

6.3 Development of the reactive-transport model

In our previous study,[22] we developed a gas phase transport model for dual porosity coalbed reservoirs and coupled it with a kinetic model based on the assumption that microbes survive only on residual pore water. However, this is not directly applicable in the assessment of commercial field applications where formation and injection waters are present in excess. Moreover, since studies have indicated that native microorganisms found in coal formations are usually nutrient-limited[12], it is also necessary to include nitrogen limitations in the kinetic model. Thus, in this study, we develop reservoir simulations in the Advanced Process and Thermal Reservoir Simulator 2011.10 (STARS),[21] by the Computer Modelling Group (CMG) with enzymatic reaction kinetics described for a multi-substrate limited case (developed in our previous study[23]). Results of gas prediction from the simulations are subsequently employed in field scale process optimization.

As described in our previous study,[22] multi-porosity coalbeds can be characterized satisfactorily by dual porosity, with the primary and secondary porosity being referred to interchangeably as macropores and micropores or fractures and matrix, respectively. Primary porosity consists of fractures or macropores (> 50 nm) and mesopores of dimensions $2 - 50$ nm, while secondary porosity consists of micropores of dimension < 2 nm[24–26]. Gas transport in this dual scale porous system is modeled by a dual step transport mechanism consisting of Darcy's flow in macropores and diffusive flow in the micropores. Micropore gas diffusion is controlled by surface desorption and diffusion through coal matrix, both of which are lumped based on a pseudo steady-state approach to treat diffusion as a one-step process. This method models matrix reponse relative to pseudo steady-state adsorbed gas concentrations

in a lumped parameter fashion; hence, it neglects the true spatial variation of the gas concentration and is therefore less accurate for the early stages of production.[24] Based on the above assumptions, we build a CMG STARS[21] physical model to conduct field scale simulations of coalbed methane production in the presence of microbial activity.

6.3.1 Reservoir characteristics

First, dual porosity characteristics of coalbeds are implemented in CMG STARS using the standard dual-porosity (DP) model.[27] According to this model, fluid transfer only occurs between matrices and fractures, and there is no direct communication between interblock matrices. Figure 6.1 shows the representation of a standard DP model. Next, since microbes can only access fractures[4,18] (or macropores of dimension >1 μm) and micropores are inaccessible to water[24,28–32] (which is required for microbial growth), microbial activity is assumed to occur only in the fractures. Hence, in our model, coal exists as a reactive component only in the fractures while the role of micropores is limited to storage.

The properties of the standard DP model are assigned as follows. The fracture volume fraction, which is the ratio between the fracture volume and the gross volume, is set to to 3%, and its total porosity is set to 100%. On filling these fractures with solid coal component at 200 $\frac{gmol}{m^3 \text{ pore volume}}$, the effective fracture porosity becomes 80%, making the total fracture porosity $0.8 \times 0.03 = 0.024$ or 2.4%. Similarly, the matrix porosity can be set to a high value and then filled with coal for an effective porosity of approximately 10%. Alternatively, the matrix porosity can be initialized directly to 10%, since the rock (or coal) present here does not participate in bioconversion. A description of reservoir properties and initial conditions in the porous system are shown in Table 6.1 and Table 6.2, respectively. Adsorption of gases in the porous spaces are defined using the ADSCOMP, ADSLANG, ADSROCK and ADMAXT functions in STARS. Parameter values corresponding to adsorption of CH_4, CO_2 and H_2 based on the Langmuir isotherm are shown in Table 6.3. Liquid- gas relative permeability values are obtained by linear/quadratic interpolation of the values shown in Table 6.4.

Communication between the matrix and fracture domains is controlled by a factor known as interporosity transmissibility. This is a function of σ, which is a shape factor depending on matrix block sizes. Among the different methods available for evaluating σ, the Kazemi-Gilman formulation is chosen. According to this,

$$\sigma = 4V_b \sum_i \frac{k_{mi}}{L_i^2}$$

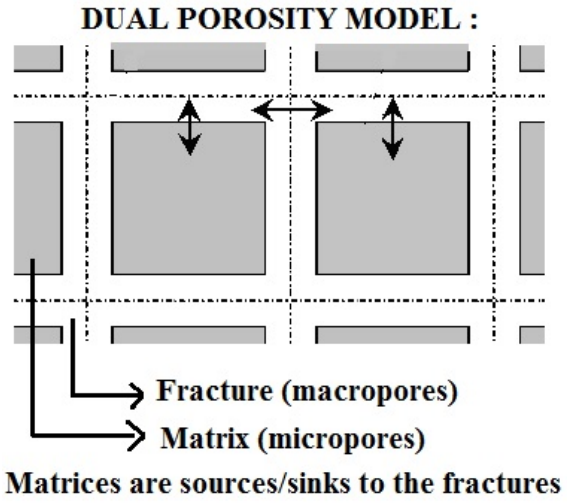

Figure 6.1: *Schematic representation of dual porosity reservoirs*

where V_b is the block volume, k_{mi} is the effective matrix permeability in all directions and L_i is the fracture spacing in x, y, z directions[21,33,34].

6.3.2 Reaction kinetic model

Having defined the reservoir properties for the model, the next issue is the reaction kinetic model. Figure 6.2 depicts the fate of matrix and fractures during coal bioconversion and shows that with an increase in reaction progress, coal is consumed only from the fractures, while the coal in the micropore blocks remain inert participating only in the diffusion of its gases. All of the components in the model are defined in Table 6.5. Gas components are defined separately for those already present in the reservoir (denoted by CH_{4i}, CO_{2i}, H_{2i}) and those produced by microbial activity (denoted by CH_4, CO_2, H_2). The multi-substrate limited enzymatic reaction kinetic model to be coupled with the transport model is based on the simplified reaction pathway in lumped species developed in our previous studies[23,35]. This is described by Equation 6.1, where $r_C, r_S, r_W, r_B, r_A, r_{CH_4}, r_{CO_2}$ are the rate of change of concentration of coal (C), solubilized coal (S), fragmented coal (W), lumped benozate (B), lumped acetate (A), methane and carbon dioxide; undergoing coal solubilization, hydrolysis, acidogenesis, acetogenesis and methanogenesis, respectively. [Nu] represents the concentration of the protein-based nitrogen rich nutrient, tryptone, that was tested in anaerobic serum bottle and coreflooding experiments for microbial stimulation to produce microbially enhanced coalbed methane[12,23,35]. Kinetic parameter values obtained by the regression of gas production data from coreflooding

Property	Unit	**Value/Description**
Grid System	-	Cartesian Rectangular
Number of grid blocks (I, J directions)	-	10
Thickness of grid block (I, J directions)	m	100
Number of grid blocks (K)	-	5
Thickness of grid block (K direction)	m	6
Depth of grid bottom from surface	m	1000
Fracture spacing (I, J directions)	m	10
Fracture spacing (K direction)	m	1
Fracture volume (as fraction of gross volume)	%	3
Matrix porosity (constant over grid system)	%	98
Fracture porosity (constant over grid system)	%	99.9
Matrix permeability (I, J, K directions)	mD	0.001
Fracture permeability (Unstimulated)(I, J, K directions)	mD	0.1
Fracture permeability (Stimulated)(I, J, K directions)	mD	5
Transmissibility factor σ for fracture-matrix flow	-	Kazemi-Gilman formulation[21]
Effective micropore porosity	%	10
Overall macropore porosity	%	2.4

Table 6.1: *Reservoir properties in the CMG STARS model.*

Property	unit	Value
Reservoir pressure	MPa	10
S_w matrix	-	0
S_w fracture	-	0.5
S_g matrix	-	1
S_g fracture	-	0.5
Fraction of methane and carbon dioxide adsorbed in the matrix in gas phase	-	0.5
Fraction of free methane and carbon dioxide in gas phase in fractures	-	0.5
Fraction of H_2O in water phase in fractures	-	0.99
Fraction of $[A]$ in water phase in fractures	-	0.01
Coal concentration in matrix	$\frac{\text{gmol}}{m^3 \text{ pore volume}}$	850
Coal concentration in fracture	$\frac{\text{gmol}}{m^3 \text{ pore volume}}$	200

Table 6.2: *Initial reservoir conditions for the base case run.*

	$\mathbf{CH_4}$	$\mathbf{CO_2}$	$\mathbf{H_2}$
ADSLANG Term 1	100	250	50
ADSLANG Term 3	10000	10000	10000
Maximum rock adsorption capacity specified by ADMAXT			
ADMAXT (macropores)	0.1	0.2	0.005
ADMAXT (micropores)	0	0	0

Table 6.3: *Adsorption properties of gas components in micropore spaces. ADSLANG inputs Langmuir isotherm parameters, Term 1 corresponding to V_l (m^3/m^3), Term 3 corresponding to P_l (kPa).*

MATRIX; Linear Interpolation		
S_l	K_{rg}	K_{rog}
0	0.0001	0
1	0	1
FRACTURE; Quadratic Interpolation		
S_l	K_{rg}	K_{rog}
0	1	0
1	0	1

Table 6.4: *End points for linear/quadratic interpolation of liquid-gas relative permeability values. K_{rg} and K_{rog} are the relative gas and water permeabilities, respectively.*

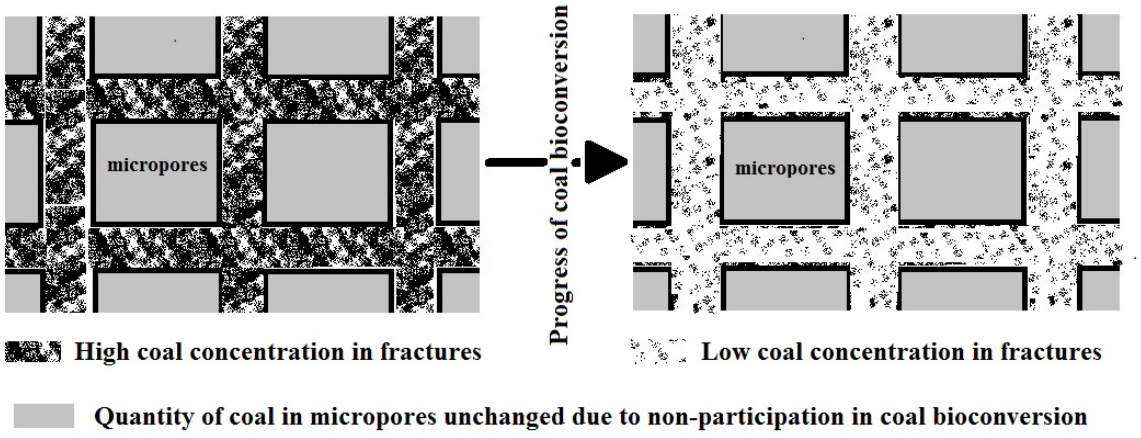

Figure 6.2: *Depiction of coal concentrations in primary and secondary porosities with progress of bioconversion.*

Component	Unit	**Value/Description**
Solid components	-	Coal (C)
Coal molecular weight	kg/gmol	1.444
Coal solid density	kg/m^3	1422
Water phase components	-	Water (H_2O) Solubilized coal (S) Fragmented coal (W) Lumped benzoate (B) Lumped acetate (A) Nutrient (nitrogen-rich) (Nu)
Gas phase components	-	Free/desorbed methane (CH_{4i}) Free/desorbed carbon dioxide (CO_{2i}) Free/desorbed hydrogen(H_{2i}) Biogenic methane(CH_4) Biogenic carbon dioxide(CO_2) Biogenic hydrogen(H_2)

Table 6.5: *Components/species used in the CMG STARS model.*

experiments are retained[23] in this model.

$$r_C = -ke^{S_n[Nu]}\left(\frac{C}{C_0}\right)^{2/3}([S^*]-[S]) \tag{6.1a}$$

$$r_S = ke^{S_n[Nu]}\left(\frac{C}{C_0}\right)^{2/3}([S^*]-[S]) - \frac{[Nu]}{k_1+[Nu]}b[S] \tag{6.1b}$$

$$r_W = 10\frac{[Nu]}{k_1+[Nu]}b[S] - \frac{[Nu]}{k_2+[Nu]}\left(\frac{\mu_1[W]}{Ks_1+[W]+\frac{Ks_1}{Ks_2}[Nu]}\right) \tag{6.1c}$$

$$r_B = \frac{[Nu]}{k_2+[Nu]}\left(\frac{\mu_1[W]}{Ks_1+[W]+\frac{Ks_1}{Ks_2}[Nu]}\right) + \frac{\mu_2[Nu]}{Ks_2+[Nu]+\frac{Ks_2}{Ks_1}[W]} - d\frac{[Nu]}{k_3+[Nu]}[B] \tag{6.1d}$$

$$r_A = 3\frac{[Nu]}{k_3+[Nu]}d[B] - \frac{[Nu]}{k_4+[Nu]}\left(\frac{e[A]}{f+[A]+[A]^2/g}\right) \tag{6.1e}$$

$$r_{Nu} = -\frac{\mu_3[Nu]}{Ks_2+[Nu]+\frac{Ks_2}{Ks_1}W]} - K_{Nus}[Nu] \tag{6.1f}$$

$$r_{CH_4} = \frac{[Nu]}{k_4+[Nu]}\frac{e[A]}{(f+[A]+[A]^2/g)} \tag{6.1g}$$

$$r_{CO_2} = \left(\frac{\mu_1[Nu][W]}{(k_2+[Nu])(Ks_1+[W]+\frac{Ks_1}{Ks_2}[Nu])}\right) + \frac{d[Nu][B]}{k_3+[Nu]} + r_{CH_4} \tag{6.1h}$$

These enzymatic kinetics for coal bioconversion are incorporated into the CMG STARS model. Reaction stoichiometry is defined with functions STOREAC, STOPROD and RPHASE. Reaction rates of the form $r = kC_1^aC_2^b$ are defined using RORDER (for a, b), FREQFAC (for k) and RXCRITCON (in the case of solid components). For reactions of the form $r' = \frac{r}{(1+Ax)^B}$, where x is a component concentration, RXCMPFAC is used. Due to limitations of the input format in CMG STARS, some modifications have to be made to the kinetic model, as discussed in the following section.

Incorporation of reaction kinetics into the CMG STARS model

- Similar to our previous study,[22] coal solubilization reaction kinetics is modeled based on the assumption that macropore spaces are composed of N spherical coal particles of radius R_0. The corresponding solubilization rate is incroporated into CMG STARS by two parallel reactions as

$$\frac{d[C]}{dt} = r_1 + r_2;\ r_1 = k[S^*]\left(\frac{C}{C_0}\right)^{2/3} \text{ and } r_2 = -k[S]\left(\frac{C}{C_0}\right)^{2/3}$$

where r_1 and r_2 are the rates of reaction 1 and 2 respectively (see Table C1).

Also, we assume the solubilization rate constant to increase with increase in porosity (i.e., decrease in particle radius), so as to denote the increase in the surface area made available for solubilization. This is defined with the functions PERMCK and PERMSCALE in CMG STARS. Using PERMCK, the permeability is made to vary with fluid porosity via the Carmen-Kozeny formulation, $k(\phi) = k\phi_0 \left(\frac{\phi}{\phi_0}\right)^{2.5} \left(\frac{1-\phi}{1-\phi_0}\right)^2$. PERMSCALE is then used to define scaling factors for the solubilization rate constant at different permeability values.

- Kinetic parameter values used in the simulation are obtained from our previous study.[23] Since the values of k_1, k_2, k_3, k_4 are low, the kinetic rate terms corresponding to nutrient limitation in solubilization, acidogenesis, acetogenesis and methanogenesis are approximated as $\frac{[Nu]}{k_i+[Nu]} \approx 1$.

- The reaction rate for methanogenesis is given by

$$r_A = \frac{e[A]}{f + [A] + [A]^2/g}; \text{ with } e = 471\frac{mol}{m^3}\text{day}^{-1}, f = 215\frac{mol}{m^3}, g = 0.0011\frac{mol}{m^3} \tag{6.2}$$

  In accordance with the Haldane model structure for the kinetic rate in Equation 6.2, the reaction rate profile increases from zero within a narrow concentration range and then decreases to zero (refer Figure 6.3a). Since the available functional capabilities in STARS does not permit input of the reaction rate expression in this form, we rewrite the rate expression with a perturbation variable $\epsilon = \frac{[A]}{c_2}$, where c_2 is a large number relative to low acetate concentrations, as

$$r_A = \frac{e'}{1 + k'[A]} - \left(\frac{1-\epsilon}{\epsilon}\right) K + \text{ constant} \tag{6.3}$$

  On nonlinear regression of Equation 6.4 against rate data generated with Equation 6.2, we get

$$r_A = \frac{0.52}{1 + 0.68[A]} - \frac{10000}{[1 + 6666667[A]]} \tag{6.4}$$

  which is formatted in CMG STARS as two reactions (reactions 7 and 8 in Table C1). Figure 6.3 compares the rate data generated by Equations 6.2 and 6.4. The regressed model deviates from the original kinetic expression (in Equation 6.2) at very low acetate concentrations. Thus, the initial acetate concentration in the simulations is kept at non-zero values to avoid errors in estimation.

- Finally, lumped benzoate production rates in the presence of competition be-

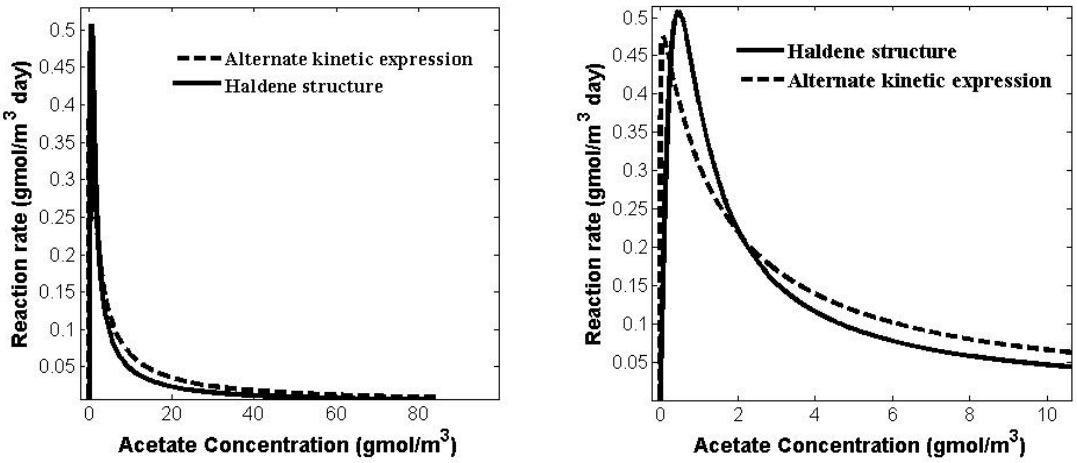

(a) **(b)**

Figure 6.3: *(a) Comparison of rate data generated using the Haldane model (Equation 6.2) and the regressed model (Equation 6.4), (b) zoomed view of Figure 6.3a, indicating deviation of regressed model at low acetate concentrations.*

tween $[W]$ and $[Nu]$ is given by

$$r_{[B]\text{ from }[W]} = \frac{\mu_1[W]}{Ks_1 + [W] + \frac{Ks_1}{Ks_2}[Nu]}; r_{[B]\text{ from }[Nu]} = \frac{\mu_2[Nu]}{Ks_2 + [Nu] + \frac{Ks_2}{Ks_1}[Nu]}$$

are simplified by the approximation, $\frac{[W]}{Ks_1} \approx 0$; eliminating the competition of $[W]$ against $[Nu]$ to produce benzoate. The simplified form is

$$r_{[B]\text{ from }[W]} = \frac{\frac{\mu_1}{Ks_1}[W]}{1 + \frac{1}{Ks_2}[Nu]}; r_{[B]\text{ from }[Nu]} = \frac{\frac{\mu_2}{Ks_2}[Nu]}{1 + \frac{1}{Ks_2}[Nu]}$$

Incorporation of the reaction kinetic model into CMG STARS is described in Table C.1 in the appendix.

6.3.3 Well patterns and operating conditions

A horizontal producer well is simulated with perforations running through grid blocks [1:10, 5, 1], while four 4 horizontal injector wells are simulated at each corner of the grid block. The injector and the producer wells are all considered to be of the same radius, approximately 3 inches. Well perforations and operating constraints are shown

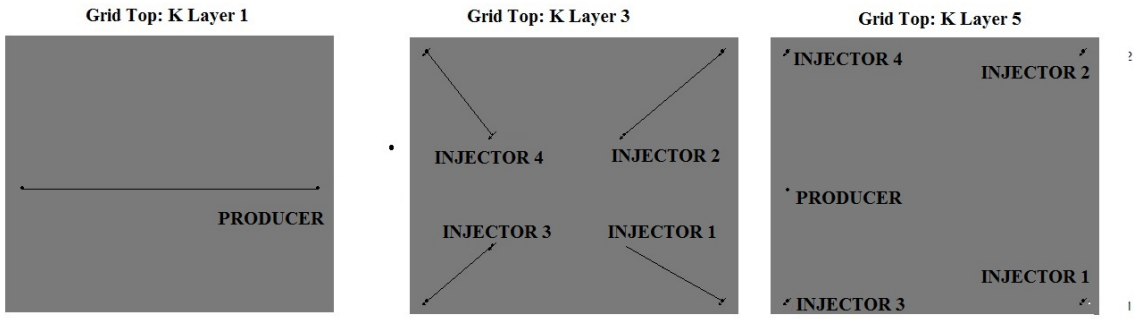

Figure 6.4: *Well perforations in the vertical layers of the reservoir.*

in Table 6.6. Figure 6.4 shows the perforations of the wells at different layers in the vertical direction (K). It is to be noted that directional drilling is the common technique applied to coal seams since they are generally interspersed between different geologic formation layers.[36,37] The physical model built in CMG STARS is then employed for simulations of microbially enhanced coalbed methane. Simulations are performed in reservoirs with natural fractures (low permeability) and stimulated fractures (high permeability). In practice, the low permeability of pre-existing fractures can be modified by artificial stimulation methods such as hydraulic fracturing. Apart from water, fracturing can also be achieved with inert gases such as nitrogen and carbon dioxide or foams containing water and inert gases with a foaming agent, air or air-to-air mixture injection and electrothermal bed stimulation.[38–40]

6.4 Optimization studies

Finally, the results of the model-based simulation runs are applied in the optimization of methane production under varying operating conditions. The cumulative methane generation is considered to be the objective cost function, which can be modified with weighed penalties for high nutrient costs, operating pressure requirements, related water management costs, etc. Optimization is performed using the CMG DECE algorithm available in the CMG CMOST toolbox. CMG DECE is an optimization method that sequentially applies an exploration stage, where the parameter space is randomly explored, and a controlled evolution stage, where candidate values are evaluated and rejected or retained.

Well					
Producer	Index	Perforations			FLOW TO
	1	1	5	5	SURFACE
	2	1	5	1	1
	3	10	5	1	2
	Minimum Bottom Hole operating pressure				300 kPa
Injector 1	Index	Perforations			FLOW FROM
	1	10	1	5	SURFACE
	2	10	1	3	1
	3	7	3	3	2
Injector 2	Index	Perforations			FLOW FROM
	1	10	10	5	SURFACE
	2	10	10	3	1
	3	7	7	3	2
Injector 3	Index	Perforations			FLOW FROM
	1	1	1	5	SURFACE
	2	1	1	3	1
	3	3	3	3	2
Injector 4	Index	Perforations			FLOW FROM
	1	1	10	5	SURFACE
	2	1	10	3	1
	3	3	7	3	2

Table 6.6: *Well perforations and operating constraints of the injector and producer wells.*

Proxy model and robust optimization

Uncertainty persists in the parameter values for kinetic and transport, since many of these are extrapolated from smaller scales to the reservoir model. We perform robust optimization to account for this uncertainty; however, this places a prohibitive computational burden. We resolve this by developing proxy/surrogate models based on a multivariate polynomial chaos expansion framework developed in our previous study[41].

Polynomial chaos expansion (PCE) is a method used for uncertainty propagation in nonlinear dynamic systems. It was first introduced by Wiener as homogeneous chaos in 1938[42], and is derived from the Cameron Martin theorem which states that an expansion in Hermite polynomials in Gaussian random variables converges in the L_2 sense for any arbitrary stochastic process with a finite second moment[43]. Xiu et al.[44] later identified optimal trial bases from the Askey family of orthogonal polynomials to represent stochastic processes, which became known as the Wiener-Askey polynomial chaos. A stochastic ouptut X is represented by a truncated polynomial chaos expansion as

$$X(\theta) = \sum_{j=0}^{p} a_j \Psi_j(\xi)$$

where Ψ_j belongs to an orthogonal basis set, chosen based on the probability distribution of the random source.

A stochastic proxy model incroporating uncertainty information into an input-output relation can be built in this framework using Legendre orthogonal polynomials (associated with a constant weighing function) in the input variables[41]. The method is motivated by the rationale that an input variable varying within a specified range may be represented by a random variable belonging to a uniform distribution. Although this is a computationally superior technique for robust optimization compared to other methods,[45–47] its reliability depends on the accuracy of the proxy model parameters. Parameter estimation is usually performed using two approaches: Galerkin projection,[48] with Gaussian quadrature rules applied for evaluation of the resulting multivariate integrals, and linear regression. A key issue with this method is the large dimensionality of the expansions, which increases with the number of input variables and the degree of nonlinearity. To deal with this, we propose that the polynomials in the expansion be chosen based on ranking of correlation indices. However, other methods such as hyperbolic index sets or least-angle regression, which are used extensively in sparse polynomial expansions, may also be suitable.[49–51]

6.5 Results and discussion

Simulation of microbially enhanced methane production is performed for two cases: one corresponding to natural fractures, with fracture permeability = 0.1 mD (obtained on history match of production data from Manville wells in our previous study[22]), and the other for the case of stimulated fractures, with fracture permeability = 5 mD. Injector and producer wells are configured as discussed in section 3.3. During operation, injectors are assigned a maximum bottomhole pressure constraint of 10 MPa, and the nutrient fraction in the injected fluid is assigned to be 0.3. For cases where the external nutrient supply is cut off, the injectors are shut down. Thus, a total of four different cases are simulated. Cases 1 and 2 simulate low permeability reservoirs in the absence and presence of external nutrient injection, respectively, and cases 3 and 4 are the corresponding simulations for high permeability reservoirs.

Figure 6.5 shows nutrient dispersion in reservoirs with low and high permeabilities and shows that nutrient dispersion (over a period of 200 days) is greater when the permeability is higher. Figures 6.6 and 6.7 show the quantities of biogenic and free & desorbed methane for each of the cases. It is to be noted that these simulations are performed for a non-zero initial acetate concentration in the fractures. The net cumulative methane generation in high permeability reservoirs is almost an order of magnitude higher than that in low permeability reservoirs. Figure 6.8 compares biogenic methane generation, while Table 6.7 shows the percentage of biogenic methane in the total methane recovery for each of the cases. The absolute biogenic methane recovery as well as the percentage of biogenic methane in the total methane recovered are the highest for case 4 (high permeability with nutrient injection), while these indicators are almost similar for cases 1 and 2 (low permeability reservoirs). Although the absolute value of biogenic methane generated is higher, the percentage of biogenic methane recovery is lower in case 3 compared to cases 1 and 2. This is due to the increase in free and desorbed methane production in the high permeability reservoir (case 3) compared to the low permeability reservoirs.

Since the reservoir with stimulated fractures responds better to nutrient injection, it was investigated for maximization of total methane recovery. The nutrient fraction in the injection fluid ($f_{nutrient}$) and maximum bottomhole pressure (BHP) at all four injectors were the operating conditions that were varied. Figure 6.9a shows a 3D surface plot of cumulative methane production at nutrient fractions varying between 0 - 0.5 and injector bottomhole pressures (BHP) varying between 10 - 20 MPa. Figure 6.9b provides the contours of this surface based on varying the BHP. It can be observed that the cumulative methane production increases with an increase in nutrient fraction at lower BHP. However, at higher BHP, an increase in the nutrient fraction causes the cumulative methane production to increase to a maximum before

reducing, with the nutrient fraction at which the maximum is reached being smaller as the BHP increases.

Proxy model and Robust optimization

The output variable Y is the cumulative methane generated at the end of 200 days. The subset of input variables and uncertain model parameters chosen is shown in Table 6.8. The input variables u_1 and u_2 are scaled such that they can be expanded with a sequence of Legendre polynomials orthogonal on the interval $[-1, 1]$. Similarly, uncertain parameters ξ_1 and ξ_2 are normalized by scaling the variables as $\frac{\xi_i - \mu_i}{\sigma_i}$, where μ_i and σ_i are the mean and standard deviation of ξ_i, $i = 1, 2$. Equation 6.5a shows the output variable Y, expanded with first order Legendre polynomials in u_1 and u_2, followed by expansion of the deterministic coefficients L, M and N in Equation 6.5b using first order Hermite polynomials in ξ_1 and ξ_2.

$$Y = L + Mu_1 + Nu_2 \tag{6.5a}$$
$$\equiv (Y_0 + Y_1\xi_1 + Y_2\xi_2) + (Y_3 + Y_4\xi_1 + Y_5\xi_2)u_1 + (Y_6 + Y_7\xi_1 + Y_8\xi_2)u_2 \tag{6.5b}$$

As the order of the expansion increases, the number of terms in the expansion can increase upto $N_{terms} = \frac{(n+p)!}{n!p!}$, where n is the number of parameters in the expansion and p is the order of the expansion. In order to choose the dominant terms in the expansion, the pairwise linear correlation coefficients between the output Y and the expansion polynomials $u_1, u_2, u_1\xi_1, u_1^2 - 0.33, \ldots$ are evaluated and ranked. Based on this, it was observed that the terms ξ_1, $u_1^2 - 0.33$, u_1u_2 & $u_1 \times u_1^2 - 0.33$ have the most correlation with the output variable, Y. Thus, a proxy model is built as shown in Equation 6.6 with model parameters estimated by linear regression against the simulation output of the CMG STARS model at 88 randomly generated sets of $[u_1, u_2, \xi_1, \xi_2]$. Figure 6.10 compares simulations of the full model at about 1000 collocation points, against the estimated proxy model at those points.

$$\begin{aligned} Y &= Y_0 + Y_1\xi_1 + Y_2(u_1^2 - 0.33) + Y_3u_1u_2 + Y_4u_1(u_1^2 - 0.33) \\ Y_0 &= 577250, Y_1 = 28600, Y_2 = 84390, Y_3 = 57970, Y_4 = 28830 \end{aligned} \tag{6.6}$$

It is seen that the significant terms in the proxy model only contain ξ_1. This indicates that the effect of uncertainty in the quantity of coal in macropores is lesser compared

to permeability of the reservoir. Next, the proxy model is used in robust optimization with an objective function defined as

$$\max_{u_1,u_2} P = (1-\alpha) * E(Y, u_1, u_2, \xi_1, \xi_2) - \alpha V(Y, u_1, u_2, \xi_1, \xi_2) \tag{6.7}$$

where P is the cumulative methane production, E and V are the expectation and variance of the cumulative methane production predicted by the proxy model over ξ_1, ξ_2 and α is the degree of caution in the results. Statistical metrics E and V are easily evaluated using Equation 6.6 giving

$$\begin{aligned} E(Y, u_1, u_2, \xi_1, \xi_2) &= Y_0 + Y_2(u_1^2 - 0.33) + Y_3 u_1 u_2 + Y_4 u_1(u_1^2 - 0.33) \\ V(Y, u_1, u_2, \xi_1, \xi_2) &= Y_1^2 \end{aligned} \tag{6.8}$$

Figure 6.11 shows the objective cost function P over a range of u_1 and u_2, while Figure 6.12 provides the contours of this surface at varying BHP. A local optimum occurs at low nutrient fraction and high injector BHP, whereas the global optimum occurs at high nutrient fraction and high injector BHP. The value of the expectation of the cumulative methane production at low nutrient fraction and high injector BHP, which was the global maximum in the nominal deterministic optimization procedure, is in fact very low under the robust optimization strategy. This indicates the strong effect of the macropore permeability ξ_1 under such operating conditions since, any uncertainty in its value can lead to the deterministic optimum no longer being valid. Thus, operating at low nutrient fraction at high injector pressures could result in large variability and therefore unreliability of the deterministic optimization. It is to be noted that in this case, since the variance of the objective function V is independent of u_1 or u_2, the location of the robust optimal point does not vary with changing degree of caution α.

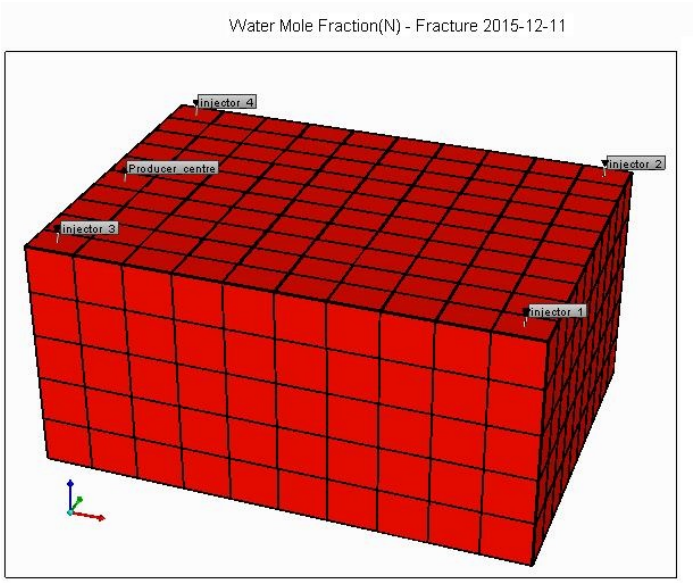

(a) *Tight reservoir (fracture permeability = 0.1 mD).*

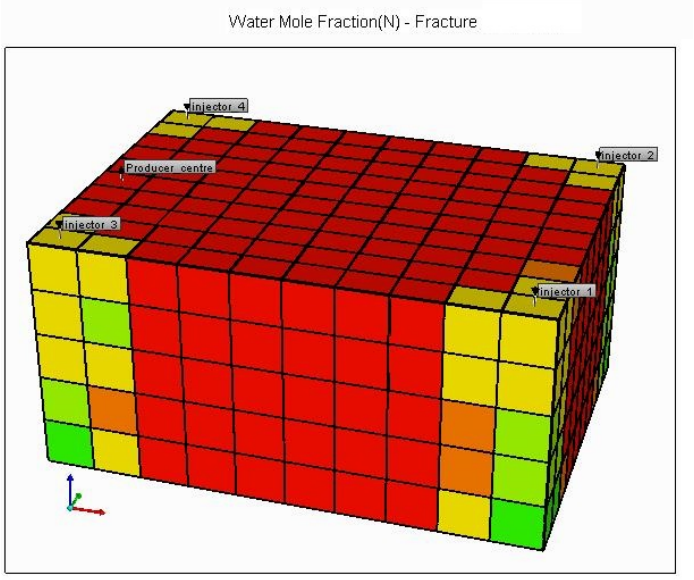

(b) *Reservoir with stimulated fractures (fracture permeability = 5 mD).*

Figure 6.5: *Nutrient concentration in coalbed reservoirs with natural and stimulated fractures.*

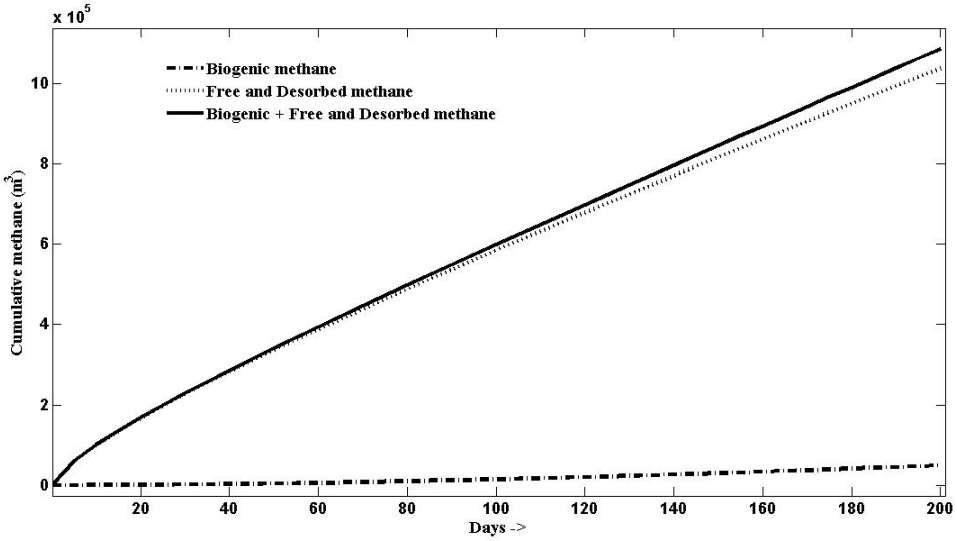

(a)

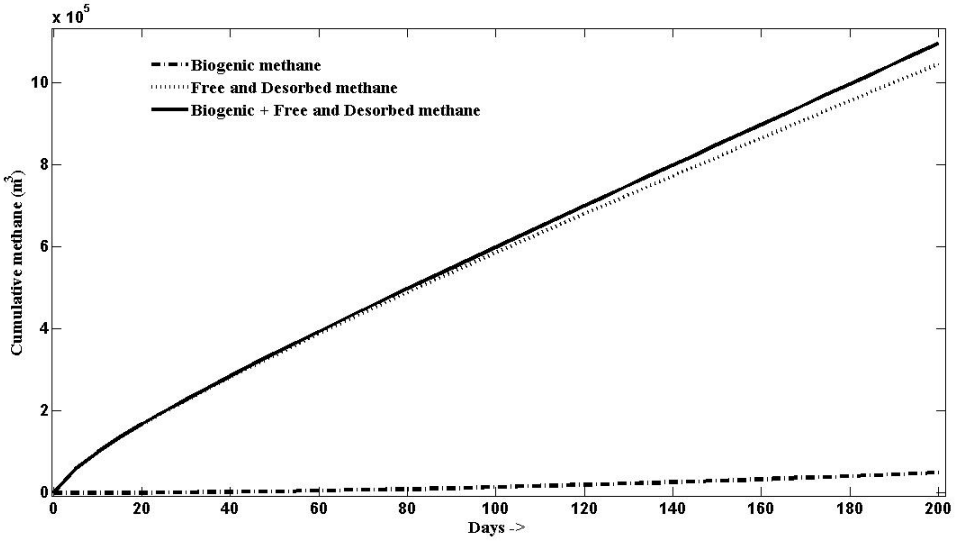

(b)

Figure 6.6: *Quantities of biogenic, free and desorbed methane from CBM reservoirs with natural fractures (permeability = 0.1 mD) (a) with and (b) without nutrient injection.*

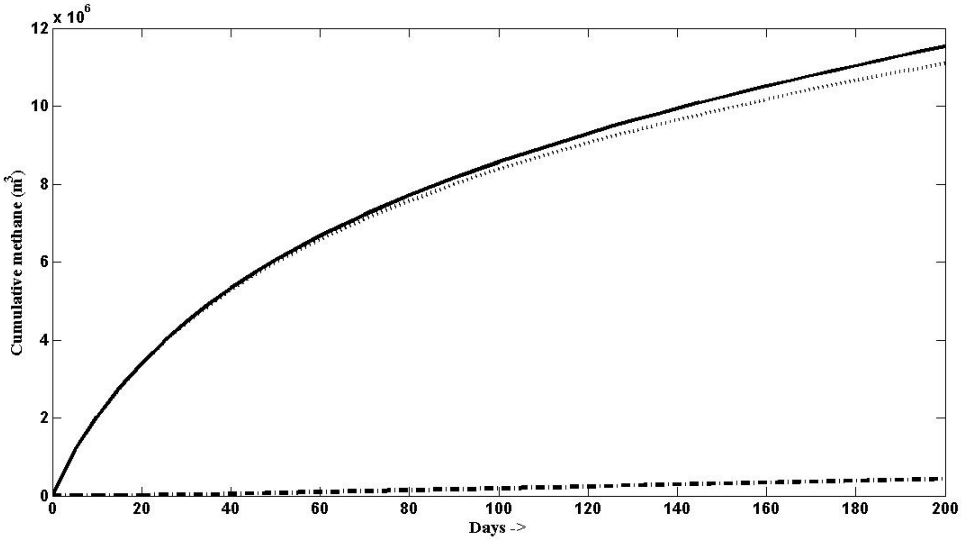

(a)

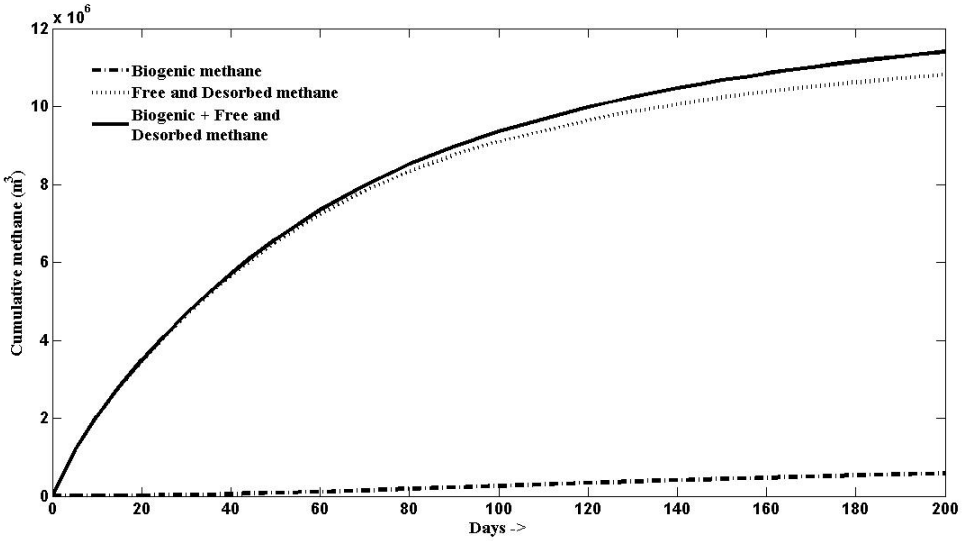

(b)

Figure 6.7: *Quantities of biogenic, free and desorbed methane from CBM reservoirs with stimulated fractures (permeability = 5 mD) (a) with and (b) without nutrient injection.*

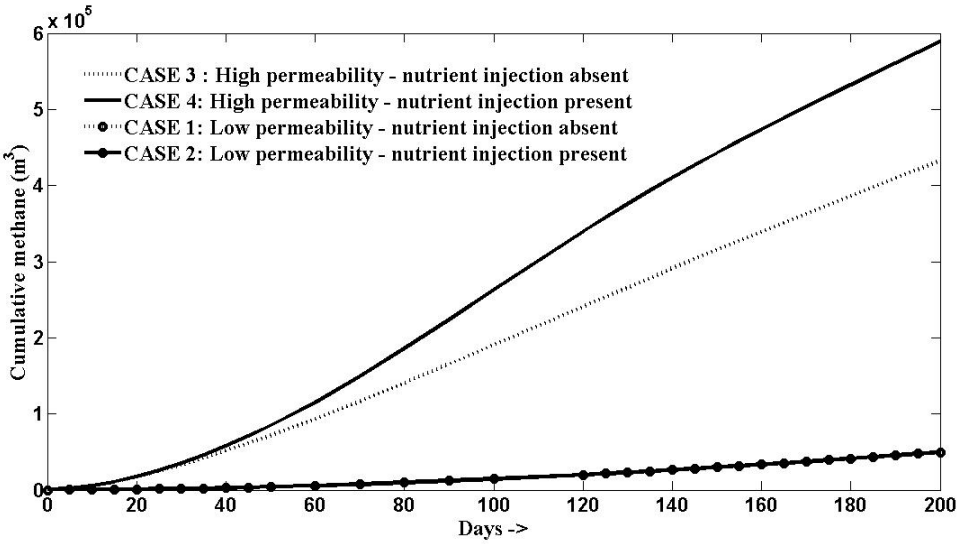

Figure 6.8: *Comparison of biogenic methane generated in CBM reservoirs with natural and stimulated fractures, with and without nutrient injection.*

Index	Case	Percentage of biogenic methane
1	Low permeability without nutrient injection	4.53
2	Low permeability with nutrient injection	4.54
3	High permeability without nutrient injection	3.75
4	High permeability with nutrient injection	5.17

Table 6.7: *Percentage of biogenic methane in total methane recovery.*

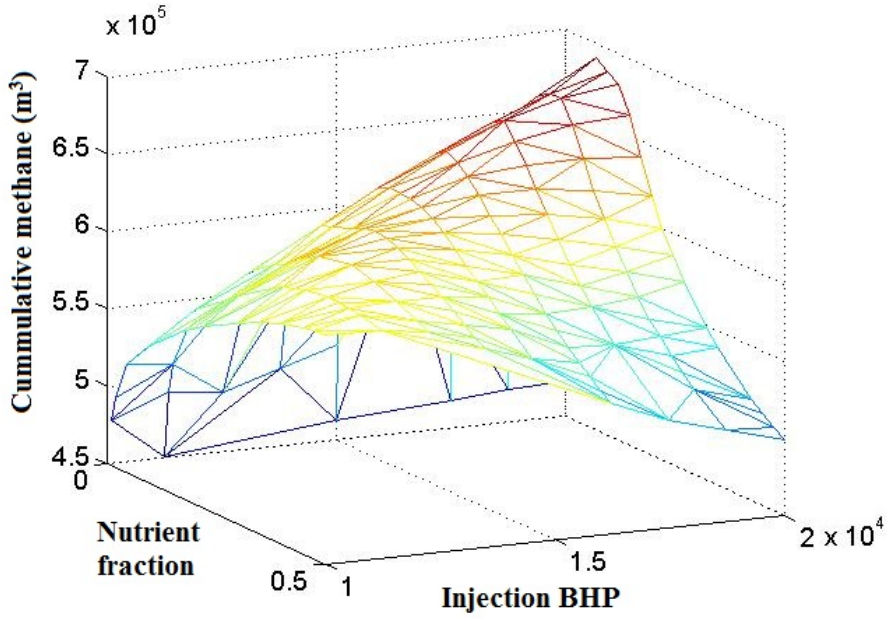

(a) *3D surface plot for cumulative biogenic methane production at varying nutrient fractions and injection bottomhole pressures (kPa).*

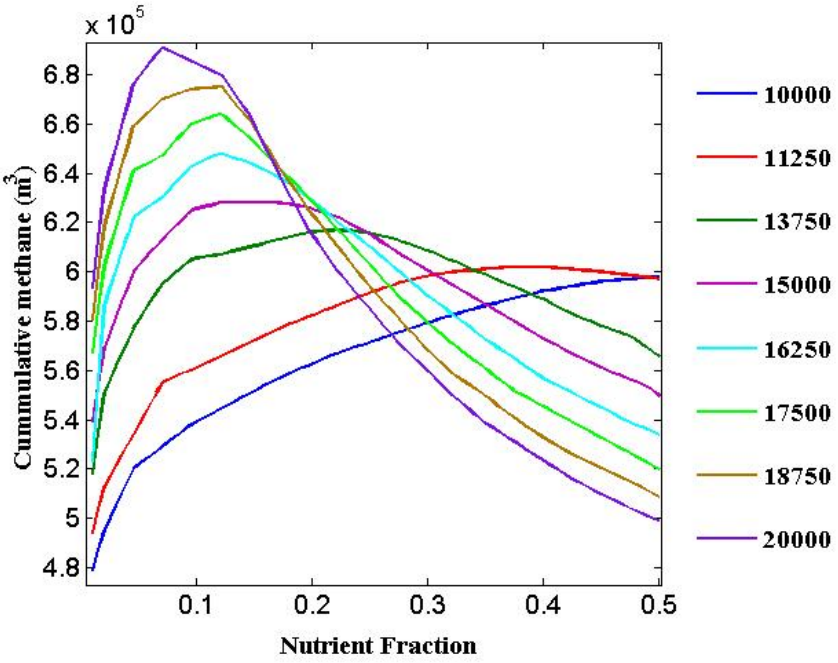

(b) *Contour plots depicting variation of cumulative biogenic methane production with nutrient injection at different injection BHP pressures (kPa).*

Figure 6.9: *The variation of microbially enhanced biogenic methane production with nutrient injection and injection bottomhole pressure (BHP).*

Variable	Description	Parameter range
u_1	Fraction of nutrient composition in injection fluid	[0.001 0.5]
u_2	Injector bottomhole pressure	[10 20] MPa
ξ_1	Isotropic fracture permeability	Gaussian distribution; $N(5,1)$ mD
ξ_2	Initial coal quantity in fractures	Gaussian distribution; $N(200,25)$ $\frac{\text{gmol}}{m^3}$

Table 6.8: *Inputs and uncertain parameters in the proxy model.*

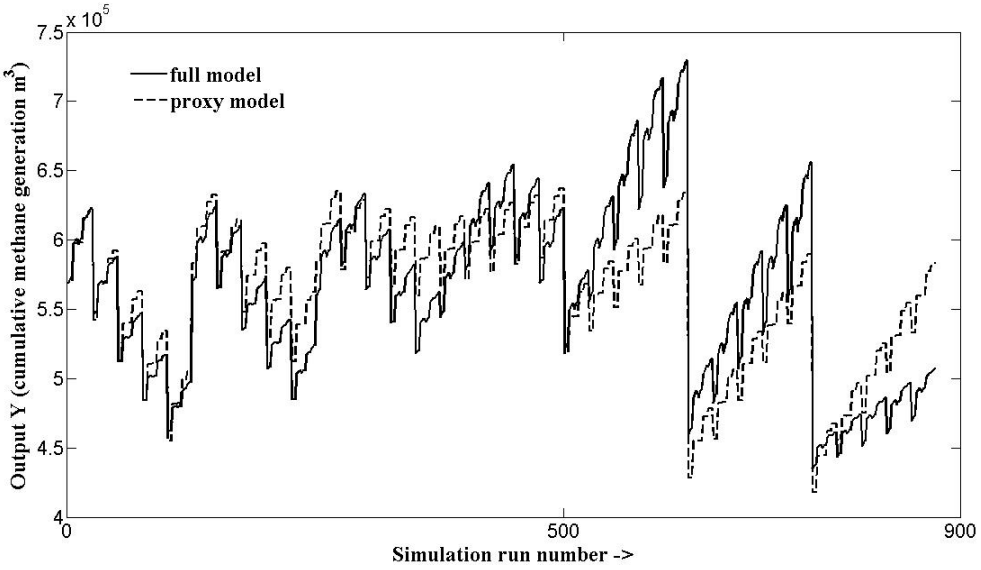

Figure 6.10: *Comparison of predictions of cumulative methane production for the reservoir model in CMG STARS and the proxy model.*

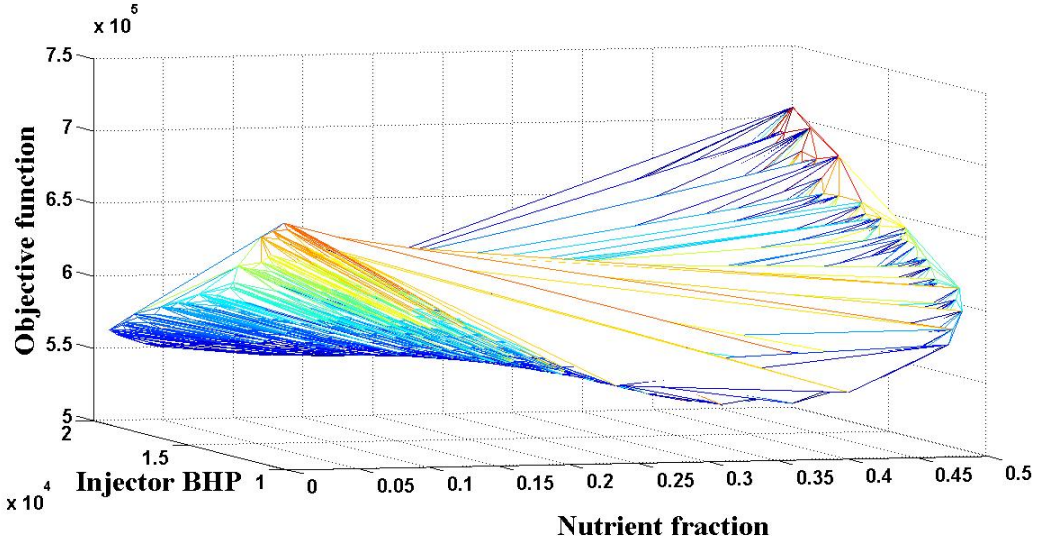

Figure 6.11: *Response surface for the robust optimization strategy.*

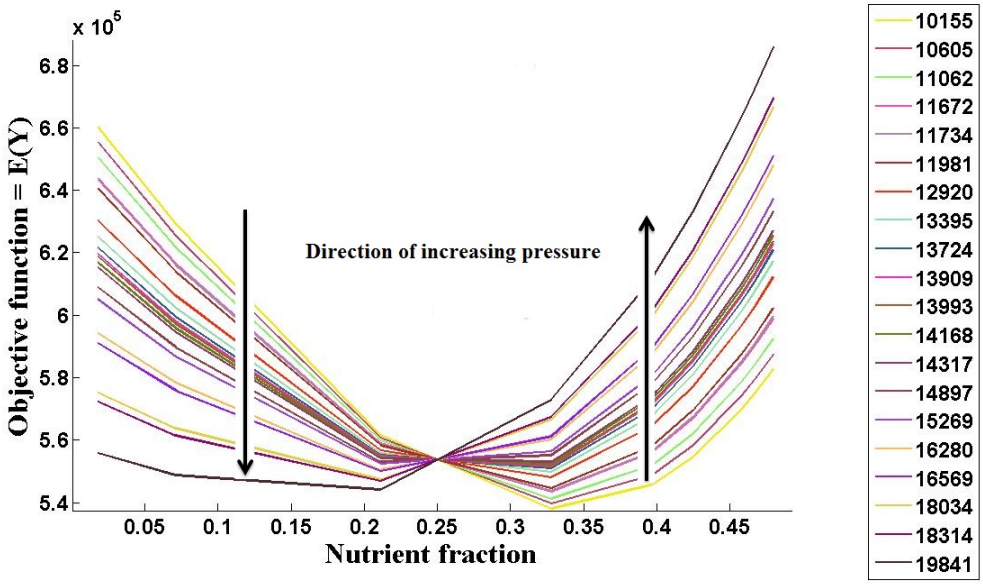

Figure 6.12: *Contour plots depicting variation of expectation of the cumulative biogenic methane production over the range of normally distributed values of mcropore permeability, with nutrient injection at different injection BHP pressures (kPa).*

6.6 Conclusion

Simulations of microbially enhanced coal bed methane were performed with the reservoir simulator, CMG STARS. A standard dual porosity model was described with the matrix-fracture transmissibility factor evaluated by the Kazemi-Gilman formulation. Since microbes and water required for microbial growth can exist only in macropores, coal bioconversion was assumed to occur only in the fractures with the coal in the micropores acting only as a storage reserve for the gases. The sorption behaviour of methane, carbon dioxide and hydrogen was defined by Langmuir isotherms, and finally, the microbial chain reactions were incorporated into the simulator. The physical model was then simulated for a specific well pattern, with and without external nutrient injection. Since naturally occurring coal fractures are insufficient for nutrient dispersion, nutrient effects were significant only under high permeability, which can be obtained by stimulated fractures. Next, the model based simulations were used in the optimization of coalbed methane production at varying nutrient fraction in the injected fluid and injector bottomhole pressures (BHP). It was observed that at lower injector BHP, the cumulative methane generation increases with an increase in the nutrient fraction in the injection fluid. However, at higher BHP, the cumulative methane generation reaches a maximum and then decreases with an increase in nutrient concentration. Lastly, in order to account for model parameter uncertainties, robust optimization strategies were tested based on a stochastic proxy model built in a polynomial chaos expansion framework. The stochastic proxy model was built for coal bed methane production at varying nutrient fraction and injector bottomhole pressure, in the presence of uncertainty from macropore permeability and coal quantity in macropores. Robust optimal points evaluated based on the proxy model indicate a local optimum at low nutrient concentration and low injector BHP, and a global optimum at high nutrient concentration and high injector BHP. Moreover, it was observed that the effect of uncertainty in macropore permeability is significant at the optimum operating regions evaluated under nominal optimization studies, implying that under those conditions, there is a high chance for field tests to deviate from model-based predictions, unless uncertainty is taken into account in the prediction and optimization. Also, since there is no significant interaction between uncertain variables and input variables, the location of the robust optimal point did not shift for varying degrees of caution.

References

[1] Stevens, P. The 'Shale Gas Revolution': Hype and Reality. *Chatham House, London*, 2010.

[2] Senthamaraikkannan, G. and Prasad, V. Coalbed methane. In M.R.Riazi and Gupta, R., editors, *Coal Production and Processing Technology*. Taylor & Francis Group, (in press).

[3] Stiller, B., Bocek, T., Hecht, F., Machado, G., Racz, P., and Waldburger, M. Coal Bed Methane (CBM) market analysis by application (Industrial, Power Generation, Residential, Commercial and Transportation) and Segment Forecasts To 2020. Technical report, Grand View Research, 2014.

[4] Ritter, D., Vinson, D., Barnhart, E., Akob, D. M., Fields, M. W., Cunningham, A. B., Orem, W., and McIntosh, J. C. Enhanced microbial coalbed methane generation: A review of research, commercial activity, and remaining challenges. *International Journal of Coal Geology*, 146:28–41, 2015.

[5] Martini, A., Walter, L., Budai, J., Ku, T., Kaiser, C., and Schoell, M. Genetic and temporal relations between formation waters and biogenic methane: Upper Devonian Antrim Shale, Michigan Basin, USA. *Geochimica et Cosmochimica Acta*, 62(10):1699–1720, 1998.

[6] Ulrich, G. and Bower, S. Active methanogenesis and acetate utilization in Powder River Basin coals, United States. *International Journal of Coal Geology*, 76(1):25–33, 2008.

[7] Parkes, R. J., Cragg, B. A., and Wellsbury, P. Recent studies on bacterial populations and processes in subseafloor sediments: a review. *Hydrogeology Journal*, 8(1):11–28, 2000.

[8] Rice, D. D. and Claypool, G. E. Generation, accumulation, and resource potential of biogenic gas. *AAPG Bulletin*, 65(1):5–25, 1981.

[9] Harris, S. H., Smith, R. L., and Barker, C. E. Microbial and chemical factors influencing methane production in laboratory incubations of low-rank subsurface coals. *International Journal of Coal Geology*, 76(1):46–51, 2008.

[10] Singh, D. N., Kumar, A., Sarbhai, M. P., and Tripathi, A. K. Cultivation-independent analysis of archaeal and bacterial communities of the formation water in an Indian coal bed to enhance biotransformation of coal into methane. *Applied microbiology and biotechnology*, 93(3):1337–1350, 2012.

[11] Opara, A., Adams, D., Free, M., McLennan, J., and Hamilton, J. Microbial production of methane and carbon dioxide from lignite, bituminous coal, and coal waste materials. *International Journal of Coal Geology*, 96:1–8, 2012.

[12] Penner, T. J., Foght, J. M., and Budwill, K. Microbial diversity of western canadian subsurface coal beds and methanogenic coal enrichment cultures. *International Journal of Coal Geology*, 82(1):81–93, 2010.

[13] Jones, E. J., Voytek, M. A., Corum, M. D., and Orem, W. H. Stimulation of methane generation from nonproductive coal by addition of nutrients or a microbial consortium. *Applied and Environmental Microbiology*, 76(21):7013–7022, 2010.

[14] Papendick, S. L., Downs, K. R., Vo, K. D., Hamilton, S. K., Dawson, G. K., Golding, S. D., and Gilcrease, P. C. Biogenic methane potential for Surat Basin, Queensland coal seams. *International Journal of Coal Geology*, 88(2):123–134, 2011.

[15] Huang, Z., Urynowicz, M. A., and Colberg, P. J. Stimulation of biogenic methane generation in coal samples following chemical treatment with potassium permanganate. *Fuel*, 111:813–819, 2013.

[16] Pfeiffer, R., Ulrich, G., and Finkelstein, M. Chemical amendments for the stimulation of biogenic gas generation in deposits of carbonaceous material, April 13 2010. US Patent 7,696,132.

[17] Volkwein, J. Method for in situ biological conversion of coal to methane, June 13 1995. US Patent 5,424,195.

[18] Scott, A. and Guyer, J. Method of generating and recovering gas from subsurface formations of coal, carbonaceous shale and organic-rich shales, February 19 2004. US Patent 10,640,273.

[19] Mahaffey, W., Bradfish, J., Haveman, S., Sutton, B., and Greaser, L. Dispersion of compounds for the stimulation of biogenic gas generation in deposits of carbonaceous material, February 6 2014. US Patent 20140034297.

[20] Pfeiffer, R., Ulrich, G., Vanzin, G., Dannar, V., DeBruyn, R., and Dodson, J. Biogenic fuel gas generation in geologic hydrocarbon deposits, January 5 2010. US Patent 7,640,978.

[21] Computer Modelling Group: Calgary, Alberta, Canada. *Computer Modelling Group STARS Version 2011.10 Users Guide*, 2011.

[22] Senthamaraikkannan, G., Gates, I., and Prasad, V. Development of multiscale microbial kinetics coupled gas transport model for simulation of biogenic coalbed methane production. *(submitted)*, 2015.

[23] Senthamaraikkannan, G., Gates, I., and Prasad, V. Modeling, estimation and optimization of biogenic methane production in coreflooding experiments. *(submitted)*, 2015.

[24] Wei, X., Wang, G., Massarotto, P., Golding, S., and Rudolph, V. Numerical simulation of multicomponent gas diffusion and flow in coals for CO_2 enhanced coalbed methane recovery. *Chemical engineering science*, 62(16):4193–4203, 2007.

[25] Shi, J. and Durucan, S. A bidisperse pore diffusion model for methane displacement desorption in coal by CO_2 injection. *Fuel*, 82(10):1219–1229, 2003.

[26] Ryu, Z., Zheng, J., Wang, M., and Zhang, B. Characterization of pore size distributions on carbonaceous adsorbents by DFT. *Carbon*, 37(8):1257–1264, 1999.

[27] Gong, B. *Effective models of fractured systems*. Ph.D. thesis, Stanford University, 2007.

[28] Bustin, R. and Clarkson, C. Geological controls on coalbed methane reservoir capacity and gas content. *International Journal of Coal Geology*, 38(1):3–26, 1998.

[29] King, G. R., Ertekin, T., and Schwerer, F. C. Numerical simulation of the transient behavior of coal-seam degasification wells. *SPE Formation Evaluation*, 1(02):165–183, 1986.

[30] Kolesar, J., Ertekin, T., and Obut, S. The unsteady-state nature of sorption and diffusion phenomena in the micropore structure of coal: Part 1-theory and mathematical formulation. *SPE Formation Evaluation*, 5(01):81–88, 1990.

[31] Prinz, D. and Littke, R. Development of the micro-and ultramicroporous structure of coals with rank as deduced from the accessibility to water. *Fuel*, 84(12):1645–1652, 2005.

[32] Goktas, B. and Ertekin, T. Production performance analysis of cavity-completed wells. In *SPE Eastern Regional Meeting*. Society of Petroleum Engineers, 1998.

[33] Lee, B. and Tan, T. Application of a multiple porosity/permeability simulator in fsractured reservoir simulation. In *SPE Symposium on Reservoir Simulation*. Society of Petroleum Engineers, 1987.

[34] Kazemi, H., Merrill Jr, L., Porterfield, K., and Zeman, P. Numerical simulation of water-oil flow in naturally fractured reservoirs. *Society of Petroleum Engineers Journal*, 16(06):317–326, 1976.

[35] Senthamaraikkannan, G., Budwill, K., Gates, I., Mitra, S., and Prasad, V. Kinetic modeling of the biogenic production of coalbed methane. *(submitted)*, 2015.

[36] U.S. Environmental Protection Agency (U.S. EPA). Directional drilling technology. Retrieved July 21, 2015 from `www.epa.gov/cmop/docs/dir-drilling.pdf`.

[37] Dogwood Initiative. Coalbed methane: Best Practices in British Columbia. Retrieved July 21, 2015 from `http://dogwoodinitiative.org/publications/reports/coalbed-methane-best-practices-for-british-columbia`.

[38] U.S. Environmental Protection Agency (U.S. EPA). Characteristics of coalbed methane production and associated hydraulic fracturing practices, In Evaluation of Impacts to Underground Sources of Drinking Water by Hydraulic Fracturing of Coalbed Methane Reservoirs. Retrieved July 21, 2015 from `http://www.epa.gov/ogwdw/uic/pdfs/cbmstudy_attach_uic_ch03_cbm_practices.pdf`, 2004.

[39] Gale, J. and Freund, P. Coal-Bed Methane Enhancement with CO_2 Sequestration Worldwide Potential. *Environmental Geosciences*, 8(3):210–217, 2001.

[40] Griffiths, M. and Severson-Baker, C. Unconventional Gas: The Environmental Challenges of Coalbed Methane Development in Alberta. Technical report, Pembina Institute for Appropriate Development, Drayton Valley, AB, Canada, 2003.

[41] Senthamaraikkannan, G. and Prasad, V. Stochastic proxy modelling for coalbed methane production using orthogonal polynomials. In *Proc. 9th IFAC Symposium on Advanced Control of Chemical Processes*. June 2015.

[42] Wiener, N. The homogeneous chaos. *American Journal of Mathematics*, pages 897–936, 1938.

[43] Dutta, P. and Bhattacharya, R. Nonlinear estimation with polynomial chaos and higher order moment updates. In *American Control Conference (ACC), 2010*, pages 3142–3147. IEEE, 2010.

[44] Xiu, D. and Karniadakis, G. E. The Wiener–Askey polynomial chaos for stochastic differential equations. *SIAM Journal on Scientific Computing*, 24(2):619–644, 2002.

[45] Mandur, J. and Budman, H. A polynomial-chaos based algorithm for robust optimization in the presence of Bayesian uncertainty. In *Proc. 8th IFAC symposium on Advanced Control of Chemical Processes*. 2012.

[46] Xiong, F., Xue, B., Yan, Z., and Yang, S. Polynomial chaos expansion based robust design optimization. In *International Conference on Quality, Reliability, Risk, Maintenance, and Safety Engineering (ICQR2MSE), 2011*, pages 868–873. IEEE, 2011.

[47] Molina-Cristobal, A., Parks, G., and Clarkson, P. Finding robust solutions to multi-objective optimisation problems using polynomial chaos. In *Proc. 6th ASMO UK/ISSMO Conference on Engineering Design Optimization*. 2006.

[48] Ghanem, R. and Dham, S. Stochastic finite element analysis for multiphase flow in heterogeneous porous media. *Transport in Porous Media*, 32(3):239–262, 1998.

[49] Blatman, G. and Sudret, B. Adaptive sparse polynomial chaos expansion based on least angle regression. *Journal of Computational Physics*, 230(6):2345–2367, 2011.

[50] Blatman, G. and Sudret, B. Sparse polynomial chaos expansions and adaptive stochastic finite elements using a regression approach. *Comptes Rendus Mécanique*, 336(6):518–523, 2008.

[51] Blatman, G. and Sudret, B. Efficient computation of global sensitivity indices using sparse polynomial chaos expansions. *Reliability Engineering & System Safety*, 95(11):1216–1229, 2010.

Chapter 7

Conclusions and Future work

7.1 Concluding remarks

Microbial enhancement of coalbed methane is a valuable prospect for improved recovery from existing as well as new gas wells. Although there is a growing body of work on fundamental and commercial research of MECoM (microbially enhanced coalbed methane), several key questions related to effective implementation of MECoM technology on a commercial scale still remain. The major factors deterring the development of simulation tools that can aid in the conceptualization and assessment of field scale MECoM recovery are the complexity and variability of coal and the associated microbiota, complicated biodegradation mechanisms that are not fully understood, incomplete knowledge of reactant transport within coal and the inaccessible nature of coal seams. Addressing these issues, we have developed multiscale models with reasonable predictive capabilities for the quantification of biogenic methane production based on a scaling approach, incorporating information from the laboratory to the field scale. The work presented in this thesis hence provides a framework for the analysis, optimization and control of commercial MECoM recovery.

In Chapter 2, we focussed on the first challenge - kinetic modeling of coal bioconversion. By considering the major reaction classes in coal bioconversion, i.e., solubilization, hydrolysis, acidogenesis, acetogeneis and methanogenesis; and taking into account information on dominant intermediates from anaerobic serum bottle experiments, we have proposed a simplified reaction pathway using lumped species, with acetoclastic methanogenesis as the dominant methanogenic pathway and the nutrient tryptone being assumed to produce a pool of benzoate. A kinetic model was then derived using a diffusion layer model for solubilization, simple Monod models for hydrolysis, acidogenesis and acetogenesis and a Haldane type model for methanogenesis

to account for substrate inhibition from acetate. Following model validation against experimental coal bioconversion data from many different coal samples, both with and without nutrient addition, a sensitivity analysis revealed that parameters controlling solubilization and methanogenesis affect methane production the most. Additionally, the kinetic model was used to infer the concentrations of intermediate products in the bioconversion of coal and to devise optimal operating strategies for maximizing the production of methane and/or intermediate products.

In Chapter 3, we applied the kinetic model to predict methane production in core-flooding experiments, which attempt to mimic CBM reservoir conditions in terms of porosity, fluid migration and high pressure conditions. The kinetic model was modified to accomodate varying nitrogen substrate limitations along the core and the adsorption kinetics of the dissolved gases onto solid coal. Using a tanks-in-series model to simulate plug flow in the core, kinetic parameters were estimated by non-linear regression against experimental data using particle swarm optimization (PSO). The estimated model was then used to study the effect of operating conditions and alternate injection patterns. Model-based experimental design was evaluated using D-optimal criterion. Finally, model reduction based on computational singular perturbation was conducted, reducing the number of parameters by 5 without much effect on the simulated model responses.

In Chapter 4, we developed a multiscale microbal reaction kinetic-coupled gas transport model for simulation of coalbed methane (CBM) production from reservoirs with ongoing anaerobic breakdown of coal. Based on the assumption of dual porosity characteristics in coal seams, gas transport equations were derived for a 1D radial coal bed reservoir by considering laminar flow and gas slippage in macropores and gas diffusion from micropores, driven by desorption. The multiscale stiff transport equations were non-dimensionalized to produce dimensionless numbers that can provide insight into the dominant physical process at various scales. A global sensitivity analysis of transport model parameters was conducted by the Morris OAT (one-at-a-time) method, which indicated that gas mobility and the surface diffusion constant affected the gas production the most. Following this, history matching of gas production data from Manville wells in Alberta was performed by solving the transport equations using the Levenberg-Marquardt method.

To deal with the effects of parametric uncertainty, we developed a technique of stochastic proxy modeling based on a multivariate polynomial chaos expansion framework in Chapter 5. For simplification, proxy model was built for coalbed methane production Y in the absence of microbial kinetics at varying producer well bottom-hole pressures, in the presence of uncertainty from normally distributed parameter values of the micropore diffusion time constant. By treating the input variable as a random variable from a uniform distribution, the output is expanded with Legendre

polynomials in the input and the associated deterministic coefficients are expanded with Hermite polynomials in the uncertain parameter. The coefficients of the basis functions in the proxy model are estimated by Galerkin projection using Gaussian quadrature. Alternatively, a proxy model was also developed based on knowledge of the underlying functional relation between the input and output variables. The results indicate that the latter method gives better predictions compared to the former, although the input-output relation is not always easily identifiable. The stochastic proxy model developed was then used for robust optimization of gas production. It is seen that the optimal point varies depending on the degree of caution in the robust optimization strategy.

In Chapter 6, model development in the previous chapters were integrated in the simulation of microbially enhanced coal bed methane in the simulation environment of CMG STARS. A standard dual porosity model was described with the matrix-fracture transmissibility factor evaluated by the Kazemi-Gilman formulation. Since microbes and water required for microbial growth can exist only in macropores, coal bioconversion was assumed to occur only in the fractures with the coal in the micropores acting only as a storage reserve for the gases. Sorption behaviour and reaction kinetics were incorporated into the simulator. The physical model was then simulated for a specific well pattern, with and without external nutrient injection. Since naturally occurring coal fractures are insufficient for nutrient dispersion, nutrient effects were significant only under high permeability, which can be obtained by stimulated fractures. The simulations were used in the optimization of coalbed methane production at varying nutrient fractions in the injected fluid and injector bottomhole pressures (BHP). Finally, in order to account for uncertainties in the macropore permeability and the coal quantity in the macropores, robust optimization strategies were tested based on a stochastic proxy model built in a polynomial chaos expansion framework. It was observed that the effect of uncertainty in macropore permeability is significant at the optimum operating regions evaluated under nominal optimization studies, implying that under those conditions, there is a high chance for field tests to deviate from model-based predictions. Also, since there is no significant interaction between the uncertain parameters and the input variables, the location of the robust optimal point did not shift for varying degrees of caution.

Thus we have presented a multiscale modeling framework for analysis, optimization and control of commercial MECoM recovery. The proposed models assess kinetic effects at the scale of bottle experiments, kinetic effects in the presence of gas attachment behaviour at the scale of coreflooding experiments, transport effects at the reservoir scale and finally coupled transport and kinetic effects at reservoir as well as field scales. As was seen, the effect of microbial kinetics in an already producing coal seam is not significant, unless a combination of stimulation strategies can improve methanogenesis, followed by solubilization rate parameters by 10-folds along

with increased fracture spacing that will allow dispersion of nutrients aiding in biostimulation.

7.2 Future work

The work in this thesis provides a framework for building simulation tools that can be enable commercial applications of microbially enhanced coalbed methane. However, there is a lot of scope for improvement, too. Some of the work that will be pursued in the near future are presented below.

- Coal seams are usually interspersed between geological layers of fine-grained sediments (shales and limestones) and coarser sediments (siltstones and sandstones) due to the sedimentation of sand, silt and clay along over buried swamps. Production simulations can therefore be performed for such field scale models interconnected by layers of varying permeabilities.
- The objective cost functions considered in this work only maximize cumulative methane generation. There are no penalties attached to increased nutrient consumption or pump operating capacity. Based on real-time estimates of such costs, we would rework the optimization strategies employed in this study can be reworked.
- The proxy model developed in this study contains only two operating parameters and two uncertain parameters. However, the number of uncertain parameters are much higher and so are the number of operating parameters in real application. Moreover, we have considered parameters such as macopore porosity and permeability to be isotropic, when they are usually highly anisotropic. The following modifications can be made to deal with these issues.
  - If it can be assumed that the uncertainty in the intrinsic hydaulic conductivity of the macropore porosity is a second order process with a known covariance, the stochastic process can be expanded into a denumerable number of random variables using Karhunen-Loeve expansions. Based on the resulting subset of random variables, proxy models that account for spatially varying uncertain parameters can be constructed.
  - In order to identify significant terms in the polynomial expansion for proxy model development, pairwise correlations were employed. However, there are many other techniques related to sparse PCE meta-models. It would be a good idea to compare results from different approaches in order to improve the accuracy of the resulting proxy model.

Bibliography

[1] Kessel, J. A. S. and Russell, J. B. The effect of pH on ruminal methanogenesis. *FEMS Microbiology Ecology*, 20(4):205–210, 1996.

[2] Kim, I. S., Hwang, M. H., Jang, N. J., Hyun, S. H., and Lee, S. Effect of low pH on the activity of hydrogen utilizing methanogen in bio-hydrogen process. *International Journal of Hydrogen Energy*, 29(11):1133–1140, 2004.

[3] Patching, T. and Mikhail, M. Studies of gas sorption and emission on Canadian coals. *CIM Bulletin*, 79(887):104–109, 1986.

[4] International Energy Agency. *Key World Energy Statistics 2010*. URL `http://dx.doi.org/10.1787/9789264095243-en/`.

[5] Das, L., Gulati, R., and Gupta, P. A comparative evaluation of the performance characteristics of a spark ignition engine using hydrogen and compressed natural gas as alternative fuels. *International Journal of Hydrogen Energy*, 25(8):783–793, 2000.

[6] Turrio-Baldassarri, L., Battistelli, C. L., Conti, L., Crebelli, R., De Berardis, B., Iamiceli, A. L., Gambino, M., and Iannaccone, S. Evaluation of emission toxicity of urban bus engines: Compressed natural gas and comparison with liquid fuels. *Science of the Total Environment*, 355(1):64–77, 2006.

[7] Al-Jubori, A., Johnston, S., Boyer, C., Lambert, S. W., Bustos, O. A., Pashin, J. C., and Wray, A. Coalbed methane: Clean energy for the world. *Oilfield Review*, 21(2):4–13, 2009.

[8] Budwill, K., Koziel, S., and Vidmar, J. Advancements in understanding and enhancing biogenic methane production from coals. In *Canadian Unconventional Resources Conference*. Society of Petroleum Engineers, 2011.

[9] Gray, N. D., Sherry, A., Larter, S. R., Erdmann, M., Leyris, J., Liengen, T., Beeder, J., and Head, I. M. Biogenic methane production in formation waters from a large gas field in the North Sea. *Extremophiles*, 13(3):511–519, 2009.

[10] Converse, D., Hinton, S., Hieshima, G., Barnum, R., and Sowlay, M. Process for stimulating microbial activity in a hydrocarbon-bearing, subterranean formation, April 8 2003. US Patent 6,543,535.

[11] Jin, S., Bland, A., and Price, H. Biogenic methane production enhancement systems, November 16 2010. US Patent 7,832,475.

[12] Scott, A. R. Improving Coal Gas Recovery with Microbially Enhanced Coalbed Methane. In Mastalerz, M., Glikson, M., and Golding, S., editors, *Coalbed Methane: Scientific, Environmental and Economic Evaluation*, pages 89–110. Springer Netherlands, 1999. ISBN 978-90-481-5217-9.

[13] Lawrence, A. W. and McCarty, P. L. Kinetics of methane fermentation in anaerobic treatment. *Journal (Water Pollution Control Federation)*, 41(2):R1–R17, 1969.

[14] Stadtman, T. and Barker, H. Studies on the methane fermentation. VII. Tracer experiments on the mechanism of methane formation. *Arch. Biochem.*, 21:256–264, 1949.

[15] Lee, C. J., Prasad, V., and Lee, J. M. Stochastic nonlinear optimization for robust design of catalysts. *Industrial and Engineering Chemistry Research*, 50(7):3938–3946, 2011.

[16] Kennedy, J. and Eberhart, R. Particle swarm optimization. In *Encyclopedia of Machine Learning*, pages 760–766. Springer, 2010.

[17] Kotsyurbenko, O. R., Chin, K.-J., Glagolev, M. V., Stubner, S., Simankova, M. V., Nozhevnikova, A. N., and Conrad, R. Acetoclastic and hydrogenotrophic methane production and methanogenic populations in an acidic West-Siberian peat bog. *Environmental Microbiology*, 6(11):1159–1173, 2004.

[18] Demirel, B. and Scherer, P. The roles of acetotrophic and hydrogenotrophic methanogens during anaerobic conversion of biomass to methane: A review. *Reviews in Environmental Science and Biotechnology*, 7(2):173–190, 2008.

[19] Joulian, C., Patel, B., Ollivier, B., Garcia, J.-L., and Roger, P. A. Methanobacterium *Oryzae sp. nov.*, a novel methanogenic rod isolated from a Philippines ricefield. *International Journal of Systematic and Evolutionary Microbiology*, 50(2):525–528, 2000.

[20] Bekins, B. A., Warren, E., and Godsy, E. M. A comparison of zero-order, first-order, and Monod biotransformation models. *Groundwater*, 36(2):261–268, 1998.

[21] Simkins, S. and Alexander, M. Models for mineralization kinetics with the variables of substrate concentration and population density. *Applied and Environmental Microbiology*, 47(6):1299–1306, 1984.

[22] Lokshina, L. Y., Vavilin, V. A., Kettunen, R. H., Rintala, J. A., Holliger, C., and Nozhevnikova, A. N. Evaluation of kinetic coefficients using integrated Monod and Haldane models for low-temperature acetoclastic methanogenesis. *Water Research*, 35(12):2913–2922, 2001.

[23] Flores, R. M., Rice, C. A., Stricker, G. D., Warden, A., and Ellis, M. S. Methanogenic pathways of coal-bed gas in the Powder River Basin, United States: the geologic factor. *International Journal of Coal Geology*, 76(1):52–75, 2008.

[24] Rice, D. D. Composition and origins of coalbed gas. *Hydrocarbons from coal: AAPG Studies in Geology*, 38:159–184, 1993.

[25] Faiz, M. and Hendry, P. Significance of microbial activity in Australian coal bed methane reservoirs – a review. *Bulletin of Canadian Petroleum Geology*, 54(3):261–272, 2006.

[26] D Strapoc, D., Mastalerz, M., Dawson, K., Macalady, J., Callaghan, A. V., Wawrik, B., Turich, C., and Ashby, M. Biogeochemistry of microbial coal-bed methane. *Annual Review of Earth and Planetary Sciences*, 39:617–656, 2011.

[27] Hatcher, P. G. and Clifford, D. J. The organic geochemistry of coal: from plant materials to coal. *Organic Geochemistry*, 27(5-6):251–257, 1997.

[28] Senthamaraikkannan, G., Budwill, K., Gates, I., Mitra, S., and Prasad, V. Kinetic modeling of the biogenic production of coalbed methane. *(submitted)*, 2015.

[29] Yoon, H., Klinzing, G., and Blanch, H. Competition for mixed substrates by microbial populations. *Biotechnology and Bioengineering*, 19(8):1193–1210, 1977.

[30] Okpokwasili, G. and Nweke, C. Microbial growth and substrate utilization kinetics. *African Journal of Biotechnology*, 5(4), 2006.

[31] Jalali, J. *A coalbed methane simulator designed for the independent producers.* Master's thesis, West Virginia University, 2004.

[32] Orem, W., Tatu, C., Varonka, M., Lerch, H., Bates, A., Engle, M., Crosby, L., and McIntosh, J. Organic substances in produced and formation water from unconventional natural gas extraction in coal and shale. *International Journal of Coal Geology*, 126:20–31, 2014.

[33] Davidson, K. Modeling microbial food webs. *Marine Ecology Progress Series*, 145(1):279–296, 1996.

[34] Bryant, M., Tzeng, S., and Robinson, I. Nutrient requirements of methanogenic bacteria. *Urbana*, 101:61801, 1971.

[35] Stephen, A., Adebusuyi, A., Baldygin, A., Shuster, J., Southam, G., Budwill, K., Foght, J., Nobes, D. S., and Mitra, S. K. Bioconversion of coal: new insights from a core flooding study. *RSC Advances*, 4(43):22779–22791, 2014.

[36] Lam, S. and Goussis, D. The CSP method for simplifying kinetics. *International Journal of Chemical Kinetics*, 26(4):461–486, 1994.

[37] Zagaris, A., Kaper, H. G., and Kaper, T. J. Two perspectives on reduction of ordinary differential equations. *Mathematische Nachrichten*, 278(12-13):1629–1642, 2005.

[38] Lam, S. Using CSP to understand complex chemical kinetics. *Combustion Science and Technology*, 89(5-6):375–404, 1993.

[39] Heller, R., Vermylen, J., and Zoback, M. Experimental investigation of matrix permeability of gas shales. *AAPG bulletin*, 98(5):975–995, 2014.

[40] IHS Inc. AccuMap oil and gas database for Alberta, Canada, 2013.

[41] Saltelli, A. Sensitivity analysis: Could better methods be used? *Journal of Geophysical Research: Atmospheres (1984–2012)*, 104(D3):3789–3793, 1999.

[42] Pekot, L. J. Matrix shrinkage and permeability reduction with carbon dioxide injection. Coal-Seq II Forum, Washington DC, 2003.

[43] Harris, S. H., Smith, R. L., and Barker, C. E. Microbial and chemical factors influencing methane production in laboratory incubations of low-rank subsurface coals. *International Journal of Coal Geology*, 76(1):46–51, 2008.

[44] Singh, D. N., Kumar, A., Sarbhai, M. P., and Tripathi, A. K. Cultivation-independent analysis of archaeal and bacterial communities of the formation water in an Indian coal bed to enhance biotransformation of coal into methane. *Applied microbiology and biotechnology*, 93(3):1337–1350, 2012.

[45] Opara, A., Adams, D., Free, M., McLennan, J., and Hamilton, J. Microbial production of methane and carbon dioxide from lignite, bituminous coal, and coal waste materials. *International Journal of Coal Geology*, 96:1–8, 2012.

[46] Penner, T. J., Foght, J. M., and Budwill, K. Microbial diversity of western canadian subsurface coal beds and methanogenic coal enrichment cultures. *International Journal of Coal Geology*, 82(1):81–93, 2010.

[47] Jones, E. J., Voytek, M. A., Corum, M. D., and Orem, W. H. Stimulation of methane generation from nonproductive coal by addition of nutrients or a microbial consortium. *Applied and Environmental Microbiology*, 76(21):7013–7022, 2010.

[48] Huang, Z., Urynowicz, M. A., and Colberg, P. J. Stimulation of biogenic methane generation in coal samples following chemical treatment with potassium permanganate. *Fuel*, 111:813–819, 2013.

[49] Papendick, S. L., Downs, K. R., Vo, K. D., Hamilton, S. K., Dawson, G. K., Golding, S. D., and Gilcrease, P. C. Biogenic methane potential for Surat Basin, Queensland coal seams. *International Journal of Coal Geology*, 88(2):123–134, 2011.

[50] Wainwright, H. M., Finsterle, S., Jung, Y., Zhou, Q., and Birkholzer, J. T. Making sense of global sensitivity analyses. *Computers & Geosciences*, 65:84–94, 2014.

[51] Laxminarayana, C. and Crosdale, P. J. Role of coal type and rank on methane sorption characteristics of Bowen Basin, Australia coals. *International Journal of Coal Geology*, 40(4):309–325, 1999.

[52] Ritter, D., Vinson, D., Barnhart, E., Akob, D. M., Fields, M. W., Cunningham, A. B., Orem, W., and McIntosh, J. C. Enhanced microbial coalbed methane generation: A review of research, commercial activity, and remaining challenges, 2015.

[53] Bustin, R. and Clarkson, C. Geological controls on coalbed methane reservoir capacity and gas content. *International Journal of Coal Geology*, 38(1):3–26, 1998.

[54] Branicki, M. and Majda, A. J. Fundamental limitations of polynomial chaos for uncertainty quantification in systems with intermittent instabilities. *Comm. Math. Sci*, 11(1):55–103, 2013.

[55] Dutta, P. and Bhattacharya, R. Nonlinear estimation with polynomial chaos and higher order moment updates. In *American Control Conference (ACC), 2010*, pages 3142–3147. IEEE, 2010.

[56] Gautschi, W. Algorithm 726: ORTHPOL–a package of routines for generating orthogonal polynomials and Gauss-type quadrature rules. *ACM Transactions on Mathematical Software (TOMS)*, 20(1):21–62, 1994.

[57] Kewlani, G. and Iagnemma, K. A stochastic response surface approach to statistical prediction of mobile robot mobility. In *Intelligent Robots and Systems, 2008. IROS 2008. IEEE/RSJ International Conference on*, pages 2234–2239. IEEE, 2008.

[58] Jalal, J. and Mohaghegh, S. D. A coalbed methane reservoir simulator designed and developed for the independent producers. In *SPE Eastern Regional Meeting*. Society of Petroleum Engineers, 2004.

[59] Ghanem, R. and Dham, S. Stochastic finite element analysis for multiphase flow in heterogeneous porous media. *Transport in Porous Media*, 32(3):239–262, 1998.

[60] Webster, M. D., Tatang, M. A., and McRae, G. J. Application of the probabilistic collocation method for an uncertainty analysis of a simple ocean model. *MIT Joint Program on the Science and Policy of Global Change*, 1996.

[61] Xiu, D. and Karniadakis, G. E. The Wiener–Askey polynomial chaos for stochastic differential equations. *SIAM Journal on Scientific Computing*, 24(2):619–644, 2002.

[62] Eldred, M., Webster, C., and Constantine, P. Evaluation of non-intrusive approaches for Wiener-Askey generalized polynomial chaos. In *Proceedings of the 10th AIAA Non-Deterministic Approaches Conference, number AIAA-2008-1892, Schaumburg, IL*, volume 117, page 189. 2008.

[63] Fagiano, L. and Khammash, M. Simulation of stochastic systems via polynomial chaos expansions and convex optimization. *Physical Review E*, 86(3):036702, 2012.

[64] Wei, X., Wang, G., Massarotto, P., Golding, S., and Rudolph, V. Numerical simulation of multicomponent gas diffusion and flow in coals for CO2 enhanced coalbed methane recovery. *Chemical Engineering Science*, 62(16):4193–4203, 2007.

[65] Xiong, F., Xue, B., Yan, Z., and Yang, S. Polynomial chaos expansion based robust design optimization. In *Quality, Reliability, Risk, Maintenance, and Safety Engineering (ICQR2MSE), 2011 International Conference on*, pages 868–873. IEEE, 2011.

[66] Molina-Cristobal, A., Parks, G., and Clarkson, P. Finding robust solutions to multi-objective optimisation problems using polynomial chaos. In *Proc. 6th ASMO UK/ISSMO Conference on Engineering Design Optimization*. 2006.

[67] Mandur, J. and Budman, H. A polynomial-chaos based algorithm for robust optimization in the presence of Bayesian uncertainty. In *Proc. 8th IFAC symposium on advanced control of chemical processes*. 2012.

[68] Nagy, Z. and Braatz, R. Distributional uncertainty analysis using power series and polynomial chaos expansions. *Journal of Process Control*, 17(3):229–240, 2007.

[69] Senthamaraikkannan, G., Gates, I., and Prasad, V. Development of multi-scale microbial kinetics coupled gas transport model for simulation of biogenic coalbed methane production. *(submitted)*, 2015.

[70] Wiener, N. The homogeneous chaos. *American Journal of Mathematics*, pages 897–936, 1938.

[71] Senthamaraikkannan, G., Gates, I., and Prasad, V. Modeling, estimation and optimization of biogenic methane production in coreflooding experiments. *(submitted)*, 2015.

[72] Parkes, R. J., Cragg, B. A., and Wellsbury, P. Recent studies on bacterial populations and processes in subseafloor sediments: a review. *Hydrogeology Journal*, 8(1):11–28, 2000.

[73] Martini, A., Walter, L., Budai, J., Ku, T., Kaiser, C., and Schoell, M. Genetic and temporal relations between formation waters and biogenic methane: Upper Devonian Antrim Shale, Michigan Basin, USA. *Geochimica et Cosmochimica Acta*, 62(10):1699–1720, 1998.

[74] Ulrich, G. and Bower, S. Active methanogenesis and acetate utilization in Powder River Basin coals, United States. *International Journal of Coal Geology*, 76(1):25–33, 2008.

[75] Rice, D. D. and Claypool, G. E. Generation, accumulation, and resource potential of biogenic gas. *AAPG Bulletin*, 65(1):5–25, 1981.

[76] U.S. Environmental Protection Agency (U.S. EPA). Directional drilling technology. Retrieved July 21, 2015 from `www.epa.gov/cmop/docs/dir-drilling.pdf`.

[77] U.S. Environmental Protection Agency (U.S. EPA). Characteristics of coalbed methane production and associated hydraulic fracturing practices,

In Evaluation of Impacts to Underground Sources of Drinking Water by Hydraulic Fracturing of Coalbed Methane Reservoirs. Retrieved July 21, 2015 from http://www.epa.gov/ogwdw/uic/pdfs/cbmstudy_attach_uic_ch03_cbm_practices.pdf, 2004.

[78] Stiller, B., Bocek, T., Hecht, F., Machado, G., Racz, P., and Waldburger, M. Coal Bed Methane (CBM) market analysis by application (Industrial, Power Generation, Residential, Commercial and Transportation) and Segment Forecasts To 2020. Technical report, Grand View Research, 2014.

[79] Gale, J. and Freund, P. Coalbed methane enhancement with CO_2 sequestration worldwide potential. *Environmental Geosciences*, 8(3):210–217, 2001.

[80] Griffiths, M. and Severson-Baker, C. Unconventional gas: The environmental challenges of coalbed methane development in Alberta. Technical report, Pembina Institute for Appropriate Development, Drayton Valley, AB, Canada, 2003.

[81] Dogwood Initiative. Coalbed methane: Best Practices in British Columbia. Retrieved July 21, 2015 from http://dogwoodinitiative.org/publications/reports/coalbed-methane-best-practices-for-british-columbia.

[82] Volkwein, J. Method for in situ biological conversion of coal to methane, June 13 1995. US Patent 5,424,195.

[83] Blatman, G. and Sudret, B. Adaptive sparse polynomial chaos expansion based on least angle regression. *Journal of Computational Physics*, 230(6):2345–2367, 2011.

[84] Blatman, G. and Sudret, B. Sparse polynomial chaos expansions and adaptive stochastic finite elements using a regression approach. *Comptes Rendus Mécanique*, 336(6):518–523, 2008.

[85] Blatman, G. and Sudret, B. Efficient computation of global sensitivity indices using sparse polynomial chaos expansions. *Reliability Engineering & System Safety*, 95(11):1216–1229, 2010.

[86] Stevens, P. The 'Shale Gas Revolution': Hype and Reality. 2010.

[87] Pfeiffer, R., Ulrich, G., and Finkelstein, M. Chemical amendments for the stimulation of biogenic gas generation in deposits of carbonaceous material, April 13 2010. US Patent 7,696,132.

[88] Mahaffey, W., Bradfish, J., Haveman, S., Sutton, B., and Greaser, L. Dispersion of compounds for the stimulation of biogenic gas generation in deposits of carbonaceous material, February 6 2014. US Patent 20140034297.

[89] Pfeiffer, R., Ulrich, G., Vanzin, G., Dannar, V., DeBruyn, R., and Dodson, J. Biogenic fuel gas generation in geologic hydrocarbon deposits, January 5 2010. US Patent 7,640,978.

[90] Computer Modelling Group: Calgary, Alberta, Canada. *Computer Modelling Group STARS Version 2011.10 Users Guide*, 2011.

[91] Senthamaraikkannan, G. and Prasad, V. Stochastic proxy modelling for coalbed methane production using orthogonal polynomials. In *Proc. 9th IFAC Symposium on Advanced Control of Chemical Processes*. June 2015.

[92] Lee, B. and Tan, T. Application of a multiple porosity/permeability simulator in fsractured reservoir simulation. In *SPE Symposium on Reservoir Simulation*. Society of Petroleum Engineers, 1987.

[93] Kazemi, H., Merrill Jr, L., Porterfield, K., and Zeman, P. Numerical simulation of water-oil flow in naturally fractured reservoirs. *Society of Petroleum Engineers Journal*, 16(06):317–326, 1976.

[94] Prinz, D. and Littke, R. Development of the micro-and ultramicroporous structure of coals with rank as deduced from the accessibility to water. *Fuel*, 84(12):1645–1652, 2005.

[95] Goktas, B. and Ertekin, T. Production performance analysis of cavity-completed wells. In *SPE Eastern Regional Meeting*. Society of Petroleum Engineers, 1998.

[96] Kolesar, J., Ertekin, T., and Obut, S. The unsteady-state nature of sorption and diffusion phenomena in the micropore structure of coal: Part 1-theory and mathematical formulation. *SPE Formation Evaluation*, 5(01):81–88, 1990.

[97] Gong, B. *Effective models of fractured systems*. Ph.D. thesis, Stanford University, 2007.

[98] King, G. R., Ertekin, T., and Schwerer, F. C. Numerical simulation of the transient behavior of coal-seam degasification wells. *SPE Formation Evaluation*, 1(02):165–183, 1986.

[99] Shi, J. and Durucan, S. A bidisperse pore diffusion model for methane displacement desorption in coal by CO_2 injection. *Fuel*, 82(10):1219–1229, 2003.

[100] Ryu, Z., Zheng, J., Wang, M., and Zhang, B. Characterization of pore size distributions on carbonaceous adsorbents by DFT. *Carbon*, 37(8):1257–1264, 1999.

[101] Gamson, P., Beamish, B., and Johnson, D. Coal microstructure and secondary mineralization: their effect on methane recovery. *Geological Society, London, Special Publications*, 109(1):165–179, 1996.

[102] Gamson, P. D., Beamish, B., and Johnson, D. P. Coal microstructure and micropermeability and their effects on natural gas recovery. *Fuel*, 72(1):87–99, 1993.

[103] Mohaghegh, S. and Ertekin. A type-curve solution for coal seam degasification wells producing under two-phase flow conditions. In *SPE Annual Technical Conference and Exhibition*. Society of Petroleum Engineers, 1991.

[104] Ertekin, T., King, G. A., and Schwerer, F. C. Dynamic gas slippage: a unique dual-mechanism approach to the flow of gas in tight formations. *SPE formation evaluation*, 1(01):43–52, 1986.

[105] Remner, D. J., Ertekin, T., Sung, W., and King, G. R. A parametric study of the effects of coal seam properties on gas drainage efficiency. *SPE Reservoir Engineering*, 1(6):633–646, 1986.

[106] Sung, W., Ertekin, T., and Schwerer, F. The development, testing, and application of a comprehensive coal seam degasification model. In *SPE Unconventional Gas Technology Symposium*. Society of Petroleum Engineers, 1986.

[107] Sawyer, W., Paul, G., and Schraufnagel, R. Development and Application of A 3-D Coalbed Simulator. In *Annual Technical Meeting*. Petroleum Society of Canada, 1990.

[108] Manik, J., Ertekin, T., and Kohler, T. Development and validation of a compositional coalbed simulator. In *Canadian International Petroleum Conference*. Petroleum Society of Canada, 2000.

[109] Reeves, S. and Pekot, L. Advanced reservoir modeling in desorption-controlled reservoirs. In *SPE Rocky Mountain Petroleum Technology Conference*. Society of Petroleum Engineers, 2001.

[110] Thararoop, P., Karpyn, Z. T., and Ertekin, T. Development of a multi-mechanistic, dual-porosity, dual-permeability, numerical flow model for coalbed methane reservoirs. *Journal of Natural Gas Science and Engineering*, 8:121–131, 2012.

[111] King, G. Numerical simulation of the simultaneous flow of methane and water through dual porosity coal seams during the degasification process. Technical report, Pennsylvania State Univ., University Park (USA), 1985.

[112] Clarkson, C. R., Jordan, C. L., Ilk, D., and Blasingame, T. A. Production data analysis of fractured and horizontal CBM wells. In *SPE Eastern Regional Meeting*. Society of Petroleum Engineers, 2009.

[113] Wu, Y.-S. and Pruess, K. Gas flow in porous media with Klinkenberg effects. *Transport in Porous Media*, 32(1):117–137, 1998.

[114] Gilman, A. and Beckie, R. Flow of coal-bed methane to a gallery. *Transport in porous media*, 41(1):1–16, 2000.

[115] Senthamaraikkannan, G. and Prasad, V. Coalbed methane. In M.R.Riazi and Gupta, R., editors, *Coal Production and Processing Technology*. Taylor & Francis Group, (in press).

[116] Mazumder, S., Wolf, K., Van Hemert, P., and Busch, A. Laboratory experiments on environmental friendly means to improve coalbed methane production by carbon dioxide/flue gas injection. *Transport in porous media*, 75(1):63–92, 2008.

[117] Nobakht, M., Moghadam, S., and Gu, Y. Mutual interactions between crude oil and CO2 under different pressures. *Fluid phase equilibria*, 265(1):94–103, 2008.

[118] Shen, P., Wang, J., Yuan, S., Zhong, T., and Jia, X. Study of enhanced-oil-recovery mechanism of alkali/surfactant/polymer flooding in porous media from experiments. *Spe Journal*, 14(02):237–244, 2009.

[119] Vlachos, D., Mhadeshwar, A., and Kaisare, N. S. Hierarchical multiscale model-based design of experiments, catalysts, and reactors for fuel processing. *Computers & Chemical Engineering*, 30(10):1712–1724, 2006.

[120] Asprey, S. and Macchietto, S. Designing robust optimal dynamic experiments. *Journal of Process Control*, 12(4):545–556, 2002.

[121] Bromhal, G. S., Sams, W. N., Jikich, S., Ertekin, T., and Smith, D. H. Simulation of CO2 sequestration in coal beds: The effects of sorption isotherms. *Chemical Geology*, 217(3):201–211, 2005.

[122] Burruss, R. C. CO2 adsorption in coals as a function of rank and composition: A task in usgs research on geologic sequestration of CO2. In *Presentation on the Second International Forum on Geologic Sequestration of CO_2 in Deep, Unmineable Coalseams (Coal-Seq II), Washington DC*. 2003.

[123] Achyuthan, K. E., Achyuthan, A. M., Adams, P. D., Dirk, S. M., Harper, J. C., Simmons, B. A., and Singh, A. K. Supramolecular self-assembled chaos:

polyphenolic lignin's barrier to cost-effective lignocellulosic biofuels. *Molecules*, 15(12):8641–8688, 2010.

[124] Payne, D. and Ortoleva, P. A model for lignin alterationpart I: a kinetic reaction-network model. *Organic geochemistry*, 32(9):1073–1085, 2001.

[125] Fakoussa, R. and Hofrichter, M. Biotechnology and microbiology of coal degradation. *Applied Microbiology and Biotechnology*, 52(1):25–40, 1999.

[126] Bodzek, D. and Marzec, A. Molecular components of coal and coal structure. *Fuel*, 60(1):47–51, 1981.

[127] Marzec, A. Towards an understanding of the coal structure: A review. *Fuel Processing Technology*, 77:25–32, 2002.

[128] Ferry, J. and Wolfe, R. Anaerobic degradation of benzoate to methane by a microbial consortium. *Archives of Microbiology*, 107(1):33–40, 1976.

[129] Green, M. S., Flanegan, K. C., and Gilcrease, P. C. Characterization of a methanogenic consortium enriched from a coalbed methane well in the Powder River basin, USA. *International Journal of Coal Geology*, 76(1):34–45, 2008.

[130] Zeikus, J., Wellstein, A., and Kirk, T. Molecular basis for the biodegradative recalcitrance of lignin in anaerobic environments. *FEMS Microbiology Letters*, 15(3):193–197, 1982.

[131] Young, L. and Frazer, A. The fate of lignin and lignin-derived compounds in anaerobic environments. *Geomicrobiology Journal*, 5(3-4):261–293, 1987.

[132] Faison, B., Scott, C., and Davison, B. Biosolubilization of coal in aqueous and non-aqueous media. *Preprints of the American Chemical Society, Div. Fuel Chem., United States*, 33(conf 8809269), 1988.

[133] Cohen, M. S., Feldman, K. A., Brown, C. S., and Gray, E. T. Isolation and identification of the coal-solubilizing agent produced by *Trametes versicolor*. *Applied and Environmental Microbiology*, 56(11):3285–3291, 1990.

[134] Cohen, M. S. and Gabriele, P. D. Degradation of coal by the fungi *Polyporus versicolor* and *Poria monticola*. *Applied and Environmental Microbiology*, 44(1):23–27, 1982.

[135] Cohen, M., Aronson, H., Feldman, K., Brown, C., and Gray Jr, E. Recent progress in cell-free solubilization of coal. *Preprints of the American Chemical Society, Div. Fuel Chem.; United States*, 33(conf-8809269-), 1988.

[136] Makgato, M., Moitsheki, L., Shoko, L., Kgobane, B., Morgan, D., and Focke, W. W. Alkali-assisted coal extraction with polar aprotic solvents. *Fuel Processing Technology*, 90(4):591–598, 2009.

[137] Noyes, A. A. and Whitney, W. R. The rate of solution of solid substances in their own solutions. *Journal of the American Chemical Society*, 19(12):930–934, 1897.

[138] Shuler, M. L. and Kargi, F. *Bioprocess engineering*. Prentice Hall New York, 2002.

[139] Colberg, P. J. and Young, L. Biodegradation of lignin-derived molecules under anaerobic conditions. *Canadian Journal of Microbiology*, 28(7):886–889, 1982.

[140] Keith, C., Bridges, R., Fina, L., Iverson, K., and Cloran, J. The anaerobic decomposition of benzoic acid during methane fermentation. *Archives of Microbiology*, 118(2):173–176, 1978.

[141] Colberg, P. and Young, L. Aromatic and volatile acid intermediates observed during anaerobic metabolism of lignin-derived oligomers. *Applied and Environmental Microbiology*, 49(2):350–358, 1985.

[142] Balba, M. and Evans, W. C. The methanogenic fermentation of aromatic substrates. *Biochem. Soc. Trans*, 5:302–304, 1977.

[143] Shlomi, E. R., Lankhorst, A., and Prins, R. Methanogenic fermentation of benzoate in an enrichment culture. *Microbial Ecology*, 4(3):249–261, 1977.

[144] Evans, W. C. and Fuchs, G. Anaerobic degradation of aromatic compounds. *Annual Reviews in Microbiology*, 42(1):289–317, 1988.

[145] Buswell, A. M. and Hatfield, W. D. Anaerobic fermentations. *Bull*, 32:., 1936.

[146] Barker, H. A. On the biochemistry of the methane fermentation. *Archiv für Mikrobiologie*, 7(1-5):404–419, 1936.

[147] Buswell, A. and Mueller, H. Mechanism of methane fermentation. *Industrial & Engineering Chemistry*, 44(3):550–552, 1952.

[148] Stadtman, T. C. Methane fermentation. *Annual Reviews in Microbiology*, 21(1):121–142, 1967.

[149] Hayatsu, R., Winans, R. E., McBETH, R. L., Scott, R. G., Moore, L. P., and Studier, M. H. Structural characterization of coal: lignin-like polymers in coals. *Am. Chem. Soc., Div. Fuel Chem., Prepr.;(United States)*, 24(CONF-790415-P2), 1979.

[150] Nozhevnikova, A. N., Nekrasova, V., Ammann, A., Zehnder, A. J., Wehrli, B., and Holliger, C. Influence of temperature and high acetate concentrations on methanogenensis in lake sediment slurries. *FEMS Microbiology Ecology*, 62(3):336–344, 2007.

[151] Fedorak, P. M. and Hrudey, S. E. The effects of phenol and some alkyl phenolics on batch anaerobic methanogenesis. *Water Research*, 18(3):361–367, 1984.

[152] Healy, J. and Young, L. Anaerobic biodegradation of eleven aromatic compounds to methane. *Applied and Environmental Microbiology*, 38(1):84–89, 1979.

[153] Okino, M. S. and Mavrovouniotis, M. L. Simplification of mathematical models of chemical reaction systems. *Chemical Reviews*, 98(2):391–408, 1998.

[154] Jacob, S. M., Gross, B., Voltz, S. E., and Weekman, V. W. A lumping and reaction scheme for catalytic cracking. *AIChE Journal*, 22(4):701–713, 1976.

[155] Susilawati, R., Esterle, J. S., Golding, S. D., and Mares, T. E. Microbial methane potential for the South Sumatra basin coal: Formation water screening and coal substrate bioavailability. *Energy Procedia*, 65:282–291, 2015.

[156] Wawrik, B., Mendivelso, M., Parisi, V. A., Suflita, J. M., Davidova, I. A., Marks, C. R., Van Nostrand, J. D., Liang, Y., Zhou, J., and Huizinga, B. J. Field and laboratory studies on the bioconversion of coal to methane in the San Juan Basin. *FEMS Microbiology Ecology*, 81(1):26–42, 2012.

[157] Krüger, M., Beckmann, S., Engelen, B., Thielemann, T., Cramer, B., Schippers, A., and Cypionka, H. Microbial methane formation from hard coal and timber in an abandoned coal mine. *Geomicrobiology Journal*, 25(6):315–321, 2008.

[158] Thielemann, T., Cramer, B., and Schippers, A. Coalbed methane in the Ruhr basin, Germany: a renewable energy resource? *Organic Geochemistry*, 35(11):1537–1549, 2004.

[159] Westermann, P., Ahring, B. K., and Mah, R. A. Temperature compensation in *Methanosarcina barkeri* by modulation of hydrogen and acetate affinity. *Applied and Environmental Microbiology*, 55(5):1262–1266, 1989.

[160] Rebac, S., Ruskova, J., Gerbens, S., Van Lier, J. B., Stams, A. J., and Lettinga, G. High-rate anaerobic treatment of wastewater under psychrophilic conditions. *Journal of Fermentation and Bioengineering*, 80(5):499–506, 1995.

[161] Hitzman, D. Use of bacteria in the recovery of petroleum from underground deposits. May 25 1965. US Patent 3,185,216.

[162] Flores, R. M. Coalbed methane: from hazard to resource. *International Journal of Coal Geology*, 35(1):3–26, 1998.

[163] Cokar, M., Ford, B., Kallos, M., and Gates, I. New gas material balance to quantify biogenic gas generation rates from shallow organic-matter-rich shales. *Fuel*, 104:443–451, 2013.

[164] Kirk, M. F., Martini, A. M., Breecker, D. O., Colman, D. R., Takacs-Vesbach, C., and Petsch, S. T. Impact of commercial natural gas production on geochemistry and microbiology in a shale-gas reservoir. *Chemical Geology*, 332:15–25, 2012.

[165] Strapoc, D., Mastalerz, M., Eble, C., and Schimmelmann, A. Characterization of the origin of coalbed gases in southeastern illinois basin by compound-specific carbon and hydrogen stable isotope ratios. *Organic Geochemistry*, 38(2):267–287, 2007.

[166] Soot, P. Tax incentives spur development of coalbed methane. *Oil & Gas Journal*, 89(23):40, 1991.

[167] Broadhead, R. F. Petroleum geology of the mcgregor range, otero county, new mexico. *Transactions Southwest Section AAPG Convention*, pages 40–55, 2002.

[168] Young, E. . Shale gas and coal bed methane: Potential sources of sustained energy in the future. Technical report, 2010. URL `http://www.ey.com/Publication/vwLUAssets/Shale_gas_and_coal_bed_methane/$File/Shale_gas_and_coal_bed_methane_-__Potential_sources_of_sustained_energy_in_the_future.pdf`.

[169] U.S. Environmental Protection Agency (U.S. EPA). Technical Development Document for the Coalbed Methane (CBM) Extraction Industry. Technical report, 2013. URL `http://water.epa.gov/scitech/wastetech/guide/oilandgas/upload/cbmttd2013.pdf`.

[170] U.S. Environmental Protection Agency (U.S. EPA). Characteristics of coalbed methane production and associated hydraulic fracturing practices, 2004. URL `http://water.epa.gov/type/groundwater/uic/class2/hydraulicfracturing/wells_coalbedmethanestudy.cfm`.

[171] White, C. M., Smith, D. H., Jones, K. L., Goodman, A. L., Jikich, S. A., LaCount, R. B., DuBose, S. B., Ozdemir, E., Morsi, B. I., and Schroeder, K. T. Sequestration of carbon dioxide in coal with enhanced coalbed methane recovery: A review. *Energy & Fuels*, 19(3):659–724, 2005.

[172] Jones, E. J., Voytek, M. A., Warwick, P. D., Corum, M. D., Cohn, A., Bunnell, J. E., Clark, A. C., and Orem, W. H. Bioassay for estimating the biogenic methane-generating potential of coal samples. *International Journal of Coal Geology*, 76(1):138–150, 2008.

[173] Faiz, M. Microbial influences on coal seam gas reservoirsa review. In *Bac-Min Conf., Bendigo, Vic., Aust. The Aust. Inst. Min. Metall. Publ. Ser*, volume 6, pages 133–42. 2004.

[174] Scott, A. R. and Guyer, J. E. Method of generating and recovering gas from subsurface formations of coal, carbonaceous shale and organic-rich shales. February 19 2004. US Patent 20040033557.

Appendix A

Appendix to Chapter 3

A.1 Reduced kinetic model obtained on ignoring the fast reaction subspace : CSP

At $t_0 > 28$ days, one mode is exhausted.

$$\frac{d[C]}{dt} = -ke^{S_n[Nu]}\left(\frac{C}{C_0}\right)^{2/3}([S^*]-[S]) \approx 0 \text{ (dormant)}$$

$$\frac{d[S]}{dt} \approx 0$$

$$\frac{d[W]}{dt} \approx 10ke^{S_n[Nu]}\left(\frac{C}{C_0}\right)^{2/3}([S^*]-[S]) - \frac{\mu_1[W]}{Ks_1+[W]+Ks_1/Ks_2[Nu]}$$

$$\frac{d[B]}{dt} = \frac{\mu_1[W]}{Ks_1+[W]+Ks_1/Ks_2[Nu]} + \frac{\mu_2[Nu]}{Ks_2+[Nu]+Ks_2/Ks_1[W]} - d[B]$$

$$\frac{d[A]}{dt} = 3d[B] - \frac{e[A]}{f+[A]+[A]^2/g}$$

$$\frac{d[CH_4]}{dt} = \frac{e[A]}{f+[A]+[A]^2/g} - r_{CH_4ads}$$

$$\frac{d[CH_{4s}]}{dt} = r_{CH_4ads}$$

$$\frac{d[CO_2]}{dt} = \frac{3\mu_1[W]}{Ks_1+[W]+Ks_1/Ks_2[Nu]} + d[B] + \frac{e[A]}{f+[A]+[A]^2/g} - r_{CH_4ads} - r_{CO_2ads};$$

$$\frac{d[CO_{2s}]}{dt} = r_{CO_2ads}$$

$$\frac{d[Nu]}{dt} = r_{Nu}$$

For a brief period between 37 and 40 days, one more mode is exhausted, giving $r_{CO_2des} \approx 0$. However, after 40 days, there are a total of 3 exhausted modes.

$$\begin{aligned}
\frac{d[C]}{dt} &= -ke^{S_n[Nu]}\left(\frac{C}{C_0}\right)^{2/3}([S^*]-[S]) \approx 0(\text{dormant}) \\
\frac{d[S]}{dt} &\approx 0 \\
\frac{d[W]}{dt} &\approx 10ke^{S_n[Nu]}\left(\frac{C}{C_0}\right)^{2/3}([S^*]-[S]) - \frac{\mu_1[W]}{Ks_1+[W]+Ks_1/Ks_2[Nu]} \\
\frac{d[B]}{dt} &\approx 0 \\
\frac{d[A]}{dt} &\approx 10ke^{S_n[Nu]}\left(\frac{C}{C_0}\right)^{2/3}([S^*]-[S]) + \frac{2\mu_1[W]}{Ks_1+[W]+Ks_1/Ks_2[Nu]} \\
&\quad + \frac{3\mu_2[Nu]}{Ks_2+[Nu]+Ks_2/Ks_1[W]} - \frac{e[A]}{f+[A]+[A]^2/g} - 0.7r_{Nu} \\
\frac{d[Nu]}{dt} &= r_{Nu} \\
\frac{d[CH_4]}{dt} &= \frac{e[A]}{f+[A]+[A]^2/g} - r_{CH_4ads};\ \text{and}\ \frac{d[CH_{4s}]}{dt} = r_{CH_4ads} \\
\frac{d[CO_2]}{dt} &+ \frac{d[CO_{2s}]}{dt} \approx \frac{4\mu_1[W]}{Ks_1+[W]+Ks_1/Ks_2[Nu]} + \frac{\mu_2[Nu]}{Ks_2+[Nu]+Ks_2/Ks_1[W]} \\
&\quad + \frac{e[A]}{f+[A]+[A]^2/g} - r_{CH_4ads}; r_{CO_2} \approx 0
\end{aligned}$$

Appendix B

Appendix to Chapter 5

B.1 Proxy model development for dynamic input variables

This work was presented in the poster session at the FEGRS symposium, 2013.

When input variables are dynamic, proxy models accounting for uncertainty cannot be developed by the use of orthogonal polynomials, as described in Chapter 5. To deal with such cases, we have developed an alternate technique, wherein an ensemble of black-box time series models are identified at different collocation points and the deterministic coefficients of the time series model are then regressesed against a polynomial chaos expansion.

A short experiment of this technique was conducted with the tanks-in-series-model for the coreflooding experiment, developed in Chapter 3. The dynamic feed rate is considered to be the input parameter in the proxy model, whereas the initial coal quantity is assumed to tbe the uncertain parameter. Figure B.1 shows the input PRBS signal used in the identification of time series models at an ensemble of collocation points. Figure B.2 shows good prediction by a second order ARX model at one collocation point. Coefficients of time series models are then regressed against a

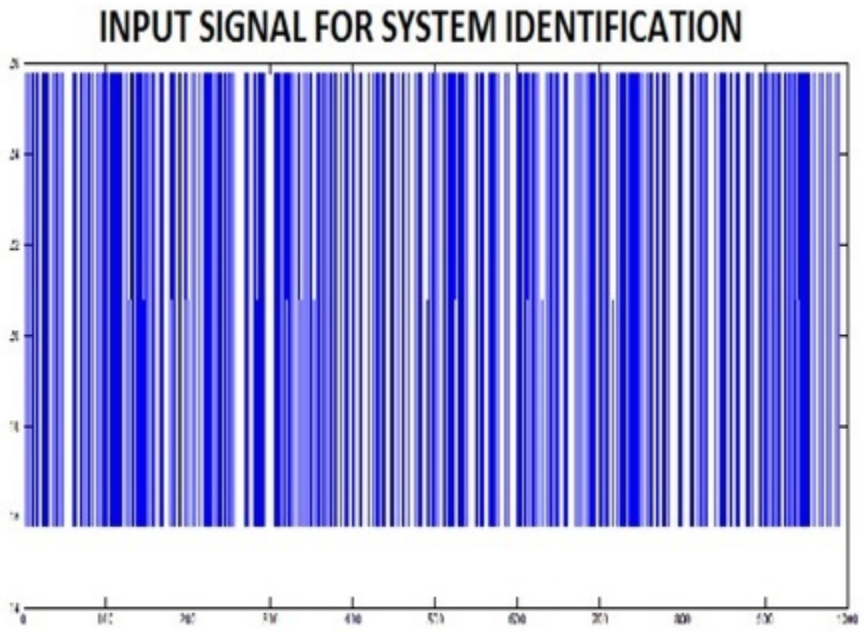

Figure B.1: *PRBS input signal used in model identfication*

polynomial chaos expansion as shown in Figure B.3.

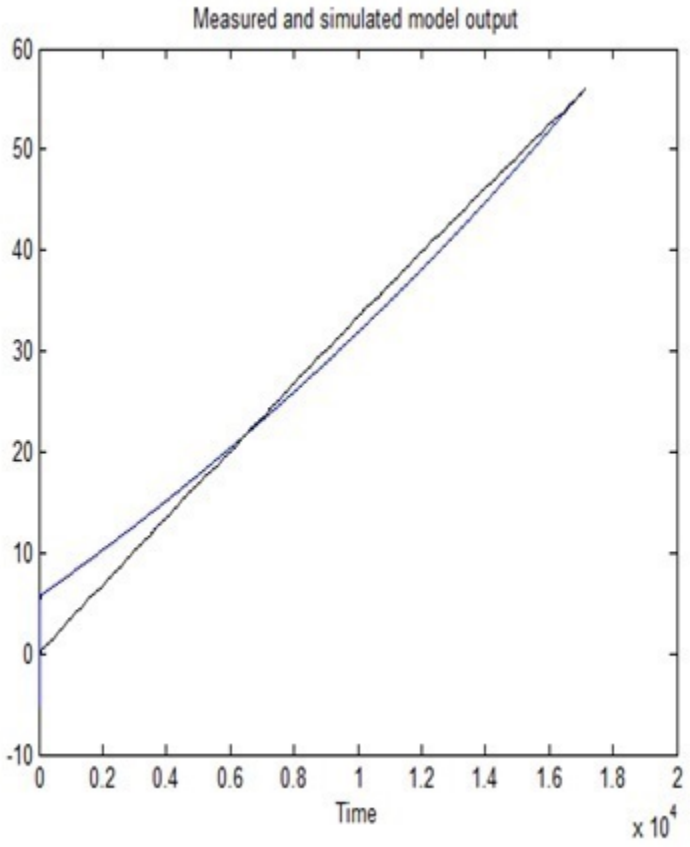

Figure B.2: *ARX model at one collocation point*

r	s	t
1.93	-0.9305	7.05E-06
1.932	-0.9317	6.78E-06
1.932	-0.9317	6.98E-06
1.931	-0.9313	6.83E-06
1.933	-0.933	6.59E-06
1.933	-0.9331	6.66E-06
1.931	-0.9312	6.73E-06
1.934	-0.9339	6.52E-06
1.93	-0.93	7.05E-06
1.931	-0.9308	7.07E-06

s = -0.0276 + 0.0004*e1 + 0.0003*e2 - 0.0179*(e1^2-1) - 0.0291*(e1*e2) - 0.0097 *(e2^2-1)

Polynomial Chaos Expansion for the parameter s

ARX MODEL:

y(t) = r*y(t-1) + s*y(t-2) + t*u(t-1) + e(t)

Figure B.3: *Polynomial chaos expansion of the coefficients of the ensemble of ARX models*

Appendix C

Appendix to Chapter 6

C.1 Enzymatic reaction network input to the CMG STARS model

	'H$_2$O'	'S'	'W'	'B'	'A'	'Nu'	'CH$_4$'	'CO$_2$'	'H$_2$'	'Coal'	'CH$_{4i}$'	'CO$_{2i}$'	'H$_{2i}$'
Reaction 1: C → S Reaction rate: $-k[S^*]\left(\frac{C}{C_0}\right)^{2/3}$													
STOREAC	0	0	0	0	0	0	0	0	0	1	0	0	0
STOPROD	0	0	0	0	0	0	0	0	0	0	0	0	0
RPHASE	0	1	0	0	0	0	0	0	0	4	0	0	0
RORDER	0	0	0	0	0	0	0	0	0	0.67	0	0	0
RXCRITCON	'Coal'	0.01											
FREQFAC	2×10^{-7}												
	'H$_2$O'	'S'	'W'	'B'	'A'	'Nu'	'CH$_4$'	'CO$_2$'	'H$_2$'	'Coal'	'CH$_{4i}$'	'CO$_{2i}$'	'H$_{2i}$'
Reaction 2: S → C Reaction rate: $k[S]\left(\frac{C}{C_0}\right)^{2/3}$													
STOREAC	0	1	0	0	0	0	0	0	0	0	0	0	0
STOPROD	0	0	0	0	0	0	0	0	0	1	0	0	0
RPHASE	0	1	0	0	0	0	0	0	0	4	0	0	0
RORDER	0	1	0	0	0	0	0	0	0	0.67	0	0	0
RXCRITCON	'Coal'	0.01											
FREQFAC	10^{-8}												

PERMSCALE defined for reactions 1 and 2 to indicate variation in solubilization rate constant with permeability

	'H$_2$O'	'S'	'W'	'B'	'A'	'Nu'	'CH$_4$'	'CO$_2$'	'H$_2$'	'Coal'	'CH$_{4i}$'	'CO$_{2i}$'	'H$_{2i}$'
Reaction 3: S + 41H$_2$O → 10W + 41H$_2$ Reaction rate: $b[S]$													
STOREAC	41	1	0	0	0	0	0	0	0	0	0	0	0
STOPROD	0	0	10	0	0	0	0	0	41	0	0	0	0
RPHASE	1	1	1	0	0	0	0	0	3	0	0	0	0
RORDER	0	1	0	0	0	0	0	0	0	0	0	0	0
FREQFAC	2.4												
	'H$_2$O'	'S'	'W'	'B'	'A'	'Nu'	'CH$_4$'	'CO$_2$'	'H$_2$'	'Coal'	'CH$_{4i}$'	'CO$_{2i}$'	'H$_{2i}$'
Reaction 4: W + Nu + 3H$_2$O → B + 5H$_2$ + 3CO$_2$ + Nu Reaction rate: $\frac{\mu_1'[W]}{1+1/Ks_2[Nu]}$													
STOREAC	3	0	1	0	0	1	0	0	0	0	0	0	0
STOPROD	0	0	0	1	0	1	0	3	5	0	0	0	0
RPHASE	1	0	1	1	0	1	0	3	3	0	0	0	0

RORDER	0	0	1	0	0	0	0	0	0	0	0	0	0
RXCMPFAC	'N '	W	2	1									
FREQFAC	0.024												
	'H_2O'	'S'	'W'	'B'	'A'	'Nu'	'CH_4'	'CO_2'	'H_2'	'Coal'	'CH_{4i}'	'CO_{2i}'	'H_{2i}'
Reaction 5: Nu → Nu + B Reaction rate: $\frac{\mu_2'[Nu]}{1+1/Ks_2[Nu]}$													
STOREAC	0	0	0	0	0	1	0	0	0	0	0	0	0
STOPROD	0	0	0	0.01	0	0.999	0	0	0	0	0	0	0
RPHASE	0	0	0	1	0	1	0	0	0	0	0	0	0
RORDER	0	0	0	0	0	1	0	0	0	0	0	0	0
RXCMPFAC	'N'	W	2	1									
FREQFAC	1.5												
	'H_2O'	'S'	'W'	'B'	'A'	'Nu'	'CH_4'	'CO_2'	'H_2'	'Coal'	'CH_{4i}'	'CO_{2i}'	'H_{2i}'
Reaction 6: B + 6H_2O → 3A + 3H_2 + CO_2 Reaction rate: $d[B]$													
STOREAC	6	0	0	1	0	0	0	0	0	0	0	0	0
STOPROD	0	0	0	0	3	0	0	1	3	0	0	0	0
RPHASE	1	0	0	1	1	0	0	3	3	0	0	0	0
RORDER	0	0	0	1	0	0	0	0	0	0	0	0	0
FREQFAC	0.1												
	'H_2O'	'S'	'W'	'B'	'A'	'Nu'	'CH_4'	'CO_2'	'H_2'	'Coal'	'CH_{4i}'	'CO_{2i}'	'H_{2i}'
Reaction 7: A → P Reaction rate: $\frac{0.52}{1+0.68[A]}$													
STOREAC	0	0	0	0	1	0	0	0	0	0	0	0	0
STOPROD	0	0	0	0	0	0	1	1	0	0	0	0	0
RPHASE	0	0	0	0	1	0	3	3	0	0	0	0	0
RORDER	0	0	0	0	0	0	0	0	0	0	0	0	0
RXCMPFAC	'A'	W	0.68		1								
FREQFAC	0.52												
Reaction 8: A → P Reaction rate: $-\frac{10000}{1+6666667[A]}$													
STOREAC	0	0	0	0	1	0	0	0	0	0	0	0	0
STOPROD	0	0	0	0	0	0	1	1	0	0	0	0	0
RPHASE	0	0	0	0	1	0	3	3	0	0	0	0	0

RORDER	0	0	0	0	-1	0	0	0	0	0	0	0	0
RXCMPFAC	'A'	W		6.6E+6	1								
FREQFAC	10000												

C.2 Input data file for CMG STARS

The following is the DAT file corresponding to flow in high permeability reservoir in the presence of nutrient injection

RESULTS SIMULATOR STARS 201110

INUNIT SI

WSRF WELL TIME

WSRF GRID TIME

WSRF SECTOR TIME

OUTSRF GRID CMPDENO CMPDENW FLUXRC FLUXSC FPOROS MOLDENG MOLDENO MOLDENW PERMI PERMJ PERMK PRES SG SO MOLE SOLCONC SW VPOROS VPOROSGEO W WATMOB Y Z

OUTSRF GRID PRES SG SO SOLCONC SW TEMP W X Y Z

OUTSRF WELL LAYER ALL

OUTSRF WELL MASS COMPONENT ALL

OUTSRF WELL MOLE COMPONENT ALL

WPRN GRID 0

OUTPRN GRID NONE

OUTPRN RES NONE

RESULTS XOFFSET 0.0000

RESULTS YOFFSET 0.0000

RESULTS AXES-DIRECTIONS 1.0 1.0 1.0

**21 ============== GRID AND RESERVOIR DEFINITION ==========

grid cart 10 10 5 ** 3D cartesian grid

depth 1 1 1 1000

NULL MATRIX CON 1

NULL FRACTURE CON 1

kdir UP

di con 100

dj con 70

dk con 6

dualpor

difrac con 10

djfrac equalsi

dkfrac con 1

frfrac con 0.03

por matrix con 0.98

POR FRACTURE CON 0.999

permi matrix con 0.001

permi fracture con 5 ** Fracture properties

permj matrix con 0.001

permj fracture con 5 ** Fracture properties

permk matrix con 0.001

permk fracture con 5 ** Fracture properties

PINCHOUTARRAY CON 1

SECTORARRAY 'Matrix' MATRIX CON 1

SECTORARRAY 'Fracture' FRACTURE CON 1

*end-grid

ROCKTYPE 1

permck 2.5

MODEL 13 12 6 6

COMPNAME H2O S W B A N H2O CH4 CO2 H2 CH4i CO2i H2i

CMM

0.018 1.444 0.21 0.122 0.06 1.22 0.016 0.044 0.002 0.016 0.044 0.002 1.444

IDEALGAS

TCRIT

0 0 0 0 0 0 0 0 0 0 0 0 0

TEMR 25

TSURF 25

$SOLID_DEN$ coal 1422 0 0

MASSDEN

0 0 0 0 0 0

CP

0 0 0 0 0 0

AVISC

0 0 0 0 0 0

**COMPNAME H2O S W B A N H2O CH4 CO2 H2 CH4i CO2i H2i coal

**CMM 0.018 1.444 0.21 0.122 0.06 1.22 0.016 0.044 0.002 0.016 0.044 0.002 1.444

** Reaction specification

STOREAC

0 0 0 0 0 0 0 0 0 0 0 0 1

STOPROD 0 1 0 0 0 0 0 0 0 0 0 0 0 RPHASE

0 1 0 0 0 0 0 0 0 0 0 0 4 RORDER

0 0 0 0 0 0 0 0 0 0 0 0 0.67

FREQFAC 2.00E-07

RXCRITCON coal 0.01

PERMSCALE

** effpt freqt 5 1

5.5 1.2

6 1.3

**COMPNAME H2O S W B A N H2O CH4 CO2 H2 CH4i CO2i H2i coal

**CMM 0.018 1.444 0.21 0.122 0.06 1.22 0.016 0.044 0.002 0.016 0.044 0.002 1.444

** Reaction specification STOREAC

0 1 0 0 0 0 0 0 0 0 0 0 0 STOPROD

0 0 0 0 0 0 0 0 0 0 0 0 1

RPHASE

0 1 0 0 0 0 0 0 0 0 0 0 4

RORDER

0 1 0 0 0 0 0 0 0 0 0 0 0.67

FREQFAC 1.00E-08

RXCRITCON coal 0.01

PERMSCALE

** effpt freqt

5 1 5.5 1.2

6 1.3

**COMPNAME H2O S W B A N H2O CH4 CO2 H2 CH4i CO2i H2i coal

**CMM 0.018 1.444 0.21 0.122 0.06 1.22 0.016 0.044 0.002 0.016 0.044 0.002 1.444

STOREAC

41 1 0 0 0 0 0 0 0 0 0 0 0

STOPROD

0 0 10 0 0 0 0 0 41 0 0 0 0

RPHASE

1 1 1 0 0 0 0 0 3 0 0 0 0

RORDER

0 1 0 0 0 0 0 0 0 0 0 0 0 FREQFAC 2.4

**COMPNAME H2O S W B A N H2O CH4 CO2 H2 CH4i CO2i H2i coal

**CMM 0.018 1.444 0.21 0.122 0.06 1.22 0.016 0.044 0.002 0.016 0.044 0.002 1.444

STOREAC 3 0 1 0 0 1 0 0 0 0 0 0 0

STOPROD

0 0 0 1 0 1 0 3 5 0 0 0 0

RPHASE

1 0 1 1 0 1 0 3 3 0 0 0 0

RORDER

0 0 1 0 0 0 0 0 0 0 0 0 0 FREQFAC 0.024

RXCMPFAC N W 2 1

**COMPNAME H2O S W B A N H2O CH4 CO2 H2 CH4i CO2i H2i coal

**CMM 0.018 1.444 0.21 0.122 0.06 1.22 0.016 0.044 0.002 0.016 0.044 0.002 1.444

STOREAC

0 0 0 0 0 1 0 0 0 0 0 0 0 0 STOPROD

0 0 0 0.01 0 0.999 0 0 0 0 0 0 0 0 RPHASE

0 0 0 1 0 1 0 0 0 0 0 0 0 0

RORDER

0 0 0 0 0 1 0 0 0 0 0 0 0 0

FREQFAC 1.5

RXCMPFAC N W 2 1

**COMPNAME H2O S W B A N H2O CH4 CO2 H2 CH4i CO2i H2i coal

**CMM 0.018 1.444 0.21 0.122 0.06 1.22 0.016 0.044 0.002 0.016 0.044 0.002 1.444 STOREAC

6 0 0 1 0 0 0 0 0 0 0 0 0 0 STOPROD

0 0 0 0 3 0 0 1 3 0 0 0 0 0

RPHASE 1 0 0 1 1 0 0 3 3 0 0 0 0 0

RORDER

0 0 0 1 0 0 0 0 0 0 0 0 0 0

FREQFAC 0.1 **COMPNAME H2O S W B A N H2O CH4 CO2 H2 CH4i CO2i H2i coal

**CMM 0.018 1.444 0.21 0.122 0.06 1.22 0.016 0.044 0.002 0.016 0.044 0.002 1.444

STOREAC

0 0 0 0 1 0 0 0 0 0 0 0 0

STOPROD

0 0 0 0 0 0 1 1 0 0 0 0 0 RPHASE

0 0 0 0 1 0 3 3 0 0 0 0 0 RORDER

0 0 0 0 0 0 0 0 0 0 0 0 0 FREQFAC 0.52

RXCMPFAC 'A' W 0.68 1

**COMPNAME H2O S W B A N H2O CH4 CO2 H2 CH4i CO2i H2i coal

**CMM 0.018 1.444 0.21 0.122 0.06 1.22 0.016 0.044 0.002 0.016 0.044 0.002 1.444
STOREAC

0 0 0 0 0 0 1 1 0 0 0 0 0

STOPROD

0 0 0 0 1 0 0 0 0 0 0 0 0 RPHASE

0 0 0 0 0 0 3 3 0 0 0 0 0

RORDER 0 0 0 0 0 0 0 0 0 0 0 0 0

FREQFAC 10000

RXCMPFAC 'A' W 6666667 1

$solid_den$ CH4i 0.66 0 0

$solid_den$ CO2i 1.98 0 0 $solid_den$ H2i 0.09 0 0

$solid_den$ CH4 0.66 0 0

solid$_d$*en* CO2 1.98 0 0 *solid*$_d$*en* H2 0.09 0 0

**124 ========== ROCK-FLUID PROPERTIES ==========

rockfluid

rpt 1 WATWET ** ——— MATRIX ———

swt smoothend quad

** Sw krw krow 0 0 1 1 1 0

slt ** Liquid-gas relative permeabilities smoothend linear

** Sl Krg Krog ** —- —— ——

0 0.0001 0

1 0 1

rpt 2 WATWET ** ——— FRACTURE ———

swt

smoothend quad ** Sw krw krow 0 0 1

1 1 0

slt ** Liquid-gas relative permeabilities

smoothend cubic

** Sl Krg Krog ** —- —— ——

0 1 0

1 0 1

**155 Assign rel perm sets

krtype matrix con 1

krtype fracture con 2

adscomp CH4i gas ** Reversible adsorption of aqueous surfactant

adslang 100 0 10000 ** Langmuir isotherms at 2 tempertures adsrock 1

admaxt 0.1

adsrock 2

admaxt 0

adscomp CO2i gas

adslang 250 0 10000 adsrock 1

admaxt 0.2

adsrock 2

admaxt 0

adscomp H2i gas

adslang 50 0 10000

adsrock 1

admaxt 0.05 adsrock 2

admaxt 0

adscomp CH4 gas ** Reversible adsorption of aqueous surfactant

adslang 100 0 10000 ** Langmuir isotherms at 2 tempertures

adsrock 1

admaxt 0.1

adsrock 2 admaxt 0

adscomp CO2 gas

adslang 250 0 10000

adsrock 1

admaxt 0.2

adsrock 2

admaxt 0

adscomp H2 gas

adslang 50 0 10000

adsrock 1

admaxt 0.05

adsrock 2

admaxt 0

**158 ========== INITIAL CONDITIONS ==========

initial VERTICAL OFF

INITREGION 1

pres matrix con 10000

pres fracture con 10000

sw matrix con 0 ** So by difference, since Sg = 0

sg matrix con 1

sw fracture con 0.5 ** So by difference, since Sg = 0

sg fracture con 0.5

**Property: Gas Mole Fraction(CH4i) Max: 0.5 Min: 0.5

MFRAC GAS CH4i MATRIX CON 0.5

**Property: Gas Mole Fraction(CO2i) Max: 0.5 Min: 0.5

MFRAC GAS CO2i MATRIX CON 0.5

**Property: Water Mole Fraction(H2O) Max: 0.9 Min: 0.9 MFRAC WAT H2O FRACTURE CON 0.99

**Property: Water Mole Fraction(A) Max: 0.1 Min: 0.1 MFRAC WAT A FRACTURE CON 0.01

**Property: Gas Mole Fraction(CH4i) Max: 0.5 Min: 0.5 MFRAC GAS CH4i FRACTURE CON 0.5

**Property: Gas Mole Fraction(CO2i) Max: 0.5 Min: 0.5

MFRAC GAS CO2i FRACTURE CON 0.5 **Property: Initial Solid Concentration(coal) (gmole/m3) Max: 850 Min: 850

CONC SLD coal MATRIX CON 850

**Property: Initial Solid Concentration(coal) (gmole/m3) Max: 200 Min: 200 CONC

SLD coal FRACTURE CON 200

temp matrix con 25

temp fracture con 25

**177 ========== NUMERICAL CONTROL ==========

numerical ** All these can be defaulted. The definitions ISOTHERMAL

CONVERGE TOTRES NORMAL UPSTREAM KLEVEL

RUN

DATE 2015 5 25

DTWELL 0.1 **

WELL Producer

PRODUCER Producer

OPERATE MIN BHP 300. CONT **UBA ff Status Connection

** rad geofac wfrac skin

GEOMETRY K 0.086 0.08 1. 0.

PERF GEOA Producer

**UBA ff Status Connection 1 5 5 1. OPEN FLOW-TO 'SURFACE' REFLAYER

1 5 1 1. OPEN FLOW-TO 1

10 5 1 1. OPEN FLOW-TO 2 **

WELL injector1

INJECTOR UNWEIGHT injector1

INCOMP WATER 0.7 0. 0. 0. 0 0.3

OPERATE MAX BHP 15000. CONT

** rad geofac wfrac skin

GEOMETRY K 0.086 0.249 1. 0.

PERF GEOA injector1

**UBA ff Status Connection

10 1 5 1. OPEN FLOW-FROM 'SURFACE' REFLAYER

10 1 3 1. OPEN FLOW-FROM 1

7 3 3 1. OPEN FLOW-FROM 2

** WELL injector2

INJECTOR UNWEIGHT injector2

INCOMP WATER 0.7 0. 0. 0. 0 0.3

OPERATE MAX BHP 15000. CONT

**UBA ff Status Connection ** rad geofac wfrac skin

GEOMETRY K 0.086 0.08 1. 0.

PERF GEOA injector2 **UBA ff Status Connection

10 10 5 1. OPEN FLOW-FROM 'SURFACE' REFLAYER 10 10 3 1. OPEN FLOW-FROM 1

7 7 3 1. OPEN FLOW-FROM 2

**

WELL injector3

INJECTOR UNWEIGHT injector3

INCOMP WATER 0.7 0. 0. 0. 0 0.3 OPERATE MAX BHP 15000. CONT

** rad geofac wfrac skin GEOMETRY K 0.086 0.249 1. 0.

PERF GEOA injector3

**UBA ff Status Connection

1 1 5 1. OPEN FLOW-FROM 'SURFACE' REFLAYER

1 1 3 1. OPEN FLOW-FROM 1 3 3 3 1. OPEN FLOW-FROM 2

**

WELL injector4 INJECTOR UNWEIGHT injector4

INCOMP WATER 0.7 0. 0. 0. 0 0.3

OPERATE MAX BHP 15000. CONT

** rad geofac wfrac skin

GEOMETRY K 0.086 0.249 1. 0.

PERF GEOA injector4

** UBA ff Status Connection

1 10 5 1. OPEN FLOW-FROM 'SURFACE' REFLAYER 10 3 1. OPEN FLOW-FROM 1

3 7 3 1. OPEN FLOW-FROM 2

DTMAX 0.5

NCUTS 15

UNRELAX 0.5

time 5

time 10

time 15

time 20

time 25 time 30 time 35 time 40 time 45 time 50 time 60 time 70 time 80 time 90 time 100 time 120 time 125 time 130 time 135 time 140 time 145 time 150 time 155 time 160 time 165 time 170 time 175 time 180 time 185 time 190 time 195 time 200

STOP